Finding the bottleneck in brain rejuvenation: mechanisms underlying neural stem cell quiescence exit

By

Christopher S. Morrow

A dissertation submitted in partial fulfillment of

the requirements for the degree of

Doctor of Philosophy

(Molecular and Cellular Pharmacology)

at the

UNIVERSITY OF WISCONSIN-MADISON

2021

Date of final oral examination: 6/29/2021

The dissertation is approved by the following members of the final Oral Committee:

Darcie L. Moore, Assistant Professor, Neuroscience
Timothy M. Gomez, Professor, Neuroscience
Jill C. Wildonger, Associate Professor, Biochemistry
William M. Bement, Professor, Zoology

Acknowledgements

Graduate school has been a period full of personal and professional growth. Although I am the sole author of this dissertation, this dissertation reflects the work of myself and dozens of colleagues. Further, what I have done would not have been possible without the support of many networks of friends and family. To all of my peers, mentors, mentees, friends, and family – thank you for supporting me and contributing to who I am today.

First I thank my PhD advisor, Dr. Darcie Moore, for her dedication to my training as a scientist. Darcie has a strong passion for mentoring future scientists and always goes above and beyond to ensure that her trainees receive a comprehensive training experience. My graduate studies, future career trajectory and life have been largely impacted by Darcie's mentoring. I hope that as I continue to work as a scientist and mentor junior scientists I am able to pay forward the wisdom Darcie has bestowed upon me.

I also thank all members of the Moore Lab, past and present, for their support during my graduate career. Peer mentoring is critical to be successful in any field – whether it be about figuring out how to complete a critical experiment or to go and eat ice cream when a critical experiment doesn't work out the way you had hoped.

I also thank our collaborators and colleagues who have contributed to my success as a graduate student through providing technical and conceptual expertise. Thank you for being open to support my work down the various paths my research has taken me.

To my dissertation committee, thank you for offering your time and support to ensure I stay on track both in completing projects, publishing papers and in maintaining a career trajectory.

Much of what I do also relies upon maintaining mental sanity through the highs and lows of science. To this end, I thank my friends and family from all walks of life, particularly Scott, Cassie, Judy, Quinn and Dan.

I also thank Cassie, Judy and Dan for their comments on Chapter 1 of the dissertation in which I wrote about my work to a non-scientist audience. This was arguably the most difficult chapter to write and a fantastic exercise to reflect on what the most important parts of my work are in the greater context of the world.

Last but not least, I thank my partner Cassie for her unwavering support in my academic endeavors. Most academic scientists will tell you that one of the most important keys to success is to find a supportive partner. From simply listening to me complain about failed experiments, to being open to moving around the country/world to support my career, Cassie has played a pivotal role in any success I have had or will have.

Table of Contents

Abstract

Neurogenesis persists but dramatically declines during early aging due to a decreased capacity of neural stem cells (NSCs) to exit quiescence. Although there is much we know about NSC quiescence, our understanding of NSC quiescence remains incomplete and limited by modern technologies that exist to study NSC quiescence. To address these gaps, we first developed a novel tool to study NSC quiescence by imaging autofluorescence. Second, we identified the aggresome as a cellular program for turning over protein which is required for efficient NSC quiescence exit and a role for the intermediate filament vimentin at the aggresome. Lastly, we performed a comparative study of the aggresome in dermal fibroblasts and found that aggresomes are used cell state-specifically and identified a novel regulator of aggresome assembly, MAP3K7. Together, these data illustrate NSC quiescence exit as a dynamic, multifaceted process and provide mechanistic insight into the rate-limiting step driving the decrease in adult neurogenesis that occurs during early aging.

Chapter 1: Non-Scientist Accessible Summary of Thesis for the Wisconsin Initiative for Science Literacy

---

1.1 Preface

The Wisconsin Idea suggests that every citizen should have the opportunity to learn about publicly funded research happening in Wisconsin. To this end, the Wisconsin Initiative for Science Literacy provides an annual award for PhD thesis chapters that are written to convey research to a non-science audience. Over the past 5 years I have been a graduate student working at the University of Wisconsin-Madison in the Department of Neuroscience in a stem cell biology laboratory. During this time I have contributed to the effort to help us live longer, healthier, happier lives by studying brain stem cells in a mouse. My predominant tasks were to 1) learn how to be an effective scientist, and 2) learn new things about how life works. In Chapter 6, I will convey my experiences to a non-scientist audience by discussing a couple of key experiments which illustrate some of the work I completed in graduate school. First I will provide an introduction to the topic I have been focused on in graduate school – brain stem cell aging. I will then discuss an example of experiments I performed to help us understand how to improve brain stem cell aging. Lastly, I will speculate next steps suggested by my findings.

1.2 An effort to live a long, healthy life

Is aging inevitable? Could we stop, or even reverse aging? Although people throughout history have strived to find the fountain of youth, up until only a few decades ago, these questions seemed so hard to answer that many scientists thought it was futile to even try. It wasn't until scientists discovered that you could make worms live as much as ten times longer by changing just one out of their roughly twenty thousand genes that people started to see aging as a process that we could control. While thinking about aging can seem depressing, by the time you finish reading this chapter I hope to convince you that it is well within our power to improve human aging and that human aging is emerging as one of the greatest biological and socioeconomic challenges of our time.

While living forever may on occasion seem attractive, there are several far more important reasons to study aging that have more practical applications. As modern medicine and technology has boomed over the past century, people are living longer than they ever have before and the gained years aren't the healthiest. As you get older, your risk of getting many major diseases increases, such as many types of cancer (Lopez-Otin, Blasco et al. 2013). Modern medicine and public health has extended human lifespan (the number of years before dying), but has failed to comparably extend human healthspan (the number of years without being riddled by ailments). Thus, we are creating epidemics of age-related diseases with enormous social and economic consequences (Spector 2018). If left unaddressed, the aging population will become a significant burden for future generations. Further, as your risk for getting most major diseases increases as you get older, aging provides a unique opportunity to understand many diseases at the

same time. If we can understand why you are at higher risk for these diseases as you age, we could make progress towards tackling all of these diseases simultaneously.

Studying aging in a comprehensive way is challenging due to the complexity of the aging process. Many things change as you age, such as your hair turning grey and your muscles weakening, and figuring out which things are causing you to age versus things that are just an effect of the aging process can be difficult. To make an effective dent, we had to narrow our focus to tangible goals. Our research group focused on one component of aging: stem cell aging (Lopez-Otin, Blasco et al. 2013). Your body is composed of many different types of components, one of which is something called a cell. **Cells** are units of life that are responsible for "doing" things to keep your body functioning optimally. For example, you have red blood cells that travel through your blood to deliver oxygen from the air to different parts of your body. Your body has hundreds of different types of cells that all have different jobs that all function together in a coordinated system to make you who you are. **Stem cells** are cells in your body that have the potential to create many different types of cells in your body and to effectively regenerate select parts of your body. While stem cell activity largely declines after our childhood, adult humans still have stem cells in at least a dozen spots. The problem is that, as we age, the ability of stem cells to properly support us diminishes (Boyette and Tuan 2014). Thus, many scientists are interested in trying to understand if rejuvenating adult stem cells throughout the body could be an effective strategy to slow, stop or even reverse aging.

Our group is interested in aging and stem cell aging broadly, but more specifically we are most interested in stem cells in the brain, called **neural stem cells** (which I will refer to here as **brain stem cells**). Brain stem cells are a cell type in the brain with the

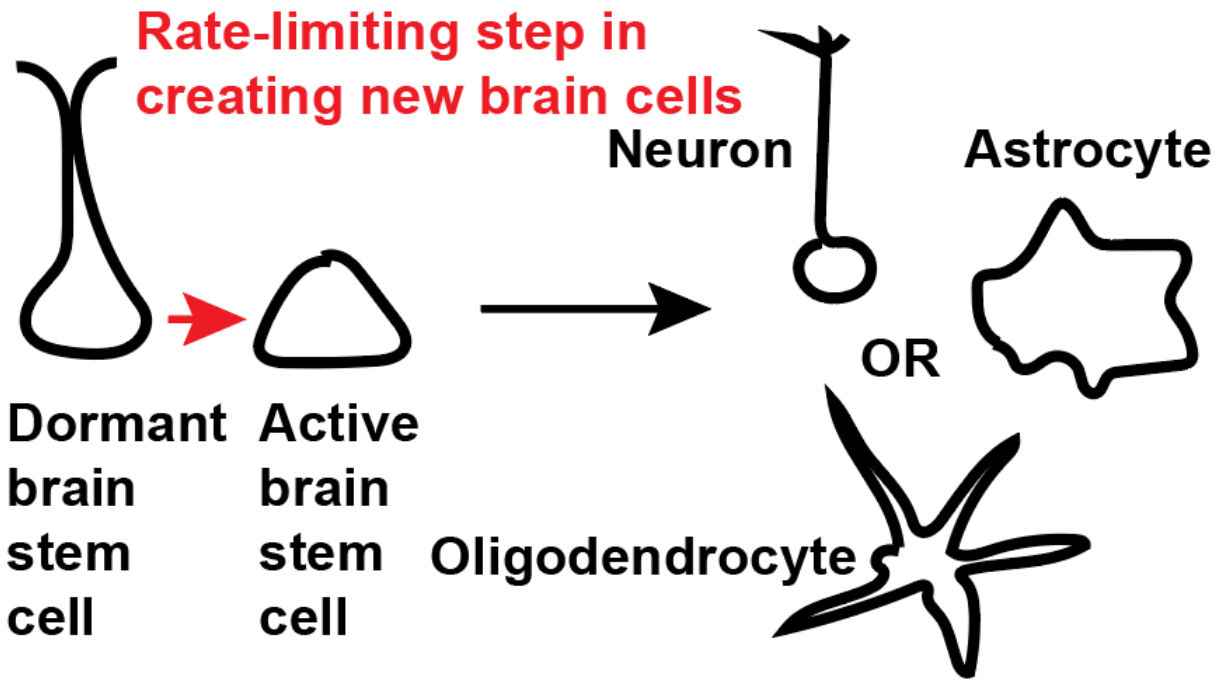

Figure 1.1 *– Schematic depicting how brain stem cells create new brain cells. White shapes outlined in black represent different cells. To make a new brain cell type, such as a neuron, astrocyte, or oligodendrocyte, dormant brain stem cells must first activate and become activated brain stem cells and then continue to mature into a specified brain cell type, such as the types of cells listed on the right. We think that a rate-limiting step in the production of new brain cells in adults is in the ability of dormant brain stem cells to become activated.*

capacity to make new brain cells (Fig. 1.1) (Goncalves, Schafer et al. 2016). The problem is that brain stem cells are largely dormant when you are an adult and are not producing new brain cell types at a rate which could substantially repair your brain when your brain would need them most (Kalamakis, Brune et al. 2019, Ibrayeva, Bay et al. 2021). For example, Alzheimer's Disease results, in part, from the destruction of brain cells (Cummings, Morstorf et al. 2014). Currently there are no effective ways to treat Alzheimer's Disease. If we could figure out how to help brain stem cells be more active we could potentially figure out ways to improve the prognosis for Alzheimer's Disease patients. Thus, many scientists such as myself have been focused on trying to understand how to make dormant brain stem cells become more active. To this end, I study brain stem cells in mice and brain stem cells in a petri dish that originate from mice and focus on trying to find ways to get them to be more active (Fig. 1.2).

During my time at the University of Wisconsin-Madison I learned many new things about brain stem cells. To convey a sample of what I learned, here I will discuss a few key experiments from one of the projects I completed where I found that brain stem cells use a cellular garbage can called the aggresome to keep themselves clean and leave the dormant state to make new brain cells and promote healthy aging.

1.3 A cellular garbage can that makes brain stem cells more efficient

In 2018, scientists found that dormant brain stem cells accumulate cell junk called protein aggregates and that they have to get rid of this junk to become activated and begin to make new brain cells (Leeman, Hebestreit et al. 2018). Cells have many ways to get rid of junk. Therefore, we wanted to see if experimenting with different ways that

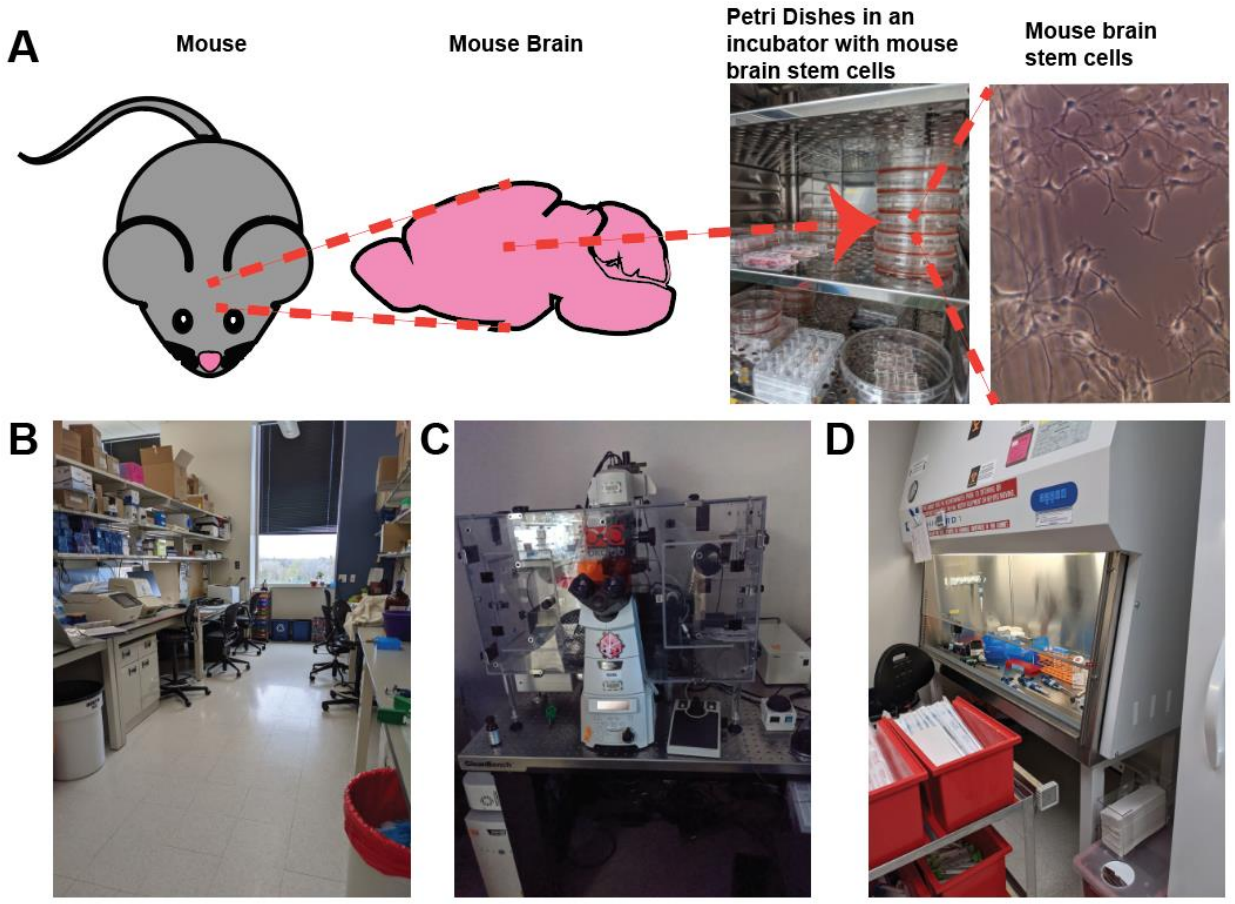

Figure 1.2 *– Pictures of the lab I work in and the cells I work with. A) Schematic showing the brain stem cells we work with. Brain stem cells are taken from a mouse brain and put in a petri dish in an incubator with cell food (the red liquid in the petri dishes). The far right image shows brain stem cells under a microscope. B) A picture of the lab space I work in. C) A picture of one of our fancier microscopes (confocal microscope). D) A picture of a "hood" – the sterile space we use to work with our brain stem cells where we can minimize the risk of contaminating them with microbes in the air.*

cells have for getting rid of junk could be an effective strategy to increase or decrease the rate at which brain stem cells activate and make new brain cells.

One way that cells can get rid of junk is through a cellular garbage can called the aggresome. The **aggresome** is a garbage can cells have that could be thought of as a staging ground for the destruction of cell junk (Fig. 1.3) (Johnston, Ward et al. 1998). The cell takes junk that needs to be destroyed and takes its tools for destroying the junk and carefully organizes them in one spot. We think that this helps a cell in many ways, such as by keeping the junk organized so it isn't sprawling out across the cell interfering with other critical tasks a cell must complete to stay healthy. Imagine living in a house without a trash can where the trash gets randomly spread everywhere rather than nicely contained in one spot. **We wanted to know if brain stem cells used the aggresome to get rid of cell junk when they activate and begin to make new brain cells.**

To see if brain stem cells used the aggresome to keep themselves clean as they activate, we took brain stem cells from a mouse and put them in a petri dish and then used a microscope to see if we could observe the aggresome forming as brain stem cells activated. To look at the aggresome, we had to treat the brain stem cells with a set of chemicals that would allow us to see different parts of the aggresome. More specifically, we looked at one part of the aggresome, called **vimentin**, which is a part of the cell's skeleton that encapsulates the aggresome. You can tell a cell is forming an aggresome if you see a condensed ball of vimentin in the middle of the cell. Excitingly, when we performed this experiment, we found that aggresomes formed when brain stem cells activated (Fig. 1.4A-B). This result supports our hypothesis that brain stem cells use the aggresome to keep themselves clean and produce new brain cells. This result also

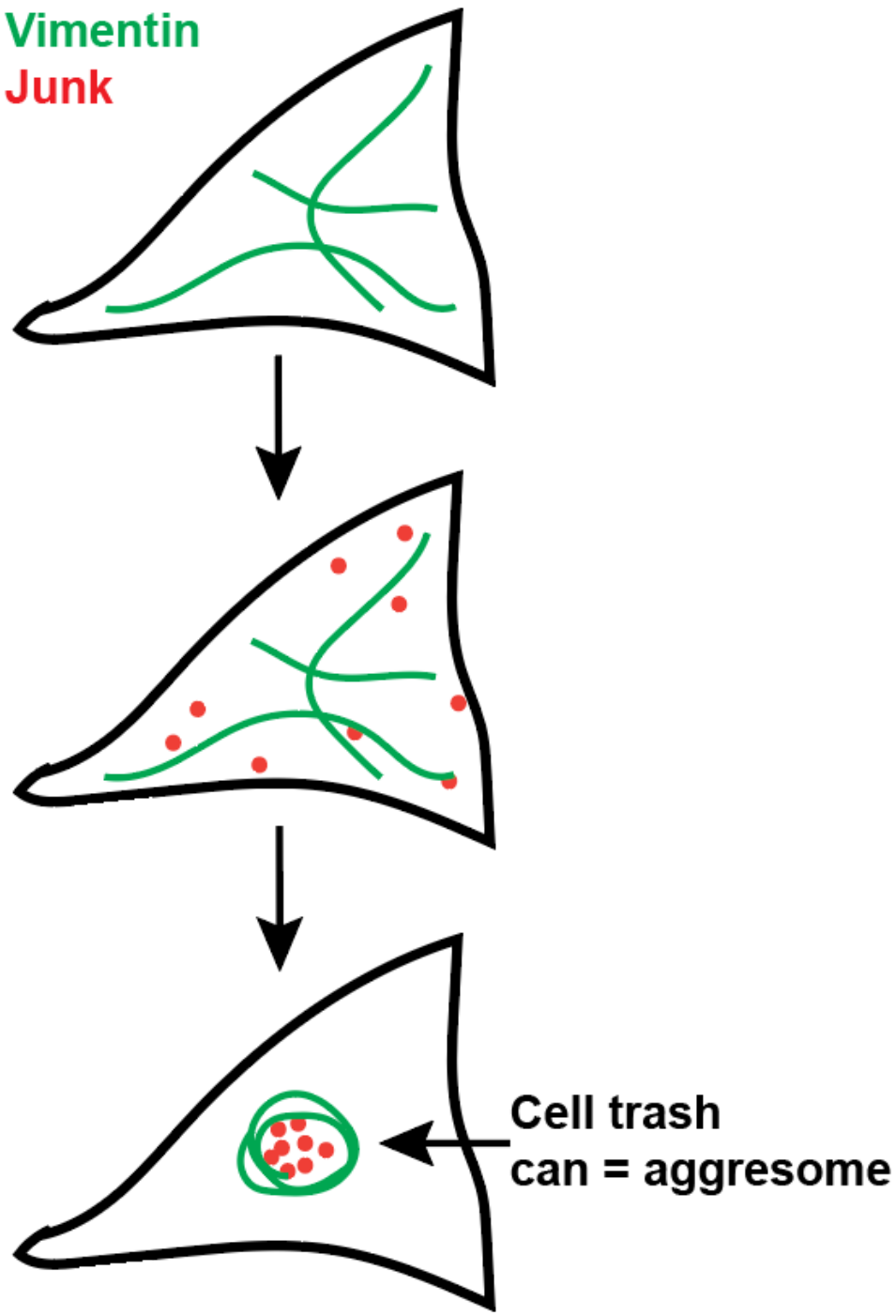

Figure 1.3 *– Schematic depicting how cells form a cellular trash can called the aggresome to get rid of cell junk (red). The white objects with a black outline are cells. During*

aggresome formation, a skeletal part of the cell called vimentin (green) forms a cage around the cell junk in the middle of the cell.

suggests that we could use the aggresome as a target to increase or decrease new brain cell production in adults.

Although we had seen that the aggresome was used by brain stem cells as they activated, we still didn't know if the aggresome was important for this process. Think of it this way, all astronauts that have been to the moon have drunk water, but drinking water doesn't mean you will end up on the moon. In other words, is the aggresome a part of what is causing brain stem cells to activate, or is the aggresome just a side-effect of other things that are happening that drive brain stem cell activation? To try and find an answer to this question, we examined brain stem cells which have an aggresome that doesn't work properly. We learned from other experiments that brain stems cells needed vimentin to efficiently degrade cell junk at the aggresome. Vimentin isn't important for forming the aggresome, but is important for getting rid of junk in the aggresome. You could think of a brain stem cell without vimentin as having a trash can that doesn't empty often enough. Therefore, to determine whether the aggresome is important for brain stem cell activation, we took mice that either had vimentin or mice that had vimentin removed and looked at their brains using a microscope to observe the rate at which dormant brain stem cells were activating. To our great excitement, we observed that brain stem cells without vimentin had a harder time activating (Fig. 1.4C). This result suggests that the aggresome is a junk clearance system that is important for a brain stem cell's ability to activate and produce new brain cells.

In conclusion, in this section I discussed key experiments from a project we completed in which we found a new way that brain stem cells keep themselves clean, a cellular garbage can called the aggresome, and that this cellular garbage serves

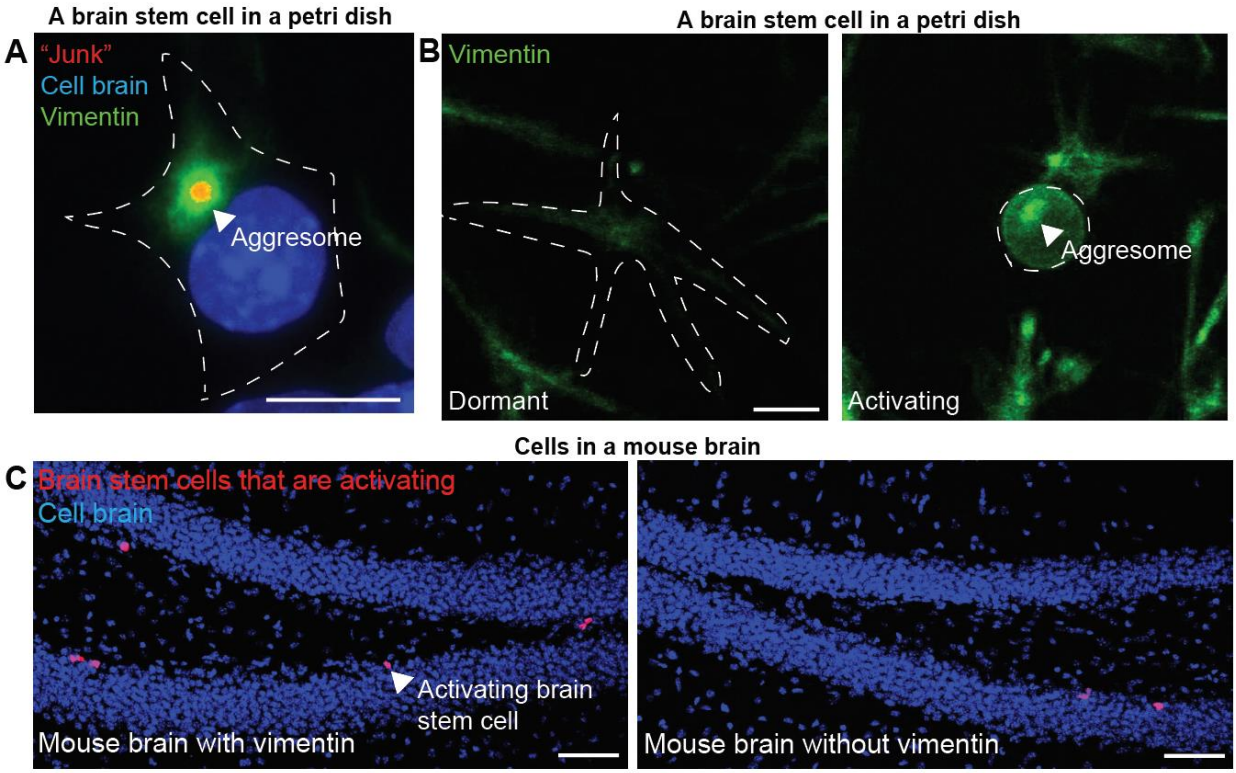

Figure 1.4 – *Data for section 6.4. A) Picture of a brain stem cell with an aggresome where we imaged junk (red), the cell's command center (nucleus; blue) and vimentin (green). Notice how vimentin forms a cage around the cell junk. This structure denoted by the white arrow is the aggresome. The cell is outlined with a white dashed line. B) Pictures of a brain stem cell in a petri dish making a vimentin cage (green) around the aggresome as it starts to activate out of a dormant state. The cell is outlined with a white dashed line. Notice how vimentin gets brighter and forms a smaller dot within the cell when activating – this is the vimentin cage. C) Pictures of a mouse brain from a mouse that either did or did not have vimentin where all nuclei were labeled (not just brain stem cells, but also other cells in the brain like neurons) in blue and brain stem cells that are activating are*

labeled in red. Notice how when vimentin is in the brain there are more red cells – indicating vimentin is important for a brain stem cell's ability to activate in the mouse brain.

important roles in the production of new brain cells. At a broader level, these experiments provide a framework explaining some of the rate-limiting steps in how the adult brain creates new brain cells which limit our brain's ability to repair itself.

1.4 Where we go from here

In this chapter, I first discussed the aging research field and discussed how scientists study stem cells to figure out whether increasing their activity can help us age more gracefully. More specifically, I discussed how scientists think a reason your brain is unable to regenerate sufficiently when suffering from brain degenerating diseases or injuries, such as Alzheimer's Disease, is tied to brain stem cells having a hard time getting out of a dormant state. In section 6.3 I summarized our work identifying a cellular garbage can called the aggresome as a critical component of a brain stem cell's ability to exit the dormant state on the path to making new brain cells. These experiments provide an example of the types of progress we have made in the laboratory towards improving brain stem cell aging. In addition to these key discoveries, we have also made new tools to identify dormant and active brain stem cells and learned more about how cells put the aggresome together. It is our ultimate hope that these advances in knowledge can continue to instruct the world-wide journey towards healthier aging.

While it may seem a bit abstract how the experiments I described above could cause you or your children to live longer, healthier lives, it might help to know that groundbreaking science almost always starts as what we have discussed in this chapter.

Many of the most significant scientific discoveries were the result of “basic science” research, which was not specifically focused on directly curing a human disease. For example, CRISPR/Cas9, the hot new gene editing technology that is arguably the discovery of the century, came from unsuspecting scientists who were studying what happens when bacteria are attacked by viruses. My point is not that my work is worthy of the title “discovery of the century,” but rather that everything we do, no matter how small it may seem, contributes to the betterment of the world, often in ways we could never fully anticipate.

Chapter 2: Introduction

2.1 Neural Stem Cell Quiescence

In 1928 when the father of modern Neuroscience, Ramon y Cajal, proclaimed that no newborn neurons were created in the brain after development, it became long-held dogma that neurons lost in adult life are not replaceable. However, as technologies developed and opportunities arose, we slowly began to learn that adult mammalian brains harbored neural stem cells (NSCs) with the capacity to generate a number of neural cell types, such as neurons, throughout life (Alvarez-Buylla, Theelen et al. 1988, Kuhn, Dickinson-Anson et al. 1996, Spalding, Bhardwaj et al. 2005) (Fig. 2.1). Neurogenic niches harboring NSCs have since been identified in at least two distinct regions of the adult brain, the subgranular zone of the dentate gyrus of the hippocampus and the subventricular zone of the lateral ventricles (Urban, Blomfield et al. 2019). Further, recent evidence suggests there additionally may be a population of NSCs in the hypothalamus (Paul, Chaker et al. 2017). Adult neurogenesis has since been shown to play a role in a variety of higher order cognitive functions, such as pattern separation, and is modulated in various diseases, such as Alzheimer's Disease (Jacobs, van Praag et al. 2000, Jacobs 2002, Sahay and Hen 2007, Sahay, Scobie et al. 2011, Choi, Bylykbashi et al. 2018, Moreno-Jimenez, Flor-Garcia et al. 2019).

While many species of adult mammals exhibit adult neurogenesis, the rate of adult neurogenesis dramatically declines during early-aging, heavily limiting the ability of the brain to regenerate after injury (Ben Abdallah, Slomianka et al. 2010). Current evidence suggests that this is not due to a lack of NSCs present in aged brains, but rather that the NSCs in the aged brain are in a reversibly non-mitotic state called quiescence

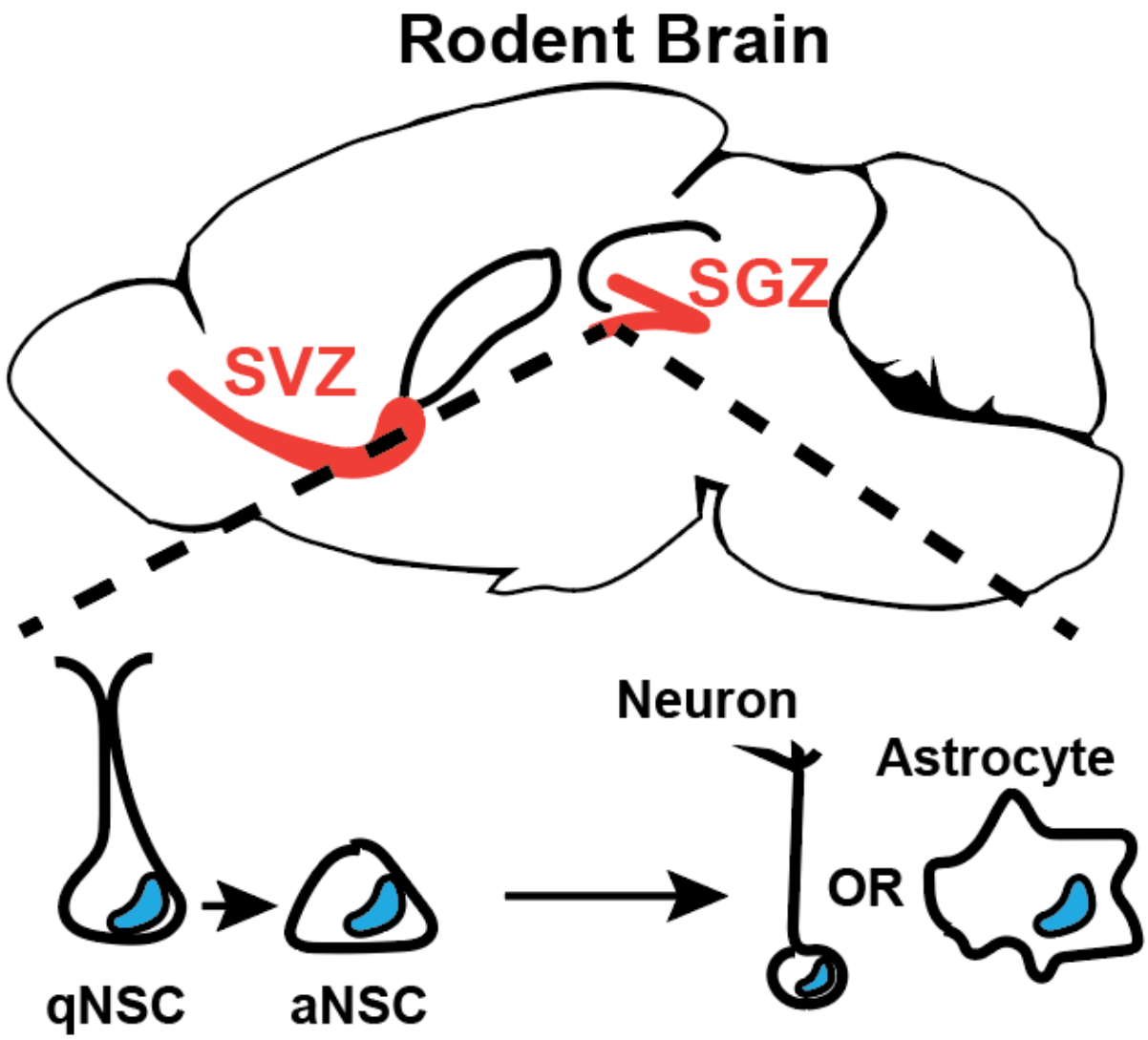

Figure 2.1 – *Neurogenesis in the adult mammalian brain. qNSCs (left) activate to become aNSCs and subsequently can differentiate to generate a number of neural cell types, such as: astrocytes and neurons. Adult neurogenesis occurs in mammals in at least two distinct zones: the subgranular zone (SGZ) and the subventricular zone (SVZ).*

(Kalamakis, Brune et al. 2019). To create a newborn neuron, a quiescent neural stem cell (qNSC) must first exit quiescence, thereby entering the cell cycle and subsequently beginning differentiation over the course of several days. Recent work suggests that the intrinsic and extrinsic barriers to exiting quiescence are greater in the aging brain and that this drives the sharp decline in adult neurogenesis during early aging (Dulken, Buckley et al. 2019, Kalamakis, Brune et al. 2019, Ibrayeva, Bay et al. 2021). Thus, the adult neurogenesis community has become heavily invested in understanding the path an NSC takes when undergoing quiescence exit, with the ultimate hope of identifying strategies to modulate quiescence exit to more broadly potentiate adult neurogenesis.

Although, these observations may seem to suggest that NSC quiescence is an "enemy" to the aging brain, it is also important to understand the critical role that NSC quiescence plays in maintaining adult neurogenesis. Preserving a subpopulation of stem cells in a quiescent state is thought to come with a number of advantages contributing to the longevity of the stem cell pool, such as a reduced mutational load, resistance to terminal differentiation, depletion of stem cell number, and reduction in stochastic damage that may accumulate over the lifespan of the organism (Urban, Blomfield et al. 2019). Thus, in any effort to modulate NSC quiescence, careful consideration should be taken to ensure that the stem cell pool is preserved to continually support adult neurogenesis throughout the rest of the organism's life.

The identification of quiescent NSCs (qNSCs) and activated NSCs (aNSCs), along with the development of markers and tools to isolate and study them, such as single-cell RNA sequencing, has provided great insight into the molecular nature of qNSCs, aNSCs and qNSC exit

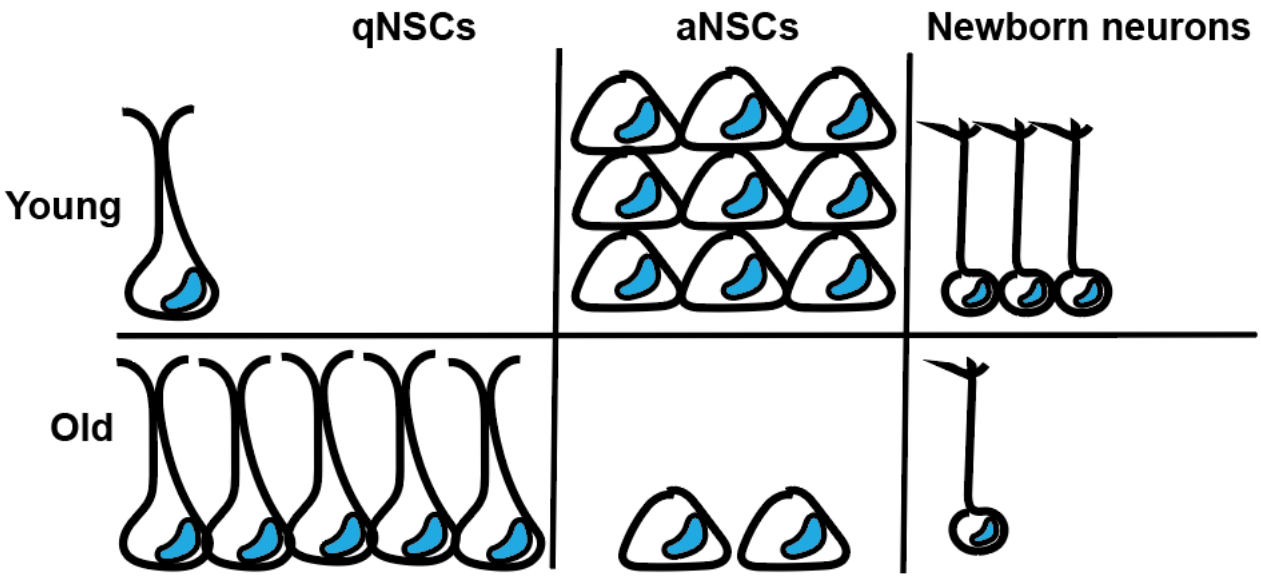

Figure 2.2 *– A model of age-related changes to adult neurogenesis. During aging the proportion of NSCs in quiescence increases and there is a reduction in the production of newborn neurons.*

(Lugert, Basak et al. 2010, Bonaguidi, Wheeler et al. 2011, Codega, Silva-Vargas et al. 2014, Llorens-Bobadilla, Zhao et al. 2015, Shin, Berg et al. 2015, Urban, van den Berg et al. 2016, Knobloch, Pilz et al. 2017, Leeman, Hebestreit et al. 2018, Pilz, Bottes et al. 2018, Zhou, Bond et al. 2018, Urban, Blomfield et al. 2019, Zhang, Boareto et al. 2019, Bottes, Jaeger et al. 2021). Together, these studies have identified widespread shifts in cell biology defining qNSCs and aNSCs, such as in their metabolic networks and in how they maintain proteostasis, much of which mimics what is observed in quiescent states in other cell types. Further, these data have begun to uncover targetable pathways which modulate NSC activation state. Here I discuss what is known about the differences between qNSCs and aNSCs, examples of how to perturb NSC activation state, and speculate future directions for the field.

2.2 The underlying biology of qNSCs and aNSCs

Targeted and unbiased studies from the past decade have revealed numerous distinctions in the cell biology of qNSCs and aNSCs (Llorens-Bobadilla, Zhao et al. 2015, Shin, Berg et al. 2015, Dulken, Leeman et al. 2017, Leeman, Hebestreit et al. 2018, Kalamakis, Brune et al. 2019). For example, as NSCs move in and out of a quiescent state, they are known to substantially remodel their metabolism (Shin, Berg et al. 2015, Beckervordersandforth 2017, Knobloch, Pilz et al. 2017, Leeman, Hebestreit et al. 2018). Although NSC quiescence comes with decreased protein synthesis and transcription, quiescence is still a highly active state, where numerous pathways become upregulated (Cheung and Rando 2013, Baser, Skabkin et al. 2017).

Metabolism – For example, while aNSCs exhibit higher levels of oxidative phosphorylation and *de novo* lipogenesis, qNSCs are associated with relatively higher levels of glycolysis and fatty acid oxidation (Knobloch, Braun et al. 2013, Shin, Berg et al. 2015, Stoll, Makin et al. 2015, Knobloch, Pilz et al. 2017). Strikingly, the Cpt1a inhibitor and metabolite malonyl CoA, was by itself sufficient to drive NSCs to exit quiescence (Knobloch, Pilz et al. 2017). This finding suggests a critical role for the cell's metabolic network in influencing NSC activation state and suggests that metabolic pathways can act as drivers rather than merely as consequences of NSC activation state. However, it is not clear why NSC cell states have such strong preferences for different sources of energy production and what advantages or consequences these decisions may confer for adult neurogenesis at large.

Proteostasis – NSC quiescence is also marked by a shift in how NSCs maintain their proteome. qNSCs exhibit higher levels of protein aggregates and higher lysosome activity, while harboring lower levels of protein synthesis and proteasome activity, compared to aNSCs (Leeman, Hebestreit et al. 2018). Further, the ability to shift proteostasis and clear the protein aggregates present in quiescence was critical for efficient NSC quiescence exit, as upregulating autophagy through overexpression of the transcription factor transcription factor EB (TFEB) was sufficient to increase the rate of NSC quiescence exit (Leeman, Hebestreit et al. 2018). Despite these initial observations, the identity and function of the protein aggregates present in qNSCs is unclear. Supporting these observations, we similarly found that protein clearance through a protein turnover mechanism called the aggresome was critical for efficient neural stem cell quiescence exit (Morrow, Porter et al. 2020).

Cell-surface receptors – qNSCs and aNSCs also differ in their expression of cell surface receptors. qNSCs are thought exist in a poised state with a number of cell surface receptors, such as Notch2, expressed on the plasma membrane awaiting cues from the niche to signal a NSC response (Shin, Berg et al. 2015, Boareto, Iber et al. 2017, Engler, Zhang et al. 2018, Zhang, Engler et al. 2018, Zhang, Boareto et al. 2019). This feature is thought to allow qNSCs to quickly adapt to environmental cues and be recruited into the cell cycle. Conversely, aNSCs are more intrinsically focused, with a downregulation of cell-cell communication networks and a larger attention being spent on proliferation and differentiation (Shin, Berg et al. 2015).

Epigenetics – Recent evidence also suggests substantive shifts in chromatin accessibility between aNSCs and aNSCs, which could explain some of the widespread shifts in the cell biology of qNSCs and aNSCs, through control of transcription (Sun Y. Maybury-Lewis 2020). Assay for Transposase Accessible Chromatin (ATAC-seq) revealed that there were many chromatin features conserved across qNSCs and aNSCs and many features which differed. Specifically, qNSCs and aNSCs differed in the accessibility of chromatin bound by pro-neurogenic transcription factors ASCL1 and NFI, whereas qNSCs and aNSCs shared chromatin profiles related to protein translation and metabolic function (Sun Y. Maybury-Lewis 2020).

Interestingly, despite sharing a cell-type identity as NSCs, qNSCs and aNSCs cumulatively exhibit substantially different cell biology, with many major aspects of their biology being rewired across NSC activation state. It is likely that there are many other differences that have yet to be revealed as the focus on NSC quiescence is still relatively

recent. How these differences influence function and optimize the roles each of these cell states plays in the biology of the brain remains to be uncovered.

2.3 Regulators of NSC Activation State

As numerous aspects of cell biology are shifted as NSCs move in and out of quiescence, it is no surprise that numerous mechanisms have been identified which influence NSC quiescence. During aging when the relative levels of NSCs exiting quiescence decreases, it is thought that this increase in NSC quiescence is mediated through extrinsic signals coming from the niche (Silva-Vargas, Maldonado-Soto et al. 2016, Yeh, Asrican et al. 2018, Kalamakis, Brune et al. 2019). Indeed, many extrinsic mechanisms influencing NSC quiescence have been identified coming from various sources, such as the vasculature and astrocytes (Wilhelmsson, Faiz et al. 2012, Silva-Vargas, Maldonado-Soto et al. 2016, Horowitz, Fan et al. 2020). However, numerous cell intrinsic mechanisms have also been identified, suggesting that NSCs may have some intrinsic capacity to control NSC quiescence as well (Urban, van den Berg et al. 2016, Leeman, Hebestreit et al. 2018, Morrow, Porter et al. 2020). It is also likely that many of these identified strategies for perturbing NSC quiescence are linked or represent different steps in a more common pathway, however, how these would be connected at this point remains less clear.

<u>Extrinsic Control of NSC quiescence</u>

Extracellular matrix (ECM) – NSCs reside in complex niches in the brain full of distinct cell types, vasculature, and a diverse ECM. One component of the ECM

composed primarily of laminins, termed fractones, was found to play a key role in maintaining NSC quiescence through modulating bone-morphogenic protein 4 (BMP4) signaling (Mercier and Douet 2014). Specifically, BMP4 was observed to bind to fractones, and in the absence of this interaction, BMP4 was freed to act on NSCs and ultimately suppress NSC proliferation. More broadly, maintaining the ECM also is thought to be critical to ensure NSCs are kept in close contact with critical signals involved in maintaining the quiescent state.

Neurotransmitters – NSC quiescence and neurogenesis are also largely subject to regulation by neurotransmitters, such as: serotonin, dopamine, glutamate, gamma aminobutyric acid, acetylcholine, neuropeptide Y and noradrenaline (Berg, Belnoue et al. 2013). Long range signals from neurons called mossy cells have been found to physically associate with NSCs and control their behavior (Yeh, Asrican et al. 2018). Such mechanisms could provide a means to quickly control neurogenesis to dynamically react to environmental changes occurring across the organism.

Local extracellular factors – Additionally, numerous factors from various sources, such as from the vasculature systemically, or from being secreted by NSCs, astrocytes and other cell types locally, also can influence NSC quiescence and neurogenesis. For example, parabiosis experiments connecting the vasculature of old and young animals revealed that factors in the aging vasculature negatively regulates neurogenesis (Villeda and Wyss-Coray 2013). Since this discovery, a number of small molecules which change during blood aging have been proposed as modulators of neurogenesis, such as glycosylphosphatidylinositol (GPI)-specific phospholipase D1 (Gpld1) (Villeda and Wyss-Coray 2013, Baruch, Deczkowska et al. 2014, Smith, He et al. 2015, Horowitz, Fan et al.

2020). Further, WNTs produced by both NSCs and astrocytes are similarly able to control NSC quiescence, where canonical WNT signaling is associated with NSC self-renewal and proliferation (Lie, Colamarino et al. 2005, Bowman, van Amerongen et al. 2013, Kalamakis, Brune et al. 2019). Lastly, recent evidence also suggests that during aging, T cells infiltrate the SVZ and secrete interferon-γ, which inhibits NSC proliferation. Thus, many factors possess the capacity to modulate NSC quiescence (Dulken, Buckley et al. 2019). How they synergize to elicit net effects remains unclear, as it is unlikely that NSCs would ever only be affected by one of these such signals at one time.

Intrinsic Control of NSC quiescence

In addition to manipulating NSC quiescence through extrinsic mechanisms, numerous reports have similarly identified ways to manipulate NSC quiescence through changing intracellular biology. NSC quiescence is marked by a broad remodeling of the metabolome, and as such, several approaches that shift cellular metabolism have been observed to elicit downstream effects on NSC cell behavior. For example, *in vitro*, qNSCs can be triggered to exit quiescence by the simple addition of malonyl CoA to the media (Knobloch, Pilz et al. 2017).

Many signaling pathways, such as the MFGE8/Integrin/ILK pathway and AKT-mTOR1 pathway have also been observed to influence NSC proliferation (Bonaguidi, Wheeler et al. 2011, Zhou, Bond et al. 2018). For example, AKT was found to be suppressed in qNSCs and deletion of this suppression led to stem cell pool depletion. Many of these pathways also have been observed to converge on a common set of transcription factors. For example, several niche signals have been found to converge on

the transcription factor ASCL1, a factor which targets a number genes, many of which are cell-cycle related genes (Urban, Blomfield et al. 2019). Degradation of ASCL1 was found to be required for NSCs to return to quiescence (Urban, van den Berg et al. 2016).

Lastly, modulating protein degradation also influences NSC quiescence. As qNSCs harbor elevated levels of aggregated proteins which must be cleared during NSC quiescence exit, it was found that upregulating autophagy through expression of TFEB during NSC quiescence exit was sufficient to increase the efficiency of the transition from quiescence to activation (Leeman, Hebestreit et al. 2018). Thus, the activated NSC identity is tied to the ability to efficiently shift proteostasis and clear waves of protein.

To date, the field has uncovered a variety of strategies to modulate NSC quiescence and neurogenesis at many different levels. It remains to be seen how these pathways and mechanisms can be integrated and which may turn out to be of more or less consequence in dictating NSC cell behavior both in pathology and during healthy aging.

2.4 Limitations in Technologies to Study Neurogenesis

While we know a great deal about the biology of qNSCs, aNSCs and what must occur for a NSC to exit quiescence, the current body of knowledge is limited by technical caveats. For example, due to challenges in accessing NSCs in the middle of the brain, the vast majority of analyses of NSCs are examining NSCs fixed in a single point in time, as opposed to dynamically tracking cell behavior over the course of time. These studies provide insight to the biology of NSCs, but lack critical insight into NSC behavior that

preceded the fixed point in time in which each analysis was performed. Further, we have also recently learned that many fundamental assumptions which paved the way for isolation and characterization of different populations of NSCs are inherently flawed. For example, intermediate filaments such as nestin and GFAP are thought to be expressed by NSCs in the brain and are used to identify and isolate NSCs. However, recent evidence suggests that NSCs change expression of these proteins as they change cell state. Nestin is predominantly thought to be expressed in aNSCs, but not qNSCs while GFAP is thought to be expressed in qNSCs but not aNSCs (Codega, Silva-Vargas et al. 2014). Many studies have used either nestin or GFAP to isolate NSCs and then further used other markers to identify which cells are aNSCs or qNSCs. While these data sets still have value, the cell-state expression of GFAP and nestin raise concerns as to whether these previous studies are actually providing an accurate picture of the differences between qNSCs and aNSCs. Limitations such as these require the development of new techniques to expand the technical toolkit.

2.5 Future Directions for the Field

The past several decades provided the adult neurogenesis community with observations and insights into many key questions posed by the field. We know that neurogenesis persists and functionally contributes to higher level cognitive function in many mammalian species throughout life. Despite some recent controversy, a large body of evidence supports the notion that neurogenesis similarly persists in adult humans. Further, clonal analyses and emerging technologies, such as *in vivo* imaging and single-

cell sequencing have culminated in stronger models for NSC behavior during mitosis and differentiation to produce newborn neurons.

Expanding upon this existing body of work, key questions for the field moving forward include, but are not limited to, the following: When the brain increases neurogenesis, what controls why some NSCs will begin to terminally differentiate and other NSCs will retain their stemness? How much of the age-dependent decline in neurogenesis is due to NSC intrinsic vs. extrinsic factors, and what are all of these factors? Are there other places in the brain where neurogenesis occurs, and of the niches we know about, how similar or different are the modes of neurogenesis in each? How discrete or continuous is NSC quiescence, and are there further substates of NSC quiescence that can predict NSC behavior? Finally, more broadly and perhaps most importantly, how can we harness the knowledge we have of how adult neurogenesis occurs to tackle the problems imposed by brain aging?

In this dissertation, I will discuss projects aimed at expanding our technical toolkit and broadening our conceptual understanding of the molecular mechanisms mediating adult neurogenesis, through focusing specifically on a rate-limiting step in adult neurogenesis, NSC quiescence exit.

Chapter 3: Autofluorescence as a biomarker to identify quiescent neural stem cells

3.1 Abstract

Neural stem cells (NSCs) in the adult brain are primarily quiescent yet can activate and enter the cell cycle to produce newborn neurons. NSC quiescence can be regulated by disease, injury, and age, however our understanding of NSC quiescence is incomplete due to technical limitations imposed by the bias of markers used to isolate each population of NSCs and the lack of live-cell labeling strategies. Fluorescence lifetime imaging (FLIM) of autofluorescence has previously been used in other cell types to study shifts in cell states driven by metabolic remodeling that change the optical properties of endogenous fluorophores. Thus, here we asked whether autofluorescence could be used to discriminate NSC activation state. We found that quiescent NSCs (qNSCs) and activated NSCs (aNSCs) have distinct autofluorescence intensity and fluorescence lifetime profiles, specifically with an enrichment of autofluorescence localizing to lipid droplets in qNSCs. NSC autofluorescence could enrich for NSC activation state using a fluorescence-activated cell sorter, predict cell behavior, and enable tracking of the dynamics of quiescence exit at single cell resolution. Finally, autofluorescent punctate signals were similarly detectable in qNSCs in the mouse brain in situ. Taken together, we describe a live-cell, label-free strategy for determining NSC activation state which expands the toolkit for studying adult neurogenesis.

3.2 Project Introduction

Neural stem cells (NSCs) are responsible for the lifelong production of newborn neurons, a process referred to as neurogenesis, in at least two distinct zones: the subventricular zone of the lateral ventricles and the subgranular zone of the dentate gyrus

in the hippocampus (Goncalves, Schafer et al. 2016). Neurogenesis consists of a quiescent NSC (qNSC) activating to become a proliferative activated NSC (aNSC) and then beginning to differentiate, first by becoming a neuroblast before fully differentiating into a newborn neuron (Goncalves, Schafer et al. 2016). Recent evidence suggests that a significant rate-limiting step in adult neurogenesis may be NSC quiescence exit, a time in which a non-dividing NSC is activated and enters the cell cycle to produce progeny (Lugert, Basak et al. 2010, Kalamakis, Brune et al. 2019, Harris, Rigo et al. 2021, Ibrayeva, Bay et al. 2021). Thus, understanding the biology of qNSCs, aNSCs and the transition from quiescence to activation has become critical to understanding adult neurogenesis. Studies over the past decade have provided insight into the biology underlying NSC quiescence, revealing widespread remodeling of metabolism and the proteome (Knobloch, Braun et al. 2013, Knobloch, von Schoultz et al. 2014, Llorens-Bobadilla, Zhao et al. 2015, Shin, Berg et al. 2015, Dulken, Leeman et al. 2017, Knobloch, Pilz et al. 2017, Leeman, Hebestreit et al. 2018, Kalamakis, Brune et al. 2019). However, these studies have been limited by the constraints of modern technologies which exist to identify, isolate and/or generate qNSCs and aNSCs. For example, intermediate filaments, such as nestin and glial fibrillary acidic protein (GFAP) are commonly used as markers to isolate NSCs, yet these proteins are differentially expressed in qNSCs and aNSCs (Codega, Silva-Vargas et al. 2014, Llorens-Bobadilla, Zhao et al. 2015, Shin, Berg et al. 2015, Leeman, Hebestreit et al. 2018, Morrow, Porter et al. 2020). To gain the most complete understanding of NSC quiescence, new tools with unique capabilities need to be applied.

Many studies have demonstrated the potential of fluorescent lifetime imaging (FLIM) of autofluorescence to study shifts in cell state and behavior in other cell types (Chance, Schoener et al. 1979, Lakowicz, Szmacinski et al. 1992, Heaster, Humayun et al. 2020, Walsh, Mueller et al. 2021). FLIM involves measuring the rate of signal decay of a fluorophore after excitation, called the fluorescent lifetime, which can be used to extrapolate biophysical properties of a fluorophore (Fig. 3.1A). For example, nicotinamide adenine dinucleotide phosphate (NAD(P)H; NADPH and NADH autofluorescence are indistinguishable and thus NAD(P)H is used to represent the combination) and Flavin adenine dinucleotide (FAD) autofluorescence can be used to resolve spatial and temporal dynamics in macrophage metabolism, and to classify T cell activation state (Heaster, Humayun et al. 2020, Sagar, Ouellette et al. 2020, Walsh, Mueller et al. 2021). Autofluorescence imaging capitalizes on the principle that as autofluorescent molecules are used by cells in different ways (e.g. binding to an enzyme, oxidation state) across cell states, identities or behaviors, their optical properties will change. For example, NAD(P)H is autofluorescent in the reduced state, whereas NAD(P) in the oxidized state is not autofluorescent (Blacker and Duchen 2016). Conversely, FAD is autofluorescent in the oxidized state, but not autofluorescent in the reduced state ($FADH_2$) (Kolenc and Quinn 2019, Walsh, Mueller et al. 2021). In addition to detecting relative levels of NAD(P)H or FAD through measuring their fluorescence intensity, FLIM can further be used to track biophysical properties of NAD(P)H and FAD. For example, NAD(P)H has a shorter fluorescence lifetime when it is not bound to an enzyme (Table 3.1) (Lakowicz, Szmacinski et al. 1992). Conversely, FAD has a longer lifetime when it is not bound to an

Table 3.1

Explanation of FLIM endpoints		
Molecule	**Endpoint**	**Meaning**
NAD(P)H	Intensity	Amount of NAD(P)H
	α1	Freely diffusing NAD(P)H
	α2	Bound NAD(P)H
	τ1	Lifetime of diffusing NAD(P)H
	τ2	Lifetime of bound NAD(P)H
FAD	Intensity	Amount of FAD
	α1	Bound FAD
	α2	Freely diffusing FAD
	τ1	Lifetime of bound FAD
	τ2	Lifetime of diffusing FAD

enzyme (Blacker and Duchen 2016, Kolenc and Quinn 2019). NAD(P)H and FAD are known to be involved in hundreds of enzymatic reactions in the cell. Thus, it can be challenging to identify the precise underlying binding partners responsible for changing NAD(P)H's fluorescence lifetime across conditions. However, regardless of what is specifically driving changes in NAD(P)H's fluorescence lifetime, seeing differences in NAD(P)H's autofluorescent intensity and lifetime can be sufficient on its own to inform on a cell's overall behavior. Thus, here we asked whether autofluorescence imaging could be used to study NSC quiescence. We observed that NSC autofluorescence could be used to classify NSC activation state and to study shifts in NSC cell state in a non-destructive manner at single-cell resolution. This strategy provides a unique tool for identifying NSC activation state using only autofluorescence.

3.3 Results (adapted from Morrow et al 2022 *in preparation*)

Autofluorescence can be used to accurately classify NSC activation state

To determine whether autofluorescence imaging could be used to classify NSC activation state, we first isolated primary hippocampal NSCs *in vitro* from 6 week-old mice and generated qNSCs and aNSCs using a previously established paradigm using bone morphogenic protein 4 (BMP4) to drive aNSCs into quiescence (Fig. 3.4A) (Mira, Andreu et al. 2010, Martynoga, Mateo et al. 2013, Knobloch, Pilz et al. 2017, Leeman, Hebestreit et al. 2018, Morrow, Porter et al. 2020). To validate this model, we pulsed aNSCs and qNSCs with the thymidine analog 5-ethynyl-2'-deoxyuridine (EdU) for one hour to label cells in S-phase, and expectedly observed a sharp reduction in the number of EdU+ cells in the quiescent condition (Fig. 3.4B). Using this paradigm, we next performed FLIM using

Table 3.2

Autofluorescence Imaging Strategies				
Name	**Microscope**	**Excitation (nm)**	**Emission (nm)**	**Rationale**
NAD(P)H	Multiphoton	750 (375 – 1P)	360-520	Optimized to image NAD(P)H
Green Autofluorescence	Multiphoton	890 (445 – 1P)	450-650	Optimized to image FAD, among other endogenous fluorophores
Lipid Droplet Autofluorescence (LDA)	Confocal/Flow Cytometer	405	~525-640 nm	Images autofluorescent lipid droplets, among other endogenous fluorophores

a multiphoton microscope on qNSCs and aNSCs *in vitro* using optical parameters designed to image the metabolic cofactors NAD(P)H (Excitation: 2 photon 750 nm, Emission: 360-520 nm) and FAD (Excitation: 2 photon 890 nm, Emission: 450-650 nm) (Fig. 3.1A) (Datta, Heaster et al. 2020). As expected from previous studies, NAD(P)H autofluorescence signal localized to mitochondria (Fig. 3.1B, Table 3.2) (Lewis, Parker et al. 2014). However, despite using excitation and emission consistent with published reports to excite FAD, we observed punctate signals in qNSCs not reminiscent of FAD, which others had shown to be diffusely spread throughout the cytoplasm (Fig. 3.1B) (Walsh, Mueller et al. 2021). Therefore, we hereafter conservatively use the title “green autofluorescence” for the FAD channel. qNSCs and aNSCs on average exhibited significantly different NAD(P)H and green autofluorescence fluorescent lifetimes and a significantly increased autofluorescent intensity in the green autofluorescence channel (Fig. 3.1C-D). Principal component analysis (PCA) of qNSCs and aNSCs using all 8 non-redundant autofluorescent endpoints (quantitative values obtained from analyzing NSC autofluorescence imaging data; Intensity, α1, τ1 and τ2 for both NAD(P)H and green autofluorescence) revealed clear separation between qNSCs and aNSCs, suggesting the predictive power of autofluorescence to assess NSC cell behavior (Table 3.1, Fig. 1E).

To further evaluate whether NSC autofluorescence could be used to predict NSC activation state, we constructed classification models using random forest machine learning and varying combinations of autofluorescent endpoint inputs (Fig. 3.1F). Receiver operator characteristic (ROC) curves illustrated that whereas training the model with only NAD(P)H intensity (purple line) resulted in poor classification no greater than randomly guessing whether a NSC was quiescent or activated, training the model with all

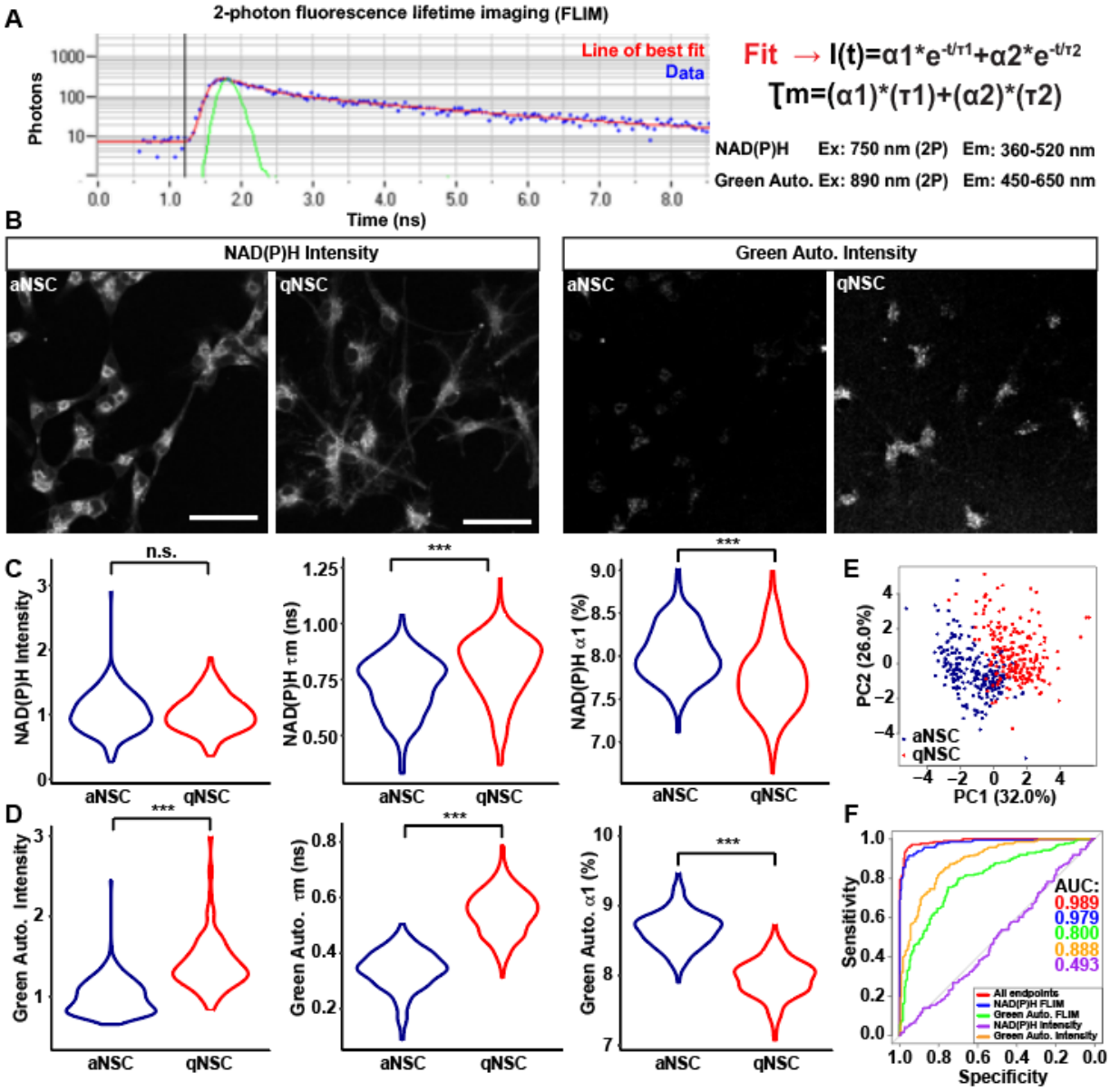

Figure 3.1 – A live-cell, label-free imaging strategy for the classification of NSC activation state. A) Schematic depicting fluorescence lifetime imaging (FLIM) analysis. Data is modeled by a biexponential decay equation. B-C) aNSCs and qNSCs were imaged for NAD(P)H and green autofluorescence intensities and fluorescence lifetimes. (B) Multiphoton intensity images of NAD(P)H and green autofluorescence in qNSCs and aNSCs. (C) Violin plots depicting intensity and representative FLIM endpoints for NAD(P)H and green autofluorescence in qNSCs (blue) and aNSCs (red) (n=446 cells,

Generalized Linear Model). D) Principle component analysis of qNSC (red) and aNSC (blue) autofluorescence imaging data (NAD(P)H and green autofluorescence intensity, α_1, τ_1, and τ_2; n=446 cells). E) Receiver operating characteristic curve depicting a random forest model generated to classify NSC activation state using NSC autofluorescence data. Different lines represent random forest models constructed using subsets of NSC autofluorescence data. Scale bars, 10 μm. ***$p < 0.001$.

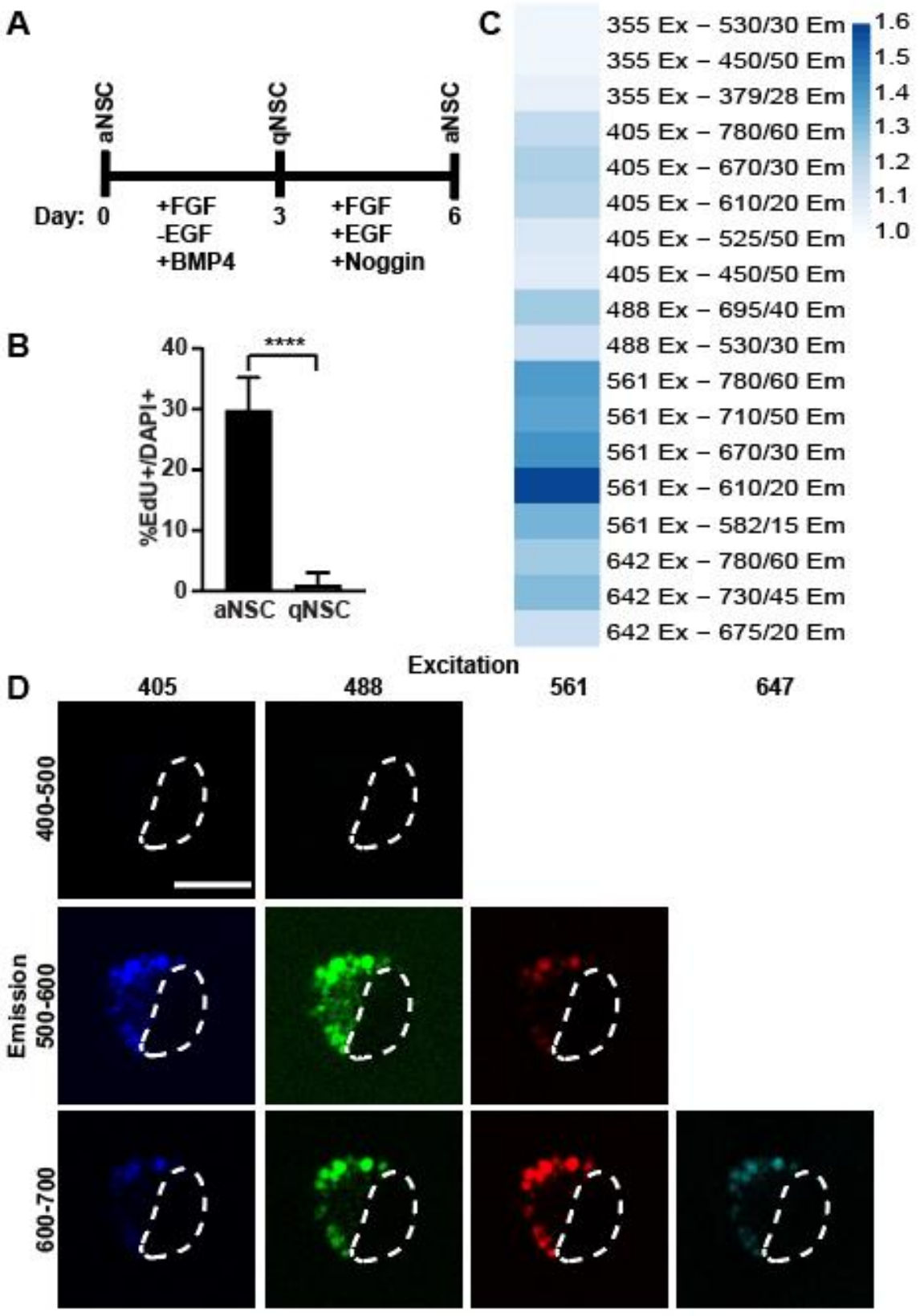
A
aNSC
qNSC
aNSC
Day: 0
+FGF
-EGF
+BMP4
3
+FGF
+EGF
+Noggin
6
B
****
%EdU+/DAPI+
40
30
20
10
0
aNSC
qNSC
C
355 Ex – 530/30 Em
355 Ex – 450/50 Em
355 Ex – 379/28 Em
405 Ex – 780/60 Em
405 Ex – 670/30 Em
405 Ex – 610/20 Em
405 Ex – 525/50 Em
405 Ex – 450/50 Em
488 Ex – 695/40 Em
488 Ex – 530/30 Em
561 Ex – 780/60 Em
561 Ex – 710/50 Em
561 Ex – 670/30 Em
561 Ex – 610/20 Em
561 Ex – 582/15 Em
642 Ex – 780/60 Em
642 Ex – 730/45 Em
642 Ex – 675/20 Em
1.6
1.5
1.4
1.3
1.2
1.1
1.0
D
Excitation
405
488
561
647
400-500
Emission
500-600
600-700

Figure 3.2 – A) Schematic of the BMP4 system for inducing reversible NSC quiescence. B) aNSCs (black bar) and qNSCs (red bar) were pulsed with EdU for 1 hour and then fixed and analyzed for %EdU+ cells (N=3, Student's t test, mean ± SD). C) Heat map depicting differences in qNSC autofluorescence relative to aNSC autofluorescence measured on a flow cytometer. D) qNSCs were imaged using a confocal microscope with excitation and emission as specified in the figure. Scale bar, 10 µm. ****$p < 0.001$.

8 endpoints (Intensity, α1, τ1 and τ2 for both NAD(P)H and green autofluorescence; red line) resulted in an almost perfect model. Additionally, subsets of autofluorescent endpoints, such as NAD(P)H FLIM, revealed strong modeling. Strikingly, we observed that a single endpoint, green autofluorescence intensity, alone was sufficient to provide robust classification of NSC activation state (Fig. 3.1F). Taken together, these data demonstrate strong differences in autofluorescence between qNSCs and aNSCs and highlight the potential of autofluorescence imaging to be used to biomark NSC activation state.

qNSCs are marked by an autofluorescent signal localizing to lipid droplets

We next investigated the identity of the green autofluorescent punctate signals present in qNSCs, but not aNSCs. To gain further insight into the optical properties of these signals, we used both confocal microscopy and fluorescent activated cell sorting (FACS) to identify where the puncta would absorb and emit light. Interestingly, we observed that puncta in qNSCs were broadly excited by 405-647 nm light and emitted between 500-700 nm (Fig. 3.2C-D). These data are further suggestive that the puncta are not representative solely of FAD, as FAD has previously been shown to not be highly excited by a 561 nm laser (Islam, Honma et al. 2013). Additionally, when measuring NAD(P)H and FAD levels in cell lysates, qNSCs and aNSCs contained similar levels of both molecules, suggesting that varying levels of these factors likely were not contributing to differences in autofluorescence intensity observed across aNSCs and qNSCs (Fig. 3.4A-B). Finally, if FAD were substantially contributing to the intensity of the autofluorescent puncta, this signal should be sensitive to treatment with Carbonyl

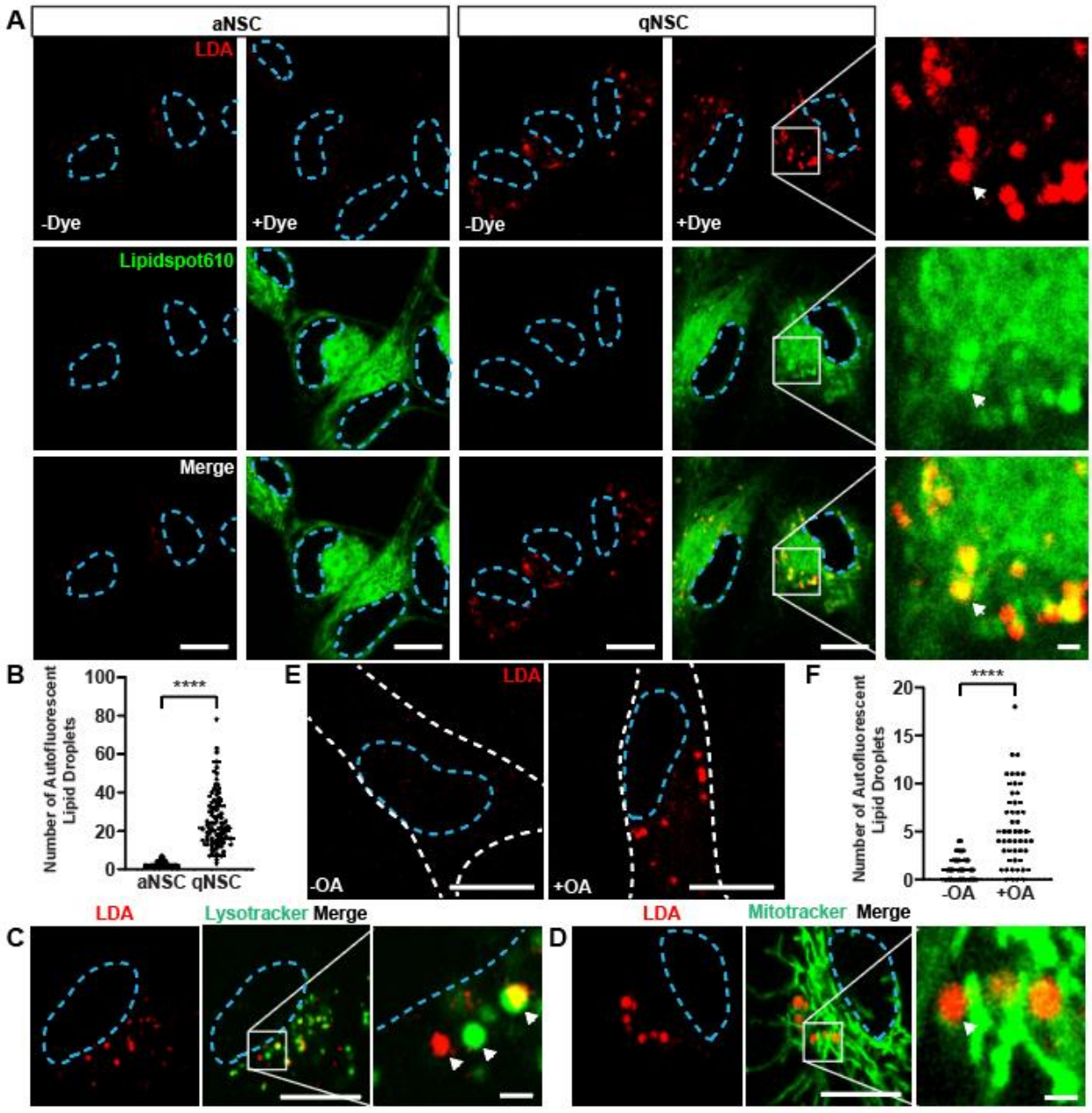

Figure 3.3 – Autofluorescence localizing to lipid droplets in qNSCs marks NSC activation state. A) qNSCs and aNSCs were labeled with LipidSpot610 and then imaged on a confocal microscope for lipids (green) and autofluorescent puncta (red, Ex: 405 nm Em: 525-560 nm). B) aNSCs (black bar) and qNSCs (red bar) were analyzed for the number of autofluorescent lipid droplets (LDA) (Ex: 405 nm Em: 580-620 nm) (N=3, Student's t test, mean ± SD). C-D) qNSCs were stained for lysosomes (Lysotracker, green) or

mitochondria (Mitotracker, green) and then imaged with a confocal microscope for each organelle marker respectively and autofluorescent puncta (red, Ex: 405 nm Em: 525-560 nm). E-F) aNSCs were either untreated or treated with 3 mM oleic acid for 2.5 hours and then imaged with a confocal microscope for autofluorescent puncta (Ex: 405 nm Em: 580-620 nm). The whole cell is outlined by a white dashed line. Samples were analyzed for the number of autofluorescent lipid droplets (Ex: 405 nm Em: 580-620 nm) (N=3, Student's t test, mean ± SD). Arrows denote autofluorescent puncta. Nuclei are outlined by a blue dotted line. White line denotes inset. Scale bars, 10 μm (outsets), 1 μm (insets). ***$p < 0.001$, ****$p < 0.0001$.

cyanide-p-trifluoromethoxyphenylhydrazone (FCCP), which should make FAD more autofluorescent, or sodium cyanide (NaCN), which should make FAD less autofluorescent (Abramov, Gegg et al. 2011, Bartolome and Abramov 2015). Whereas NAD(P)H autofluorescence in qNSCs and aNSCs was sensitive to NaCN and FCCP consistent with previous reports, treatment with FCCP and NaCN showed no effect on the green autofluorescence of qNSCs, further confirming that FAD is not contributing substantially to the green autofluorescent puncta (Fig. 3.4C-F) (Holmstrom, Baird et al. 2013).

Further examination of the morphology of the autofluorescent puncta suggested round, dynamic structures as the source of the signal. As qNSCs and aNSCs have distinct differences in lipid metabolism, and qNSCs are marked by an accumulation of lipid droplets, we hypothesized that the puncta may be autofluorescent lipid droplets (Lipid Droplet Autofluorescence; LDA) (Knobloch, Braun et al. 2013, Knobloch, Pilz et al. 2017, Leeman, Hebestreit et al. 2018). To test this, we labeled qNSCs and aNSCs with a far-red lipid dye lipidspot 610, to avoid bleed-through from the dye, and performed autofluorescence imaging using a confocal microscope to detect the puncta using a 405 nm laser (excitation) and collecting 525-560 nm. In addition to a membrane signal from lipidspot 610, autofluorescent puncta exhibited substantial overlap with the dye, suggesting that the autofluorescent signals present in qNSCs may be lipid droplets (Fig. 3.3A-B, Table 3.2). To further support this conclusion, we performed similar experiments using far-red dyes to label mitochondria (Mitotracker) and lysosomes (Lysotracker) (Fig. 3.3C-D). We observed little overlap between the autofluorescent puncta and mitochondria, confirming that the puncta were not mitochondria. However, we did interestingly detect relatively greater levels of overlap between the autofluorescent puncta

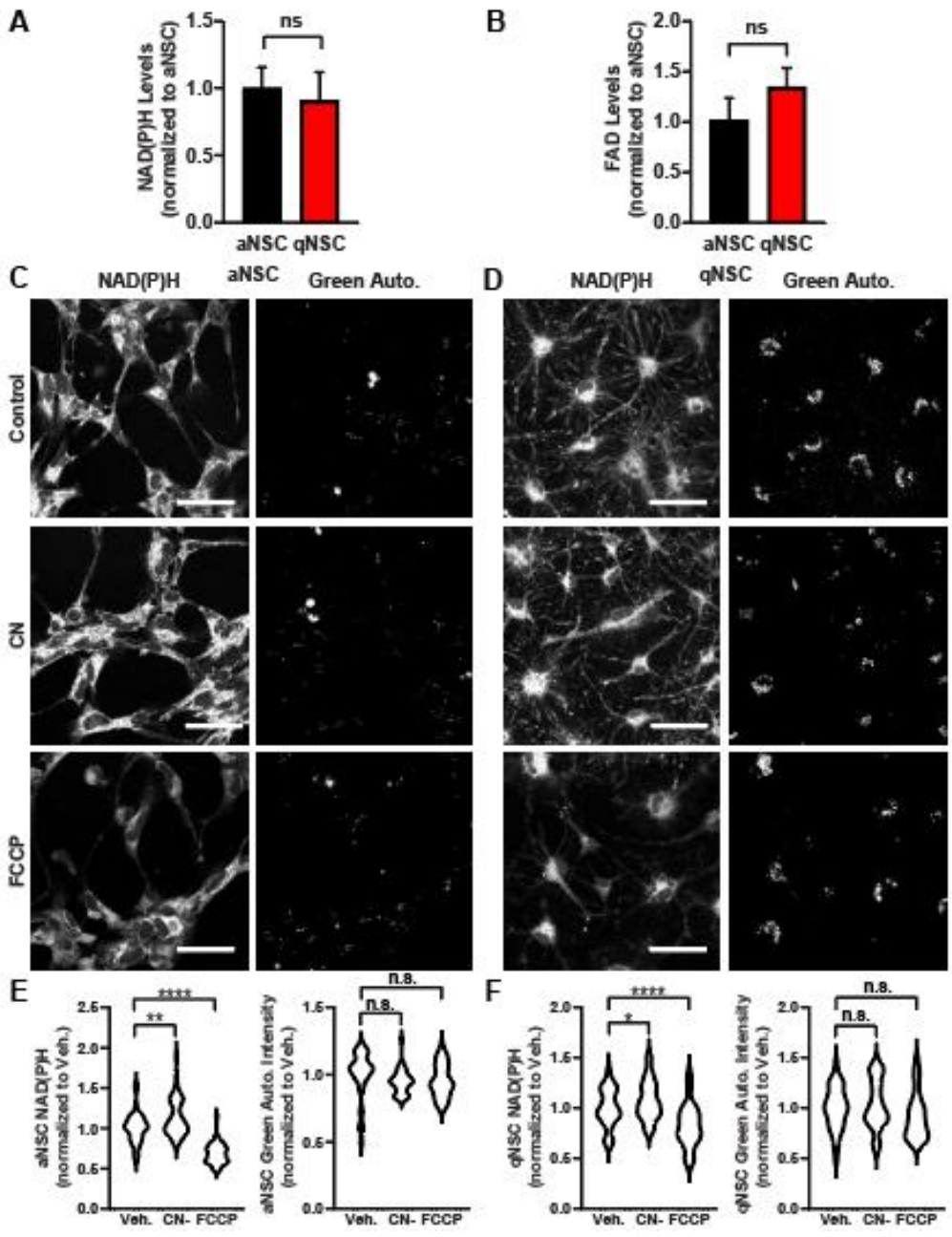

Figure 3.4 – A-B) aNSCs (black bars) and qNSCs (red bars) were lysed and analyzed for relative levels of NAD(P)H and FAD (N=3, Student's t test, mean ± SD). C) qNSCs were either untreated (control), treated with 2 mM CN^- (red bar), 1 μM FCCP (blue bar), or 1% DMSO vehicle control for 20 minutes and then analyzed for autofluorescence intensity (Ex: 405 nm Em: 580-620 nm; N=3, Student's t test, mean ± SD).

and lysosomes. Many lysosomes were clearly not autofluorescent, however, and the overlapping autofluorescent puncta and lysosomes often appeared to be only partially overlapped, suggesting they are not the same structures. This observation could also reflect the degradation of lipid droplets by autophagy (Schulze, Krueger et al. 2020).

To further test the hypothesis that the autofluorescent puncta are lipid droplets, we took advantage of the fact that treatment with oleic acid can rapidly induce formation of lipid droplets (Rohwedder, Zhang et al. 2014). We hypothesized that if the signals detected were lipid droplets, we could induce the present of autofluorescent puncta in aNSCs through treatment with oleic acid. Indeed, 1.5 hours after treatment with lipid droplets, aNSCs exhibited autofluorescent puncta that were reminiscent both in size and distribution to the puncta detected in qNSCs (Fig. 3.3E-F). Together, these experiments reveal that qNSCs are marked by the presence of autofluorescent lipid droplets.

Autofluorescence can enrich for NSC activation state from a mixed *in vitro* population of qNSCs and aNSCs

As NSC autofluorescence provides predictive power to classify NSC activation state, we next asked if we could identify qNSCs in a mixed population. As we had previously observed that qNSCs exhibited brighter autofluorescence when analyzed in a dish, we first asked whether sorting NSCs using FACS based on autofluorescence would be sufficient to enrich separately for qNSCs and aNSCs. To this end, we generated qNSCs and aNSCs, labeled both groups with a 1 hour EdU pulse, and then sorted cultured qNSCs, cultured aNSCs and a 1:1 mixture (Mix) of these two populations based

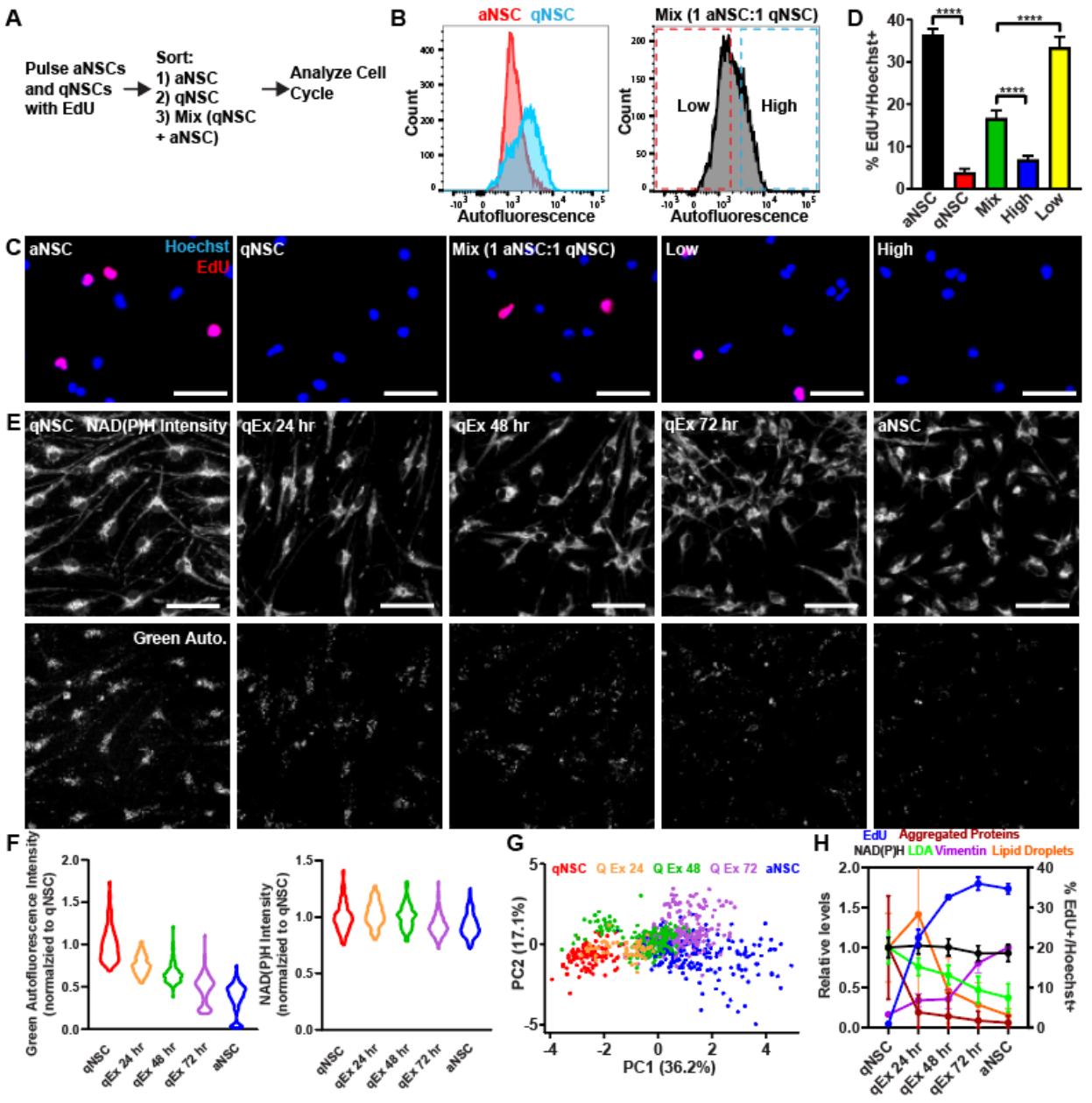

Figure 3.5 – NSC autofluorescence can enrich for activation state and reveal dynamics of quiescence exit. A-D) qNSCs and aNSCs were pulsed with EdU for 1 hour and then prepared for cell sorting either separately or in a 1 aNSC:1 qNSC mixture and then sorted based on relatively low or high autofluorescence (Ex: 405 nm Em: 580-620 nm). 3 hours after plating, cells were fixed, treated to visualize EdU (red) and nuclei (Hoechst; blue) and analyzed for %EdU+ cells (N=3, Student's t test, mean ± SD). E) NAD(P)H (top) and

green autofluorescence (bottom) multiphoton intensity images of a quiescence exit time course. F) Analysis of NAD(P)H and green autofluorescence intensity of the quiescence exit time course (n=783 cells). G) PCA of NSC quiescence exit autofluorescence imaging data (NAD(P)H and green autofluorescence intensity, α_1, τ_1, and τ_2). H) Overlay of changes in autofluorescence intensity during the quiescence exit time course combined with the proliferation rate marker (EdU; blue), aggregated proteins (Proteostat; red), vimentin (purple) and lipid droplets (nile red; orange). Scale bars, 50 μm. ****$p < 0.0001$.

on their autofluorescence intensity (FACS: 405 Excitation, 560-640 Emission) (Fig. 3.5A-B). Gates were drawn to sort the brighter (High) or dimmer (Low) NSCs in the mixed population. After sorting, cells were plated, allowed to adhere to the dish over the course of 2-3 hours, and then fixed, stained and analyzed for EdU to mark cell cycle status in each population of cells (Fig. 3.5C-D). Whereas the Mix cells exhibited a proliferation rate in between qNSCs and aNSCs, High autofluorescent cells purified from the Mix proliferated more similarly to qNSCs and Low autofluorescent cells purified from the Mix proliferated more similarly to aNSCs. Thus, FACS can be used to prospectively enrich for NSC activation state and behavior using only autofluorescence.

Autofluorescence reveals heterogeneity in the rate of quiescence exit

As NSC autofluorescence can classify NSC activation state, we next hypothesized that NSC autofluorescence could provide a window into the dynamics of NSC quiescence exit and act as an additional sensor to monitor cell behavior during NSC quiescence exit. To test this hypothesis, we used a multiphoton microscope to perform FLIM of the NAD(P)H and green autofluorescent signals on NSCs at fixed timepoints as they exited quiescence over the course of three days, and compared these data to qNSC and aNSC cultures (Fig. 3.5E-G). As expected, we observed minimal changes in NAD(P)H autofluorescence intensity as NSCs exited quiescence, whereas at the same time, the green autofluorescent intensity steadily decreased towards levels observed in aNSCs (Fig. 3.5F). These data suggest that autofluorescence could track NSC activation state at the population level. We next examined NSC autofluorescence at the single-cell level through PCA to determine whether NSC autofluorescence could identify which cells were

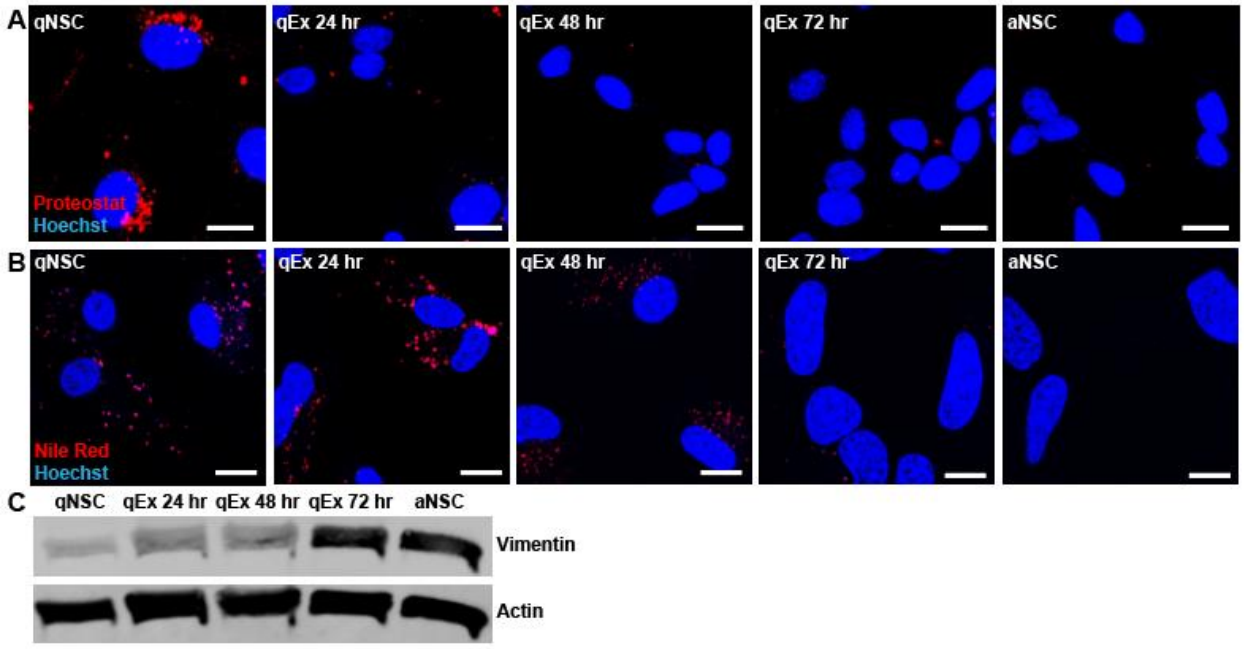

Figure 3.6 – A) Representative Proteostat images of the data shown in Fig. 3H. NSCs during the fixed quiescence exit time course were fixed and stained to visualize aggregated proteins (Proteostat; red) and nuclei (Hoechst; blue). B) Representative nile red images of the data shown in Fig. 3H. NSCs during the fixed quiescence exit time course were labeled with nile red (lipid droplets; red) and Hoechst (nuclei; blue). C) Western blot showing changes in vimentin expression during quiescence exit corresponding to the data shown in Fig. 3H. NSCs during the fixed quiescence exit time course were processed to extract total protein and vimentin and actin expression were probed by western blot. Scale bars, 10 μm.

still quiescent, which cells had begun to exit quiescence, and which cells were more "completely" activated. Interestingly, PCA revealed a step-wise trajectory of quiescence exit, and revealed the single-cell heterogeneity in the rate of quiescence exit (Fig. 3.5G). For example, cultures of qNSCs that had been treated with activation media for 24 hours contained cells that clustered within the group of qNSCs, suggesting that these cells had not begun to exit quiescence yet, while some cells had moved into an intermediate state where they did not cluster with qNSCs or aNSCs. Conversely, cultures of qNSCs that had been treated with activation media for 48 hours had cells that clustered with aNSCs that had more fully reactivated in addition to cells that clustered in an intermediate state. Importantly, the time from quiescence exit was reflected in a clear trajectory towards aNSCs, revealing the strength of autofluorescence imaging to report at single-cell resolution measures of functional, dynamic cellular changes occurring during shifts in NSC cell state. Thus, autofluorescence imaging provides a novel strategy to identify distinct substates of NSCs and track the dynamics of NSC quiescence exit.

To further establish autofluorescence imaging as a strategy to track the dynamics of quiescence exit and to create a map of the events occurring during NSC quiescence exit, we compared the autofluorescence intensity endpoints to other markers that are known to shift during NSC quiescence exit: 1) aggregated proteins labeled by the dye Proteostat, 2) EdU as a proxy for proliferation rate, 3) vimentin expression, and 4) lipid droplets labeled by nile red (Fig. 3.5G, 3.6A-C) (Leeman, Hebestreit et al. 2018, Morrow, Porter et al. 2020). Previously it was shown that as neural stem cells exit quiescence, aggregated proteins and lipid droplets decrease while proliferation markers and vimentin protein levels increase (Leeman, Hebestreit et al. 2018, Morrow, Porter et al. 2020). At

the same time points in which we performed autofluorescence imaging, we analyzed levels of each of these markers. Expectedly, we observed that as NSCs exited quiescence, they became more proliferative, cleared the Proteostat+ aggregated proteins, degraded lipid droplets, and increased vimentin expression. Interestingly, we observed that while EdU and Proteostat changed relatively rapidly, green autofluorescence intensity, Nile Red labeled lipid droplets, and vimentin expression changed more gradually as NSCs progressed towards activation. This observation suggests that the changes in lipid droplet metabolism that occur during NSC quiescence exit may progress relatively slower compared to other markers which change during NSC quiescence exit. Altogether, these data provide proof-of-principle for how NSC autofluorescence can be used to study NSC quiescence, both through using NSC autofluorescence to enrich for NSC activation state, and to establish the dynamics of NSC quiescence exit.

Autofluorescent puncta are detectable in qNSCs in the mouse brain

Our *in vitro* observations also raised the prospect that autofluorescence imaging could be used to study NSC quiescence in the brain. To address whether autofluorescent features observed *in vitro* in qNSCs and aNSCs are conserved in the mouse brain, we optimized a protocol for live-cell imaging of qNSCs in organotypic slice cultures (Wang and Andreasson 2010). A recent report identified that adeno-associated virus serotype 4 (AAV4) particles stereotaxically injected into the dentate gyrus with target genes expressed under the cytomegalovirus (CMV) promoter were largely specific for qNSCs (Crowther, Lim et al. 2018). Therefore, we generated AAV4 particles with a CMV promoter

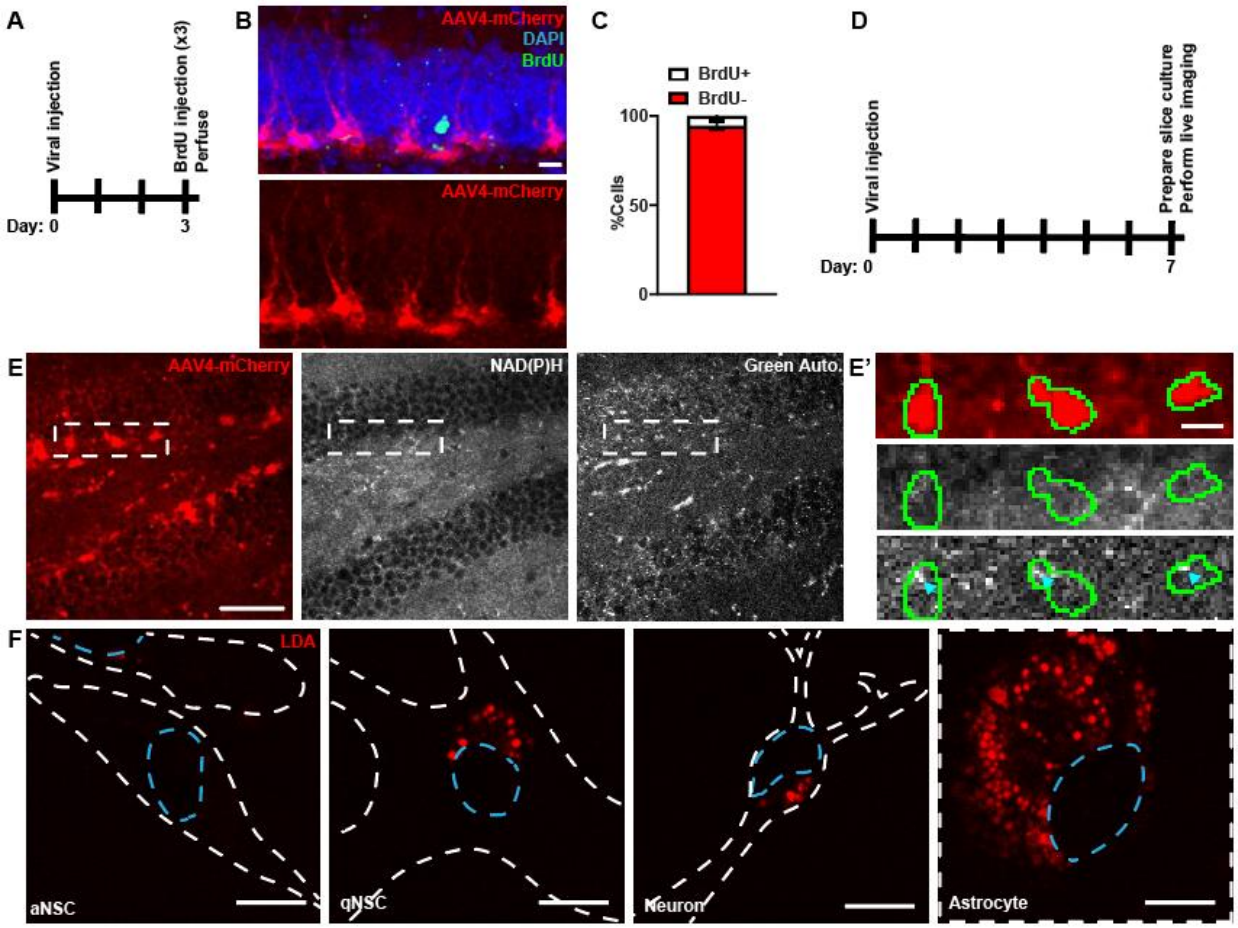

Figure 3.7 – Autofluorescent puncta are detectable in qNSCs in the mouse brain. A-C) Mice were stereotaxically injected with AAV4-CMV-mCherry viral particles into the dentate gyrus of the hippocampus, allowed to recover for 3 days before receiving three BrdU injections (200 mg/kg) two hours apart prior to perfusion. Brains were extracted, sectioned and immunostained to visualize BrdU (green), mCherry (red) and nuclei were labeled by DAPI (blue). AAV4-CMV-mCherry+ cells were counted as BrdU+ (white bar) or BrdU- (red bar) (n=3, mean ± SD). D-E) Mice were stereotaxically injected with AAV4-CMV-mCherry viral particles into the dentate gyrus of the hippocampus, allowed to recover for 7 days. Brains were extracted and live, organotypic slice-cultures were prepared. Slices were immediately imaged with a multiphoton microscope for mCherry

(red), NAD(P)H (white) and green autofluorescence (white). Green lines denote the edge of qNSCs. Blue arrows denote autofluorescent puncta. F) aNSCs, qNSCs, neurons and astrocytes were imaged to detect LDA (red). Blue dotted line outlines nucleus. White dotted line outlines the cell. Scale bars, 50 μm (B, E outset), 10 μm (E inset, F).

driving expression of cytosolic mCherry, a fluorophore compatible with our multiphoton fluorescence lifetime autofluorescence imaging strategy.

Following validation of AAV4-CMV-mCherry labeling of qNSCs (Fig. 3.7A-C), we next performed autofluorescence imaging on qNSCs in the mouse brain. Following stereotaxic injection of AAV4-CMV-mCherry into the dentate gyrus, and seven days to allow for expression of the viral reporter that was detectable in live slices, we generated acute organotypic slice cultures to image autofluorescence in qNSCs in the mouse brain (Fig. 3.7D). Similar to our *in vitro* observations, we observed the presence of autofluorescent punctate signals specifically in the green autofluorescence channel (Fig. 3.7E). Closer examination revealed the puncta were similarly present in qNSCs in the mouse brain. Thus, NSC autofluorescence may be used *in vivo* to mark NSC activation state.

Interestingly, we also observed the presence of green autofluorescence puncta in regions outside the subgranular zone, where qNSCs would not be, suggesting that other cell types similarly harbor autofluorescent lipid droplets. Thus, we hypothesized that other neural cell types such as neurons or astrocytes may similarly be marked by an accumulation of autofluorescent lipid droplets. To test this hypothesis, we derived neurons and astrocytes *in vitro* by differentiating NSCs using a previously optimized protocol and imaged lipid droplet autofluorescence in neurons and astrocytes compared to qNSCs and aNSCs (Morrow, Porter et al. 2020). Consistent with our previous findings we observed that aNSCs did not have substantial levels of lipid droplets, whereas qNSCs, neurons, and particularly astrocytes all exhibited substantial levels of lipid droplet

autofluorescence (Fig. 3.7F). Thus, *in vivo* lipid droplet autofluorescence can be visualized in other neuronal cell types including neurons and astrocytes.

3.4 Discussion

NSC autofluorescence provides a new tool to understand the biology of NSCs and the processes they undergo to generate newborn neurons. Using NSC autofluorescence to identify NSC cell states and behaviors may offer significant technical advantages (e.g. live-cell, label-free) without the biases and disadvantages of other canonical markers. For example, intermediate filaments such as nestin, vimentin and glial fibrillary acidic protein (GFAP) are often used to identify NSCs in the brain, in combination with other markers, however, these proteins are highly differentially expressed between qNSCs and aNSCs (Codega, Silva-Vargas et al. 2014, Llorens-Bobadilla, Zhao et al. 2015, Shin, Berg et al. 2015, Leeman, Hebestreit et al. 2018, Morrow, Porter et al. 2020). Therefore, studies relying on these markers may be missing important subpopulations of NSCs in their analyses. Studies of NSCs using various NSC-specific promoters also identify NSCs with distinct behaviors (Pilz, Bottes et al. 2018, Bottes, Jaeger et al. 2021, Ibrayeva, Bay et al. 2021). Thus, additional tools that aren't reliant on promoter-driven expression of proteins could be useful in constructing a more comprehensive view of NSC quiescence. NSC autofluorescence also provides a platform to identify nuanced sub-states of NSC behavior. For example, in our NSC quiescence exit timelapse we were able to identify NSCs that were transitioning between quiescence and activation, as opposed to still quiescent or already fully activated. As this technology continues to develop, NSC

autofluorescence could be used to further identify NSC substates both *in vitro* and *in vivo* as NSCs exit quiescence and differentiate.

Past using NSC autofluorescence to identify distinct cell states, it could also be useful to understand what is specifically driving the changes in autofluorescence, rather than just broadly seeing the changes as a reflection of changes in cellular metabolism. We found that one of the most robust autofluorescent markers of NSC quiescence was an accumulation of autofluorescent signal localizing to lipid droplets. However, it remains unclear what specific molecule(s) is localizing to lipid droplets in qNSCs that causes them to be autofluorescent. The fact that there are dozens of well-known, and likely many unknown, highly autofluorescent molecules in the cell, combined with the broad spectral absorption and emission of qNSC lipid droplets makes it challenging to identify what molecule is driving the autofluorescence (Datta, Heaster et al. 2020). Identifying the source of this signal could provide new insight into mechanisms underlying NSC quiescence.

Taken together, here we describe a live-cell, label-free tool to study NSC quiescence at the single-cell level, with promise for the study of other types of stem cells and shifts in other types of NSC cell behavior, such as differentiation. We found that NSC autofluorescence was sufficient to predict NSC activation state in the absence of any exogenous labels. qNSCs in particular were marked by an autofluorescent signal localizing to lipid droplets. NSC autofluorescence could be used to track the dynamics of NSC quiescence exit and to enrich for NSC activation state using a cell sorter. Finally, we provide evidence that autofluorescence imaging may be used to study NSC quiescence in the brain *in vivo*.

3.5 Materials and Methods

Mice

C57BL/6J mice were purchased from the Jackson Laboratory and used to establish a colony which was then used for experiments to isolate NSCs for *in vitro* experiments and for the animal experiments described in this manuscript. Only males between 6 and 12 weeks of age were used for this study. All facilities used for maintaining the colony of mice used in this study have been approved by the Research Animal Resources and Compliance (RARC) at UW-Madison.

Imaging Paradigms/Microscopes

Multiphoton Imaging – Fluorescence lifetime images were captured on an Ultima (Bruker) two-photon microscope paired with a Nikon TiE body with a Chameleon Ultra II femtosecond-pulsed tunable Ti:Sapphire laser source (Coherent Inc., Santa Clara, CA, USA), a H7422PA-40 GaAsP photomultiplier tube (Hamamatsu Corporation, Bridgewater, NJ, USA) and a SPC-150 (Becker & Hickl) TCSPC card, using a Nikon CFI Apo LWD Lambda S 40XC water immersion objective. NAD(P)H was imaged by tuning the laser to 750 nm for two-photon excitation and collecting light using a 440/80 nm bandpass filter (Chroma). Green autofluorescence was imaged by tuning the laser to 890 nm for two-photon excitation and collecting light using a 550/100 nm bandpass filter (Chroma). mCherry was imaged by tuning the laser to 740 nm for two-photon excitation

and collecting light using a 550/100 nm bandpass filter (Chroma). The field of view (256x256pixels) was scanned for 60 seconds with a 4.7 microsecond pixel dwell time.

Confocal Imaging – Confocal images were acquired using a Nikon C2 confocal microscope equipped with one fixed and one tunable GaAsP detector using excitation and emission described in the text. In general, autofluorescence images represent a single optical plane in the cell taken with 2-4x averaging. NSC autofluorescence is ~50-100x dimmer than conventional fluorophores, and thus, significantly higher powers are needed to visualize the signals described in this study. qNSC autofluorescent puncta are relatively photostable, whereas oleic acid induced autofluorescent puncta were much dimmer and required much more care to avoid photobleaching to visualize. Specific excitation and emission parameters vary by experiment as listed in either Table 3.2 or each figure legend.

Fluorescent Activated Cell Sorting/Flow Cytometry – A BD FACSAria high speed cell sorter was used for all cell sorting experiments. A BD LSR II flow cytometer was used for analysis experiments. Specific excitation and emission parameters vary by experiment as listed in either Table 3.2 or each figure legend.

<u>NSC Dissection and Culturing</u>

NSCs were isolated from the hippocampus by dissecting hippocampi from 3-5 male mice into cold HBSS, pooling samples, and then dissociating the tissue using

GentleMACS Dissociator (Miltenyi Biotec) and MACS Neural Tissue Papain Dissociation Kit (Miltenyi Biotec 130-092-628) using the manufacturer's protocol with added myelin removal, similar to previously described protocols (Moore, Pilz et al. 2015, Morrow, Porter et al. 2020). aNSCs were cultured as previously described at 37°C/5% CO2 in serum-free media (aNSC media): DMEM/F12 GlutaMax (Invitrogen 10565018) with B27 (1:50, Invitrogen 17504044), penicillin-streptomycin-fungizone (1:100, Invitrogen 15140122), and 20 ng/mL FGF-2 and EGF (PeproTech 100-18B and AF-100-15) (Moore, Pilz et al. 2015, Morrow, Porter et al. 2020). When culturing aNSCs as monolayers, cells were additionally treated with 5 µg/mL Heparin (Sigma H3149).

To image aNSCs as monolayers, aNSCs were plated onto glassware suitable for imaging (such as Fisher Scientific 12-565-337 or Ibidi 80826-G500) that was precoated with poly-L-ornithine for 1 hour at 37°C (PLO; 10 µg/mL plastic, 50 µg/mL glass, Sigma P3655) and laminin for 3 hours at 37°C (5 µg/mL, Sigma L2020). To create single cell suspensions for plating aNSCs, aNSCs were trypsinized using the following protocol: Cells were pelleted in a centrifuge at 120xg for 4 minutes and then treated with 0.05% trypsin (Invitrogen 25300-054) made in Versene (Thermo Fisher 15040066) at 37°C for 5 minutes (Morrow, Porter et al. 2020). Cells were then treated with twice the volume of trypsin inhibitor (Sigma T6522) for 2 minutes at room temperature, mechanically triturated and then pelleted again in a centrifuge by spinning at 120xg for 4 minutes. Single cells were then suspended and plated in aNSC media.

To generate qNSCs, aNSCs were plated onto PLO- and laminin-coated plates and treated with BMP-4, with FGF-2 and without EGF (qNSC media), using previously described protocols (Mira, Andreu et al. 2010, Martynoga, Mateo et al. 2013, Knobloch,

Pilz et al. 2017, Leeman, Hebestreit et al. 2018, Morrow, Porter et al. 2020). qNSC media is similar to aNSC media with the exception of the removal of EGF and the addition of 50 ng/mL BMP-4 (Fisher Scientific 5020BP010). After initial induction of quiescence, qNSCs were fed at least once every two days and were considered quiescent after 3 days of qNSC media treatment. For inducing quiescence exit, qNSCs were treated with aNSC media with the addition of 0.5 µg/mL the BMP-4 antagonist noggin (PeproTech 120-10C) to more reproducibly induce quiescence exit.

To differentiate NSCs into neurons and astrocytes, aNSCs were plated on PLO- and laminin-coated dishes. One day later after aNSCs adhered to the dish, NSCs had FGF and EGF removed from the media and were allowed to differentiate for 14 days prior to imaging. Media was changed at least 3 times per week. Neurons and astrocytes were identified through distinct morphologies.

EdU Pulse

To measure the proliferation rate of NSCs, cells were pulsed with 10 µM EdU (Invitrogen C10337) to label cells progressing through S-phase of the cell cycle for 1 hour at 37°C. Following the pulse with EdU, cells were fixed in 4% paraformaldehyde (PFA) at room temperature (RT) for 15 minutes, and then treated to visualize EdU using a click-chemistry kit (Invitrogen C10337). To quantify EdU pulses, cells were costained with 20 µM Hoechst (Thermo Fisher Scientific 62249) to label nuclei of all cells. The total number of EdU+ and Hoechst+ cells were then counted across at least three experiments performed on different days and analyzed per image.

Analysis of Fluorescence Lifetime Imaging Data

Fluorescent lifetime images were analyzed using SPCImage version 8.3. For each fluorescent lifetime image, background was removed through thresholding (value of 50 for NAD(P)H, value of 5 for green autofluorescence). Fluorescence lifetime decays were deconvolved from the instrument response function and modeled by fitting to a biexponential decay equation: $I(t) = \alpha_1 * e^{-t/\tau 1} + \alpha_2 * e^{-t/\tau 2} + C$, when I(t) is the autofluorescent intensity as a function of time (t) after the laser pulse, α_1 and α_2 are fractional contributions ($\alpha_1 + \alpha_2 = 1$) of long and short lifetime components, τ_1 and τ_2 reflect the short and long lifetime components and C represents background photons. The fluorescence lifetime (T_m) was defined as: $T_m = \alpha_1 * \tau_1 + \alpha_2 * \tau_2$. After fitting the data, average fluorescence lifetime and intensities were calculated per cell examining only the cytoplasm. To identify cytoplasm, CellProfiler was used to generate masks around the entire cell and the cell's nucleus and then nuclear space was subtracted from the whole cell to identify only cytoplasmic signal. Average endpoint values for each cell, were obtained by using R to calculate average values using the CellProfiler generated cytoplasm masks.

Dimension Reduction Analyses

PCA was used to reduce the dimensions of NSC autofluorescence imaging data using the PCA() function in R. To perform the PCA, non-redundant NSC autofluorescence endpoints (intensity, α_1, τ_1, and τ_2) were normalized to values within 0 and 1 and used for the analysis.

Machine Learning Analyses

Random Forest models were developed to assess the capacity of NSC autofluorescence to classify NSC activation state using the randomForest() function in R and used to generate the representative ROC plots shown in this manuscript (Andy Liaw 2002). Non-redundant NSC autofluorescence endpoints (intensity, α_1, τ_1, and τ_2) were normalized to values within 0 and 1 and then varying subsets of these endpoints, as described in the text, were used to generate each Random Forest model.

Autofluorescence Imaging with Organelle Dyes

To image NSC autofluorescence with various markers of other organelles in the cell, qNSCs were generated as described above and then treated with the following dyes and specifications. Lysotracker Deep Red (Thermo Fisher Scientific L12492) was added to qNSCs at a dilution of 1:1000 and incubated on qNSCs for 10 minutes in the incubator. Cells were washed three times prior to imaging. LipidSpot 610 (Biotium 70069-T) was added to qNSCs at a dilution of 1:1,000 and incubated on qNSCs for 10 minutes in the incubator. Cells were washed three times prior to imaging. Mitotracker red CM H (Thermo Fisher Scientific M7513) was added to qNSCs at a dilution of 1:100,000 and incubated on qNSCs for 5 minutes in the incubator. Cells were washed three times prior to imaging. To avoid bleed through from the dyes, autofluorescence was imaged by exciting with a 405 nm laser and collecting 525-560 nm light.

Flow Cytometry NSC Cell State Enrichment Assays

A BD FACSAria high speed cell sorter was used to sort NSCs. qNSCs and aNSCs were pulsed with EdU for one hour as described above in the incubator and then put into

single cell suspension – aNSCs by trypsinizing and qNSCs by just mechanically lifting from the dish. Cells were counted and then a 1:1 mix of aNSCs and qNSCs was made. All samples were put in phosphate buffered saline on ice until completion of the sort. On the cytometer forward and side scatter was used to identify single cells and then NSCs were sorted by autofluorescence using a 405 nm laser to excite and collecting light between 565 and 645 nm. Gates were drawn to collect the brighter or dimmer NSCs and then samples were collected and plated on to glassware coated in PLO and laminin. 2-3 hours after plating following cell sorting (after cells adhered to the dish) samples were fixed in 4% PFA for 15 minutes at room temperature. Cells were then stained and analyzed for EdU as described above.

Quiescence Exit Timelapse

qNSCs were generated and then sequentially treated with activation media in such a way that qNSCs that had been exiting quiescence for 0 hours, 24 hours, 48 hours, 72 hours and aNSCs could be imaged at the same time. Multiphoton FLIM autofluorescence imaging was performed and analyzed as discussed above. To perform the quiescence exit EdU pulse, samples were prepared for each step in the time course and then treated, processed and analyzed as discussed in the “EdU Pulse” section of the methods.

To label aggregated proteins with Proteostat (Enzo ENZ-51035-0025), NSCs were prepared for each part of the time course and then fixed in 4% PFA for 15 minutes at room temperature. Cells were stained in accordance with the manufacturer’s protocol. In brief, cells were permeabilized with 0.5% triton in 0.5 mM ethylenediaminetetraacetic acid (EDTA) in PBS for 30 minutes at room temperature and stained with Hoechst (1:5,000)

to visualize nuclei and Proteostat (1:1,000) for 30 minutes at room temperature. Following staining with the dyes, cells were washed 3 times in PBS for 10 minutes at room temperature. To analyze Proteostat signal, number of Proteostat puncta were counted per cell over at least 5 images per condition. The experiment was repeated for a total of 3 times.

AAV4 Particle Production

AAV4 particles were produced by the Duke Viral Vector Core. The AAV4 vector was a generous gift from Dr. Juan Song.

BrdU Labeling

Mice were injected with AAV4-CMV-mCherry particles and then allowed to express for 3 days, mimicking a previously described protocol (Crowther, Lim et al. 2018). On the third day following AAV4 injection, BrdU was dissolved 0.02 g/mL in PBS and then administered to mice by intraperitoneal injection at 200 mg/kg, a total of 3 times over the course of 4 hours (each injection 2 hours apart). 2 hours following the final BrdU injection, mice were transcardially perfused with 0.9% saline followed by 4% PFA in a 0.2M phosphate buffer. Brains were then extracted and postfixed in 4% PFA overnight at 4°C and then stored in 30% sucrose in phosphate buffered saline until the brains sank (~1-3 days). Brains were then sectioned on a sliding microtome to generate 40 µm thick slices and then immunostained for the following markers: BrdU (Abcam ab6326), mCherry (Clontech 632496); to amplify mCherry signal) and 4′,6-diamidino-2-phenylindole (DAPI) (Invitrogen D1306; to label nuclei) using the following protocol. Sections were rinsed 3

times for 10 minutes in tris buffered saline (TBS) at room temperature and then incubated with 1 M HCl for 20 minutes at 37°C, incubated in 0.1 M Borate Buffer 2 times for 15 minutes at room temperature, rinsed 3 times with TBS for 10 minutes each at room temperature, blocked in 0.25% TritonX-100, 3% Donkey Serum (Millipore Sigma S30-100ML) in TBS (TBS++ buffer) for 1 hour at room temperature, incubated with primary antibodies overnight at a dilution of 1:500 in TBS++ at 4°C, rinsed 3 times in TBS at room temperature for 10 minutes, incubated with secondary antibodies 1:500 for 1.5 hours at room temperature in TBS++, incubated with DAPI (1:1,000 in TBS) for 5 minutes at room temperature, and then rinsed 2 times in TBS at room temperature prior to mounting slides.

Samples were then imaged and analyzed to determine whether mCherry+ cells were BrdU+. Representative series of brain sections (~8 slices per series) were analyzed over a total of 3 animals. All mCherry+ cells in the dentate gyrus were analyzed.

Stereotaxic Injections and Organotypic Slice Culture Experiment

To inject AAV4 particles into the dentate gyrus of the mouse brain, we adapted previously reported protocols (Crowther, Lim et al. 2018, Pilz, Bottes et al. 2018). Mice were anesthetized with isoflurane, and then mounted in a stereotaxic frame (Stoelting). Optixcare Pet Eye Lubricant (Amazon B0799LS6ZY) was applied periodically to maintain eye lubrication. The incision site was sterilized with Betadine and then cut to access the skull. The incision site was then anesthetized with a splash block of 50:50 lidocaine/bupivacaine. Following local anesthetic, two holes were drilled manually with a needle over the dentate gyrus at coordinates: AP -2.0 mm, ML +/- 1.4 mm. A Hamilton syringe (Sigma-Aldrich 20734) loaded with AAV4 particles was then inserted into each

hole (one at a time) and inserted down 2.8 mm ventral to the cortical surface. After inserting the needle, the needle was left for 2 minutes, and then 1 uL of AAV4 (~1*10^8 particles/uL) was injected over the course of 7 minutes. Following injection of the virus, the needle was left for an additional two minutes prior to removing the needle and proceeding. Following removal of the needle, the skin was moistened with 0.9% saline, and then resealed with a chemical suture (3M Vetbond Tissue Adhesive). Animals were administered 5mg/kg Meloxicam through IP injection as a preemptive anesthetic following surgery. Following surgeries, animals were monitored until they woke up and then administered additional meloxicam in the days following surgery as necessary if any signs of discomfort were observed.

To generate slice cultures, we adapted a previously published protocol (Wang and Andreasson 2010). 7 days following injection (viral expression was not detectable in live slices until ~7 days after injection) mice were euthanized and brains were extracted and immersed in ice-cold 70% ethanol for 2 minutes. Following ethanol, and brains were mounted onto the stage with superglue and then sectioned at 400 µm thick on a Leica VT1000S vibratome in ice-cold dissection media (95.2 g/L Hank's Balanced salt (Sigma H2387), 4.2 mM $NaHCO_3$, 10 mM HEPES (Thermo Scientific 15630106), 33.3 mM Glucose, 1X Penicillin/Streptomycin (Invitrogen 15140122), 0.3% BSA (Sigma-Aldrich A2153-50G), 12 mM $MgSO_4$-$7H_2O$). Following slice generation, slices were placed in culturing medium (50% MEM (Invitrogen 11575032, 25% Hank's Balanced Salt (Invitrogen 24020117), 25% Horse Serum (Invitrogen 26050070, 12.5 mM HEPES, 1X Penicillin/Streptomycin (Thermo Scientific 15630106), 35 mM Glucose), placed in a 37°C/5%CO_2 incubator and imaged within 3 hours.

Statistics and replicates

Experiments, unless otherwise noted, were replicated on at least three separate days with at least three technical replicates each day as applicable. Significance and analyses were performed in either R Studio, Microsoft Excel, or GraphPad Prism using tests indicated in the figure legends. To analyze multiphoton imaging data (FLIM data), a Generalized Linear Model was formed to assess significance in R Studio. All other statistical tests were performed in GraphPad Prism.

Data Accessibility/Code

In addition to supplementary data files attached to this manuscript, all code and data will be available upon reasonable request to the corresponding author: Dr. Darcie L. Moore (darcie.moore@wisc.edu).

Chapter 4: Vimentin coordinates protein turnover at the aggresome during neural stem cell quiescence exit

4.1 Abstract

Maintaining a healthy proteome throughout life is critical for proper somatic stem cell function, yet the complexities of the stem cell response to increases in damaged or aggregated proteins remain unclear. Here we demonstrate that adult neural stem cells (NSCs) utilize aggresomes to recover from disrupted proteostasis, and describe a novel function for the intermediate filament vimentin in proteostasis as a spatial coordinator of proteasomes to the aggresome. In the absence of vimentin, NSCs have a reduced capacity to exit quiescence, a time when NSCs are required to clear a wave of aggregated proteins, and demonstrate an early age-dependent decline in proliferation and neurogenesis. Taken together, these data reveal a significant role for vimentin and aggresomes in the regulation of proteostasis during quiescent NSC activation.

4.2 Background: Vimentin's role in proteostasis (adapted from Morrow and Moore 2020 *Cytoskeleton*)

Maintaining protein homeostasis (proteostasis) is critical for an organism's ability to properly function and avoid disease (Douglas and Dillin 2010). To ensure proteostasis is maintained, cells have evolved three primary systems which are thought to respond to elevated levels of misfolded, damaged or mutant proteins: chaperones, the ubiquitin-proteasome system, and autophagy. Chaperones are a class of proteins that, amongst many functions, are able to bind to proteins and assist in their refolding or target them for degradation by protein degradation systems (Barral, Broadley et al. 2004). The ubiquitin-proteasome system involves a network of proteins that first identify proteins destined for degradation, label them with polyubiquitin, and subsequently target them to proteasomes

for proteolysis (Collins and Goldberg 2017). Finally, autophagy consists of the loading of larger protein inclusions into autophagosomes which then can fuse with acidified lysosomes to denature proteins via an acidic environment and lysosomal proteases (Wong and Cuervo 2010). Collectively, in healthy organisms and in many pathological contexts, these mechanisms are sufficient to maintain proteostasis. However, there are also many situations in which these systems fail to sufficiently turn over protein which ultimately result in disrupted proteostasis and impaired cellular viability (Douglas and Dillin 2010).

When proteostasis is disrupted, cells may employ additional mechanisms to ensure proper cellular function is maintained. One of these mechanisms involves the trafficking of proteins destined for degradation by dynein motor proteins along microtubules to the centrosome, which is surrounded by a cage composed of the IF vimentin. This structure is referred to as the aggresome (Johnston, Ward et al. 1998, Johnston, Illing et al. 2002, Kawaguchi, Kovacs et al. 2003, Iwata, Riley et al. 2005) (Fig. 4.1). The terms “inclusion bodies” and “aggresomes” have been used somewhat interchangeably to describe protein aggregates that are dispersed throughout the cytoplasm. However, here we define the “aggresome” as a distinct cytoplasmic structure rich in proteins destined for degradation present at the centrosome/nuclear bay that is dependent on microtubules to form and which resides within a cage comprised of IFs (Johnston, Ward et al. 1998). Since the aggresome was first identified in 1998, much has become clear about mechanisms driving aggresome formation and clearance, and the numerous healthy and pathological contexts in which the aggresome is utilized by cells

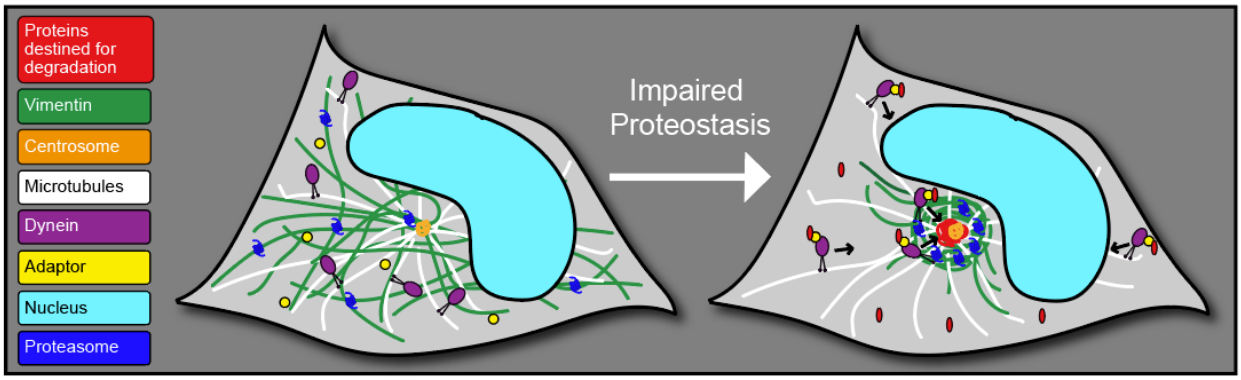

Figure 4.1 *– Schematic of aggresome formation. During conditions where proteostasis becomes disrupted, proteins destined for degradation (red) are trafficked by dynein (purple) and adapter proteins (yellow) along microtubules (white) to the centrosome (orange), accompanied by a collapse of the IF vimentin (green) and a redistribution of proteasomes (dark blue) to the nuclear bay.*

Table 4.1 – *Diverse phenotypes in vimentin KO organisms/cells*

Vimentin KO Phenotype	Source
Immune response	
Reduced replication of murine cytomegalovirus	*(Roy, Kapoor et al. 2020)*
Reduced activation of the inflammasome	*(Xiao, Xie et al. 2018)*
Reduced fibroblast proliferation, keratinocyte differentiation, and wound healing	*(Cheng, Shen et al. 2016)*
Reduced lung inflammation following bleomycin exposure	*(dos Santos, Rogel et al. 2015)*
Longer tail bleeding time	*(Da, Behymer et al. 2014)*
Increased acute colitis	*(Mor-Vaknin, Legendre et al. 2013)*
Impaired microglia activation	*(Jiang, Slinn et al. 2012)*
Impaired glial scar formation (in combination with GFAP KO)	*(Pekny, Johansson et al. 1999)*
Structural support	
Increased mechanical stress generation	*(van Loosdregt, Weissenberger et al. 2018)*
Increased actin stress fiber assembly and contractility	*(Jiu, Peranen et al. 2017)*
Death in response to renal mass reduction	*(Terzi, Henrion et al. 1997)*
Impaired flow-induced dilation in mesenteric resistance arteries	*(Henrion, Terzi et al. 1997)*
Reduced cytoplasmic stiffness	*(Guo, Ehrlicher et al. 2013)*
Reduced lymphocyte rigidity	*(Brown, Hallam et al. 2001)*
Higher expression of sub-endothelial basement membranes	*(Langlois, Belozertseva et al. 2017)*
Reduced collagen production	*(Challa and Stefanovic 2011)*
Compromised endothelial integrity	*(Nieminen, Henttinen et al. 2006)*
Development	
Cerebellar development defects and impaired motor coordination	*(Colucci-Guyon, Gimenez et al. 1999)*
Disrupted vascular smooth muscle cell differentiation	*(van Engeland, Suarez Rodriguez et al. 2019)*
Impaired mammary gland development	*(Peuhu, Virtakoivu et al. 2017)*
Disrupted endothelial differentiation of embryonic stem cells	*(Boraas and Ahsan 2016)*
Decreased axonal outgrowth and uptake of C3bot	*(Adolf, Leondaritis et al. 2016)*
Altered arterial remodeling	*(Schiffers, Henrion et al. 2000)*
Disrupted Notch signaling and impaired angiogenesis	*(Antfolk, Sjoqvist et al. 2017)*
Intermediate filament network formation	
Disrupted GFAP network	*(Galou, Colucci-Guyon et al. 1996)*
Disrupted nestin polymerization	*(Park, Xiang et al. 2010)*
Impaired desmin filament formation	*(Geerts, Eliasson et al. 2001)*
Motility/Migration	
Increased motility of caveolin-1 vesicles	*(Shi, Fan et al. 2020)*
Impaired directional cell migration	*(Vakhrusheva, Endzhievskaya et al. 2019)*
Miscellaneous	
Disrupted subcellular localization of Na-glucose transporters	*(Runembert, Couette et al. 2004)*
No obvious phenotypes in vimentin KO mice	*(Colucci-Guyon, Portier et al. 1994)*
Decreased astrocyte activation (in combination with GFAP KO)	*(Wilhelmsson, Faiz et al. 2012)*
Reduced ability to respond to proteotoxic stress	*(Morrow, Porter et al. 2020)*
Increased rearrangement of the mitochondrial genome	*(Bannikova, Zorov et al. 2005)*
Reduced fibroblast proliferation rate and inability to immortalize	*(Tolstonog, Shoeman et al. 2001)*

(French, van Leeuwen et al. 2001, Johnston, Illing et al. 2002, Kawaguchi, Kovacs et al. 2003, Olzmann, Li et al. 2008, Xu, Graham et al. 2013, Morrow, Porter et al. 2020). However, the role of vimentin at the aggresome has remained largely unexplored.

Vimentin is a type III IF comprised of a central rod domain with a head and tail domain on either side, and is expressed in numerous cell types throughout the body in many organisms (Perreau, Lilienbaum et al. 1988, Schaffeld, Herrmann et al. 2001, Herrmann and Aebi 2004, Danielsson, Peterson et al. 2018). Vimentin is able to polymerize either by itself or heteropolymerize with other IFs into non-polar unit length filaments which can assemble into full length filaments (Steven, Hainfeld et al. 1983, Herrmann, Haner et al. 1996). Two decades ago, vimentin knockout (KO) mice were created and observed to develop and reproduce with no obvious phenotypes, suggesting that vimentin may be dispensable for the organism's general viability (Colucci-Guyon, Portier et al. 1994). However since then, numerous reports have emerged suggesting that although vimentin is not important for early-development, vimentin becomes critical during a response to a wide variety of challenges (Table 4.1) (Terzi, Henrion et al. 1997, Rogel, Soni et al. 2011, Cheng, Shen et al. 2016, Danielsson, Peterson et al. 2018). For example, vimentin is now recognized as a critical player in directional migration during wound healing (Rogel, Soni et al. 2011). Vimentin also has been observed to dynamically upregulate in response to challenges such as heat shock and cadmium chloride treatment (Vilaboa, Garcia-Bermejo et al. 1997). Thus, the precedent of vimentin being a stress response protein supports the notion that vimentin could be important for recovering proteostasis in the cell after a cellular stress which impairs proteostasis. Here we review investigations of vimentin's function in maintaining proteostasis at the aggresome, and

discuss the implications of vimentin's function at the aggresome in both healthy organisms and in numerous pathologies and diseases.

Vimentin's function at the aggresome

The identification of vimentin's presence at the aggresome more than 2 decades ago suggested a new role for this IF. Despite this observation, while many studies have utilized vimentin as a marker of aggresome formation, few have addressed vimentin's function in proteostasis at the aggresome. To address this question, we recently investigated vimentin's function at the aggresome in mouse primary hippocampal neural stem cells (NSCs) (Morrow, Porter et al. 2020). Interestingly, vimentin KO NSCs were still able to form an aggresome, demonstrating that vimentin is not essential for aggresome formation. However, vimentin KO NSCs displayed a decreased capacity to recover from impaired proteostasis both after a transient challenge with the proteasome inhibitor MG132 *in vitro* and during NSC quiescence exit *in vitro* and *in vivo*, a time when NSCs must clear a wave of proteins to activate and enter the cell cycle. Vimentin KO NSCs not only displayed reduced viability after a transient pulse with the proteasome inhibitor MG132, but also an increased accumulation of aggregated proteins. Vimentin KO NSCs compensated for defects in protein clearance by increasing autophagy, however were still unable to recover to the same extent as WT NSCs. Further, we identified through co-immunoprecipitation that vimentin bound several types of proteostasis-related machineries at the aggresome, suggesting that vimentin is critical for efficient protein turnover by acting as a scaffold for these machineries at the aggresome. Immunostaining and proximity ligation assays confirmed that proteasomes, identified in the co-

immunoprecipitation, were enriched at the aggresome in WT NSCs, but not in vimentin KO NSCs. Thus, this suggested that vimentin's function at the aggresome was, at least in part, to localize proteasomes to the aggresome for efficient protein turnover. However, the extent to which this mechanism drives the phenotypes reported in vimentin KO NSCs is not fully clear as numerous other proteostasis machineries, such as ribosomal proteins and chaperone proteins, were also pulled down by vimentin in NSCs. Vimentin KO in NSCs also resulted in a loss of nestin and Glial fibrillary acidic protein (GFAP) IFs, making it difficult to understand if the phenotypes observed in NSCs were vimentin-specific or due to the loss of these other IF proteins. Interestingly, there was no compensation by any other IF in the absence of vimentin. Together, these findings suggest that vimentin's repositioning of proteasomes to the aggresome in NSCs following impaired proteostasis is critical to essential cellular functions.

Similar to our hypothesis that vimentin is critical for positioning cellular components in the cell, it has also been proposed that vimentin is a regulator of autophagosome and lysosome distribution in HEK293 cells, and that vimentin potentiates autophagy (Biskou, Casanova et al. 2019). This study utilized treatment with the compound Withaferin A (WFA), which binds vimentin and inhibits filament formation, to perturb the filamentous vimentin network and probe for downstream consequences. WFA treatment induced a redistribution of vimentin protein to the aggresome along with autophagosomes and lysosomes. Further, WFA perturbed autophagy through disruption of autophagosome-lysosome fusion (Biskou, Casanova et al. 2019). However, WFA has been found to be cytotoxic even in vimentin KO cells, suggesting that WFA is not specific to targeting vimentin (Bargagna-Mohan, Hamza et al. 2007). For example, WFA also has been

observed to perturb the cell's microtubule network (Grin, Mahammad et al. 2012). WFA's prevention of vimentin polymerization also could result in increases in vimentin degradation which could overwhelm protein turnover systems and lead to measurable perturbations in autophagy such as what was reported. This scenario is further supported by the recent observation that vimentin can be degraded by autophagy (Park, Yoon et al. 2020). Thus, it would be interesting to reexamine these findings in a vimentin KO or KD cell line which may be less limited by the non-specific activities of WFA.

Additionally in line with the view that vimentin can function through binding and localizing of cellular components to different regions within the cytoplasm, vimentin has been reported to increase activity of the intracellular calcium channel inositol 1,4,5-trisphosphate (IP3) receptor type 1 (IP3R1) through sequestering the negative IP3R1 regulator, IP3R1-interacting protein released with IP3 (IRBIT), to the aggresome (Bauer, Hudec et al. 2012). However, this role for vimentin was suggested to be detrimental to the cell's capacity to maintain proteostasis, as increased IP3R1 activity was previously connected with increased aggregation of overexpressed mutant Huntington protein in Neuro-2a cells (Bauer, Hudec et al. 2011). In line with this model, vimentin overexpression in Neuro-2a cells increased levels of overexpressed aggregated Huntingtin protein and mild vimentin knock-down (KD) decreased levels of overexpressed aggregated Huntingtin protein (Bauer, Hudec et al. 2012). Whereas overexpressing proteins such as vimentin could be detrimental to a cell by introducing an overabundance of proteins that interfere with cellular processes or compete with endogenous proteins that require degradation, how vimentin KD results in an increased capacity to maintain proteostasis in Neuro-2a cells overexpressing Huntingtin protein is less clear compared

with our model in which vimentin is beneficial for the cell's capacity to maintain proteostasis (Morrow, Porter et al. 2020). As mutant Huntingtin has an increased propensity to aggregate, rendering it resistant to degradation by the proteasome, vimentin's function in localizing proteasomes to the aggresome may be less consequential for degrading these proteins (Thibaudeau, Anderson et al. 2018). Further, due to the complexity and variety of dynamically regulated pathways that are able to compensate for impaired nodes of the cell's proteostasis network, it is also possible that weak KD of vimentin could be acting as a type of hormesis for the cell which then becomes exacerbated in a stronger KD or full vimentin KO cells. Finally, as the authors utilized both Neuro-2a cells and HeLa cells, both of which are cancer cell lines, it may be interesting to see if similar effects are seen in primary cells, as cancer cells may have modified their methods of responding to disruptions in proteostasis (see below a further discussion on cancer in part II),

Vimentin and the aggresome also can be asymmetrically inherited during mitosis (Rujano, Bosveld et al. 2006, Ogrodnik, Salmonowicz et al. 2014, Moore, Pilz et al. 2015, Morrow, Porter et al. 2020). Thus, any functions that vimentin may serve in interphase, such as what is described above, can be asymmetrically distributed between two daughter cells after mitosis and could lead to distinct cell behavioral outcomes. Indeed, the daughter cell inheriting more vimentin and the aggresome is associated with a relatively longer cell-cycle length and an increased chance of undergoing apoptosis (Ogrodnik, Salmonowicz et al. 2014, Moore, Pilz et al. 2015). However, it remains unclear if inheriting more vimentin and the aggresome would always be bad for the cell. For example, daughter cells inheriting more vimentin-associated proteins, such as

proteasomes, could be better equipped to handle specific circumstances compared to daughter cells with less inherited proteasomes (Morrow, Porter et al. 2020). It has not yet been determined whether daughter cells which inherit more or less vimentin have different capacities to maintain proteostasis after mitosis.

Together, while the field has now answered several key questions about vimentin's function in proteostasis, this topic remains largely understudied. Additional research is needed to reconcile unresolved discrepancies, as numerous elements could factor into conflicting findings, such as: cell type, KO of vimentin as opposed to KD of vimentin, and different techniques to measure or enhance protein accumulation (endogenous labeling of aggregated proteins as opposed to mutant Huntingtin overexpression). What these studies do agree upon is that vimentin interacts with a diverse set of proteins and that, whether for the better or the worse, perturbing vimentin potentiates the cell's capacity to maintain proteostasis.

Organismal implications for vimentin's function at the aggresome

Although vimentin KO mice retain the ability to develop and reproduce normally, vimentin plays numerous critical roles throughout the body, and can be upregulated in pathological contexts (Danielsson, Peterson et al. 2018). As mounting evidence supports a role for vimentin in the cell's proteostasis network, vimentin's action at the aggresome could be a putative mechanism underlying previously established vimentin KO phenotypes.

Many reports have demonstrated general reduced cellular function in vimentin KO cells (Galou, Gao et al. 1997, Terzi, Henrion et al. 1997, Vilaboa, Garcia-Bermejo et al.

1997, Lundkvist, Reichenbach et al. 2004, Perez-Sala, Oeste et al. 2015, Boraas and Ahsan 2016, Cheng, Shen et al. 2016). For example, vimentin KO fibroblasts display a slower proliferation rate (Cheng, Shen et al. 2016), and vimentin KO embryonic stem cells have a reduced capacity to differentiate down a endothelial lineage (Boraas and Ahsan 2016). These findings suggest that vimentin's functions within the cell are important for maintaining basic cellular functions which could translate into the numerous phenotypes reported in vimentin KO organisms (Table 4.1) (Danielsson, Peterson et al. 2018). Although vimentin's previously established mechanisms of action could contribute to these phenotypes, such as vimentin's function in cell motility and adhesion, it is also possible that these phenotypes are the result of an impaired capacity to maintain proteostasis through mechanisms such as what is described above (Danielsson, Peterson et al. 2018). Closer examination for the presence of aggresome formation in these cells would shed light on whether vimentin's function at the aggresome is playing a role in these phenotypes.

Vimentin's function in proteostasis may also be important for an organism's defense against pathologies and diseases throughout the body. For example, vimentin and the aggresome are studied in the lung where they respond to insults such as exposure to cigarette smoke or lung pathologies such as Chronic Obstructive Pulmonary Disease (COPD), which can display elevated ubiquitinated protein levels and impaired proteostasis (Min, Bodas et al. 2011, Tran, Ji et al. 2015, Shivalingappa, Hole et al. 2016). Further, many diseases and stimuli can induce disrupted proteostasis in the liver, some of which culminate in aggresome formation (French, van Leeuwen et al. 2001, Bardag-Gorce, Riley et al. 2004, French, Mendoza et al. 2016, French, Masouminia et al. 2017).

Thus, there are plenty of pathological contexts which may warrant vimentin's action at the aggresome. However, not all cell types throughout the body express vimentin. Therefore, it would be important to verify that the cell type being studied either already expressed vimentin or upregulated vimentin as a complement to aggresome formation to understand if vimentin is playing a role in these circumstances. In the event that vimentin is not expressed, other IFs could play an analogous role to vimentin. Indeed, in mouse motor neuron-neuroblastoma cells the neurofilament network was observed to collapse around aggresomes formed by overexpression of a truncated androgen receptor with a 112-glutamine repeat *in vitro* (Taylor, Tanaka et al. 2003). It remains unclear if this observation would translate to bonafide neurons *in vivo*. Further, as many intermediate filaments heteropolymerize, it is likely that many intermediate filament proteins (such as nestin and GFAP) could be similarly enriched in the cage surrounding the aggresome and that these proteins could be performing functions analogous to vimentin (Steven, Hainfeld et al. 1983, Morrow, Porter et al. 2020).

Further supporting the notion that vimentin plays a role in pathologies across the body, vimentin is also upregulated in tissues during several pathologies where proteostasis is disrupted. For example, neurons in a mouse model of Alzheimer's Disease (Tg2576), which normally don't express vimentin once mature, upregulate vimentin during disease progression (Levin, Acharya et al. 2009). Further, vimentin also has been found in human Alzheimer's Disease amyloid plaques (Liao, Cheng et al. 2004, Rudrabhatla, Jaffe et al. 2011). Finally, vimentin expression is increased generally during aging in tissues, such as the brain (Xu, Gao et al. 2016, Benayoun, Pollina et al. 2019). A recent quantitative proteomic analysis during aging in the hippocampus, an area critical for

learning and memory, found vimentin as one of 35 upregulated genes out of 4582 that were analyzed (Xu, Gao et al. 2016). One explanation may be that vimentin is upregulated in reactive astrocytes; however, it could also be that vimentin becomes activated to respond to the disruptions in proteostasis that are sustained in the brain during aging (Wang, Bekar et al. 2004).

While there are numerous scenarios in which vimentin's activity at the aggresome could be interpreted as beneficial, there are also scenarios in which the organism sustains greater consequences from an optimally functioning vimentin-caged aggresome such as in cancers and viral infection. Aggresomes and vimentin are widely studied chemotherapeutic targets in combination with proteasome inhibitors in cancers such as multiple myeloma, breast cancer and pancreatic cancer (Nawrocki, Carew et al. 2006, Komatsu, Moriya et al. 2013, Mishima, Santo et al. 2015, Park, Yoon et al. 2020). Interestingly, indirectly inhibiting aggresome function synergistically increases cytotoxicity associated with proteasome inhibition in a pancreatic cancer xenograft (Nawrocki, Carew et al. 2006). Other studies have reported that vimentin KO tumors have an impaired ability to metastasize, which may be mediated by a reduced capacity to migrate (Liu, Lin et al. 2015). However, an alternative explanation may be that vimentin KO tumors have a decreased capacity to maintain proteostasis. Together, these findings combined with vimentin's role in proteostasis suggest that vimentin could be viewed as a target for not only reducing tumor metastasis, but also the tumor's ability to maintain proteostasis.

Aggresomes have also been implicated in the cell's response to viral infection. While the precise mechanism(s) by which viruses benefit from hijacking the aggresome are not fully clear, cells with impaired aggresome formation display reduced viral

propagation, suggesting that an optimally functioning aggresome would be beneficial for viruses and detrimental for the organism (Nozawa, Yamauchi et al. 2004, Liu, Shevchenko et al. 2005). Thus, vimentin also could be viewed potentially as a target to reduce the virus' capacity to propagate. These examples suggest that an optimally functioning aggresome may provide cellular benefits that may not always be beneficial to the organism and that it may not always be desirable to utilize vimentin to increase the cell's capacity to recover proteostasis.

There are many examples of vimentin and the aggresome dynamically responding to numerous different healthy and pathological stimuli. Recent data investigating vimentin's role in maintaining proteostasis at the aggresome provides a new consideration for vimentin in a myriad of diverse cellular functions and phenotypes. Future research will be needed to fully understand how this mechanism functions with other established roles of vimentin in these diverse conditions.

Future Directions

Evidence suggests that vimentin plays numerous unique roles in the cell, many of which fall under the umbrella of the cell's response to stress. While many components of vimentin's function in these processes are known, the field is still limited by the absence of critical and effective tools. For example, currently there is no mouse line that allows for conditional knock-out of vimentin, but only a full vimentin KO mouse that has had vimentin removed throughout development in all cell types. Therefore, all studies to date in vimentin KO mice are limited by any compensatory mechanisms that this line has generated to adapt to vimentin KO, and in the inability to determine cell-specific effects.

Further, many studies investigating vimentin's presence and function at the aggresome have relied on visualizing vimentin through overexpression of vimentin fused to a fluorophore, which could also be inducing artificial phenotypes that are less reminiscent of endogenous vimentin. Despite technical limitations, it is clear that vimentin expression and distribution in the cell are dynamic and functionally important in many cell types in numerous contexts. Improved tools can be used to resolve discrepancies in the understanding of vimentin's role in proteostasis and further reveal how *in vitro* studies in cell lines translate into organismal changes *in vivo*.

As vimentin and IFs are expressed in a tissue-specific manner, it will be interesting to determine how cell types that don't express vimentin maintain proteostasis through compensation by other nodes of the proteostasis network. For example, it is well-established that impairments in the ubiquitin-proteasome system can lead to increases in autophagy and vice versa (Dikic 2017). Further, revealing how species such as *Drosophila melanogaster* were able to evolve in the absence of IFs may reveal mechanisms of compensation by other mechanisms (Bohnekamp, Cryderman et al. 2016). Both of these phenomena may be explained by the fact that many roles of vimentin involve increased resilience to cellular challenges that would only become important in specific settings. These roles are also often redundant and provide increased efficiency in a cellular process, rather than an essential function that the cell could not complete otherwise. Additionally, as expression of vimentin has been shown to be harmful for organisms in specific scenarios such as cancer or viral infection, it may be that organisms have carefully evolved to only use vimentin in places where they are needed most to minimize their potential to cause harm to the organism. Vimentin's cell-type specific

expression raises the prospect that not all cells are using all of the tools nature has provided them with to maintain proteostasis. Identifying the molecular determinants driving vimentin's function in maintaining proteostasis could lead to development of targeted therapies that can modulate cellular proteostasis and ultimately improve diseases resulting from impaired proteostasis.

4.3 Project Introduction

Proper somatic stem cell function for lifelong tissue maintenance relies on the cell's ability to maintain proteostasis, a fine balance between the synthesis and degradation of proteins which is controlled by a network of protein pathways (Vilchez, Simic et al. 2014). Failure to maintain proteostasis leads to an accumulation of misfolded, damaged or aggregated proteins, which is a hallmark of aging and is correlated with stem cell dysfunction (Lopez-Otin, Blasco et al. 2013, Audesse, Dhakal et al. 2019, Rodriguez-Fernandez, Qi et al. 2019). Though proteostasis is recognized as a critical component of cellular function, therapeutic interventions for restoring proteostasis during aging or in pathology remain limited, driving a need for a more complete understanding of the cell's response to accumulated proteins destined for degradation.

One way that stem cells can regulate this imbalance is through mitosis, where they can asymmetrically segregate damaged or ubiquitinated proteins to one of their daughter cells (Rujano, Bosveld et al. 2006, Bufalino, DeVeale et al. 2013, Moore, Pilz et al. 2015, Moore and Jessberger 2017). Neural stem cells (NSCs), the somatic stem cells of the brain, co-segregate ubiquitinated proteins with the intermediate filament (IF) vimentin

during mitosis, suggesting vimentin as a potential player in protein clearance (Moore, Pilz et al. 2015). While a number of studies have investigated the role of IFs in NSCs, revealing an essential role for nestin during development and a role for phosphorylated vimentin in NSC differentiation, vimentin's role in protein clearance in NSCs remains unknown (Park, Xiang et al. 2010, Chen, Puschmann et al. 2018).

Previously it has been shown in cell lines that following impaired proteostasis, accrued misfolded or damaged proteins can be trafficked to the centrosome and surrounded by a vimentin cage in a structure referred to as the aggresome (Johnston, Ward et al. 1998, Rujano, Bosveld et al. 2006, Ogrodnik, Salmonowicz et al. 2014). While much is known about how aggresomes form and how to induce their formation *in vitro* in cell lines, the endogenous role of aggresomes and how specifically they enhance recovery from disrupted proteostasis has remained elusive (Kawaguchi, Kovacs et al. 2003, Ouyang, Ali et al. 2012, Ogrodnik, Salmonowicz et al. 2014). Here we asked if NSCs utilize aggresomes to maintain NSC proteostasis, and what function vimentin plays in these structures.

4.4 Results (adapted from Morrow et al 2020 Cell Stem Cell)

Tagging of endogenous vimentin in primary mouse NSCs to monitor aggresome formation

To unravel vimentin's role in maintaining NSC proteostasis, we used CRISPR/Cas9 to add an mNeon fluorophore to genomic vimentin at its 3' end in mouse primary hippocampal NSCs to dynamically visualize vimentin without overexpression

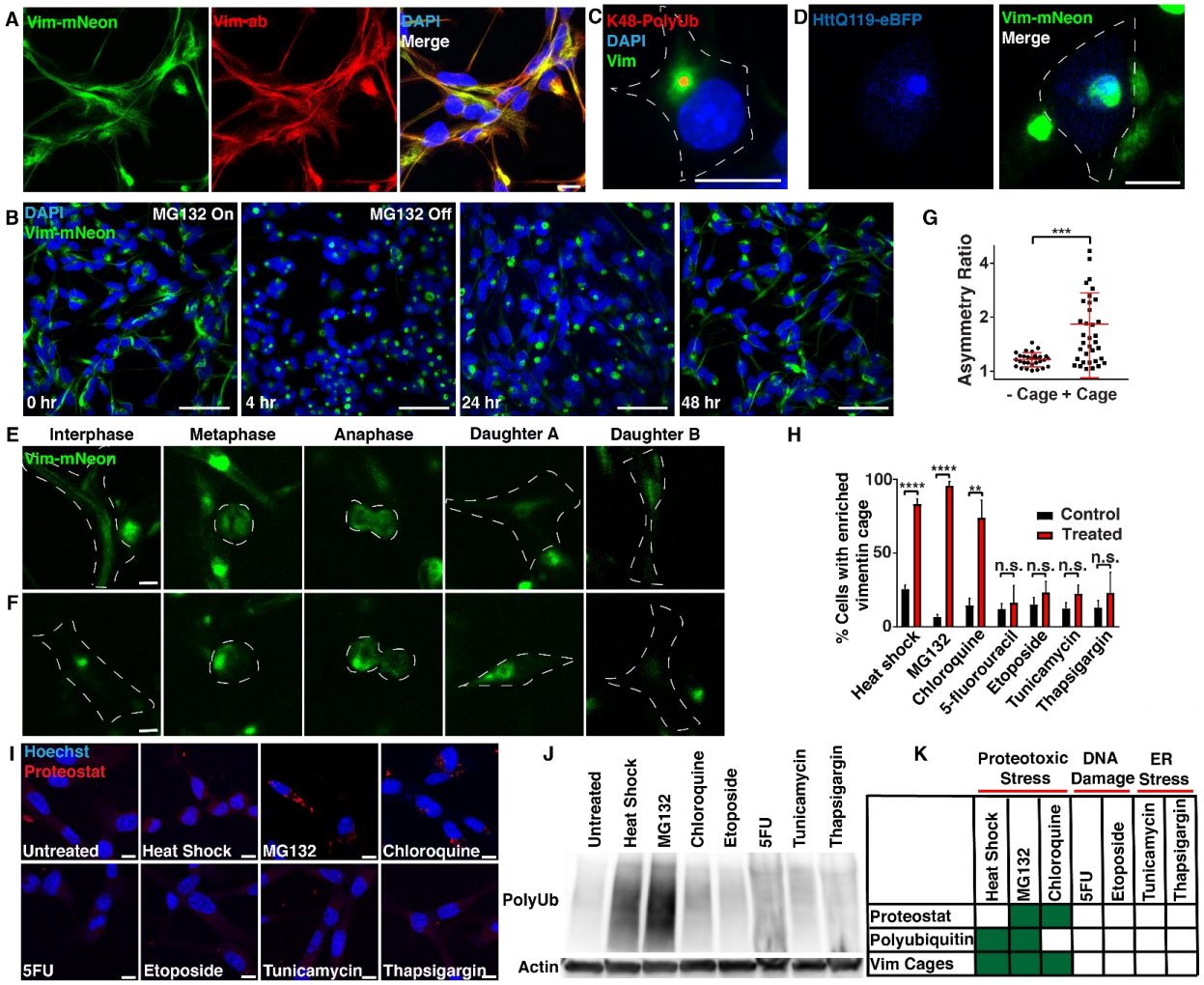

Figure 4.2 - NSCs form aggresomes surrounded by vimentin cages in response to a loss of proteostasis that are asymmetrically inherited during mitosis. *A) Vimentin-mNeon (green) NSCs were immunostained for vimentin (red). B) Vimentin-mNeon NSCs (green) were treated with 5 μM MG132 for 4 hours to transiently disrupt proteostasis, and allowed to recover for up to 48 hours. C) Vimentin-mNeon NSCs were treated with 2 μM MG132 or 0.02% DMSO for 18 hours and then immunostained for K48pUb (red). D) Vimentin-mNeon NSCs (green) were live-imaged 24 hours after electroporation with a construct that expresses a mutant Huntingtin protein (HttQ119; blue). E-G) Representative frames and quantitation of asymmetry from timelapse imaging of*

*vimentin-mNeon NSCs in either untreated conditions or following a 20 minute heat shock at 45°C, that proceeded through mitosis either with or without a vimentin cage formed in interphase (n≥29; Mann-Whitney test; mean ± SD). H) Quantification of vimentin cage formation in response to a heat shock of 20 minutes at 45°C, 5 µM MG132 or 10 µM chloroquine for 6 hours, 50 nM 5-fluorourucil or 100 nM etoposide for 24 hours, and 1 µg/mL tunicamycin or 1 µM thapsigargin for 6 hours (red bars) next to their appropriate DMSO or untreated controls (black bars) (N=3; Two-way ANOVA with post-hoc Tukey's test; mean ± SD). I) NSCs treated as indicated in Fig. 1H were stained with Proteostat (aggregated proteins; red). (N=3; Two-way ANOVA with post-hoc Tukey's test; mean ± SD). J) Western blot against polyubiquitin and β-actin in total fraction (soluble and insoluble) protein lysates generated from NSCs stressed as indicated in Fig. 1H alongside an untreated control. K) Chart depicting cellular stress conditions that induced changes in aggregated protein levels (Proteostat), polyubiquitin levels, or vimentin cages. Scale bars, 10 µm (A, C-F, I) 50 µm (B). White line denotes edge of the cell. Nuclei were labeled with DAPI or Hoechst (blue). **p<0.01, ***p<0.001, ****p<0.0001.*

(Fig. 4.2A). We performed fluorescence activated cell sorting (FACS) to purify mNeon-expressing NSCs, and immunostained against vimentin protein. Vimentin antibody signal strongly co-localized with mNeon (Fig. 4.2A), suggesting the tag accurately reported vimentin filament formation and that the NSCs had successfully integrated a low level of tagged vimentin (Fig. 4.3A), limiting its interference in mature filament formation. Vimentin tagging also did not affect NSC morphology, proliferation, differentiation, or motility (Fig. 4.2A, 4.3B-E).

To identify if vimentin-mNeon NSCs could form vimentin cages that surround aggresomes in response to a loss of proteostasis, we treated WT and vimentin-mNeon NSCs with the reversible proteasome inhibitor MG132 or DMSO for 4 hours, and then immunostained against vimentin throughout the course of treatment and during recovery (Fig. 4.1B, 4.3F-H). We defined a vimentin cage as a cage-like structure located at the centrosome in the nuclear bay including >50% of the vimentin signal within each individual cell (Fig. 4.3F). We found that NSCs form a vimentin cage with similar dynamics, as visualized with both mNeon signal and vimentin antibody staining (Fig. 4.3G-H). Importantly, we confirmed that these vimentin cages indeed surrounded an aggresome, as vimentin-mNeon surrounded K48-linked polyubiquitin-rich (K48pUb) aggregates, Proteostat-labeled aggresomes, and overexpressed aggregation-prone proteins at the centrosome (Fig 4.2C-D, 4.3I-M). Taken together, these data show that we have created a genetically encoded fusion tag of vimentin in primary mouse NSCs that accurately reports aggresome formation through monitoring of the vimentin cage, and does not interfere with IF formation or NSC function.

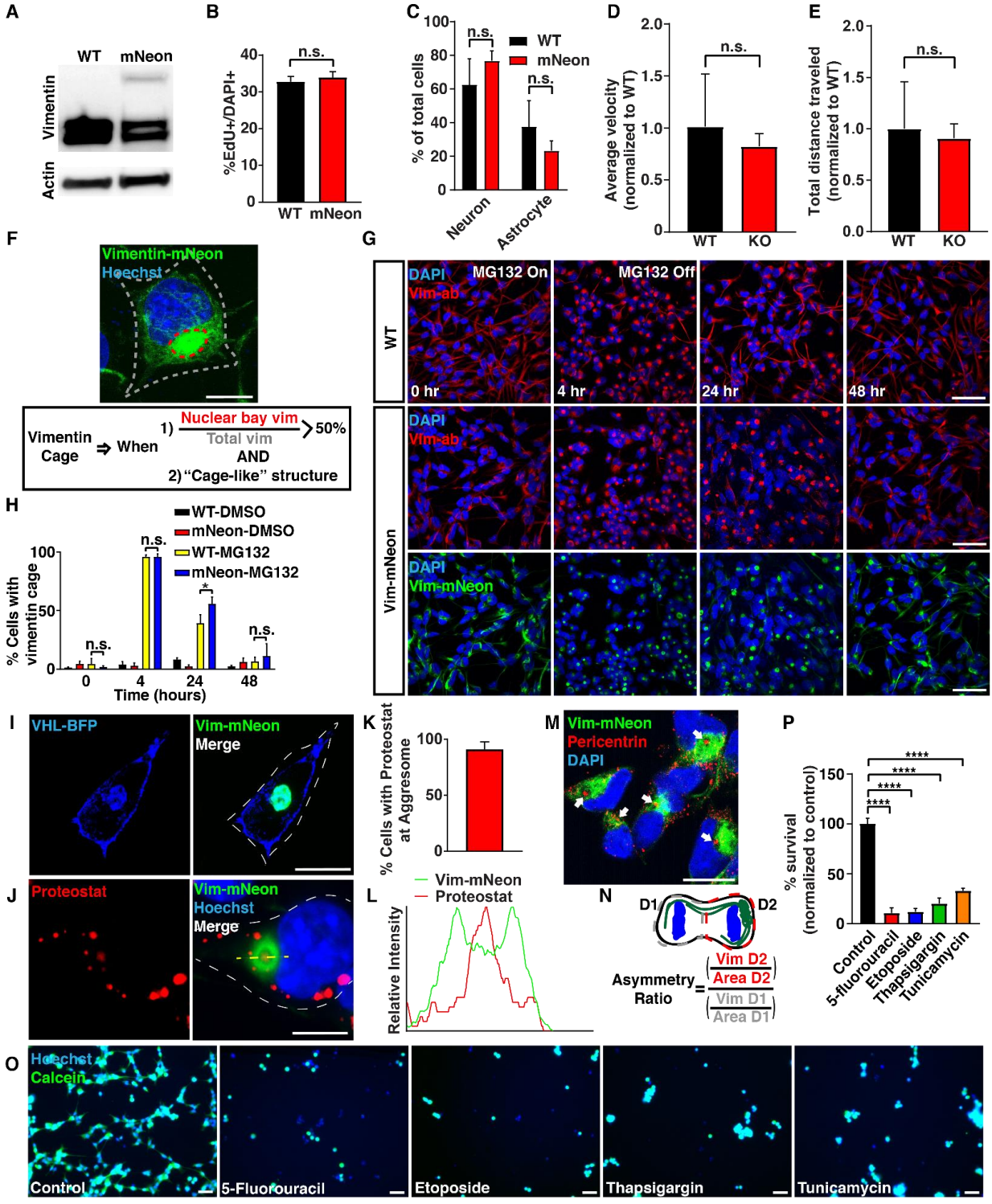

Figure 4.3 – *A) Protein was extracted from WT and vimentin-mNeon NSCs and run on a western blot probing for vimentin and β-actin levels. B) WT (black bar) and vimentin-mNeon (red bar) NSCs were pulsed with EdU for 1 hour and then fixed and analyzed for*

percent EdU+ cells. (n=3; Student's t-test; mean ± SD). C) WT or vimentin-mNeon NSCs were differentiated for 14 days by removing growth factors, and then quantified for generation of neurons (MAP2ab) or astrocytes (GFAP). (n=3; Student's t-test; mean ± SD). D-E) WT and vimentin mNeon-NSC timelapse images were analyzed for average velocity or total distance traveled to quantify cell motility. (N=3; Student's t-test; mean ± SD). F-H) WT and Vimentin-mNeon NSCs (green) were treated with 5 μM MG132 for 4 hours to induce a transient loss of proteostasis, allowed to recover for up to 48 hours, and stained with a vimentin antibody to analyze the percentage of vimentin cages. (N=3; Two-way ANOVA with post-hoc Tukey's test; mean ± SD). I) Vimentin-mNeon NSCs (green) were electroporated with a construct expressing the mutant tumor suppressor Von Hippel-Lindau (VHL; blue) and imaged 24 hours later. J-K) Vimentin-mNeon NSCs were stressed with 5 μM MG132 for 4 hours and then immunostained for vimentin (green), stained with Proteostat (red), and quantified for the percentage of cells that had Proteostat puncta present at or within the vimentin cage. L) Intensity histogram along the yellow dotted line in J depicting vimentin and Proteostat fluorescence. M) Vimentin-mNeon NSCs were stressed with 5 μM MG132 for 2 hours and then immunostained for pericentrin (centrosome; red). White arrows indicate centrosomes. N) Schematic depicting quantitation of asymmetry during mitosis. O-P) Images and quantification of survival (living cells labeled by Calcein AM; green) of WT NSCs after modification of drug treatment stress paradigms that did not induce vimentin cage formation in initial experiments (50 nM 5-fluorourucil for 48 hours, 100 nM etoposide for 48 hours, 1 μg/mL tunicamycin for 9 hours, and 1 μM thapsigargin for 9 hours). (n=3; Two-way ANOVA with post-hoc Tukey's test; mean ± SD). Scale bars, 10 μm (I, J, M), 50 μm (G, O). Nuclei were

*labeled with DAPI or Hoechst (blue). White line denotes edge of the cell. *p<0.05, ****p<0.0001.*

Vimentin cages form during interphase in response to increased levels of ubiquitinated or aggregated proteins

Using an overexpression system, we previously found that vimentin is asymmetrically segregated between two daughter cells during NSC mitosis (Moore, Pilz et al. 2015). To better understand vimentin dynamics and aggresome formation throughout the cell cycle in endogenously tagged vimentin-mNeon NSCs, we performed timelapse imaging. Similar to reports in cell lines (Rujano, Bosveld et al. 2006, Ogrodnik, Salmonowicz et al. 2014), we found that vimentin asymmetry during mitosis in NSCs was tightly linked to aggresome formation in interphase (Fig. 4.2E-G, 4.3N). Thus, we next asked what drives vimentin cage formation in NSCs during interphase.

Vimentin has been shown to react to cellular stress by becoming upregulated and collapsing to form a cage around the aggresome (Vilaboa, Garcia-Bermejo et al. 1997, Johnston, Ward et al. 1998, Rujano, Bosveld et al. 2006, Ogrodnik, Salmonowicz et al. 2014). To determine if vimentin responds to all cellular stresses with cage formation, we measured the percentage of NSCs which formed a vimentin cage in response to different cellular challenges. We found that heat shock, inhibition of proteasomes (MG132), and inhibition of autophagy (chloroquine) significantly increased the percentage of NSCs forming a vimentin cage, whereas drugs that caused DNA damage (5-fluorouracil, etoposide), or ER stress (tunicamycin, thapsigargin) did not affect vimentin cage formation (Fig. 4.2H), even if taken to a concentration that kills the cells (Fig. 4.3O-P). As the aggresome has been shown to consist of aggregated and ubiquitinated proteins (Johnston, Ward et al. 1998, Ogrodnik, Salmonowicz et al. 2014), in these treatments we also measured the levels of aggregated proteins using the dye Proteostat, and the total

(soluble and insoluble) amount of polyubiquitinated proteins in western blots. We found that Proteostat signal was increased only with MG132 or chloroquine treatment, whereas total polyubiquitinated protein levels were increased with heat shock and MG132 (Fig. 4.2I-J). These experiments demonstrate that vimentin cage formation occurs in NSCs in response to increases in aggregated and/or ubiquitinated proteins, further supporting the hypothesis that NSCs make aggresomes specifically in response to a loss of proteostasis (Fig. 4.2K).

Vimentin is not necessary for aggresome formation in NSCs

Despite the report of vimentin at the aggresome, its role has been unclear (Johnston, Ward et al. 1998). Previous studies suggest that vimentin cages form first prior to deposition of proteins marked for degradation, and trafficking of polyubiquitinated aggregates to the aggresome is thought to be mediated through the microtubule network, histone deacetylase 6 (HDAC6) and dynein (Kawaguchi, Kovacs et al. 2003, Ouyang, Ali et al. 2012, Ogrodnik, Salmonowicz et al. 2014). To determine if vimentin is necessary for aggresome formation, we first used CRISPR/Cas9 to create three vimentin KO lines in primary mouse hippocampal NSCs (KO), as well as a control NSC line treated with a non-targeting guide RNA (WT; Fig. 2A, S2A). Vimentin KO NSCs had decreased expression of the IFs glial fibrillary acidic protein (GFAP) and nestin (Fig. 4.5B), however displayed no differences in NSC proliferation, differentiation, or motility (Fig. 4.5C-F). To determine if vimentin is required for aggresome formation, we treated WT and vimentin KO NSCs with MG132 to induce an increase in misfolded or damaged proteins, and found that both WT and vimentin KO NSCs made K48pUb aggresomes in the nuclear bay (Fig.

4.4B). These data reveal that vimentin is not necessary for aggresome formation, or basic NSC function. What then is vimentin's role at the aggresome in NSCs?

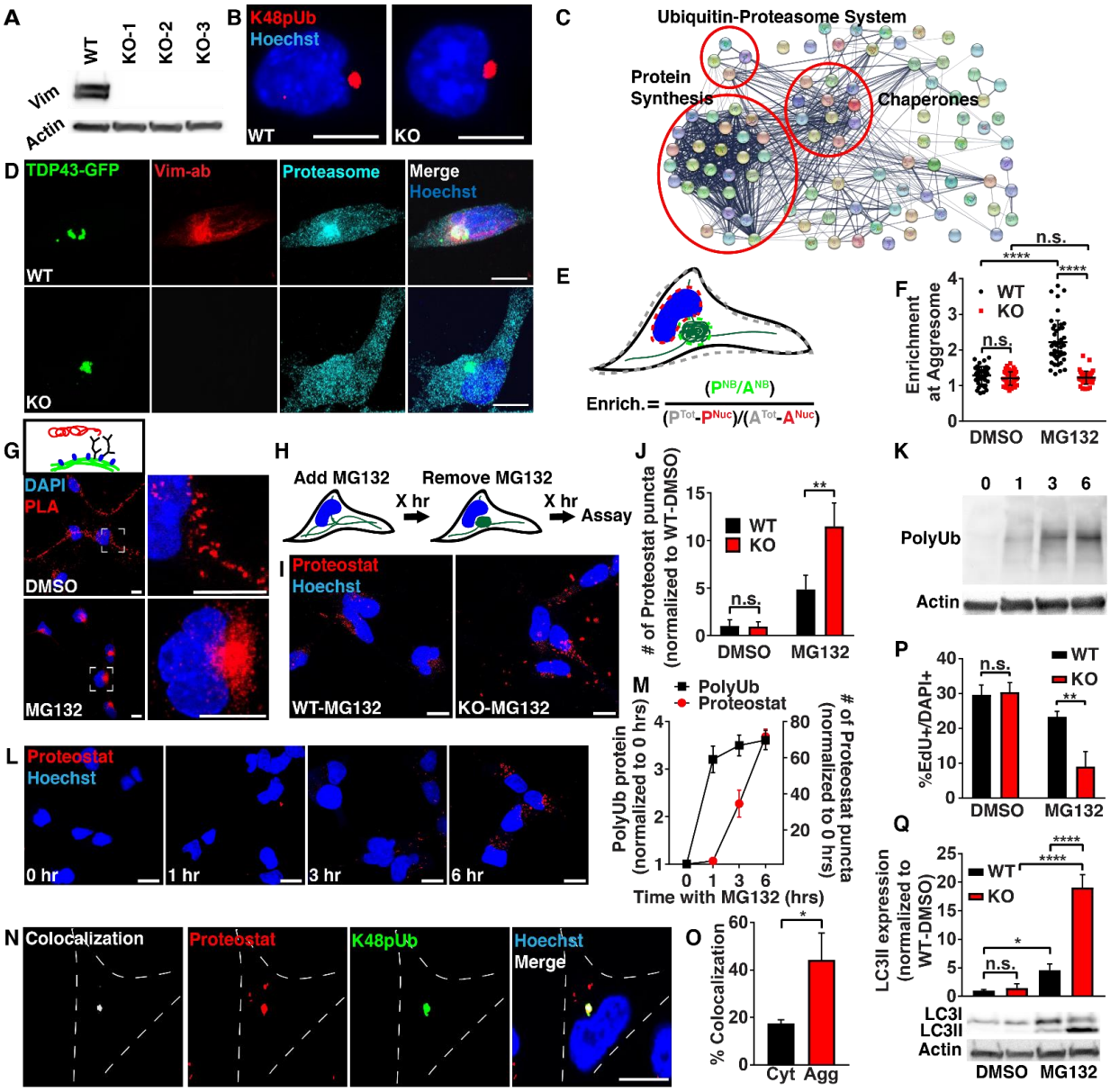

Figure 4.4 – Vimentin KO NSCs fail to localize proteasomes to the aggresome and demonstrate a reduced capacity to recover proteostasis. *A) WT and 3 vimentin KO clones were probed by western blot for vimentin and β-actin protein levels. B) WT and vimentin KO NSCs were treated with 2 μM MG132 for 16 hours and then immunostained for K48pUb (red). C) Functional protein association network generated from LC-MS/MS on proteins co-immunoprecipitated with vimentin-mNeon following 5 μM MG132 for 4*

hours, and visualized using String. D) WT and vimentin KO NSCs 24 hours after electroporation with a construct expressing the C-terminal fragment of TDP-43-GFP were fixed and immunostained for vimentin (red) and the α5 subunit of the proteasome (cyan). E-F) WT (black dots) and vimentin KO (red dots) NSCs were stressed with 0.05% DMSO or 5 μM MG132 for 4 hours and then fixed and immunostained for the α5 subunit of the proteasome and quantitated for proteasome enrichment at the aggresome by measuring Proteasome Intensity (P) and Area (A) of the nuclear bay (NB), nucleus (Nuc) or entire cell (Tot). (n≥45 cells; Mann-Whitney test; mean ± SD). G) WT NSCs were treated with 0.05% DMSO or 5 μM MG132 for 4 hours and then fixed and probed with a proximity ligation assay (red) against vimentin and the α5 subunit of the proteasome. H) Graphic outlining treatment and recovery scheme for experiments in Fig. 2I, P and Q. I-J) WT (black bar) and vimentin KO (red bar) NSCs were treated with 0.05% DMSO or 5 μM MG132 for 4 hours and then allowed to recover for 2 hours before fixing and staining aggregated proteins with the dye Proteostat (red). (N=3; Two-way ANOVA with post-hoc Tukey's test; mean ± SD). K-M) WT NSCs were treated with 5 μM MG132 for 0, 1, 3 and 6 hours and then stained with Proteostat (red) or analyzed for total fraction (soluble and insoluble) polyubiquitin levels on a western blot. (N=3; Two-way ANOVA with post-hoc Tukey's test; mean ± SD). N-O) WT NSCs were treated with 5 μM MG132 for 4 hours and then fixed and immunostained for K48pUb (green) and stained for Proteostat (red). Colocalization of Proteostat signal overlapping with K48pUb either in the cytosol (Cyt) or within the vimentin cage (Agg) was quantified using Imaris. (n=30; Student's t-test; mean ± SD) P) WT (black bar) and vimentin KO (red bar) NSCs were treated with 0.05% DMSO or 5 μM MG132 for 4 hours and then allowed to recover for 2 hours. During the last hour

*of treatment, cells were pulsed with EdU for 1 hour and then fixed and analyzed for percent EdU+ NSCs. (N=3; Two-way ANOVA with post-hoc Tukey's test; mean ± SD). Q) WT (black bar) and vimentin KO (red bar) NSCs were treated with 0.02% DMSO or 2 μM MG132 for 24 hours and then allowed to recover for 1 hour before analyzing LC3I and LC3II protein on a western blot. (N=3; Two-way ANOVA with post-hoc Tukey's test; mean ± SD). Scale bars, 10 μm. Nuclei were labeled with Hoechst (blue). *p<0.05, **p<0.01, ****p<0.0001.*

Vimentin interacts with proteins important in the maintenance of NSC proteostasis

To identify what proteins interact with vimentin at the aggresome, we performed a co-immunoprecipitation against mNeon in our vimentin-mNeon NSCs in both control and MG132-stressed conditions, followed by liquid chromatography-mass spectrometry (LC-MS/MS) to identify proteins that interact either directly or indirectly with vimentin (Fig. 4.4C). Interestingly, in comparison to control untagged NSCs transfected with cytosolic mNeon, we found a strong presence of nodes important for protein homeostasis, such as heat shock proteins and chaperones for protein re-folding, ribosomal proteins and elongation factors for protein translation, and proteasomes for protein degradation (Fig. 4.4C). These results suggest that vimentin is acting as an organizer of proteins that regulate the balance of protein synthesis, refolding, and degradation – processes critical for the maintenance of proteostasis.

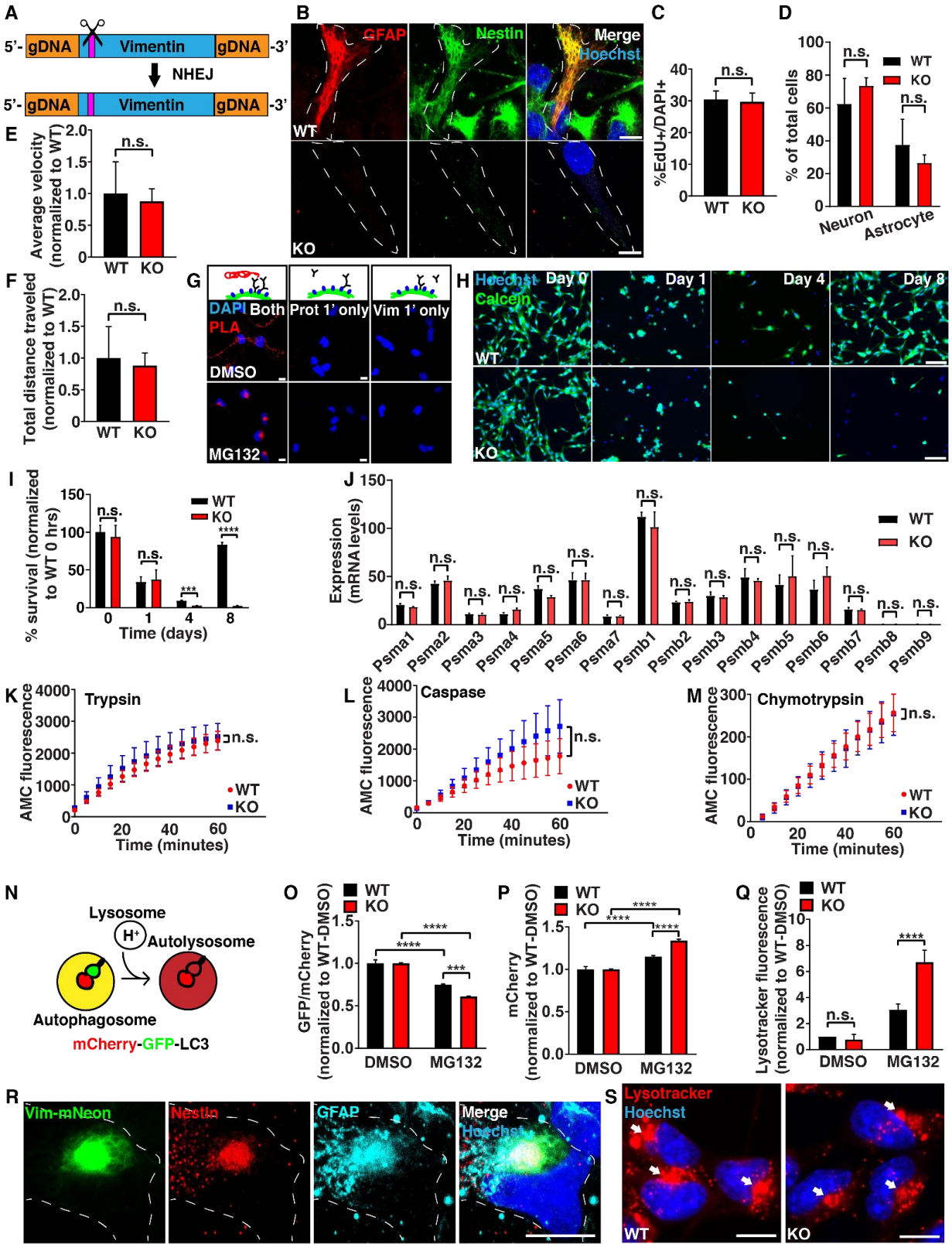
A
5'- gDNA Vimentin gDNA -3'
NHEJ
5'- gDNA Vimentin gDNA -3'
B
GFAP
Nestin
Merge
Hoechst
WT
KO
C
%EdU+/DAPI+
n.s.
WT KO
D
% of total cells
n.s.
WT
KO
Neuron
Astrocyte
E
Average velocity (normalized to WT)
n.s.
WT KO
F
Total distance traveled (normalized to WT)
n.s.
WT KO
G
DAPI Both
Prot 1' only
Vim 1' only
PLA
DMSO
MG132
H
Hoechst
Calcein
Day 0
Day 1
Day 4
Day 8
WT
KO
I
% survival (normalized to WT 0 hrs)
WT
KO
n.s.
***
****
Time (days)
J
Expression (mRNA levels)
WT
KO
Psma1 Psma2 Psma3 Psma4 Psma5 Psma6 Psma7 Psmb1 Psmb2 Psmb3 Psmb4 Psmb5 Psmb6 Psmb7 Psmb8 Psmb9
K
Trypsin
AMC fluorescence
n.s.
WT
KO
Time (minutes)
L
Caspase
AMC fluorescence
n.s.
WT
KO
Time (minutes)
M
Chymotrypsin
AMC fluorescence
n.s.
WT
KO
Time (minutes)
N
Lysosome
H+
Autolysosome
Autophagosome
mCherry-GFP-LC3
O
GFP/mCherry (normalized to WT-DMSO)
WT
KO
****
***
DMSO MG132
P
mCherry (normalized to WT-DMSO)
WT
KO
****
DMSO MG132
Q
Lysotracker fluorescence (normalized to WT-DMSO)
WT
KO
n.s.
****
DMSO MG132
R
Vim-mNeon
Nestin
GFAP
Merge
Hoechst
S
Lysotracker
Hoechst
WT
KO

Figure 4.5 *– A) Schematic of CRISPR/Cas9-based vimentin KO NSC generation strategy. B) WT and vimentin KO NSCs were immunostained for GFAP (red) and nestin (green). C) WT (black bar) and vimentin KO (red bar) NSCs were pulsed with EdU for 1 hour and then fixed and analyzed for percent EdU+ cells. (N=3; Student's t-test; mean ± SD). D) WT or vimentin KO NSCs were differentiated for 14 days and then quantified for generation of neurons (MAP2ab) or astrocytes (GFAP). (n=3; Student's t-test; mean ± SD). E-F) WT and vimentin mNeon-NSCs live-cell imaging timelapses were analyzed for average velocity or total distance traveled to quantify cell motility. (N=3; Student's t-test; mean ± SD). G) (Controls for Fig. 2G) WT NSCs were treated with 0.05% DMSO or 5 μM MG132 for 4 hours and then fixed and probed with a proximity ligation assay (red) against vimentin and the α5 subunit of the proteasome, with negative controls shown here using probes for only one antibody. H-I) WT (black bar) and vimentin KO (red bar) NSCs were treated transiently with 5 μM MG132 for 8 hours and then were monitored for cell survival over the course of the following week (normalized to day 0). Living cells are labeled by calcein (green). (N=3; Two-way ANOVA with post-hoc Tukey's test; mean ± SD). J) Proteasome subunit mRNA levels from total RNA sequencing data generated from WT and vimentin KO NSCs (n=3; Two-way ANOVA with post-hoc Tukey's test; mean ± SD). K-M) Proteasome activity assays performed on protein lysates generated from WT (red) or vimentin KO (blue) NSCs measuring caspase-like, trypsin-like and chymotrypsin-like proteasome activity (N=3; Student's t-test; mean ± SD). N-P) WT (black bar) and vimentin KO (red bar) NSCs were lentivirally transduced with mCherry-GFP-LC3. 7 days after viral transduction both cell types were treated either with 0.02% DMSO or 2 μM MG132 for 24 hours and then were allowed to recover for 1 hour without drug before analyzing mCherry*

*and GFP fluorescence. (N=3; Two-way ANOVA with post-hoc Tukey's test; mean ± SD). Q) WT (black bar) and vimentin KO (red bar) NSCs were treated with 0.05% DMSO or 5 μM MG132 for 4 hours and then allowed to recover for 2 hours before staining with the dye Lysotracker (lysosomes; red) (N=3; Two-way ANOVA with post-hoc Tukey's test; mean ± SD). R) Vimentin-mNeon (green) NSCs were treated with 5 μM MG132 for 4 hours, fixed and immunostained for nestin (red) and GFAP (cyan). S) WT and vimentin KO NSCs were treated with 5 μM MG132 for 1 hour and then stained with the dye Lysotracker (lysosomes; red). Nuclei were labeled with Hoechst (blue). Scale bars, 10 μm (B, R, S), 100 μm (H). White lines denote edge of the cell. ***p<0.001, ****p<0.0001.*

Vimentin spatially localizes proteasomes to aggresomes in response to cellular stress

Proteasomes, multi-subunit protein complexes which primarily process polyubiquitinated proteins for degradation, previously have been identified at aggresomes and inclusion bodies, and also were present in our vimentin interactome (Wigley, Fabunmi et al. 1999, Hao, Nanduri et al. 2013, Ogrodnik, Salmonowicz et al. 2014, Schipper-Krom, Juenemann et al. 2014). To visualize this potential interaction, we electroporated the aggregation prone C-terminal domain of TDP43-GFP into NSCs to induce aggresome formation and then performed immunostaining against the α5 subunit in the catalytic 20S portion of the proteasome (Fig. 4.4D). WT NSCs made a vimentin cage surrounding TDP43-GFP at the aggresome, and as our mass spectrometry data suggested, the vimentin cage was strongly enriched with proteasomes (Fig. 4.4D-F). Using a Duolink proximity ligation assay (PLA) which results in labeling if proteins are within 40nm of each other, we applied antibodies against vimentin and the same α5 proteasome subunit and detected a strong signal at the aggresome in WT NSCs, supporting an interaction between vimentin and proteasomes (Fig. 4.4G, 4.5G). Interestingly, interactions between proteasomes and vimentin were also present along vimentin filaments in unstressed conditions (Fig. 4.4G), suggesting these interactions are maintained following stress as vimentin filaments collapse to the nuclear bay, bringing proteasomes to the aggresome. Strikingly, while vimentin KO NSCs could still form an aggresome, there was no enrichment of proteasomes at the aggresome, revealing that vimentin is required for proteasome localization to the aggresome (Fig. 4.4D-F). Thus, our data suggest that proteasome-mediated protein turnover at the aggresome may be impaired in vimentin KO NSCs and may impact their ability to recover from disrupted proteostasis.

Vimentin KO NSCs demonstrate a reduced ability to recover from a loss of proteostasis

Initial papers characterizing vimentin KO mice reported limited phenotypes in these animals (Colucci-Guyon, Portier et al. 1994); however, further studies showed that in conditions of stress, vimentin KO mice had poor outcomes (Terzi, Henrion et al. 1997, Lundkvist, Reichenbach et al. 2004). We thus asked how might vimentin KO NSCs respond when challenged with a loss of proteostasis if they are unable to deliver proteasomes to the aggresome? To address this question, we created a stress/recovery paradigm where we treated WT or vimentin KO NSCs with MG132 or DMSO for 4 hours to disrupt proteostasis, followed by a 2 hour recovery prior to analysis (Fig. 4.4H). Using the dye Proteostat to measure the levels of aggregated proteins, we found that whereas basally there was no difference in the amount of aggregated proteins in WT and vimentin KO NSCs, following disrupted proteostasis, vimentin KO NSCs had significantly increased levels of aggregated proteins during recovery (Fig. 4.4H-J). This finding suggests that vimentin KO NSCs are less able to degrade proteins that accumulate as a result of proteasome inhibition with MG132. To better understand the temporal dynamics of this aggregated protein formation, we measured total (soluble and insoluble) polyubiquitinated protein levels and Proteostat labeling, indicative of aggregated proteins, at different timepoints during MG132 treatment in WT NSCs. We found that after treatment with MG132, ubiquitin levels increased and were maintained, followed by a delayed increase of Proteostat signal, suggesting that when ubiquitinated proteins are unable to be degraded, they aggregate (Fig. 4.4K-M). Further, we observed a high degree of co-localization between K48pUb proteins and Proteostat labeled aggregated proteins

at the aggresome (Fig. 4.4N-O). These data propose a model whereby the lack of proteasome localization in vimentin KO NSCs to the aggresome may result in inefficient degradation of misfolded or polyubiquitinated proteins, leading to an increase in aggregated proteins.

We next asked if the increased amount of aggregated protein following a loss of proteostasis in vimentin KO NSCs affects NSC behavior. Using a one hour pulse of EdU to label NSCs in S phase following the stress/recovery paradigm, we found that whereas the percentage of EdU+ NSCs under basal conditions was not different between WT and vimentin KO cells with DMSO treatment, disruption of proteostasis with MG132 treatment resulted in decreased proliferation in vimentin KO NSCs during a 2 or 8 day recovery period (Fig. 4.4P, 4.5H-I), indicating a negative consequence of the increased aggregated protein levels on NSC function. Taken together, these data show that vimentin KO NSCs basally have no measured phenotype, yet during a recovery following a loss of proteostasis they have significantly increased levels of aggregated proteins, and decreased proliferation that was unable to improve even after an extended recovery time.

Proteasome expression and activity is not changed in vimentin KO NSCs

To confirm that these effects were not due to differential expression of proteasome components in vimentin KO NSCs, we performed RNA sequencing of WT and vimentin KO NSCs, and found no difference in the amount of mRNA of proteasome components between genotype (Fig. 4.5J). Further, to determine if proteasome function is altered in vimentin KO NSCs, we lysed WT and KO NSCs, losing all spatial information, and subjected them to a proteasome activity assay, which utilizes non-fluorescence

substrates that upon cleavage by different enzymes of the proteasome, become fluorescent. All measured substrates testing chymotrypsin, trypsin, and caspase activities showed similar proteasome activity levels in WT and vimentin KO NSCs during recovery after a loss of proteostasis (Fig. 4.5K-M), indicating that proteasomes in vimentin KO NSCs have normal function. Taken together, these experiments demonstrate that there is no change in proteasome expression or activity in vimentin KO NSCs, suggesting the lack of spatial localization of proteasomes to the aggresome due to vimentin KO may be the main driver of increased protein aggregation and decreased proliferation measured in vimentin KO NSCs.

Vimentin KO NSCs upregulate autophagy in response to increased levels of aggregated proteins

Another arm of cellular protein degradation is autophagy, where autophagosomes engulf large aggregates which fuse with acidic lysosomes to degrade proteins (Yu, Chen et al. 2018). To determine if vimentin KO NSCs compensate for defects in proteasome-mediated protein degradation, we measured LC3II protein levels in WT and vimentin KO NSCs treated with DMSO or MG132 followed by recovery (Fig. 4.4Q). In line with our previous observations, we observed no differences between WT and vimentin KO NSCs in the DMSO condition, but during recovery from MG132 treatment, vimentin KO NSCs had increased autophagic flux indicated by increased levels of LC3II, suggesting that vimentin KO NSCs are more dependent on autophagy to recover proteostasis (Fig. 4.4Q). This was further confirmed using lentiviral overexpression of mCherry-GFP-LC3 in WT and vimentin KO NSCs. This peptide localizes to autophagosomes (GFP+ and mCherry+)

and then during fusion of autophagosomes with an acidified lysosome (mCherry+), GFP is denatured, giving a readout for autophagic flux (Fig. 4.5N). Similarly, following MG132 treatment to disrupt proteostasis, vimentin KO NSCs expressing mCherry-GFP-LC3 demonstrated increased autophagic flux (Fig. 4.5O), as well as increased mCherry signal demonstrating increased utilization of lysosomes (Fig. 4.5P). This increase in lysosomes following MG132 treatment and recovery in vimentin KO NSCs was also visualized using Lysotracker (Fig. 4.5Q). Taken together, these data provide evidence to support a model where, following an inability to spatially localize proteasomes to the aggresome, multi-ubiquitinated proteins begin to aggregate, and vimentin KO NSCs increase autophagy to improve protein aggregate clearance.

Vimentin protein is downregulated in qNSCs, and forms cages only during quiescence exit

When might NSCs experience such a loss of proteostasis in the body? Adult NSCs in the brain are primarily quiescent, but can activate, re-entering the cell cycle to divide and giving rise to neurogenic progeny (Goncalves, Schafer et al. 2016). Recently, it has been shown that quiescent NSCs (qNSCs) of the subventricular zone (SVZ) have increased levels of protein aggregates (Proteostat), which are removed through autophagy during activation into the cell cycle (Leeman, Hebestreit et al. 2018). Using a well-established protocol to induce quiescence in NSCs *in vitro* by adding BMP4 for 3 days, followed by BMP4 removal for 3 days to transition NSCs back into an activated cycling state (Mira, Andreu et al. 2010, Martynoga, Mateo et al. 2013, Knobloch, Pilz et al. 2017) (Fig. 4.6A, 4.7A), we found that quiescent primary mouse hippocampal NSCs

also had increased levels of protein aggregates, as measured by Proteostat labeling, which were cleared during quiescence exit (Fig. 4.6A-B). As we had previously shown that vimentin responds to increases in protein aggregates by making an aggresome surrounded by a vimentin cage (Fig. 4.2), we asked if vimentin would respond to increased protein aggregates in qNSCs with cage formation. To address this question, we imaged vimentin-mNeon NSCs prior to quiescence induction, after full quiescence was reached, and two days during the transition to activation (Fig. 4.6A). We found that qNSCs downregulate vimentin protein, and surprisingly, do not form vimentin cages in the presence of increased protein aggregates (Fig. 4.6B-E). Using timelapse microscopy of vimentin-mNeon NSCs during quiescence exit, we found that prior to the first cell division following BMP4 removal, vimentin is upregulated and forms a cage in interphase, resulting in asymmetric inheritance of the vimentin cage to one of the daughter cells (Fig. 4.6F-H). Interestingly, vimentin mRNA is upregulated in qNSCs (Fig. 4.6I), suggesting the NSCs are primed to respond with upregulation and cage formation in the transition to activation. Taken together, these results demonstrate that vimentin protein is downregulated in qNSCs, and does not respond with cage formation to increased levels of protein aggregates in quiescence; however, upon quiescence exit, vimentin is upregulated and forms a cage prior to mitosis, resulting in an asymmetric segregation of the aggresome to one daughter cell.

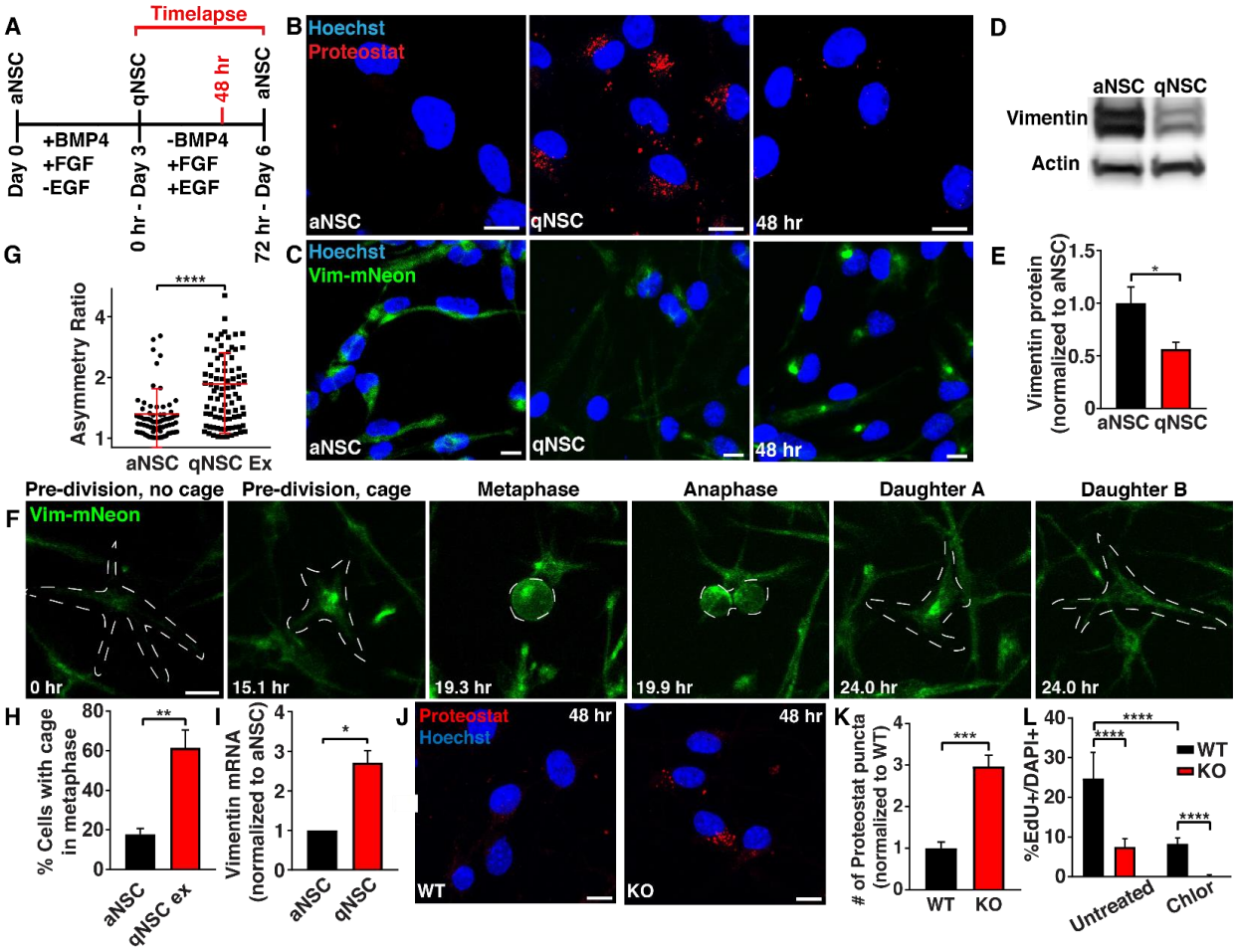

Figure 4.6 - NSCs form aggresomes during quiescence exit, and vimentin KO NSCs have a reduced capacity to exit quiescence in vitro. *A) Schematic outlining critical experimental time points examined during an in vitro quiescence paradigm. B) aNSCs, qNSCs or qNSCs exiting quiescence for 48 hours were fixed and stained with Proteostat (aggregated proteins; red). C) Images of vimentin-mNeon (green) aNSCs, qNSCs or qNSCs exiting quiescence for 48 hours. D-E) aNSCs and qNSCs were probed by western blot for vimentin and β-actin protein levels. (N=3; Student's t-test; mean ± SD). F) Representative division of a vimentin-mNeon NSC during quiescence exit. G-H) Quantification of vimentin asymmetry during mitosis (G) and presence of vimentin cages in metaphase prior to mitosis (H) in vimentin-mNeon aNSCs or qNSCs during quiescence*

*exit. (n≥71; Mann-Whitney test; mean ± SD). I) aNSCs and qNSCs were analyzed by qRT-PCR for vimentin mRNA expression levels. (N=3; Student's t-test; mean ± SD). J-K) WT or vimentin KO NSCs exiting quiescence for 48 hours were stained with Proteostat (aggregated proteins; red). (N=3; Student's t-test; mean ± SD). L) WT or vimentin KO NSCs exiting quiescence for 48 hours in either an untreated condition or in the presence of 1 μM chloroquine were pulsed for 1 hour with EdU before analysis. (N≥3; Two-way ANOVA with post-hoc Tukey's test; mean ± SD). Scale bars, 10 μm. Nuclei were labeled with Hoechst (blue). White line denotes edge of the cell. *p<0.05, **p<0.001 ***p<0.001, ****p<0.0001.*

Vimentin KO NSCs demonstrate a reduced capacity to exit quiescence *in vitro*

As we had shown that vimentin forms a cage around the aggresome during the transition from quiescence to activation, we asked if vimentin was necessary for quiescence exit. To test this, we induced full quiescence in WT and vimentin KO NSCs, and then began the transition to activation. Forty-eight hours into this transition (Fig. 4.6A), we stained for Proteostat and found that vimentin KO NSCs have increased levels of aggregated proteins (Fig. 4.6J-K) and lysosomes (Fig. 4.7B-C), mimicking our results disrupting proteostasis using MG132, and suggesting an impairment in protein degradation during activation. Further, we found that vimentin KO NSCs had decreased proliferation as measured by EdU (S phase), Ki67 (cell cycle), and phosphohistone H3 (PH3; late G2 and M) (Fig. 4.6L, 4.7D-E), suggesting a reduced ability to exit quiescence. Proliferation rates during quiescence exit were approximately half in vimentin KO NSCs (Fig. 4.6L), suggesting this is not the only mechanism driving quiescence exit. As autophagy was previously determined also to contribute to quiescence exit (Leeman, Hebestreit et al. 2018), we again induced quiescence in Vimentin WT and KO NSCs, though this time adding chloroquine to inhibit autophagy during quiescence exit. Interestingly, we found that autophagy inhibition during quiescence activation in vimentin KO NSCs rendered the cells fully unable to exit quiescence (Fig. 4.6L), suggesting that vimentin's caging and proteasome localization, as well as autophagy are both playing roles in quiescence exit in NSCs.

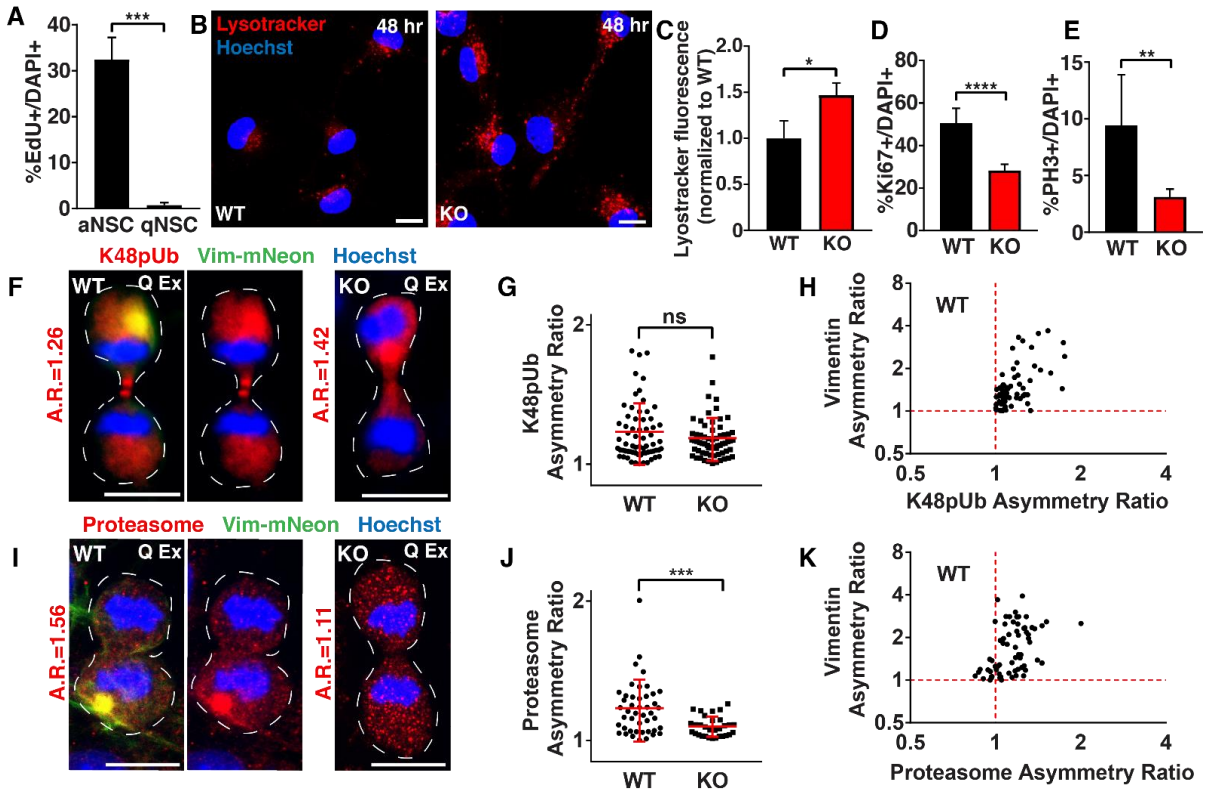

Figure 4.7 – *A) aNSCs or qNSCs were pulsed with EdU for 1 hour and then fixed and analyzed for percent EdU+ cells. (n=3; Student's t-test; mean ± SD). B-C) WT or vimentin KO NSCs exiting quiescence for 48 hours were stained with the dye Lysotracker (lysosomes; red). (N=3; Student's t-test; mean ± SD). D-E) WT and vimentin KO NSCs exiting quiescence for 48 hours were fixed and immunostained for Ki67 (cells not in G_0), and phosphohistone H3 (PH3; late G2/M phase). (n=3; Student's t-test; mean ± SD). F-N) Vimentin-mNeon (WT; green) NSCs and vimentin KO NSCs exiting quiescence were immunostained for either F-H) K48pUb or I-K) proteasome. Asymmetry ratio (A.R.) of proteasome or K48pUb is indicated beside each image. (n≥39; Mann-Whitney test; mean ± SD). Nuclei are labeled by Hoechst. Scale bars, 10 µm. *p<0.05, **p<0.01, ***p<0.001, ****p<0.0001.*

During quiescence exit, vimentin KO NSCs fail to asymmetrically segregate proteasomes during mitosis

Our finding that NSCs asymmetrically segregate vimentin during quiescence exit suggested that vimentin may be involved in coordinating the asymmetric segregation of different cellular cargoes such as polyubiquitin and proteasomes during mitosis. To address this question, we imaged vimentin-mNeon and vimentin KO NSCs during quiescence exit and quantified asymmetry of vimentin, K48pUb, and proteasomes in these divisions (Fig. 4.7F-K). In WT NSCs, K48pUb and proteasomes were primarily asymmetrically inherited during mitosis by the daughter cell that inherited more vimentin (Fig. 4.7F, H; (Moore, Pilz et al. 2015)). Interestingly, vimentin KO NSCs retained the ability to asymmetrically segregate K48pUb proteins during mitosis (Fig. 4.7F-G), a finding unsurprising in light of our observation that vimentin is not involved in aggresome formation (Fig. 4.4B). While vimentin was not required for asymmetric segregation of K48pUb proteins, vimentin was critical for the asymmetric segregation of proteasomes during mitosis (Fig. 4.7I-J). Taken together, these data suggest that vimentin KO NSCs asymmetrically segregate polyubiquitin to daughters without providing them with an enrichment of proteasomes to adequately clear this burden. In addition to vimentin's roles in interphase at the aggresome, vimentin's role in the asymmetric segregation of proteasomes could also contribute to the vimentin KO phenotypes we observe at the population level.

NSCs asymmetrically segregate the aggresome *in vivo*

To determine if vimentin cage formation and asymmetric segregation of vimentin during mitosis is conserved in a physiologic setting *in vivo*, we performed immunofluorescence to visualize endogenous vimentin in the dentate gyrus of 7 week-old Nestin-GFP mice. While NSC divisions in brain slices are rare, we observed the asymmetric segregation of vimentin in a dividing Nestin+ NSC, supporting our *in vitro* data, and previously published overexpression studies in embryonic NSCs (Fig. 4.8A, S4B) (Moore, Pilz et al. 2015). Additionally, we were also able to observe enrichment of vimentin in the nuclear bay of a small number of NSCs in interphase (Fig. 4.8B). These data collectively suggest that *in vivo*, NSCs can utilize aggresomes during quiescence exit and cell division.

NSCs in vimentin KO mice have a decreased ability to exit quiescence *in vivo*

As vimentin KO leads to a decreased ability to exit from quiescence *in vitro,* and we observed vimentin cages to be formed *in vivo*, we asked if vimentin KO animals would demonstrate a reduced ability of NSCs to exit quiescence *in vivo*. Previously it was shown that following temozolamide (TMZ) treatment, dividing NSCs are depleted, leading to qNSC activation to replenish the population (Garthe, Behr et al. 2009, Knobloch, Pilz et al. 2017) (Fig. 4.9A). We performed 3 days of TMZ injections in WT and vimentin KO mice followed by a 3 day recovery. Prior to perfusion, mice received 3 EdU injections (Fig. 4.8C). We found that vimentin KO NSCs had decreased levels of EdU+ cells in the subgranular zone (SGZ) following TMZ treatment as compared to WT mice, suggesting that vimentin is necessary for efficient quiescent exit not only *in vitro*, but also *in vivo* in hippocampal NSCs (Fig. 4.8D-E).

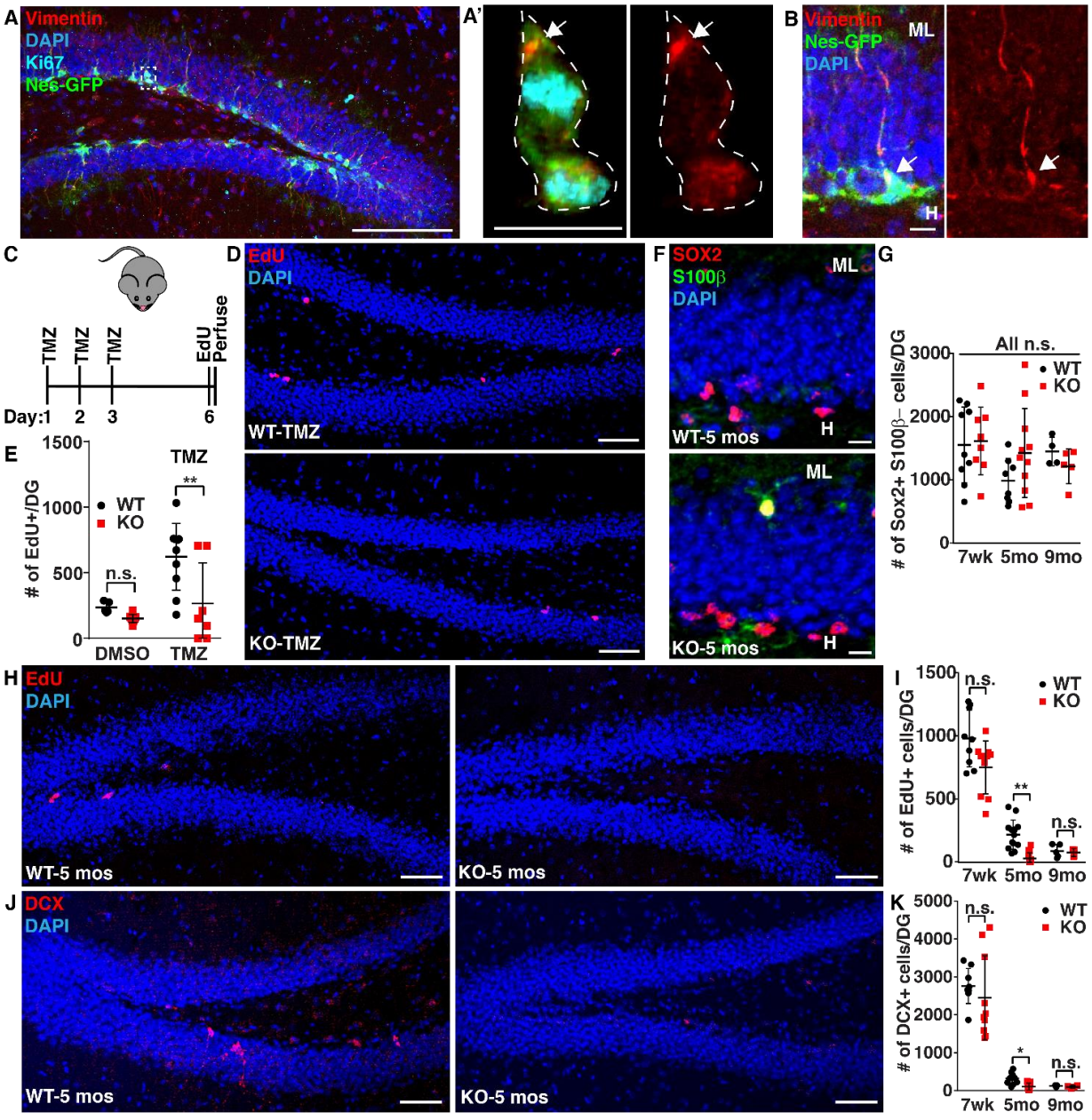

Figure 4.8 – NSCs in vimentin KO mice demonstrate a reduced capacity to exit quiescence following a stimulus and during early aging. *A-B) 7 week old Nestin-GFP mouse brain sections were immunostained for GFP (NSCs; green), vimentin (red) and Ki67 (cyan). A' was created by making a 3-D mask of the cytoplasmic GFP signal around the dividing cell (Imaris), revealing only intracellular staining. White line denotes edge of cells. C-E) 7 week old WT or vimentin KO mice were treated with 25 mg/kg TMZ or DMSO*

*once per day for 3 consecutive days and then allowed to recover for 3 days before being injected with 50 mg/kg EdU 3 times every 3 hours, perfused 3 hours after the last EdU injection and analyzed for proliferative (EdU+) NSCs in the SGZ. (n≥4; Two-way ANOVA with post-hoc Tukey's test; mean ± SD). F-K) 7 weeks (wk), 5 months- (mo) old, or 9 months-old WT and vimentin KO mice were injected with 50 mg/kg EdU once per day for 4 days, sacrificed 1 day following the last EdU injection and then analyzed for proliferative (EdU+) NSCs in the subgranular zone, total newborn neuron (doublecortin (DCX; red)) number and total NSC number (Sox2+ (red) S100β- (green)). The hilus (H) and the molecular layer (L) are annotated in F. (n≥4; Kruskal-Wallis Test with post-hoc Dunn's test; mean ± SD). Scale bars, 100 μm (A), 50 μm (D, H, J), 10 μm (A', B, F). Nuclei were labeled with Hoechst or DAPI (blue). *p<0.05, **p<0.001.*

Hippocampal NSC proliferation and neurogenesis dramatically decreases with age, such that even by 7 months of age in the mouse, the numbers are almost at their lowest (Ben Abdallah, Slomianka et al. 2010), and the NSC niche already expresses inflammatory markers (Kalamakis, Brune et al. 2019). Recently, it has been proposed that a major factor driving reduced neurogenesis during aging is an increased time spent in quiescence, suggesting that vimentin KO animals may sustain a faster decline in proliferation and neurogenesis during aging (Kalamakis, Brune et al. 2019). To measure the differences in adult neurogenesis at different ages, we performed 4 EdU injections once per day for four days in 7 weeks-old, 5 month-old, or 9 month-old WT and vimentin KO littermates prior to perfusion. We found that vimentin KO mice exhibit a faster age-dependent decline in NSC proliferation (EdU+) and neurogenesis (DCX+), but display similar numbers of NSCs (Sox2+/S100β-) (Fig. 4.8F-K), suggesting that vimentin KO NSCs have difficulty exiting quiescence, and further supporting a role for vimentin in NSC quiescence exit.

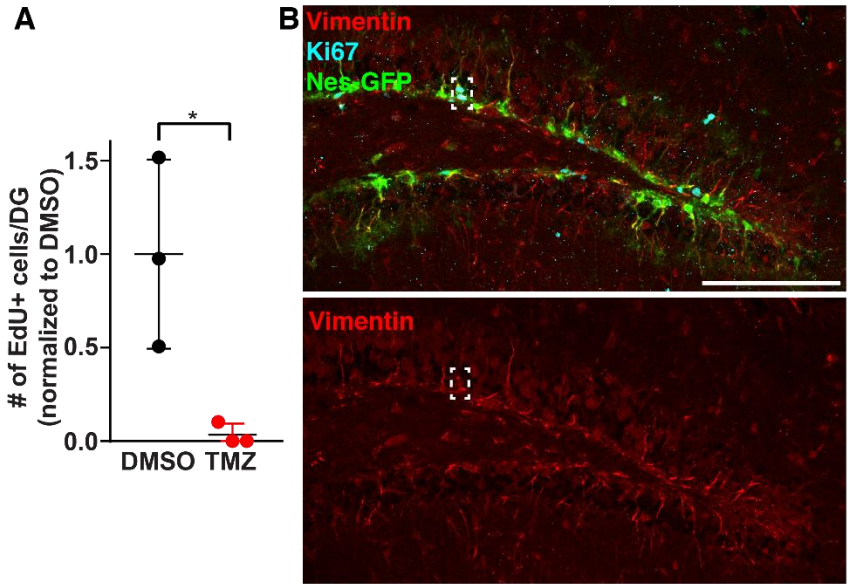

Figure 4.9. *A) WT mice were injected i.p. with DMSO (black bar) or 25 mg/kg TMZ (red bar) once per day for 3 consecutive days. They were allowed to recover for 2 hours before being injected with 50 mg/kg EdU once, and then were sacrificed 3 hours following the EdU injection and analyzed for proliferative (EdU+) NSCs. (n=3, Student's t-test; mean ± SD). B) 7 week old Nestin-GFP mouse brain sections were immunostained for GFP (NSCs; green), vimentin (red) and Ki67 (cyan). Scale bar, 100 µm. *p<0.05.*

4.5 Discussion

We show here that NSCs respond to impaired proteostasis by making an aggresome surrounded by a vimentin cage that is enriched with proteasomes. Vimentin is necessary for the spatial localization of proteasomes to the aggresome, and in its absence, in response to a loss of proteostasis, NSCs have increased protein aggregates, increased dependence on lysosomes, and decreased proliferation. While qNSCs have increased levels of protein aggregates, vimentin does not respond to this increase until the cell begins to transition to an activated state, whereby it is upregulated and forms a cage during interphase, followed by a asymmetric inheritance of vimentin, proteasomes and polyubiquitin in the first division exiting quiescence. In the absence of vimentin in vitro, qNSCs have a reduced ability to clear aggregated proteins and re-enter the cell cycle. Inhibition of autophagy in vimentin KO NSCs during activation fully prevents quiescence exit, suggesting proteasomes and autophagy work together to remove accumulated proteins that must be degraded during quiescence exit. In vivo, vimentin KO qNSCs have a decreased ability to exit from quiescence following a stimulus, and also during the early stages of aging. Importantly, we have shown that vimentin acts as an organizer for proteins that regulate cellular proteostasis, suggesting its cage formation at the aggresome localizes these proteins to the area where they are most needed. Taken together, this suggests a novel endogenous role for aggresomes during NSC quiescence exit, and for vimentin as a critical regulator of cellular proteostasis in NSCs.

The intermediate filament network

Vimentin was initially largely overlooked when a study reported that vimentin KO mice displayed no obvious phenotype (Colucci-Guyon et al., 1994), a surprising result considering vimentin's dynamically regulated expression across the body throughout development. However, subsequently many papers have demonstrated that vimentin is indeed important, but primarily in the context of the proper challenge, such as following a reduction in renal mass, severe mechanical stress in the retina, and in fibroblasts during wound healing (Lundkvist et al., 2004, Terzi et al., 1997, Cheng et al., 2016). Our study confirms that vimentin is not important for normal NSC function, however it is critical for recovery following cellular stresses that disrupt proteostasis.

Cells can express multiple IFs, and the composition varies between cell types. NSCs primarily express GFAP, nestin, and vimentin, all of which we find localized at the aggresome (Fig. 4.5R) as these proteins form heteropolymeric IFs, and display interdependence (Leduc and Etienne-Manneville, 2017, Robert et al., 2016). For example, nestin KO mice still express both vimentin and GFAP (Wilhelmsson et al., 2019), whereas GFAP is disrupted (Galou et al., 1996) and nestin is unable to polymerize in vimentin KO astrocytes and NSCs, respectively (Park et al., 2010). We have found in our vimentin KO NSCs that both nestin and GFAP do not form full length filaments (Fig. 4.5B), and GFAP has reduced expression. There also appears to be no compensation by any other IFs. Together, these findings suggest vimentin may be the critical regulator of this IF network in NSCs; however, the loss of the IF network in vimentin KO NSCs and interdependence of IF proteins make it difficult to determine

whether the effects we observe in vimentin KO NSCs are specific to the loss of vimentin, as opposed to nestin and/or GFAP.

Vimentin and protein degradation

Proteasomes previously have been reported at aggresomes and inclusion bodies, however, until now the mechanism driving this localization has not been clear (Schipper-Krom et al., 2014, Fabunmi et al., 2000, Ogrodnik et al., 2014, Wigley et al., 1999). We have demonstrated that vimentin is necessary for proteasome localization to the aggresome (Fig. 4.4D-F); yet it has not been clear what functional role the proteasomes play at the aggresome when the polyubiquitinated proteins there are thought to be largely aggregated and cleared through autophagy. Here we demonstrate that if ubiquitinated proteins are unable to be degraded, the system becomes overwhelmed, resulting in a time-dependent delayed increase in protein aggregates (Fig. 4.4M). Thus, the localization of proteasomes to the centrosomal region may assist in degrading polyubiquitinated proteins that are trafficked to the aggresome (Fabunmi et al., 2000).

Are these proteasomes at the aggresome functioning or clogged? Some studies have suggested that proteasomes are unable to function at the aggresome (Verhoef et al., 2002, Bennett et al., 2005), and yet others find they are still actively processing substrate (Schipper-Krom et al., 2014, Ogrodnik et al., 2014, Verdoes et al., 2006). These mixed results may likely be substrate specific, such that certain aggregation-prone proteins may reduce proteasome function, but not all. Another potential function of proteasomes may be through Poh1, a proteasomal deubiquitinating enzyme that

cleaves ubiquitin from proteins prior to substrate processing, releasing free ubiquitin chains when processing, which has been shown to drive the activation of HDAC6 and aggresome clearance, creating a crosstalk between the ubiquitin-proteasomal system and autophagy (Hao et al., 2013). We have found that the inability to localize proteasomes to the aggresome results in a reduced ability to recover from proteostasis, despite the cells' response of increasing lysosomes due to this imbalance (Fig. 4.4Q, 4.5N-Q), further suggesting a role for active proteasomes at the aggresome.

Are the effects of vimentin KO in NSCs specific to proteasome localization to the aggresome? Our mass spectrometry data suggest that there are likely other proteins that vimentin delivers to the aggresome such as chaperone proteins and ribosomal proteins, all taking part in the delicate balance of protein synthesis, refolding, and degradation (Fig. 4.4C). Future studies should more fully explore the interaction between vimentin and these proteins and identify whether the effects we observe are dependent on just one, or many of the proteins that vimentin may be responsible for organizing at the aggresome.

Interestingly, we did not find any autophagic proteins interacting with vimentin either directly or indirectly (Fig. 4.4C). Previously, it has been reported that vimentin may play a role in lysosomal positioning at the aggresome (Biskou et al., 2019), however, vimentin KO was not performed in that context to confirm these results. We have found that vimentin KO in NSCs does not affect lysosomal positioning following a loss of proteostasis (Fig. 4.5S). However, as discussed above, autophagy and the ubiquitin-proteasome system are likely both required for proper function, as disruption of

any protein degradation system will ultimately lead to global effects on proteostasis and influence the other.

Thus, we have found that vimentin is necessary to localize proteasomes to the aggresome, and its absence results in an imbalance in the protein degradation processes in NSCs, leading to an increased number of protein aggregates, an increase in lysosomes, and yet a reduced ability to recover from a disruption of proteostasis.

The role of vimentin in NSC quiescence exit

qNSC activation has become increasingly recognized as one of the critical barriers to neurogenesis (Kalamakis et al., 2019). Recently, Leeman et al showed that one key component driving qNSC activation is a shift in proteostasis, where a wave of aggregated proteins (Proteostat) are cleared (Leeman et al., 2018). Induction of autophagy enhanced clearance of these aggregated proteins and increased the rate of qNSC activation, suggesting a direct connection between a qNSC's ability to activate and the ability to clear aggregated proteins (Leeman et al., 2018). Our study further validates the findings that qNSCs carry an increased load of Proteostat+ aggregated proteins, here in hippocampal NSCs (Fig. 4.6B), and provides a mechanism of aggresome formation as a means for qNSCs to turn up protein turnover for efficient qNSC activation (Fig. 4.6C). Identifying the differences or upstream regulators that drive the changes in vimentin expression and response will be critical to understand the processes instructing NSC quiescence exit.

During aging, NSCs have a decreased ability to exit quiescence (Kalamakis et al., 2019, Ziebell et al., 2018, Leeman et al., 2018). While other regions of the body, and

indeed other stem cell niches experience changes with aging in rodents at more advanced ages such as 18-24 months, hippocampal NSCs show decreases in proliferation as early as 2 months, which saturate by 9 months (Ben Abdallah et al., 2010, Cho et al., 2008, Lukjanenko et al., 2019). Indeed, recently, it was shown that already by 7 months of age in the rodent (with 2 months being the next earliest time point tested), inflammatory markers were significantly increased in the neurogenic niche, which further maintained NSCs in quiescence (Kalamakis et al., 2019). In our study, we used vimentin KO mice (129S1/SvImJ) (Colucci-Guyon et al., 1994), a strain that has very low neurogenesis basally (Clark et al., 2011), to identify the role of vimentin in quiescence exit in vivo. We find that NSC proliferation and neurogenesis decline more rapidly in vimentin KO animals, further supporting a role for vimentin in regulating quiescence exit in vivo (Fig. 4.8C-K).

Asymmetric segregation of vimentin during mitosis

In the first divisions following quiescence exit, vimentin is strongly asymmetrically inherited with proteasomes and K48pUb to one of the daughter NSCs (Fig. 4.6F-G, 4.7F-K). Previously we have reported that asymmetric inheritance of vimentin during mitosis was correlated with altered proliferation, suggesting a negative effect on the inheriting daughter (Moore et al., 2015). Besides our finding that proteasomes are localized to vimentin for this asymmetric inheritance, our mass spectrometry data suggest that many additional proteins bound to vimentin could be asymmetrically inherited, potentially impacting each daughter in unique ways (Fig. 4.4C). One scenario may be that the inheriting daughter may need more time to degrade the aggregates and

polyubiquitinated proteins, reducing the proliferation rate in that cell to allow it to recover, if possible. Future studies identifying all protein cargoes asymmetrically inherited, as well as long-term timelapse in vitro or in vivo following this segregation will be needed to better understand the functional outcome of this inheritance. Importantly, we find that asymmetric inheritance of vimentin during mitosis requires interphase formation of the aggresome (Fig. 4.2E-G), establishing part of the upstream mechanisms regulating the mitotic asymmetric segregation of vimentin.

Taken together, our study provides insight into the two-decade old question of vimentin's function at the aggresome, demonstrating its role as an organizer of proteostasis-related proteins to the aggresome, and a critical regulator of cellular proteostasis in NSCs. We have further provided a function for aggresomes within a biological system, as a program that NSCs utilize to clear protein during qNSC activation. Our findings pave the way for future studies aimed at understanding the mechanisms driving vimentin cage formation, the significance of vimentin asymmetry during mitosis as a mechanism of stem cell regulation, and the application of our findings to other cell types and diseases.

4.6 Materials and Methods

Mice

In this study, male and female mice between the ages of 6 weeks and 9 months were used. Nestin-GFP mice were obtained from Xinyu Zhao (UW-Madison) which were developed by Kensaku Mori's laboratory (Yamaguchi, Saito et al. 2000). 129S-Vimtm1Cba/MesDmarkJ and C57BL/6J mice were obtained from The Jackson

Laboratory. All techniques associated with animals are described in further detail in the "Method Details" section of this document. All facilities and protocols for animal work were approved by the Research Animal Resources and Compliance (RARC) at UW-Madison. Animals had *ad libitum* access to food and water and were kept under a 12hr light-12hr dark cycle. All procedures were performed in strict accordance with all federal and institutional policies.

Cell Lines

All cell lines (aside from HEKs discussed in the viral particle generation part of the methods) in this study were NSCs derived from ~6 week old male C57BL/6 mouse hippocampi. Cultures were grown at 5% CO_2 at 37°C. Cultures were periodically tested for mycoplasma to ensure no contamination was present. More detail on specific experiments and techniques used to maintain these cell lines is listed below in the "Method Details" section.

NSC Dissection and Culture

NSCs were obtained by pooling cells extracted from the hippocampi of approximately 3-5 mice around 6 weeks old, similar to a previously described protocol (Moore, Pilz et al. 2015). Hippocampi were dissected in cold HBSS and dissociated using the GentleMACS Dissociator (Miltenyi Biotec) and MACS Neural Tissue Papain Dissociation Kit (Miltenyi Biotec 130-092-628) using the manufacturer's protocol with added myelin removal. NSCs were cultured as described previously (Moore, Pilz et al. 2015). Activated NSCs (aNSCs) were cultured with 37°C/5% CO2 in serum-free media:

DMEM/F12 GlutaMax (Invitrogen 10565018) with penicillin-streptomycin-fungizone (1:100, Invitrogen 15140122), B27 (1:50, Invitrogen 17504044), and 20 ng/mL FGF-2 and EGF (PeproTech 100-18B and AF-100-15). Cells grown as monolayers were additionally given 5ug/mL Heparin (Sigma H3149).

For imaging experiments, aNSCs were plated onto poly-L-ornithine (PLO; 10 µg/mL plastic, 50 µg/mL glass, Sigma P3655) and laminin (5 µg/mL, Sigma L2020) coated cuvettes (Fisher Scientific 12-565-337 or Ibidi 80826-G500). Cell culture dishes reaching confluency were trypsinized and split into lower densities using previously described methods (Moore, Pilz et al. 2015). Briefly, single cells were spun down at 120xg for 4 minutes, resuspended in 0.05% trypsin (Invitrogen 25300-054) in Versene (Thermo Fisher 15040066) and placed at 37°C for 5 minutes. Twice the volume of trypsin inhibitor (Sigma T6522) was added for 2 minutes, cells were mechanically triturated, and then cells were spun again at 120xg for 4 minutes before being resuspended in media and plated onto new dishes.

Quiescent NSCs (qNSCs) were cultured using a previously established protocol (Mira, Andreu et al. 2010, Martynoga, Mateo et al. 2013, Knobloch, Pilz et al. 2017) similarly to aNSCs with the exception of the removal of EGF and the addition of 50 ng/mL BMP-4 (Fisher Scientific 5020BP010). All qNSC experiments were cultured in qNSC medium on PLO- and laminin-coated wells for at least 3 days before performing quiescence experiments. For experiments observing quiescence exit, after at least 3 days of BMP-4 treatment the media was changed back to proliferation media (-BMP-4, +FGF, +EGF).

Transfections

Electroporations were performed on 4 million trypsinized NSCs resuspended in Mouse Nucleofector solution (Lonza VPG-1004) with 7 µg of Endotoxin-free DNA using the Mouse Neural Stem cell program in the Nucleofector II machine (Lonza). Electroporations were plated immediately onto glassware coated with PLO and laminin with a media change 24 hours later to remove dead cells. In overexpression experiments of varying aggregation-prone proteins, cells were imaged 24-48 hours after electroporation.

Molecular Cloning and Constructs

For design and delivery of guide RNAs (gRNAs) we used the tool at crispr.mit.edu to choose gRNA sequences, and cloned identified sequences (Table 4.1) into pSpCas9(BB)-2A-Puro (PX459) V2.0, (Addgene #62988) or pSpCas9(BB)-2A-GFP (PX458) (Addgene #48138) using a previously established cloning protocol for this vector (Ran, Hsu et al. 2013).

Table 4.1 – gRNA sequences

Name	**Purpose**	**Sequence**
Nontargeting	Control gRNA	GCGAGGTATTCGGCTCCGCG
Vimentin 1	Creating vimentin KO NSCs	CGGGTCACATAGGCGCCACC
Vimentin 2	Creating vimentin KO NSCs	GTGGCTCCGGCACATCGAGC
Vimentin 3	Creating vimentin-mNeon NSCs	GTGGCTCCGGCACATCGAGC

The vimentin-mNeon homology directed repair template was constructed by performing a four piece Gibson assembly (NEB E5510S) to ligate homology arms corresponding to vimentin's carboxyl terminus with a linker sequence (GGTGGTGGCGGTTCAGGCGGAGGTGGCTCTGGCGGTGGCGGATCG) and mNeon fluorophore sequence (Allele Biotechnology) into pENTR4-HaloTag w876-1 (Addgene #29644). To construct CMV-HttQ119-eBFP, eBFP was PCR amplified from CMV-eBFP-2A-H2B-eGFP (gift from Dr. Murray Blackmore) and ligated into CMV-HttQ119-eYFP (gift from Dr. Harm Kampinga). To construct CAG-BFP-VHL, a four piece Gibson assembly was performed ligating eBFP from CMV-eBFP-2A-H2B-eGFP, VHL-WPRE from pESC-LEU-GFP-VHL (Addgene #21053) and a linker between VHL and BFP into a CAG-GFP-PRE vector (Kaganovich, Kopito et al. 2008). Tdp43-eGFP (Addgene #28197) and GFP-Ubiquitin (Addgene #11928) were obtained from Addgene (Dantuma, Groothuis et al. 2006, Yang, Tan et al. 2010). The CAG-mNeon vector was a gift from Dr. Erik Dent.

Generation of CRISPR Mutant Model Cell Lines

CRISPR/Cas9-based mutant NSCs harboring vimentin-mNeon were generated by electroporating 4 million NSCs with the construct pSpCas9(GAATAAAAATTGCACACACT)-2A-Puro (PX459) V2.0 harboring an expression cassette for a gRNA targeting vimentin's carboxyl terminus and Cas9 (3.5 µg), as well as pENTR-vimentin-mNeon harboring a template for repairing vimentin's endogenous locus with the insertion of a linker peptide sequence and an mNeon fluorophore (3.5 µg) as described in the transfection section of the methods. Seven to ten days after electroporation, a pool of vimentin-mNeon NSCs were isolated through

fluorescence-activated cell sorting (FACS) using a BD FACSAria high speed cell sorter. CRISPR/Cas9-based vimentin KO NSCs were generated by electroporating NSCs with two gRNAs (CGGGTCACATAGGCGCCACC and GTGGCTCCGGCACATCGAGC) targeting vimentin's amino terminus in the backbone. NSCs were single cell sorted using a BD FACSAria high speed cell sorter into a plastic flat-bottomed 96 well plate coated with PLO and laminin, and allowed to expand for approximately one month. Approximately 20.83% of these clones survived, and were initially screened for vimentin protein expression by immunostaining for vimentin on a duplicated plate. Clones with a lack of vimentin filaments by immunostaining were further validated for vimentin KO by a western blot. Alongside vimentin KO NSCs, a control strain was generated by treating NSCs with a non-targeting (NT) gRNA (GCGAGGTATTCGGCTCCGCG) that were similarly sorted and expanded. All experiments with vimentin KO and NT NSCs are examining a pooling of 3 full vimentin KO or NT clones.

Microscopy/Live Cell Imaging

All images displayed in this study were taken using either a Nikon C2 confocal microscope or a Zeiss widefield epifluorescent microscope. Live cell time-lapses were performed on the Nikon C2 confocal with humidity, CO_2 and temperature control. Typically, imaging of NSCs involved 1 µm step sizes with total stack size ranging from 10-20 µm. Live cell time-lapses typically had images collected every 8 minutes to ensure no divisions were missed unless otherwise noted.

Differentiation Assays

For assessing the ability of NSCs to differentiate in different conditions, aNSCs were plated at a seeding density of 50,000 per one well on a 12 well cuvette (Fisher Scientific 12-565-337). 24 hours later FGF, EGF and heparin were removed from the media and cells were fed with this differentiation media every other day for two weeks. After two weeks, cells were fixed and stained for MAP2ab (neurons) and GFAP (astrocytes). A blinded observer counted the total number of MAP2ab or GFAP positive cells in 10 images of three technical replicates per condition. The experiment was repeated three times on three different days.

Motility Assays

To determine if there were any differences in the migratory behaviors of NSCs in any conditions listed in the text, we performed live cell imaging of NSCs in different conditions acquiring a single image every 5 minutes and used the “manual track” plug-in in FIJI to assess average velocity and total distance traveled over the course of the timelapse. At least 30 cells were traced for each condition for as long as possible before the timelapse ended or the cells were lost. The experiment was repeated three times on three different days.

Proteasome Activity Assays

To measure proteasome activity in protein lysates of NSCs in different conditions we adapted a protocol from Vilchez et al (Vilchez, Boyer et al. 2012). Cells were cultured as described in the text and then pelleted. Immediately cells were resuspended in proteasome activity buffer (50mM Tris-HCl, pH 7.5, 250mM sucrose, 5mM $MgCl_2$, 0.5mM

EDTA and 1mM dithiothreitol) and lysed by passing through a 27-gauge needle ten times. Lysates were clarified by centrifugation at 15,000xg for 10 minutes at 4°C. Protein concentration was quantified using the DC protein assay (Bio-Rad 5000112). 15-25 µg of protein were loaded into wells in a flat bottom 96 well plate for the assay. Each well received the same amount of protein, 2 mM adenosine triphosphate (Fisher ICN15026605), 0.37 mM proteasome substrate (caspase – Z-Leu-Leu-Glu-AMC (Enzo BML-ZW9345), chymotrypsin – Suc-Leu-Leu-Val-Tyr-AMC (Enzo BML-P802), trypsin – Boc-Leu-Arg-Arg-AMC (Enzo BML-BW8515)), and then diluted to a final volume of 100 µL per well with proteasome activity buffer. Plates were immediately placed in a plate reader set to excite at 380 nm and collect 460 nm, taking a datapoint every 5 minutes for 1 hour at 37°C. Three 96-well reactions were averaged for each technical replicate, repeated on three separate days. For each substrate that was loaded in the plate a reaction was set up with no protein and subtracted from each experimental well.

Detecting vimentin cage formation in response to treatment with different cellular stressors

To determine doses of drugs used to stress NSCs, a dose response curve was utilized to determine lethal doses and timings with each drug. Cells were treated with MG132 (Sigma M7449), chloroquine (Sigma C6628), etoposide (from UW-Madison oncology department), thapsigargin (Sigma), 5-fluorourucil (from UW-Madison oncology department), and tunicamycin (Sigma) as indicated in the text. Cells were heat shocked at 45°C for 20 minutes. All experiments involving stressed cells were performed on monolayers plated on PLO and laminin at a starting density of 50,000 cells per well of a

4 well cuvette (Fisher Scientific 12-565-337). NSCs in each condition were imaged in their entirety with a 1 µm step size – 10 images per condition with three technical replicates per condition. For quantitating the presence of vimentin cages in response to cellular stress we defined a cell as having a vimentin cage if >50% of its vimentin was localized to the nuclear bay in a tight cage-like conformation. Cages were counted manually by a blinded observer that was instructed on this definition analyzing data from 3 experiments completed on three different days.

Quantitating Asymmetry in vimentin-mNeon NSCs based on prior cage formation in interphase

To assess asymmetry of vimentin during mitosis in the presence or absence of a vimentin cage being formed in interphase, we performed live cell imaging of vimentin-mNeon NSCs either in untreated conditions, or 12 hours after a heat shock, taking an image every 8 minutes with 1 µm step size. Divisions were categorized into two categories based on if the NSCs (1) had a cage or (2) did not have a cage in interphase before mitosis occurred. For each of these two bins, asymmetry was quantified by drawing a region of interest (ROI) around each daughter cell in late anaphase and placing the inheritance of the daughter with more vimentin normalized to area over the sum of the total vimentin in the division normalized to area to create an asymmetry ratio.

Proteostat Staining

For assays involving labelling with the dye Proteostat (Enzo 51035-K100), NSCs were fixed with 4% paraformaldehyde for 15 minutes at room temperature. NSCs were

permeabilized with 0.5% Triton and 3 mM EDTA in PBS for 30 minutes at room temperature, and then stained with Proteostat 1:10,000 in PBS for 30 minutes at room temperature. Proteostat was washed twice with PBS for 10 minutes at room temperature. To quantify changes in Proteostat labeling across different treatments, we instructed a blinded observer to count the number of puncta present in each individual cell. For each condition, 10 images of at least three technical replicates were quantified.

Lysotracker Staining

For labeling NSC lysosomes with the dye Lysotracker, we incubated NSCs in medium with 1:1000 LysotrackerRED (Thermo L7528) for 20 minutes with 2 µM Hoechst at 37°C. Cells were washed twice with warm media before imaging immediately. For analysis of Lysotracker staining in different conditions, raw integrated density was measured in a region of interest (ROI) drawn by a blinded observer around each cell using Fiji. Either 10 images of at least 3 replicates were fully counted or at least 300 cells per replicate were analyzed. Each Lysotracker experiment was repeated at least 3 times.

Calcein Live Cell Staining

Calcein AM (Invitrogen L3224) was diluted 1:1,000 with 2 µM Hoechst in NSC media and applied to living cells for 15 minutes at 37°C. Cells were immediately imaged after 15 minutes. For quantification of calcein, 10 images were taken randomly throughout each well of each of 3 technical replicates. For every image in each condition, calcein positive cells were counted by a blinded observer. The experiment was repeated 3 times.

Graphs depict 3 technical replicates from one repeat that are representative of the observations of the other replicates completed on different days.

mNeon co-immunoprecipitation/Mass spectrometry

20 million vimentin-mNeonGreen NSCs that were (1) treated with 0.05% DMSO for 4 hours, (2) treated with 5 µM MG132 for 4 hours, or (3) WT NSCs overexpressing mNeon for 72 hours and treated with 0.05% DMSO for 4 hours were pelleted, and resuspended in lysis buffer (10 mM TrisHCl, 150 mM NaCl, 0.5 mM EDTA, 0.5% NP-40) for 30 minutes. Lysates were incubated with mNeonGreen TRAP-A Linked Agarose Beads (Chromotek, nta-20) for 1 hour. Beads were subsequently pelleted and washed with dilution/wash buffer (10 mM TrisHCl, 150 mM NaCl, 0.5 mM EDTA). Bound proteins were eluted by incubation with 0.2M glycine pH 2.5 followed by neutralization with 1M Tris pH 10.4. Protein samples were reduced with 10 mM DTT for 30 minutes at 37°C, alkylated in the dark with 55 mM indole-3-acetic acid for 45 minutes at 37°C, and digested overnight at 37°C with two 0.5 µg Sequencing Grade Trypsin (Promega PRV5111) additions throughout the incubation. The digest reaction was stopped by acidification.

For LC/MS/MS, digested samples were subsequently dried on a speed vac, and processed with ZipTip (Millipore ZTC18S096) according to the manufacturer's protocol. Desalted peptides were dried under nitrogen, and resuspended in Buffer A (0.1% formic acid/water) and Buffer B (0.1% formic acid in acetonitrile). Samples were transferred to a Total Recovery Vial (Waters 186005663CV) and run on a 120 minute increasing AcN gradient, using top 10 MS/MS Q Exactive methods with 5 second dynamic exclusion enabled. A blank injection was run in-between samples to minimize carryover. Protein

identification, quantification, and analysis were done with Proteome Discoverer 1.4/2.2, SEQUEST HT, and MASCOT using Uniprot mus_musculus protein database. A decoy database was added to each search to establish control variability and false discovery rates.

For analysis of the LC/MS/MS data, genes appearing at least once in 3 technical replicates were pooled together to make one list of genes for each experimental condition. Genes appearing in any of the three control IP conditions (mNeon overexpression) were removed from the list of genes that were pulled down by vimentin in experimental conditions. All genes appearing in any of each replicate of vimentin-mNeon MG132 treated cells were put into String and used to generate gene ontology maps (Szklarczyk, Franceschini et al. 2015).

Immunostaining

Immunostaining for vimentin (1:1000, Sigma Aldrich AB5733), α5 subunit of the proteasome (1:500, Abcam ab189855), phosphohistone H3 (1:500, Abcam 14955), K48pUb (1:500, Millipore Sigma 05-1307-AF488) and Ki67 (1:500, Abcam ab15580) was performed using the following protocol. Cells were fixed in 4% PFA for 15 minutes at room temperature and then permeabilized in 0.25% triton in PBS for 30 minutes at room temperature. Cells were blocked with 20% donkey serum (Millipore Sigma S30) in antibody buffer (150mM sodium chloride, 50mM tris base, 1% bovine serum albumin, 100mM L-lysine, 0.04% sodium azide, pH 7.4) for 1 hour at room temperature (Moore, Blackmore et al. 2009). Primary antibodies were incubated in antibody buffer overnight at 4°C. The following day cells were washed with PBS three times, 10 minutes per wash, at

room temperature. Secondary antibodies were diluted 1:500 in antibody buffer and incubated on cells for 1.5 hours at room temperature. Cells were washed with PBS three times, 10 minutes per wash, at room temperature. To stain nuclei, either Hoechst (2 µM, Thermo 62249) or DAPI (2 µM, Invitrogen D1306) diluted in TBS, were added during one of the wash steps following secondary antibody incubation for 10 minutes.

Immunostaining for MAP2ab (1:500, Sigma M2320), GFAP (1:500, Dako Z0334), nestin (1:500, Thermo MA1110), and pericentrin (Abcam ab4448) were performed using the following protocol. Cells were fixed in 4% PFA for 15 minutes at room temperature and then permeabilized and blocked in 0.25% triton and 3% donkey serum (Millipore Sigma S30) in TBS (TBS++) for 30 minutes at room temperature. Cells were incubated in TBS++ with primary antibody diluted 1:100 overnight at 4°C. The following day cells were washed in TBS three times, 5 minutes per wash, at room temperature, followed by TBS++ for 15 minutes at room temperature. Secondary antibodies were diluted 1:500 in TBS++ and incubated with cells for 1 hour at room temperature. Cells were washed with TBS three times, 10 minutes per wash, at room temperature.

For immunostaining free-floating brain slices with Doublecortin (1:250, Cell Signaling Technology 4604S), SOX2 (1:250, Santa Cruz sc-17320) and S100β (1:250, Abcam ab52642), slices were washed 3 times for 5 minutes with TBS in net wells at room temperature, and blocked for 30 minutes at room temperature in TBS++ while shaking. Sections were then incubated overnight in primary antibodies diluted in TBS++ while shaking without nets. The next day, sections were washed 2x for 10 minutes with TBS in net wells while shaking, and incubated for 1 hour 30 min in secondary antibodies (1:250) diluted in TBS++ shaking without nets. After secondary incubation, sections were washed

2x for 5 minutes, incubated with DAPI (1:5000 in TBS) for 5 minutes shaking at room temperature, washed 2x for 5 minutes, and mounted on electrostatically treated slides.

For immunostaining brain slices with GFP (1:250, Abcam ab5450), vimentin (1:250, Sigma-Aldrich AB5733) and Ki67 (1:250, Abcam ab15580), 40 µm cryosections from perfused male and female 7 week old Nestin GFP mice were prepared. Sections were fixed for 15 minutes at room temperature in 4% PFA and then blocked in TBS++ for 30 minutes at room temperature. Sections were then incubated overnight in primary antibodies diluted in TBS++. The next day, sections were washed 2x for 10 minutes with TBS, and incubated for 1 hour 30 min in secondary antibodies (1:250) diluted in TBS++. After secondary incubation, sections were washed 2x for 5 minutes, incubated with DAPI (1:5000 in TBS) for 5 minutes.

In vitro EdU pulses

Cells in S-phase were labeled by a 1 hour incubation with 10 µm EdU (Invitrogen C10337) at 37°C. NSCs were fixed in 4% PFA for 15 minutes at room temperature. Visualization of EdU was achieved using a Click-it kit (Invitrogen C10337) for performing click chemistry as described in the manufacturer's protocol. For quantification of all EdU pulses, either 10 images of at least 3 replicates were fully counted or at least 300 cells per replicate were counted by a blinded observer. Each EdU experiment was repeated at least 3 times.

Proximity Ligation Assay

To perform the proximity ligation assay we used Sigma's DuoLink Proximity Ligation assay kit (Millipore Sigma DUO92101-1KT). Cells were fixed and stained as described in the immunostaining section of the methods for vimentin and proteasomes through the primary incubation step, this time using a mouse vimentin antibody (Abcam ab20346; 1:1,000). After overnight incubation with primary antibodies, NSCs were washed with buffer A from the kit twice for 5 minutes at room temperature. PLUS and MINUS probes were diluted in antibody buffer (see immunostaining section of methods) 1:5 and then applied to NSCs for 1 hour at 37°C. NSCs were washed with buffer A from the kit twice for 5 minutes at room temperature. 1xDuoLink Ligation Buffer (diluted in water) and ligase diluted 1:40 were applied to NSCs for 30 minutes at 37°C. NSCs were washed with buffer A from the kit twice for 5 minutes at room temperature. 1x DuoLink Amplification Buffer (diluted in water) with polymerase diluted 1:80 was applied to NSCs for 100 minutes at 37°C. NSCs were washed with buffer B from the kit twice for 10 minutes at room temperature and stained with Hoechst as described in the immunostaining section of the methods.

Western blot

Soluble protein fraction preparations: Frozen cell pellets were thawed on ice and resuspended in radioimmunoprecipitation assay (RIPA) buffer (150 mM NaCl, 1mM ethylenediaminetetraacetic acid (EDTA), 1% NP-40, 50 mM Tris pH 7.6). The resuspended samples were spun in a tube rotator (VWR) at 18 rpm for 20 minutes at 4°C. Spun samples were sonicated for 1 minute at room temperature using an ultrasonic bath (Branson) set at 5 degas/minute. Centrifugation was performed at 15,000xg (Beckman

Coulter) for 15 minutes at 4°C. Following centrifugation, supernatants were collected and protein concentrations of the cell lysates were measured using the DC Protein Assay (Bio-Rad 5000112) and a BioMate 3 Spectrophotometer (Thermo Fisher Scientific) at 750 nm.

Total (insoluble and soluble – for polyubiquitin blots) protein fraction preparations: To prepare total protein fractionation lysates we adapted the protocol used by Leeman et al *(21)*. NSC pellets were resuspended in 150 mM sodium chloride (Sigma S9625), 4% SDS, 50 mM N-ethylmaleimide (Invitrogen 23030), 25mM TCEP (Invitrogen 77720) (Total fraction buffer –TFB) and lysed by passing through a 27 gauge needle ten times. Cells were sonicated at 40 kHz for 5 minutes in a water bath sonicator (Branson 2510 Ultrasonic Cleaner). Resulting lysate was spun down at 15,000xg for 10 minutes at 4°C. Protein concentrations were determined using the DC protein assay (Bio-Rad 5000112). 20-30 µg of sample was loaded into each well for polyacrylamide gel electrophoresis.

Lysates were heated for 10 minutes at 90°C, loaded at 30 µg and run on 4-20% SDS-PAGE gels (Bio-Rad) for 45mins at 150V. Proteins were transferred onto PVDF membranes (Bio-Rad) at 100V for 90 minutes at 4°C. 5% milk in 0.25% triton and 3% donkey serum (Millipore Sigma S30) (TBS-T) was used to block the membranes unless otherwise noted. To detect the presence of specific proteins, the membranes were incubated overnight (rotating at 4°C) in the appropriate primary antibodies diluted per manufacturer recommendations in either 5% Milk in TBST unless otherwise noted – see antibodies below. The membranes were washed 3x (10 minutes each) in 1x TBS-T at room temperature. Blots were then incubated at room temperature in block solution with secondary antibodies listed below at room temperature for 90 minutes. Membranes were

again washed three times for 10 minutes with TBS-T before probing the membrane with a SuperSignal femto (Thermo 34095) or pico (Thermo 34577) kit. Primary antibodies were used as follows: β-actin (Bio-rad VMA00048 – 1:1,000), vimentin (Cell signaling 5741S – 1:1,000), polyubiquitin/FK1 (Enzo BML-PW8805 – 1:1,000 in BSA), LC3B (Abcam ab48394 - 1:1,000). Polyubiquitin western blots required a 5% BSA block instead of milk in all steps. Secondary antibodies conjugated to horseradish peroxidase (HRP) used were α-chicken (Promega G1351 – 1:1,000), α-rabbit (Bio-Rad 1706515 – 1:3,000), α-mouse (Bio-Rad 1706516 – 1:3,000). Images were taken using a UVP Imaging system (UVP) to detect protein bands at exposures set so that bands were below saturation.

To quantify western blot protein bands, a region of interest was drawn around each correctly sized band in Fiji to measure raw integrated density. Each integrated density was normalized to each sample's β-actin control and then had background subtracted before comparing across conditions. Graphs display the average of three representative technical replicates. All experiments were repeated at least three times on three different days.

mCherry-GFP-LC3 Experiments

HEK293FT cells were cultured in DMEM, high glucose, GlutaMAX Supplement, pyruvate (Thermo 10569044) supplemented with 10% FBS (Invitrogen 16000044), 1X MEM Non-Essential Amino Acids (Thermo 11140050) and 600 µM L-glutamine (Thermo 25030081) at 5% CO_2 and 37°C. For viral particle generation, HEK293FT cells were transfected with pCMV-VSV-G (Addgene #8454), psPAX2 (Addgene #12260) and FUW mCherry-GFP-LC3 (Addgene #110060) using polyethylenimine (PEI; Polysciences, Inc.

23966-1) (Joung, Konermann et al. 2017). Viral particles were harvested 48 hours post transfection and purified by ultracentrifugation as previously described (Moore, Pilz et al. 2015).

WT and vimentin KO NSCs were transduced with LC3-GFP-mCherry at a similar multiplicity of infection (MOI), and allowed to express virus for at least 7 days before performing any experiments. For experiments, 100,000 WT or vimentin KO NSCs in triplicates were treated with either 0.02% DMSO or 2 μM MG132 for 24 hours and then had drug removed for 1 hour before trypsinizing and analyzing GFP and mCherry fluorescence using a BD LSRII flow cytometer. The experiment was repeated 3 times and the data in this manuscript depicts one representative experiment.

Quantitative real time polymerase chain reaction (qRT-PCR)

Table 4.2 – Primers for qrtPCR

Primer Name	**Sequence**
F Psma5	AGTAGCATTGTTGTTTGGAG
R Psma5	CTTCAGAGTCATAGACTTATGG
F18S	GAACTGAGGCCATGATTAAGAG
R18S	CATTCTTGGCAAATGCTTTC
F Vim	CGGCTGCGAGAGAAATTGC
R Vim	CCACTTTCCGTTCAAGGTCAAG

Total RNA for all conditions was collected using an RNeasy Mini Kit (Qiagen). cDNA was synthesized from isolated RNA with iScriptTM cDNA Synthesis Kit (BioRad).

Real time PCR primers sequences from Sigma's KiCqStart® SYBR® Green Predesigned Primers were obtained from Sigma against Psma5, vimentin, and 18S (Table 4.2). qRT-PCR and data analysis were performed on the DNA Engine Opticon 2 System (BioRad). The 20 µl amplification mixture consisted of 2X SYBR Green Premix Ex Taq (Tli RNase H Plus) (Takara Bio), 0.2µM forward and reverse primers, and 4µl of cDNA generated from 1 µg of RNA. Thermal cycling conditions were as follows: 95°C for 1 min; 40 cycles of 94°C for 10s, 60°C for 30s, varying plate read temperatures for 1s; 68°C for 5 min; melting curve from 65°C to 95°C every 0.2°C for 1 sec each; 72°C for 5 min. Plate read temperatures were: 79°C for vimentin, and 81°C for 18S. qRT-PCR products were assessed via melt curve and gel electrophoresis analysis. All reactions were run in triplicate. All data was normalized to 18S RNA levels. Fold changes were calculated using the ΔΔCt method (Livak and Schmittgen 2001).

Quiescent exit timelapse quantifications

To observe vimentin morphology, expression, presence of vimentin cages during mitosis and asymmetry during quiescence and quiescence activation, we plated vimentin-mNeon NSCs at a seeding density of 40,000 NSCs per well of a 4-well cuvette (Fisher Scientific 12-565-337) in aNSC media. 24 hours later quiescence induction began with addition of qNSC media. After 3 days in quiescence media, NSCs were allowed to reactivate by switching back to aNSC media. Quantifications of asymmetry, kinetics of vimentin cage formation and degradation and prevalence of vimentin cage formation were performed by analysis of at least 4 movies of vimentin-mNeon NSCs in either aNSC media or during quiescence exit. To image aNSC cultures to compare to NSCS exiting

quiescence, aNSCs were plated in aNSC medium at densities of 40,000 NSCs per well of a 4-well cuvette (Fisher Scientific 12-565-337) and allowed to sit on to laminin for 24 hours before imaging began. Data displayed were pooled from 4 timelapse experiments.

Quiescent exit proteostasis assays

To observe the efficacy of NSC quiescence exit in a variety of conditions, we seeded aNSCs at 10,000 NSCs per well of a 4-well cuvette (Fisher Scientific 12-565-337). Twenty-four hours later qNSC media was added. Three days after qNSC media was first added, cells were switched back to aNSC media. Forty-eight hours into reactivation after the reintroduction of aNSC media, cells were analyzed by the assays indicated in the main text. Each condition/experiment was analyzed by averaging at least 3 technical replicates and repeating the experiment at least 3 times.

Quiescent exit quantification of vimentin, proteasome and K48pUb asymmetry

50,000 vimentin-mNeon NSCs or vimentin KO NSCs were induced into a state of quiescence in an 8-well cuvette (Ibidi 80826) using BMP-4 and then allowed to exit quiescence. During quiescence exit, when vimentin-mNeon expression came up and asymmetry was observed, cells were fixed and immunostained for K48pUb or proteasomes and then asymmetry was quantitated by measuring the raw integrated density (RID) and area of each daughter cells and then normalizing RID/area and comparing each daughter's inheritance of each cargo respectively. Cell divisions collected represent data from three experiments completed on three different days.

Quantification of K48pUb and Proteostat Overlap

WT NSCs were treated with 5 µM MG132 for 4 hours and then were fixed and immunostained for K48pUb and stained for Proteostat as described in the immunostaining and Proteostat staining sections of the methods. Cells were imaged and then loaded into Imaris, where a colocalization channel was built, thresholded to only analyze punctate signal from Proteostat or K48pUb. For each cell, the percentage of Proteostat signal that colocalized with K48pUb was quantified for Proteostat puncta that were either 1) in the aggresome within the vimentin cage or 2) in the cytosol outside the vimentin cage.

Quantification or Vimentin Cage and Proteostat Overlap

WT NSCs were treated with 5 µM MG132 for 4 hours and then were fixed and immunostained for vimentin and stained for Proteostat as described in the immunostaining and Proteostat staining sections of the methods. Cells were imaged and then loaded into Imaris, where a mask was constructed around the vimentin cage and around the cell body. Proteostat puncta for each cell were then binned into two categories: 1) Proteostat puncta that were touching or within the vimentin cage mask, or 2) Proteostat puncta that were within the cytosol but not touching or within the vimentin cage mask. A percentage was calculated and reported for the number of cells including at least one Proteostat puncta either at or within the vimentin cage. The intensity histogram was generated using Elements.

RNA Sequencing

For total RNA sequencing of vimentin KO or WT NSCs, three pellets of each cell type were spun down at the same time and sent to LC Sciences for total RNA sequencing. Cutadapt (Martin 2011) and perl scripts in house were used to remove the reads that contained adaptor contamination, low quality bases and undetermined bases. Then sequence quality was verified using FastQC (http://www.bioinformatics.babraham.ac.uk/projects/fastqc/). We used Bowtie2 (Langmead and Salzberg 2012) and Tophat2 (Kim, Pertea et al. 2013) to map reads to the genome of Mus musculus (Version: v88). The mapped reads of each sample were assembled using StringTie (Pertea, Pertea et al. 2015). Then, all transcriptomes from 6 samples were merged to reconstruct a comprehensive transcriptome using perl scripts and gffcompare (https://github.com/gpertea/gffcompare/). After the final transcriptome was generated, StringTie (Pertea, Pertea et al. 2015) and Ballgown (Frazee, Pertea et al. 2015) was used to estimate the expression levels of all transcripts.

StringTie (Pertea, Pertea et al. 2015) was used to perform expression level for mRNAs and lncRNAs by calculating FPKM (FPKM=[total_exon_fragments/mapped_reads(millions)×exon_length(kB)]). The differentially expressed mRNAs and lncRNAs were selected with log2 (fold change) >1 or log2 (fold change) <-1 and with parametric F-test comparing nested linear models (p value < 0.05) by R package Ballgown (Frazee, Pertea et al. 2015).

Animals

Male C57BL/6J mice were purchased from The Jackson Laboratory and used for isolating NSCs in *in vitro* experiments and generating *in vitro* vimentin KO NSCs. 7 week-old, 5 month-old, and 9 month-old 129S-Vimtm1Cba/MesDmarkJ (vimentin KO) mice from The Jackson Laboratory were used for *in vivo* vimentin KO experiments. In short, heterozygote mice carrying the mutated allele were intercrossed to produce experimental KO progeny and WT littermate controls. All intercrosses were maintained within the same familial generation. These mice were then genotyped according the strain specific master protocol provided by The Jackson Laboratory (Strain number 025692) through digesting tissue from ear punches, extracting genomic DNA and running a polymerase chain reaction (PCR). Nestin-GFP mice were obtained from Dr. Xinyu Zhao's laboratory (Yamaguchi, Saito et al. 2000).

Mice used in *in vivo* experiments were transcardially perfused with 0.9% saline solution followed by 4% paraformaldehyde (PFA)/0.2M phosphate buffer. Brains were removed, postfixed overnight in 4% PFA, and subsequently stored in 30% sucrose/PBS solution. These brains were then either sectioned into 40 µm thick sections using a sliding microtome and stored in CPS (25% ethylene glycol, 25% glycerol, 0.05M phosphate buffer) or sectioned on a cryostat 40 µm, immediately mounted and then frozen at -80°C. Free-floating sections were immunostained as described above. For analysis, we immunostained, imaged and quantified 2 of 12 total prepared series of slices (10 slices) per staining pair and then calculated the number of cells per dentate gyrus. Due to vimentin's disruption of the GFAP and nestin network, we used S100β as a marker for astrocytes in the subgranular zone of the dentate gyrus.

In Vivo Early Aging Study Paradigm

In the C57BL/6J mouse strain, neurogenesis is observed to decrease to minimal levels by 7 months (Ben Abdallah, Slomianka et al. 2010). Due to even lower levels of neurogenesis in the Vimtm1Cba/MesDmarkJ (vimentin KO) strain (base strain 129S2/SvPas), we used 5 months and 9 months as our early aging timepoints (Colucci-Guyon, Portier et al. 1994). EdU (Life Technologies A10044) was dissolved in 0.9% saline solution at 5 mg/mL. For the aging study, animals received four intraperitoneal (i.p.) injections of EdU (50 mg/kg) once per day for 4 days. On the fifth day (one day after the last EdU injection), the mice were perfused. All injections were administered at the same time each day.

In Vivo Temozolomide Study Paradigm

Temozolomide experiments were adapted from previously established protocols (Garthe, Behr et al. 2009, Knobloch, von Schoultz et al. 2014). Stock solutions of temozolomide (TMZ) (Sigma T2577) were dissolved fresh in DMSO at 25 mg/mL, and further diluted to 5 mg/mL in PBS the day of injections.

No recovery paradigm: Animals received 3 i.p. injections of TMZ (25 mg/kg) or were control injected with DMSO/PBS once per day for 3 days. Two hours following the last injection on the third day, mice received a single injection of EdU (50 mg/kg). Three hours after the last EdU injection, mice were sacrificed and perfused.

Three day treatment, three day recovery paradigm: Animals received 3 i.p. injections of TMZ (25 mg/kg) or were control injected with DMSO/PBS once per day for 3

days, and then left to recover for 3 days. On the third and final day of recovery, animals were injected with a single dose of EdU (50 mg/kg) every 3 hours, 3 times. Three hours after the last EdU injection, mice were sacrificed and perfused.

QUANTIFICATION AND STATISTICAL ANALYSIS

All statistical analyses were performed either in Microsoft Excel or in GraphPad Prism using tests as indicated in the figure legends. First, all data were tested for normal distribution using the Shapiro-Wilk normality test. Data sets with a normal distribution underwent parametric tests for significance, whereas data sets without a normal distribution underwent nonparametric tests for significance. When comparing two groups with normally distributed data to each other, an unpaired Student's t test was utilized. When comparing two groups with non-normally distributed data to each other, a Mann-Whitney test was utilized. When comparing more than two groups with normally distributed data, a two-way ANOVA was used followed by a post hoc Tukey's test for group comparisons. When comparing more than two groups with non-normally distributed data, a Kruskal-Wallis test was used followed by a post hoc Dunn's test for group comparisons. Results were found significant if $p < 0.05$. For cell culture experiments, "n" is equal to the number of cells analyzed. For cell culture experiments, "N" represents the number of times the experiment was repeated on different days with at least three technical replicates. For animal experiments, "n" refers to the number of animals used.

DATA AND CODE AVAILABILITY

RNA sequencing data is available via GEO: GSE136553. Processed mass spectrometry data and RNA sequencing data are available in this article's supplemental tables. All other resources used for this study are available through the Lead Contact, Darcie L. Moore (darcie.moore@wisc.edu) at reasonable request.

Chapter 5: Cell-state specific aggresome formation in fibroblasts is mediated by MAP3K7

5.1 Abstract

The aggresome is a protein degradation system used by many types of cells which consists of proteins destined for degradation being trafficked along microtubules to an enrichment of protein degradation machineries at the centrosome. Despite extensive focus on aggresomes in immortalized cell lines, it remains largely unclear how conserved the aggresome is in primary cell types, and whether aggresomes form through similar mechanisms across cell types. Here we examined the aggresome in primary mouse dermal fibroblasts and found that in response to proteasome inhibition, whereas quiescent and immortalized fibroblasts formed aggresomes, proliferating and senescent fibroblasts did not form aggresomes. Transcriptomic analysis of the fibroblast cell-state specific response to proteasome inhibition revealed that stronger stress-activated MAPK signaling was associated with aggresome formation. Lastly, we found that the MAP3K7 inhibition suppressed aggresome formation in quiescent fibroblasts. Together, our data suggest that the aggresome is not a universal component of the response to disrupted proteostasis and that MAP3K7 plays a role in aggresome formation.

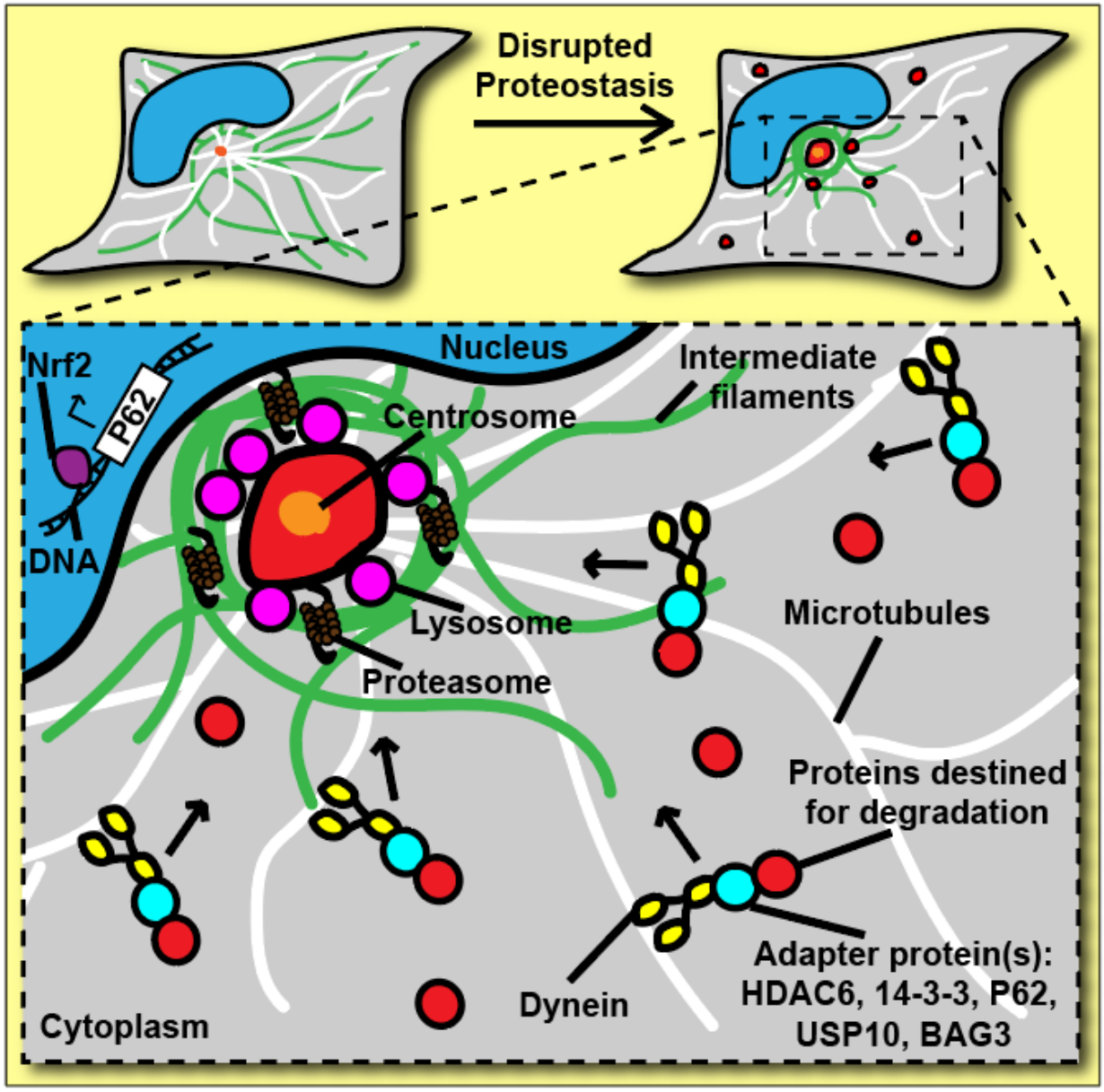

Figure 5.1 *– Simplified Aggresome Formation Schematic. During disrupted proteostasis proteins destined for degradation (red) accumulate and cells upregulate aggresome machinery with transcription factors such as Nrf2 (purple). Proteins destined for degradation are then trafficked along microtubules (white) by dynein (yellow) and adapter protein complexes (cyan) where they are localized to the centrosome (orange) within a cage comprised of intermediate filaments (green) in close spatial proximity with protein*

degradation machinery, such as proteasomes (brown) and lysosomes (pink). The nucleus is labeled in blue and the cytoplasm is in gray.

5.2 Background: Functions for the aggresome in organismal proteostasis (adapted from Morrow et al 2022 *in preparation*)

Cells constantly balance the synthesis of protein with the degradation of protein, termed proteostasis, to maintain cellular function (Chovatiya and Medzhitov 2014). Disruption of proteostasis, typically involving an accumulation of cytotoxic aggregation-prone proteins, is a common feature of a myriad of diseases throughout the organism, particularly in the brain (Ross and Poirier 2004, Douglas and Dillin 2010). To combat the onset of these diseases and maintain healthy tissue throughout life, multicellular organisms run cell intrinsic and extrinsic programs for maintaining proteostasis, which collectively comprise what is referred to as the proteostasis network (PN) (Johnston, Ward et al. 1998, Taylor and Dillin 2013, Hipp, Kasturi et al. 2019).

Within the cell there are three known, major mechanisms for responding to elevated levels of misfolded, damaged, or mutant proteins. First, the ubiquitin-proteasome system turns over proteins through recognition and labeling of the protein destined for degradation with polyubiquitin chains by ubiquitin ligases, and subsequent targeting and degradation by a protein complex called the proteasome (Collins and Goldberg 2017). Second, among many other functions, chaperone proteins can assist in the refolding or disassembly of misfolded proteins (Sontag, Samant et al. 2017, Moran Luengo, Mayer et al. 2019). Lastly, autophagy can clear aggregated proteins by loading them into autophagosomes which then fuse with acidified lysosomes that denature protein through a highly acidic environment and proteases present in lysosomes (Wong and Cuervo 2010). All of these systems have a dynamic capacity to boost activity in response to

challenges that culminate in increases in misfolded, damaged or mutant proteins (Kopito 2000, Labbadia and Morimoto 2015, Sala, Bott et al. 2017).

In addition to these three main systems for maintaining proteostasis, many cell types can respond by forming a structure called the aggresome (Johnston, Ward et al. 1998, Kopito 2000). The aggresome is formed by dynein-dependent trafficking of polyubiquitinated proteins along microtubules to the microtubule organizing center (centrosome) into a cage comprised of the intermediate filament vimentin (Fig. 5.1) (Johnston, Illing et al. 2002, Kawaguchi, Kovacs et al. 2003). At the aggresome, the cell also enriches for proteostasis-related machineries, such as proteasomes and lysosomes, to assist in clearance of proteins that have become trafficked to the aggresome (Fabunmi, Wigley et al. 2000, Riley, Li et al. 2003, Khan, Khamis et al. 2015, Morrow, Porter et al. 2020). Since initial characterization of the aggresome, numerous studies have shed light on methods for inducing aggresome formation, the mechanisms driving its formation and clearance, the cellular benefits of aggresome formation, and the tissues containing cells with the capacity to form an aggresome (Fig. 5.1) (Kawaguchi, Kovacs et al. 2003, Tanaka, Kim et al. 2004, Olzmann, Li et al. 2008, Xu, Graham et al. 2013, Jia, Wu et al. 2014, Yan 2014, Zhou, Wang et al. 2014, Nassar, Samaha et al. 2017, Takahashi, Kitaura et al. 2018, Qin, Jiang et al. 2019). Yet while the aggresome field has made progress in revealing the biology of the aggresome *in vitro*, a function for aggresomes within multicellular organisms in physiologically relevant situations has been elusive. In part I of our review, we discuss modes of aggresome induction and the cell types in which aggresomes have been identified. In part II, we discuss the benefits and consequences

of aggresome formation, providing insight into how functions of the aggresome could impact organismal physiology.

Part I: Aggresomes in Health and Disease

A large focus of aggresome research has been in identifying what induces aggresome formation, and the cell types that have the capacity to form the aggresome. Through these studies the aggresome has become established as a program for responding to disrupted proteostasis. However, many of these studies have been performed in immortalized cell lines using stress paradigms that don't always reflect the physiology of the organism, limiting our understanding of how aggresomes may be utilized in an organism. Despite these limitations, it is clear that numerous types of stimuli in various different cell lines and primary cells can stimulate the formation of an aggresome, suggesting that the aggresome is a generalized program for responding to impaired proteostasis.

Methods to Induce Aggresome Formation

To understand where and when an aggresome would form in an organism, it is important to understand what types of stimuli would or would not induce aggresome formation. Unsurprisingly, the major emerging theme from work investigating modes of aggresome formation has been that aggresomes form in response to elevated levels of proteins destined for degradation. However, due to cross-talk between different types of cellular stress, it has been difficult to identify which components of the cell's response to

stress are specifically required for aggresome formation and where these stress response pathways may converge or diverge.

The most commonly used methods for inducing aggresome formation have been through increasing the levels of proteins that need to be degraded, either through inhibiting proteasome activity, or by exogenously expressing mutant or aggregation-prone proteins. While studies often combine expression of an exogenous aggregation-prone or mutant protein with a proteasome inhibitor to induce aggresome formation, each of these techniques alone is also sufficient to induce aggresome formation in numerous cell lines and primary cells (Johnston, Ward et al. 1998, Bardag-Gorce, Riley et al. 2004, Corcoran, Mitchison et al. 2004, Pilecka, Sadowski et al. 2011, Dehvari, Mahmud et al. 2012, Ogrodnik, Salmonowicz et al. 2014, Morrow, Porter et al. 2020). This suggests that the aggresome could be a generalized response to elevated levels of proteins requiring degradation. However, not all overexpressed proteins similarly induce aggresome formation. For example, in the Cos7 cell line, overexpression of the wild-type (WT) scaffold protein Tks4 is not sufficient to induce aggresome formation, however expressing a mutant form of the protein (R43W - implicated in the Frank-ter Haar syndrome) is sufficient to induce aggresome formation (Adam, Fekete et al. 2015). Therefore, aggresome formation requires more than simply elevating levels of protein. Aggresome formation may instead reflect a cell responding to elevated levels of aberrant protein species (e.g. aggregated, mutant and misfolded) which need to be rapidly degraded or which may be difficult to degrade through alternative mechanisms. Supporting this model, other modes for disrupting proteostasis, such as inhibition of autophagy or heat shock are

similarly sufficient to induce aggresome formation (Kovacs, Lentini et al. 2006, Morrow, Porter et al. 2020).

Interestingly, cell signaling is also capable of launching aggresomes. Lipid derivatives of dopamine (N-Acyldopamine family members; LDD) induce aggresome formation in the absence of proteasome inhibition in N2a cells (Matsumoto, Inobe et al. 2018). However, whereas the ubiquitin-proteasome system is not impaired during treatment with LDD, levels of polyubiquitinated proteins increased, making it difficult to determine if the aggresome is induced by LDD signaling or if the cells just generally respond to elevated levels of polyubiquitinated proteins. A cocktail of cytokines (IFN-γ, IL-1β and TNF-α) is also sufficient to induce aggresome formation in HEK293 cells through induction of expression of nitric oxide synthase (iNOS) (Kolodziejska, Burns et al. 2005, Pandit, Kolodziejska et al. 2009). However, similar to the LDD paradigms, it remains unclear if this induction of the aggresome is specific to cellular signaling. Regardless, these experiments suggest the exciting possibility that organisms may have intracellular mechanisms for inducing aggresome formation, which could prime cells to maintain proteostasis before a challenge is present. If it is true that cell signaling alone is sufficient to turn on aggresomes, it would be interesting to understand what physiological communication pathways organisms could utilize to activate aggresomes cell non-autonomously and in which cases organisms may opt to utilize this capacity.

As is evident by the numerous types of strategies for turning on the aggresome, the aggresome is a generalized stress response program which forms in response to elevated levels of proteins destined for degradation. Further, due to the diversity of stimuli which can activate the aggresome, it is likely that there are many novel strategies for

turning on the aggresome which have yet to be revealed. Though it is still not clear where these strategies for inducing aggresomes converge or diverge and if there are multiple distinct signaling cascades which could culminate in aggresome formation.

Aggresomes Across the Organism

Since the initial characterization of the aggresome in 1998, many studies initially focused on understanding fundamental aggresome biology in immortalized cell lines. In the past decade, more attention has been spent focusing on the presence of aggresomes in primary cell lines from tissues throughout the body and the presence of aggresomes in mammalian tissue.

The Nervous System

The aggresome pathway may be particularly relevant in the brain, where numerous diseases involving impaired proteostasis are known to manifest (Ross and Poirier 2004). While many aggregation-prone proteins in neurodegenerative diseases aggregate in inclusions dispersed throughout the cytosol, or extracellularly, there are several neurodegenerative diseases which exhibit perinuclear inclusions of protein in neurons *in vivo* (e.g. amyloid plaques in Alzheimer's Disease) (Gouras, Olsson et al. 2015, Yamashita, Akamatsu et al. 2017). In post-mortem samples from patients with Parkinson's Disease (PD), the aggregation-prone protein α-synuclein aggregates and localizes to the centrosome in neo-cortical neurons (McNaught, Shashidharan et al. 2002, Olanow, Perl et al. 2004, Jucker and Walker 2013). Post-mortem amyotrophic lateral sclerosis patient samples similarly exhibited perinuclear accumulations of TDP-43 in

motoneurons in the spinal cord. However, human TDP-43 protein expressed in mice led to the formation of multiple aggregates spread throughout the cytosol in spinal cord neurons, suggesting that TDP-43's degradation through the aggresome pathway may be context specific (Xu, Gendron et al. 2010). Mutations in neurofilament heavy chain (NEFH), which is implicated in Charcot-Marie-Tooth Disease, also culminate in aggresome formation when overexpressed *in vitro* in mouse primary neurons and *in vivo* in chick embryo spinal cords (Jacquier, Delorme et al. 2017). However, it remains unclear if these observations are an artifact of overexpressing protein or if endogenous levels of this protein would elicit similar effects. Together these data illustrate that aggresomes are likely to play a role in the biology of many, though likely not all, types of neurodegeneration.

We recently have shown that a different cell type in the brain, mouse primary hippocampal neural stem cells (NSCs), have the capacity to form the aggresome in the hippocampus both *in vitro* and *in vivo* (Morrow, Porter et al. 2020). In addition to inducing aggresomes in NSCs with artificial stimuli, such as proteasome inhibition with MG132, we also observed formation of the aggresome during NSC quiescence exit *in vitro*, a time when a nondividing NSC must clear a wave of protein to enter the cell cycle and proliferate. This finding suggests that aggresomes may play a physiologically relevant role in clearing protein during quiescent NSC exit in the brain (Leeman, Hebestreit et al. 2018). Indeed, we presented evidence of vimentin cage formation in NSCs *in vivo* in the hippocampus, suggesting that aggresome formation may be conserved by NSCs endogenously *in vivo*. However, additional markers are needed to ensure that vimentin cages observed in NSCs *in vivo* are bonafide aggresomes.

Lung

Disrupted proteostasis is also a hallmark of several types of several lung pathologies, suggesting that aggresomes may be utilized to maintain proteostasis in the lung. Bronchial epithelium cells (Beas-2b) form an aggresome in response to treatment with cigarette smoke extract (Tran, Ji et al. 2015, Shivalingappa, Hole et al. 2016). While Beas-2b cells may reflect the biology of the lung only to a limited extent, this observation establishes cigarette smoke as a potential physiologic stimuli that could induce aggresome formation *in vivo*. Indeed, accumulated perinuclear ubiquitinated protein was observed in lung tissue from mice treated with cigarette smoke. However, more work is needed to conclusively say that these perinuclear accumulations of ubiquitin are aggresomes in the lung *in vivo*.

Cystic fibrosis, a disease predominantly resulting from a point mutation in a chlorine ion channel, the Cystic fibrosis transmembrane conductance regulator (CFTR), has also been an active area of aggresome research as this mutant is associated with impairments in proteostasis (Bodas and Vij 2019). Among many deleterious effects, mutated CFTR expression leads to reactive oxygen species (ROS) mediated inhibition of autophagy, which leads to an accumulation of aggregated proteins *in vivo*. Interestingly, overexpressing mutant CFTR in a nutrient starved human lung carcinoma cell line (A549), knocking-down WT CFTR in a human bronchial epithelial cell line (16HBE140-) and inhibiting CFTR function with $CFTR_{inh172}$ in 16HBE140- cells are all sufficient to induce formation of aggresomes *in vitro* (Luciani, Villella et al. 2010, Luciani, Villella et al. 2011, Villella, Esposito et al. 2013). When overexpressed in nutrient starved conditions, mutant

CFTR localized to the aggresome in A549 cells (Luciani, Villella et al. 2010). When WT CFTR was knocked-down, reduced levels of functional CFTR led to increases in ROS and activation of P62 through Beclin1 which induced aggresomes formed by, at least in part, HDAC6 and the small GTPase Rab-5 (Villella, Esposito et al. 2013). Finally, when WT CFTR was functionally inhibited, aggresome formation was also observed through a similar pathway seen in CFTR knock-down, however, in this case CFTR was also localized to the aggresome (Villella, Esposito et al. 2013). Despite these data and other reports demonstrating CFTR's capacity to be localized to the aggresome when overexpressed, it remains unclear if aggresomes would be present in untreated CF lung tissue (Johnston, Ward et al. 1998, Luciani, Villella et al. 2010, Luciani, Villella et al. 2011), and if so, what role the aggresome would specifically be playing in this disease.

Liver

Aggresomes have also been identified in the liver, as disrupted proteostasis is a hallmark of many liver pathologies, such as: alcoholic hepatitis, hepatocellular carcinoma, fatty liver in obesity, and hepatic adenoma (French, Mendoza et al. 2016). Among many other liver pathologies, these diseases share the common characteristic of the formation of protein inclusions composed of cytokeratins, called Mallory–Denk bodies (MDBs), some of which fit the criteria to be called aggresomes (Riley, Bardag-Gorce et al. 2003, French, Masouminia et al. 2017). While the term MDB can be used to discuss a broad range of protein aggregates, not all of which resemble the aggresome, at least some MDBs have been shown to be dependent on microtubules to form, further suggesting that the liver harbors aggresomes (Riley, Bardag-Gorce et al. 2003).

Skin

In response to treatment with glyoxal, a treatment that adds carboxymethyllysine (CML) to vimentin and other proteins in the cell, human dermal fibroblasts *in vitro* formed aggresomes characterized by the formation of vimentin cages and the localization of CFTR to the nuclear bay (Kueper, Grune et al. 2007). While this study further identified that vimentin was the primary target of glyoxal, it is unclear why CFTR would accumulate and similarly localize to the aggresome in this context. Vimentin cage-like structures were present in untreated, healthy human facial skin biopsies, suggesting aggresomes play a role in skin *in vivo* (Kueper, Grune et al. 2007). Interestingly, this data suggests not only that aggresomes are present *in vivo* in humans, but also that healthy human cells that are not experiencing any particular disease or pathology can form aggresomes. This suggests that aggresomes could play critical roles in healthy organismal biology and that aggresomes would not only be present in the context of some type of pathology.

Cancer

Aggresomes have been identified in several types of cancer, such as: breast cancer, pancreatic cancer and multiple myeloma (Nawrocki, Carew et al. 2006, Komatsu, Moriya et al. 2013, Moriya, Komatsu et al. 2015, Miyahara, Kazama et al. 2016). For example, human pancreatic cancer cells challenged with the proteasome inhibitor bortezomib induced a robust increase in ubiquitinated protein levels and their localization to the aggresome (Nawrocki, Carew et al. 2006). Aggresomes were also observed in a subset of pediatric medulloblastoma tumors, evident by the presence of perinuclear

vimentin cages in human patient samples (Yehia, Taha et al. 2019). Interestingly, not all pediatric medulloblastoma tumors were vimentin positive, suggesting that not all tumors, even within the same type of cancer, may use the aggresome. However, tumors also are known to dynamically change expression of intermediate filaments, such as vimentin, in later stages of development as they begin to metastasize (Strouhalova, Prechova et al. 2020). Thus, vimentin negative pediatric medulloblastoma tumors in which the aggresome is not visualized may just be earlier stage tumors. Taken together, many cancer cell lines have the capacity to utilize the aggresome. However, since most of what we know about aggresomes in tumors is from work in cell lines *in vitro*, it remains unclear how broadly these findings would translate into tumors in an organism.

Cell Type Specificity of the Aggresome

Clearly aggresome formation is conserved by many primary cell types and cell lines derived from tissues throughout the body. This begs the question of whether all cell types have the capacity to form the aggresome, and among the cell types that can form the aggresome, how similar or different they are. Interestingly, whereas expressing a cytoplasmic form of the prion protein (CyPrP) in Neuro-2a cells was sufficient to induce aggresome formation, expressing CyPrP in HeLa cells was not sufficient to induce aggresome formation (Beaudoin, Goggin et al. 2008). Instead, HeLa cells demonstrated an accumulation of smaller aggregated proteins dispersed throughout the cytoplasm, suggesting that HeLa cells may be unable to launch the aggresome in response to impaired proteostasis. However, HeLa cells still retain the capacity to form the aggresome when other challenges are applied, such as inhibition of proteasomes (Pilecka, Sadowski

et al. 2011, Salemi, Almawi et al. 2014). Thus, there is cell type specificity in how a cell will respond to disrupted proteostasis. However, it remains unclear if there are cell types which are completely unable to utilize the aggresome. Further, proteins present within the aggresome may differ between cell types, and may dictate which types of machinery are most responsible for their clearance. While aggresomes generated by overexpressing mutant huntingtin or mutant tau were able to recruit autophagy machinery to the aggresome, aggresomes formed by overexpressing mutant desmin or p38 were not able to recruit autophagic equipment to the aggresome (Wong, Tan et al. 2008). Thus, the composition of the aggresome, which could be impacted by the cell's identity, can impact how the aggresome is cleared. If the aggresome is conserved among all cell types throughout the body, there will at least be some cell-type specific modes by which the aggresome functions.

Collectively, accumulating evidence supports the idea that aggresomes are used by tissues throughout the body in many physiologically relevant contexts *in vivo*. However, due to technical limitations, many reports of aggresome formation *in vivo* are still weak, often relying on the presence of just one aggresome marker that is vaguely reminiscent of its extensively defined *in vitro* counterpart. Expanding the toolbox for visualizing aggresome formation *in vivo* will be critical for effectively identifying the presence or absence of aggresomes in organisms.

Part II. An Optimist's and Pessimist's View of the Aggresome

Evidence suggests that the aggresome operates through many distinct mechanisms to benefit the cell. These benefits are conferred through principles shared by general protein inclusions that are not aggresome-specific as well as mechanisms that are specific to the aggresome. While these mechanisms are often viewed as beneficial for an organism, there are also situations in which the aggresome's activity may be undesirable for the organism, such as in tumors and during the cell's response to viral infection. Thus, the aggresome has become established as a targetable cellular program for the potentiation of cellular viability in several pathological conditions.

The Benefits of Aggresome Formation

One of the first studies to investigate aggresome function found that among a heterogeneous culture of cells in which a proportion had formed an aggresome, those which had an aggresome were less likely undergo apoptosis (Tanaka, Kim et al. 2004). This suggests that cells which form an aggresome have a greater capacity to respond to proteotoxic challenges. As the mechanism(s) driving aggresome formation has been revealed, it has become easier to define the importance of the aggresome by studying inhibition of aggresome formation. For example, knocking-down (KD) HDAC6, an adapter protein critical for transporting ubiquitinated proteins along microtubules via dynein motors to the aggresome, in A549 cells both reduced the cell's capacity to form an aggresome and to survive a challenge with the proteasome inhibitor MG132 (Kawaguchi, Kovacs et al. 2003). Similar to KD of HDAC6, KO of Nrf2, a transcription factor which upregulates P62/SQSTM1, resulted in a failure to form an aggresome and cell death in HEK 293 cells challenged with the proteasome inhibitor MG132 (Qin, Jiang et al. 2019).

Additional evidence demonstrates similar trends where disrupting aggresome formation or aggresome-related machinery results in increased cytotoxicity (Taylor, Tanaka et al. 2003, Jones, Jourd'heuil et al. 2007, Mishima, Santo et al. 2015, Yung, Sha et al. 2016, Gerhardt, Marsh et al. 2017, Takahashi, Kitaura et al. 2018, Morrow, Porter et al. 2020). However, many strategies for inhibiting aggresome formation illicit pleotropic effects on the cell, making it difficult to determine if the increased cytotoxicity in response to aggresome inhibition is due to disrupting aggresome formation or to other non-specific effects of each paradigm. Further in support of the aggresome benefiting the cell's capacity to maintain proteostasis, aggresome-like structures (defined by a pericentrosomal localization) are relatively more abundant in fibroblasts from the long-lived naked mole rat (NMR) compared with fibroblasts from shorter-lived rodents such as mice (Sunchu, Riordan et al. 2020). Beyond the correlation of increased longevity and aggresome formation, NMR fibroblasts were also more resilient to impaired proteostasis, further suggesting that aggresome formation is cytoprotective. Past the limitations of tools for impairing aggresome formation to study aggresome function, these observations beg the question of the mechanism(s) by which the aggresome is conferring increased resilience to disruptions in proteostasis.

Due to the enrichment of proteostasis-related machineries present at the aggresome, the aggresome could be thought of as a staging ground where proteins destined for degradation are brought within close spatial proximity with protein degradation machinery for efficient protein degradation (Vora and Phillips 2016). For example, autophagosomal machineries can be recruited to the aggresome similarly in a microtubule-dependent manner (Iwata, Riley et al. 2005, Biskou, Casanova et al. 2019).

Thus, the aggresome could benefit cells by increasing efficiency of protein turnover by localizing autophagosomal machineries to proteins destined for degradation. Further, we recently demonstrated that proteasomes also are enriched at the aggresome in NSCs. NSCs which are unable to enrich for proteasomes at the aggresome (vimentin KO) accumulated aggregated proteins faster and experienced greater cytotoxicity (Morrow, Porter et al. 2020). Collectively, these examples suggest that protein turnover at the aggresome is complex, involving multiple protein degradation pathways and that the aggresome is primed for efficient protein degradation.

Aggresomes also can be asymmetrically inherited during mitosis, suggesting that mitotic cells could use the aggresome and mitosis to rid one daughter cell of the aggresome (Rujano, Bosveld et al. 2006, Ogrodnik, Salmonowicz et al. 2014, Moore, Pilz et al. 2015, Morrow, Porter et al. 2020). In this situation, one daughter cell will inherit the aggresome while the other daughter cell will be free of the contents of the aggresome. Lineage tracing experiments *in vitro* found that daughters that inherited the aggresome were more likely to take longer to undergo mitosis than the daughter that did not inherit the aggresome (Ogrodnik, Salmonowicz et al. 2014, Moore, Pilz et al. 2015). However, it remains unclear if inheriting the aggresome would always be bad for a cell (Moore and Jessberger 2017), as it could provide benefits associated with a greater inheritance of proteasomes and lysosomes that are interacting with the aggresome or a greater supply of amino acids that could be produced by clearing proteins in the aggresome.

The aggresome could also benefit cellular fitness in ways that are no different from general protein aggregation. Protein aggregation is thought to functionally impact cells through a variety of mechanisms. For example, proteins that are cytotoxic in the cytosol

could be stored in protein aggregates to reduce their capacity to interfere with other essential cellular functions throughout the cell (Ross and Poirier 2005, Jones, Jourd'heuil et al. 2007, Walther, Kasturi et al. 2015). Protein aggregation could also be considered an important precursor for efficient degradation of proteins by autophagy (Bjorkoy, Lamark et al. 2005, Iwata, Riley et al. 2005, Bjorkoy, Lamark et al. 2006). While these hypotheses have been tested more extensively in the context of protein aggregation, not specifically referencing the aggresome, these principles likely also apply to the aggresome.

The Consequences of Aggresome Formation

While the aggresome has been observed to play cytoprotective roles, aggresome formation may not always be desirable for the organism and may lead to reduced cell fitness. For example, inhibiting dynein with erythro-9-[3-2-(hydrosynonyl)] adenine (EHNA) in the NSC-34 cell line, which inhibits transport of ubiquitinated proteins to the aggresome, led to a decreased accumulation of cytotoxic protein species such as SOD1 through upregulation of ubiquitin proteasome activity (Cristofani, Crippa et al. 2017). This finding suggests that cells may in specific circumstances be better off if they are forced to compensate for accumulated cytotoxic protein species with the ubiquitin proteasome system rather than shift towards dependence on autophagy and the aggresome. Long-term aggresomes presence has also been suggested to lead to cell cycle arrest due to, at least in part, steric interference with chromosomal alignment, centrosome positioning, and spindle formation during mitosis (Lu, Boschetti et al. 2015). However, this is not supported by other groups specifically studying the mitotic asymmetric inheritance of the

aggresome in multiple cell types, where the aggresome did not inhibit mitosis (Rujano, Bosveld et al. 2006, Ogrodnik, Salmonowicz et al. 2014, Morrow, Porter et al. 2020). Further, protein aggregation at the aggresome has also been suggested to be a negative regulator of cell function through clogging proteasomes and rendering them unable to degrade future substrates (Cummings, Mancini et al. 1998, Jana, Zemskov et al. 2001). This finding is also somewhat contested, as other groups have demonstrated that proteasomes present in protein inclusions and at the aggresome are still catalytically active (Fabunmi, Wigley et al. 2000, Verdoes, Florea et al. 2006, Ogrodnik, Salmonowicz et al. 2014, Schipper-Krom, Juenemann et al. 2014). However, it is possible that the aggresome may sequester cytoprotective proteins away from the cytosol, in addition to cytotoxic proteins, which would make them inaccessible to perform critical cellular processes (Jones, Jourd'heuil et al. 2007).

Beyond normal cell function, the aggresome is also thought to play a role in the cell's response to viral infection. During infection, many viral proteins localize to the aggresome, evident by their perinuclear localization and dependence on aggresome formation machinery to assemble (Liu, Shevchenko et al. 2005, Kajitani, Satsuka et al. 2013, Banerjee, Miyake et al. 2014). This effect may be unique to certain cell types and certain viruses. For example, while the viral protein E1B55K protein from adenoviral serotypes Ad4, Ad5, Ad9 and Ad16 clearly formed aggresome-like structures in a human lung cell line (H1299), E1B55K protein from Ad12 and Ad34 did not clearly localize to the aggresome (Blanchette, Wimmer et al. 2013). Further, although some viruses form structures called viral factories that resemble aggresomes, their formation is not dependent on aggresome machinery, implying that viral factories are not aggresomes

(Munoz-Moreno, Barrado-Gil et al. 2015). It also is not clear if aggresome formation is a result of the cell trying to protect itself from infection by boosting protein clearance to remove viral components, or the virus hijacking the aggresome to propagate faster. These data suggest that the aggresome could play a functional role in viral infection. Indeed, aggresome formation accelerated the inactivation of MRE11-RAD50-NBS1 (MRN), which inhibits viral packaging and DNA replication, suggesting that the aggresome benefits viruses (Liu, Shevchenko et al. 2005). Additionally, herpes simplex virus had a 10-fold reduced capacity to propagate in cells treated with the microtubule destabilizer nocodazole, which inhibits aggresome formation (Nozawa, Yamauchi et al. 2004). Although, destabilizing microtubules is certain to induce a myriad of pleiotropic effects that could also be influencing the cell's viability and capacity to harbor the virus. However, in each of these cases, perturbing the aggresome only reduced viral viability and did not lead to a complete inability of the virus to infect the cell. Separately, bacterial infection by *Salmonella enterica* serovar Typhimurium could also induce aggresome formation (Guignot and Servin 2008), suggesting that this could be a general cellular response to foreign invasion. It remains unclear, however, whether aggresome formation would similarly augment bacterial viability. Lastly, HDAC6 was recently found to play a role in formation of aggresome-like structures which assembled in response to induction of the pyrin or pyrin domain–containing protein 3 (NLRP3) inflammasome (Magupalli, Negro et al. 2020). Localization of components of the inflammasome to the aggresome provides a mechanism to both enhance their activity, by bringing factors which need to interact closer together, and reduce their activity by increasing their degradation. Thus, it is unclear whether using the aggresome pathway to maintain the inflammasome would provide a

net benefit or drawback for a cell. Taken together, these data illustrate a function for the aggresome in the cell's immune response and provide a mechanism to modulate the strength of the cell's immune response.

Beyond the ways in which aggresome formation could be detrimental to a cell, there are also situations in which increased cellular fitness conferred by aggresome formation is not desirable for the health of the organism. The most prominent example of this is cancer. Aggresomes are relatively well-studied chemotherapeutic targets for treatment of breast and pancreatic cancer. Treating either breast cancer, multiple myeloma, or pancreatic cancer cells with proteasome inhibitors to induce proteotoxic stress together with aggresome formation inhibitors such as HDAC6 inhibitors or microtubule polymerization inhibitors, synergistically enhances the cytotoxicity of proteasome inhibitors (Catley, Weisberg et al. 2006, Nawrocki, Carew et al. 2006, Komatsu, Moriya et al. 2013, Mishima, Santo et al. 2015, Moriya, Komatsu et al. 2015, Miyahara, Kazama et al. 2016). These findings suggest that tumors have a dependence on the aggresome for maintaining viability in response to proteotoxic challenges that could be targeted for the treatment of cancer. However, HDAC inhibitors are also known to modulate tumor viability through aggresome-independent mechanisms, such as through regulating expression of apoptotic genes or growth regulators (Millward, Price et al. 2012). Thus, these pleiotropic effects could also explain the enhanced cytotoxicity reported in tumors treated with both proteasome and HDAC6 inhibitors. Closer examination of markers of proteostasis in these contexts may provide further insight into the aggresome's role in this process as opposed to other roles of HDAC proteins. Collectively, inducing aggresome formation may not always be the most desirable

outcome for the organism, even if cellular viability is increased. Aggresome formation instead should be viewed as a cellular program with the capacity to augment the capacity to maintain proteostasis and cellular viability which may be useful to target in different ways in specific pathologies and diseases.

Conclusions and Future Directions

The past two decades of aggresome research have culminated in substantial insight into the molecular mechanisms driving aggresome formation and clearance, the benefits and consequences of aggresome formation and the cell types throughout the body which have the capacity to utilize the aggresome. Aggresomes have been observed to become induced by a myriad of stimuli, primarily those that induce increases in the cytosolic levels of misfolded, damaged or mutant proteins. There is ample evidence to support aggresome formation in primary cells and cell lines derived from tissues throughout the body, however, *in vivo* evidence of aggresome formation still remains relatively limited. While there are some drawbacks to forming the aggresome, there are many benefits to aggresome formation experienced by both the cell and the organism. Collectively, these data describe the aggresome as a cellular program used to respond to disruptions in proteostasis to maintain cellular viability.

The past two decades of aggresome research, which has largely focused on studying immortalized cell lines *in vitro*, has paved the way for aggresome research to move *in vivo* to study human diseases where proteostasis is impaired and aggresomes could be functionally relevant. To move forward, the field could benefit from pursuing several goals. First, it may be constructive to revisit aggresome nomenclature. At present,

the term “aggresome” is used both to refer to the specific structure that is the topic of this review, as well as general protein aggregation. This makes reviewing aggresome literature challenging as each study must be examined carefully to determine which definition of “aggresome” is being utilized. Second, despite emerging evidence for aggresome formation throughout the body in a variety of contexts, the extent to which aggresomes do or do not play a role in healthy or pathological cell biology throughout the body is still largely unclear. If the aggresome is used as a target to disrupt in cancer or activate in neurodegenerative disease, it is essential to understand the general prevalence of aggresomes in organisms to account for off-target effects. Lastly, for cell types that have the capacity to form the aggresome, but fail to do so in disease, it will be interesting to determine whether inducing the aggresome would confer an advantage to the organism in delaying onset or slowing progression of the disease. Conversely, in cell types that lack the potential to form the aggresome, or lack at least one component of aggresome-related machinery to employ a fully functioning aggresome, we should identify ways to induce the aggresome to form or increase the aggresome’s function and determine if this is beneficial to the organism. The observation that not all cell types either 1) express all aggresome machinery or 2) launch the aggresome as readily as others suggests the exciting possibility that we can utilize the aggresome to increase the capacity of these cells to maintain proteostasis. However, it remains unclear if we can effectively and safely harness this to improve human health and disease without deleterious effects.

5.3 Project Introduction

Proper cellular function relies upon effective maintenance of the proteome by the cell's protein quality control systems, such as the ubiquitin proteasome system, autophagy and chaperone proteins (Vilchez, Saez et al. 2014). In response to environmental challenges which impair proteostasis, cells react by regulating each of these pathways to regain homeostasis. As a part of the response to impaired proteostasis, many cell types form the aggresome, a structure comprised of proteins destined for degradation being trafficked along microtubules by dynein and other adapter proteins to the centrosome within a cage comprised of the intermediate filament vimentin (Johnston, Ward et al. 1998, Kopito 2000, Johnston, Illing et al. 2002, Iwata, Riley et al. 2005, Olzmann, Li et al. 2008). It is thought that aggresome formation is cytoprotective by increasing the efficiency of protein degradation by bringing together proteins destined for degradation with protein degradation machineries and organizing damaged or misfolded proteins so they do not interfere with other cellular processes (Tanaka, Kim et al. 2004, Olzmann, Li et al. 2008).

Although substantial advances have been made in understanding how aggresomes form and function, most of what is known about the aggresome comes from studies of immortalized cell lines *in vitro*. It remains unclear whether cell line immortalization influences aggresome formation, and by extension it is difficult to understand the extent to which aggresomes are or are not used by primary cell types from across the body. To address these gaps, we investigated aggresome formation in primary mouse dermal fibroblasts isolated from the tail of mice *in vitro* in four cell states: proliferating, quiescent, senescent and immortalized. Using this model, we learned that

aggresome formation in fibroblasts is dependent on immortalization. Further, we uncovered that aggresome formation can be a cell-state specific phenotype and a novel component of MAPK signaling, MAP3K7, involved in aggresome formation.

5.4 Results (adapted from Morrow et al 2022 *in preparation*)

Aggresome formation in primary fibroblasts is cell-state specific

To determine whether primary mouse dermal fibroblasts would form the aggresome, we isolated fibroblasts from the tail of 1 month old male mice, and then in a proliferating condition, challenged the fibroblasts with the proteasome inhibitor MG132, a robust paradigm to induce aggresome formation (Johnston, Illing et al. 2002, Khan and Gasser 2016, Morrow, Porter et al. 2020). Cells were fixed and immunostained for two markers of the aggresome: 1) K48-linked ubiquitinated proteins (K48 PolyUb), which mark proteins destined for degradation which get trafficked to the aggresome, and 2) vimentin, which forms a cage around the aggresome (Fig. 5.2A-B) (Johnston, Ward et al. 1998, Johnston, Illing et al. 2002, Hao, Nanduri et al. 2013). Surprisingly, although we observed an global increase in K48 PolyUb, suggesting that MG132 was effective, we were not able to detect an obvious enrichment of K48 PolyUb in the nuclear bay of proliferating fibroblasts, and similarly were not able to observe any collapse of vimentin to form a perinuclear cage, despite high expression of vimentin in these cells. These findings suggest that proliferating primary adult fibroblasts do not retain the capacity to form the aggresome in response to proteasome inhibition.

Previous reports have demonstrated the formation of aggresomes in immortalized human embryonic fibroblast cell lines (Matsumoto, Inobe et al. 2018). Therefore, we

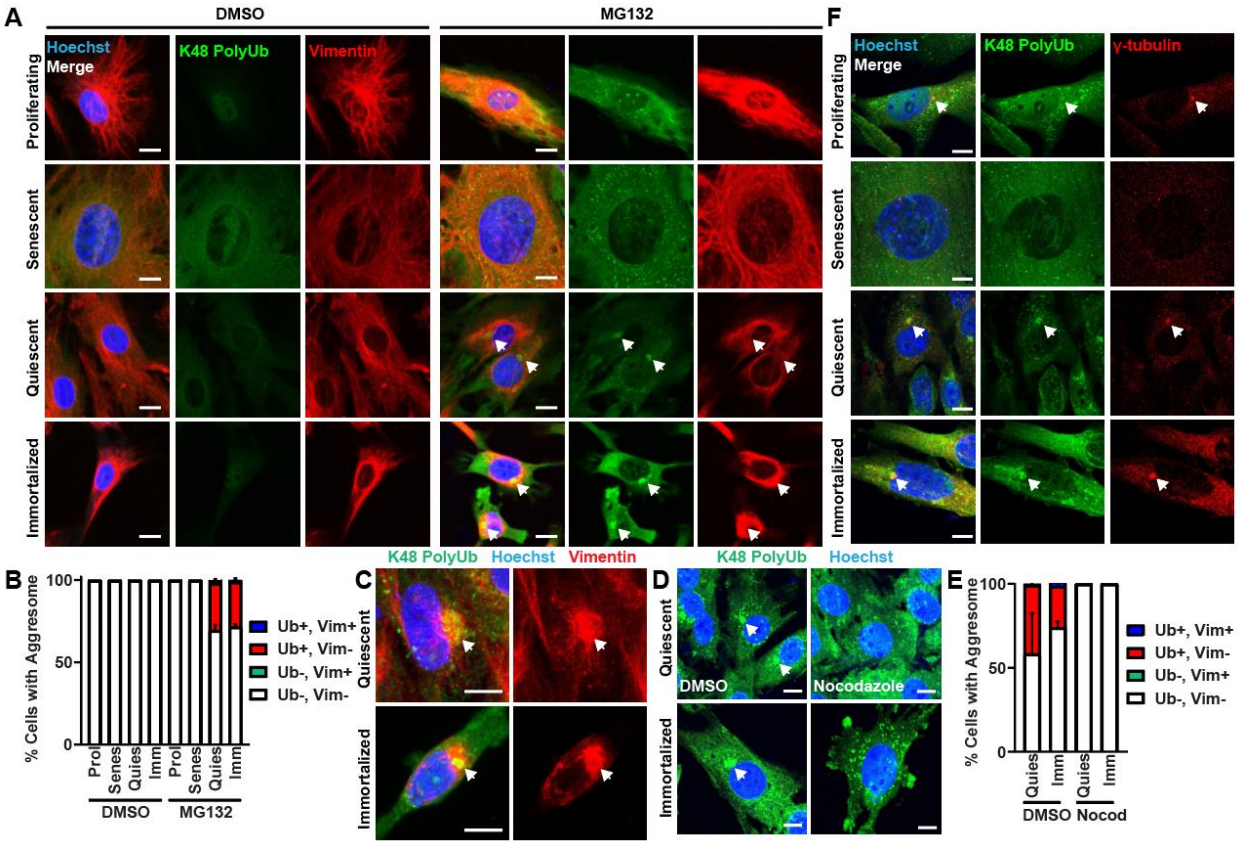

Figure 5.2 – Aggresomes are formed by fibroblasts in response to proteasome inhibition in distinct cell-states. A-B) Proliferating, senescent, quiescent and immortalized fibroblasts were treated with 0.1% DMSO or 10 μM MG132 for 8 hours prior to fixation and immunostaining for K48 PolyUb (green), vimentin (red) and nuclei (Hoechst; blue). Samples were analyzed for the proportion of cells forming aggresomes discernable by an enrichment of K48 PolyUb only (red bar), a vimentin cage only (green), both (blue) or neither (white) (N=3; Two-way ANOVA with post-hoc Tukey's test; mean ± SD). C) Examples of vimentin cages surrounding the aggresome in quiescent and immortalized fibroblasts treated with 10 μM MG132 for 8 hours prior to being fixed and immunostained as in A-B. D-E) Quiescent and immortalized fibroblasts were treated with 10 μM MG132 for 8 hours with either 0.1% DMSO or 2 mM

nocodazole prior to being fixed and immunostained for K48 PolyUb (green) and stained for nuclei (Hoechst; blue). Samples were quantified as in 1B. F) Proliferating, senescent, quiescent and immortalized fibroblasts were treated with 10 μM MG132 for 8 hours prior to being fixed and immunostained for K48 PolyUb (green), γ-tubulin (red) and stained for nuclei (Hoechst; blue) (N=3; Two-way ANOVA with post-hoc Tukey's test; mean ± SD). Arrows denote aggresomes (A,C,D) or centrosomes (F). Scale bars, 10 μm.

hypothesized that the aggresome may be used by fibroblasts specific to their cell-state. To test this hypothesis, we used proliferating primary fibroblasts to generate three additional fibroblast cell-states mimicking previously established protocols: 1) quiescent (contact inhibited), 2) senescent (replicative senescence) and 3) immortalized (expression of the SV40T antigen) (Neufeld, Ripley et al. 1987, Hutter, Unterluggauer et al. 2002, Legesse-Miller, Raitman et al. 2012). To validate each of our generated cell states, we first measured their proliferation rate by administration of EdU to label cells in S-phase and, expectedly, observed that senescent and quiescent fibroblasts exhibited a complete exit from the cell cycle, while immortalized fibroblasts became hyperproliferative (Fig. 5.3A-B). Further, as expected, senescent fibroblasts exhibited increased β-galactosidase activity and decreased expression of the nuclear envelope protein Lamin-B1 (Fig. 5.3C-F) (Wang, Ong et al. 2017). Lastly, we validated the purity of our immortalized cultures by immunostaining for the protein used to immortalize the proliferating fibroblasts, SV40T, and observed that our immortalized cultures were 100% SV40T+, suggesting that our cultures were fully composed of immortalized fibroblasts (Fig. 5.3G-H).

Using all four of these validated primary adult mouse fibroblast cultures, we next asked whether they would form the aggresome in other cell-states (Fig. 5.2A-B), again, by challenging each culture with MG132 to induce aggresome formation. Senescent fibroblasts behaved similarly to proliferating fibroblasts, exhibiting increased K48 PolyUb without forming aggresomes. However, similar to a previous report in immortalized mouse embryonic fibroblasts (Matsumoto, Inobe et al. 2018), our immortalized adult primary mouse fibroblasts were able to form aggresomes, enriching K48 PolyUb in the nuclear

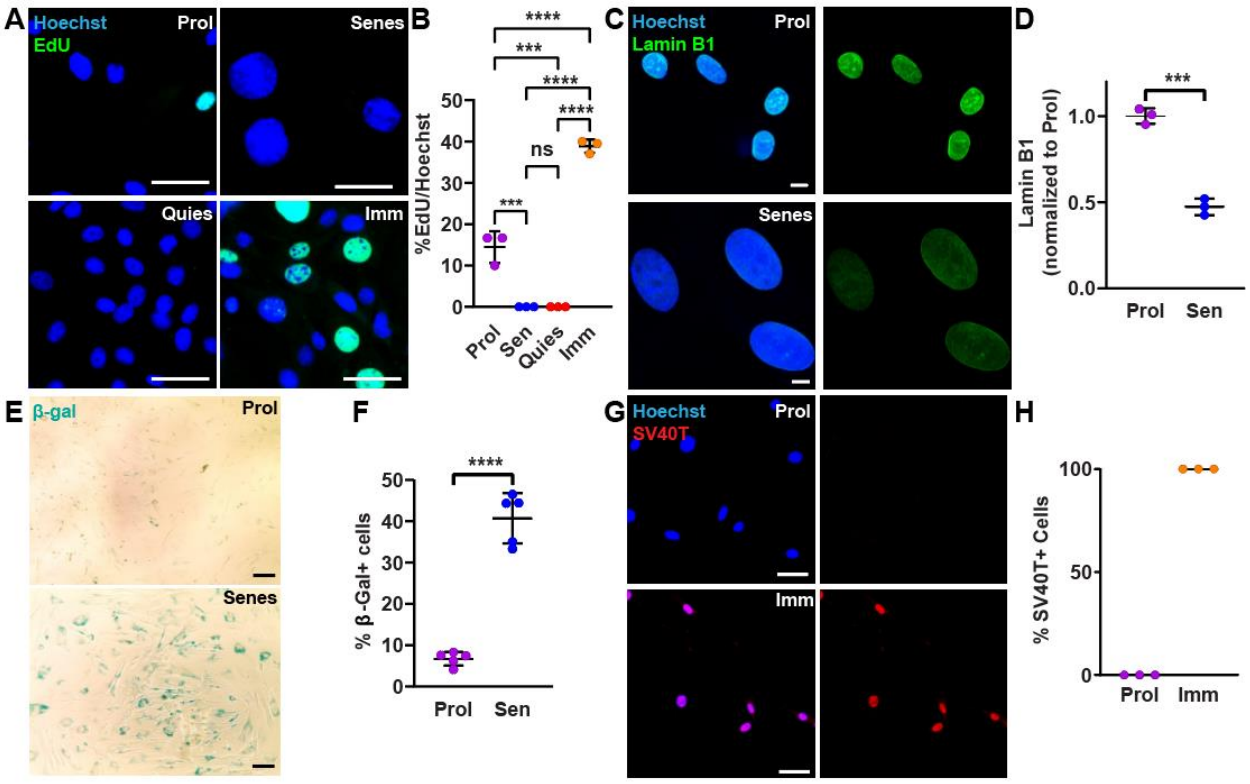

Figure 5.3 – A-B) Proliferating (purple), senescent (blue), quiescent (red) and immortalized (orange) fibroblasts were pulsed with EdU for 1 hour at 37°C prior to being fixed and stained to visualize nuclei (Hoechst; blue) and EdU (green). Cells were analyzed to identify the proportion of cells that were EdU+ (N=3; Two-way ANOVA with post-hoc Tukey's test; mean ± SD). C-D) Proliferating (purple) and senescent (blue) fibroblasts were fixed and immunostained for Lamin B1 (green) and stained for nuclei (Hoechst; blue). Samples were analyzed for relative expression of Lamin B1 (N=3; Student's t-test; mean ± SD). E-F) Bright field image of proliferating (purple) and senescent (blue) fibroblasts that were fixed and stained to visualize β-galactosidase activity (β-gal; green). Samples were analyzed for the proportion of cells positive for β-galactosidase activity (N=3; Student's t-test; mean ± SD). G-H) Proliferating (purple) and immortalized (orange) fibroblasts were fixed and immunostained for SV40T (red)

and stained for nuclei (Hoechst; blue). Samples were analyzed for the percentage of cells positive for SV40T (N=3; mean ± SD). Scale bars, 50 μm (A, E, G), 10 μm (C). ***p<0.001, ****p<0.0001.

bay. Further, quiescent fibroblasts also were able to form aggresomes in response to proteasome inhibition. These data suggest that change in cell state alone was sufficient to drive an aggresome program in fibroblasts in response to impaired proteostasis. Interestingly, in both the immortalized and quiescent fibroblast populations, whereas they did form a K48 polyUb-rich aggresome, only a small proportion of cells additionally formed collapsed vimentin cages around the aggresome (Fig. 5.2A-C). These results suggest a decoupling of vimentin cage formation and aggresome formation, further supporting previous studies in primary mouse neural stem cells (Morrow, Porter et al. 2020).

The aggresome assembles through the trafficking of proteins destined for degradation by adapter proteins and dynein motor proteins along microtubules to the centrosome (Johnston, Ward et al. 1998, Johnston, Illing et al. 2002, Kawaguchi, Kovacs et al. 2003, Olzmann, Li et al. 2008). Thus, aggresomes should colocalize with markers of the centrosome and should be sensitive to disruption of the microtubule network (Johnston, Ward et al. 1998). To further confirm the K48 polyUb-rich structures in quiescent and immortalized fibroblasts constituted bonafide aggresomes, we challenged quiescent and immortalized fibroblasts with MG132 to induce aggresome formation in the presence of the microtubule poison nocodazole to block aggresome formation, or a dimethyl sulfoxide (DMSO) vehicle control (Fig. 5.2D-E). Nocodazole efficiently blocked perinuclear enrichment of K48 PolyUb in both cell types. Further, immunostaining for a marker of the centrosome γ-tubulin, together with K48 PolyUb revealed that the perinuclear enrichments of K48 PolyUb were localized to the centrosome in both quiescent and immortalized fibroblasts (Fig. 5.2F). Together, these data support that primary adult mouse dermal fibroblasts lose or gain their ability to make aggresomes

depending on their cell-state. Specifically, quiescent and immortalized fibroblasts can make aggresomes whereas proliferating and senescent fibroblasts cannot. Moreover, the vimentin cage, a commonly cited feature of aggresomes, was dispensable for aggresome formation (Morrow, Porter et al. 2020).

Aggresomes are used by cells with diverse proteostasis networks

Among a host of other proposed functions, the aggresomes is predominantly thought to be a staging ground for protein degradation by autophagy (Olzmann, Li et al. 2008). However, evidence suggests that additional components of the cell's proteostasis network, such as proteasomes, may also play a role at the aggresome (Hao, Nanduri et al. 2013, Morrow, Porter et al. 2020). To gain more insight into how the aggresome is used in combination with other components of the cell's proteostasis network and determine if the proteostasis network used by the cell could predict aggresome formation, we profiled the proteostasis network in each fibroblast cell-state by measuring relative levels of protein synthesis, chaperone protein expression, proteasome activity, and autophagy (Fig. 5.4A).

First, we asked whether each fibroblast cell-state produced protein at relatively similar rates through protein synthesis assays by pulsing cells with puromycin to label nascent proteins. We treated proliferating, senescent, quiescent and immortalized fibroblasts with puromycin and measured relative levels of puromycin incorporation into nascent proteins by immunoblotting (Fig. 5.4B-C, 5.5A-B). Interestingly, we observed that whereas proliferating, senescent, and quiescent fibroblasts produced protein at relatively similar rates, immortalized fibroblasts exhibited significantly reduced protein synthesis

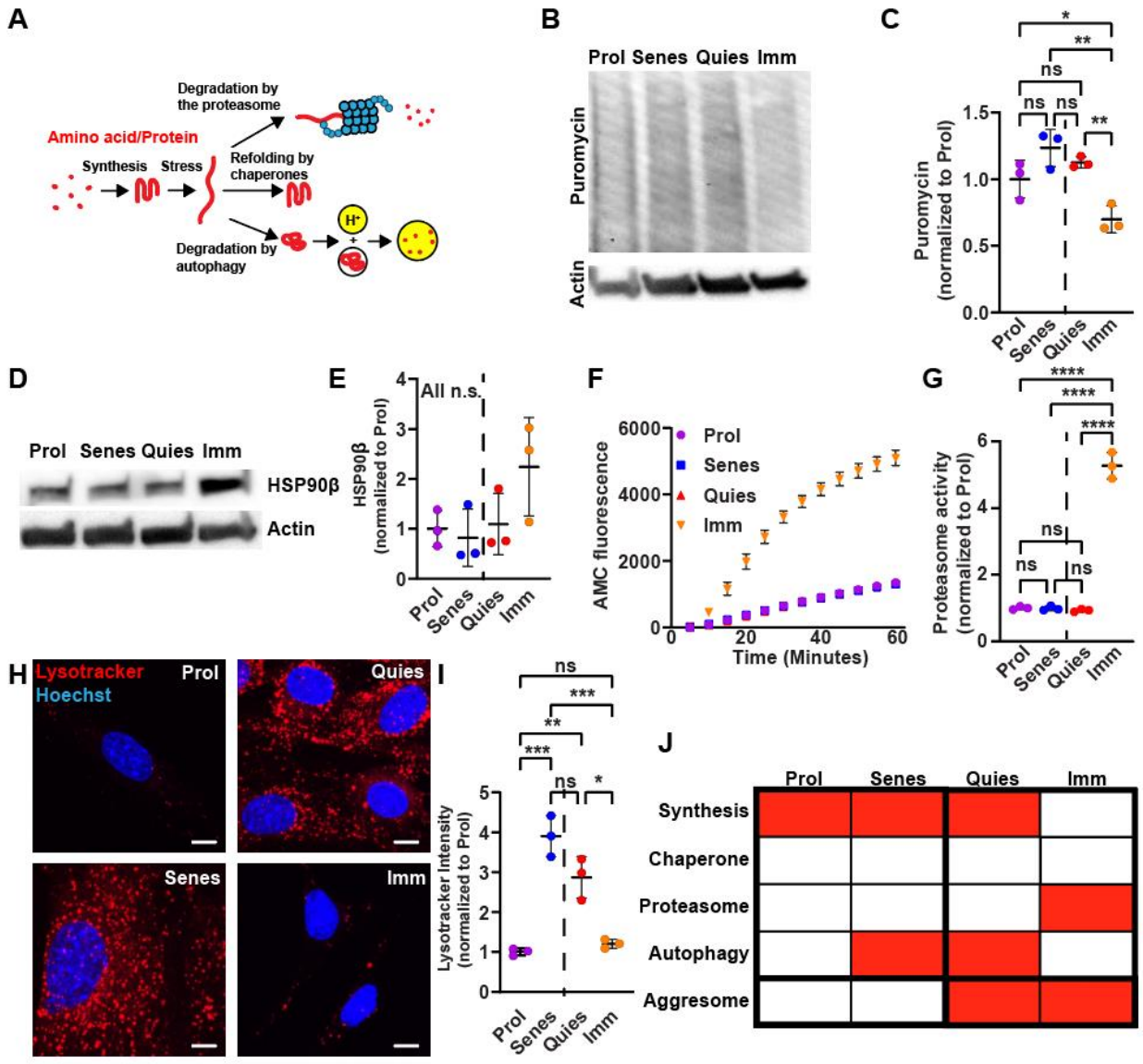

Figure 5.4 – Aggresomes are used within diverse proteostasis networks. A) Schematic representation of the cell's proteostasis network. B-C) Proliferating (purple), senescent (blue), quiescent (red) and immortalized (orange) fibroblasts were pulsed with 10 µg/mL puromycin for 10 minutes prior to soluble protein extraction and analysis by western blot. Relative levels of puromycin incorporation and actin expression were visualized by western blot. Samples were analyzed for puromycin levels relative to actin (N=3; Two-way ANOVA with post-hoc Tukey's test; mean ± SD). D-E) Proliferating (purple),

senescent (blue), quiescent (red) and immortalized (orange) fibroblasts were analyzed for soluble protein expression of HSP90β and actin by western blot (N=3; Two-way ANOVA with post-hoc Tukey's test; mean ± SD). F-G) Proliferating (purple), senescent (blue), quiescent (red) and immortalized (orange) fibroblast protein lysates were prepared and analyzed for relative levels of trypsin-like proteasome activity by measuring AMC fluorescence as a function of time (N=3; Two-way ANOVA with post-hoc Tukey's test; mean ± SD). G displays normalized AMC accumulation at 60 minutes for each sample. H-I) Proliferating (purple), senescent (blue), quiescent (red) and immortalized (orange) fibroblasts were stained and analyzed for lysosome content (Lysotracker; red) and nuclei (Hoechst; blue) (N=3; Two-way ANOVA with post-hoc Tukey's test; mean ± SD). J) Schematic summarizing the proteostasis networks experiments in each fibroblast cell-state. Darker red indicates higher levels of each node of the proteostasis network respectively. The dotted line in each panel separates cell-states that either do or do not form the aggresome. Scale bars, 10 μm. *p<0.05, **p<0.01, ***p<0.001, ****p<0.0001.

compared to the other three cell-states. Therefore, protein synthesis is not a predictor of utilization of the aggresome.

Cells also can regulate their proteome through expression of chaperone proteins which can assist in protein folding, refolding, and sequestering proteins for degradation or trafficking. Previous work has shown that chaperone protein activity, as measured by expression of the heat shock transcription factor HSF1, was not different between proliferating human fibroblasts and senescent human fibroblasts (Sabath, Levy-Adam et al. 2020). Therefore, we hypothesized that fibroblast cell-states may not significantly differentially regulate chaperone proteins. To test this hypothesis, we probed the chaperone protein network by immunoblotting for the chaperone protein HSP90β. In line with previous reports, proliferating, senescent and quiescent fibroblasts did not display differences in expression of HSP90β (Fig. 5.4D-E). We observed trends towards increased expression of HSP90β in immortalized fibroblasts compared against the other cell-states, however these trends were not significant. Thus, while fibroblast cell-states do significantly differ in the rate of protein synthesis, using HSP90β as a proxy for chaperone activity, fibroblast cell-states do not appear to differentially regulate chaperone protein levels.

To degrade proteins, cells have two primary protein degradation systems: the ubiquitin-proteasome system and autophagy. To determine whether fibroblast cell-state drove differences in protein degradation by the ubiquitin-proteasome system, we isolated protein lysates from each fibroblast cell state, and measured relative levels of proteasome activity by applying a substrate that becomes fluorescent when cleaved by the proteasome. Consistent with previous reports, proteasome activity in proliferating,

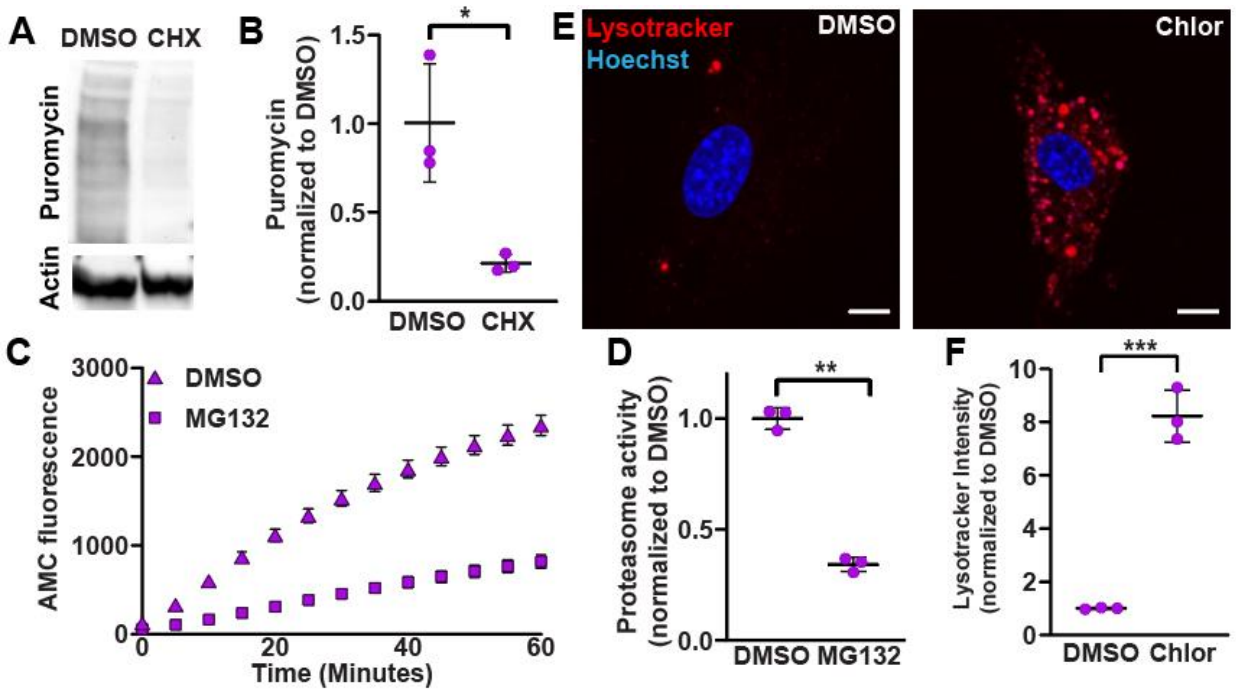

Figure 5.5 – A-B) Proliferating fibroblasts were treated with 10 µM cycloheximide or 0.1% DMSO for 10 minutes prior to addition of 10 µg/mL puromycin and then protein extraction and analysis of puromycin incorporation and actin expression by western blot. Samples were analyzed for relative puromycin incorporation relative to actin (N=3; Student's t-test; mean ± SD). C-D) Proliferating fibroblast protein lysates were prepared and treated with either a control dose of 1% DMSO or 100 µM MG132 and then analyzed for relative levels of proteasome activity by measuring AMC fluorescence as a function of time. D displays normalized AMC accumulation at 60 minutes for each sample (N=3; Student's t-test; mean ± SD). E-F) Proliferating fibroblasts were treated with either 0.1% DMSO or 1 µM chloroquine for 24 hours and then stained and analyzed for lysosome content (Lysotracker; red) and nuclei (Hoechst; blue) (N=3; Student's t-test; mean ± SD). Scale bars, 10 µm. *p<0.05, **p<0.01, ***p<0.001.

senescent and quiescent fibroblasts was similar between these cell-states, whereas immortalized fibroblasts had significantly elevated levels of proteasome activity (Legesse-Miller, Raitman et al. 2012) (Fig. 5.4F-G, 5.5C-D). Therefore, similar to protein synthesis and chaperone protein expression, proteasome activity also is not indicative of a cell's preference to form the aggresome.

Lastly, we measured relative levels of autophagy by labeling live fibroblasts with the dye Lysotracker, which fluoresces strongly in the presence of the acidic lumen of a lysosome. Previous data suggest that senescent and quiescent fibroblasts have relatively higher levels of autophagy compared to proliferating fibroblasts (Legesse-Miller, Raitman et al. 2012, Sun, Zheng et al. 2018, Rajendran, Alzahrani et al. 2019). Our data confirms these previous reports, as we observed that quiescent and senescent fibroblasts harbored higher levels of lysosomes compared to proliferating and immortalized fibroblasts (Fig. 5.4H-I, 5.5E-F, (Jia, Xue et al. 2018)). Thus, relative levels of lysosomes also do not correlate with cell-states that form aggresomes.

Taken together, fibroblast cell-states use a diverse set of proteostasis networks, and no one feature of the proteostasis network correlates with aggresome formation in fibroblasts (Fig. 5.4J). While the aggresome is largely thought to degrade protein through autophagy (Olzmann, Li et al. 2008), several reports have also suggested a role for proteasomes in protein degradation at the aggresome (Hao, Nanduri et al. 2013, Morrow, Porter et al. 2020). These data support the idea that the aggresome is used by cells in a diverse set of contexts to maintain cell fitness and that the aggresome's mode of action is more complex than degrading proteins through autophagy.

Transcriptomic profiling of the fibroblast response to MG132 reveals features associated with aggresome formation

We next used our fibroblast cell-state specific aggresome formation model to understand the mechanisms promoting aggresome formation. To this end, we generated proliferating, senescent, quiescent, and immortalized fibroblasts treated with either DMSO (no aggresome) or MG132 (aggresome), extracted RNA and submitted samples for RNA sequencing to create a resource to perform an analysis of the transcriptomic features associated with or without aggresome formation. To control for variance in global transcription rate across fibroblast cell states, we additionally performed an RNA spike-in prior to RNA extraction, normalizing to total cell number, and then normalized gene expression to the spike-in controls prior to downstream analysis (Fig. 5.7A-B) (Chen, Hu et al. 2015). Multidimensional scaling (MDS) of the transcriptomic data revealed clustering across both cell-states and treatments, suggesting MG132 similarly shifted the cell's transcriptional program (Fig. 5.6A). Further, each cell-state clustered individually, suggesting each cell-state harbored a distinct transcriptional profile. We next asked if the proteostasis networks of cells responding to MG132 would be similar or different in cells with or without aggresomes by performing MDS on only the differential expression of genes in the proteostasis network (chaperone, proteasome, autophagy) in response to MG132 (Fig. 5.6B). In support of our previous data (Fig. 5.4), we observed that each cell-state harbored a distinct proteostasis network transcriptional response to proteasome inhibition (Fig. 5.6B). Further, we asked how each node of the proteostasis network reacted in response to proteasome inhibition in each cell-state. We constructed heat maps and measured the average fold change of chaperone, proteasome and

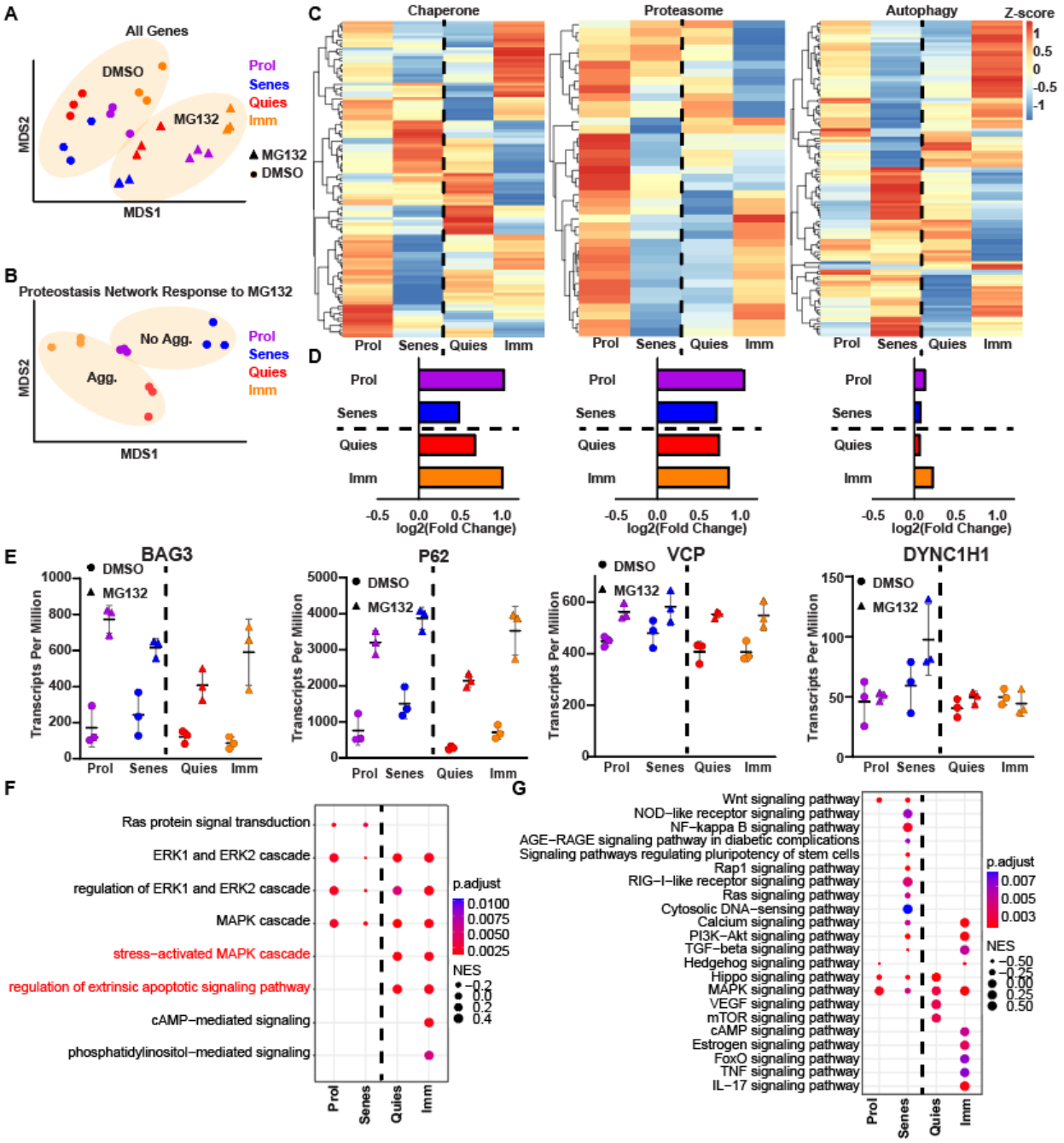

Figure 5.6 – Transcriptional profiling of the fibroblast cell-state specific response to proteasome inhibition reveals stress-activated MAPK signaling associated with aggresome formation. A) MDS analysis of the global transcriptomes of proliferating (purple), senescent (blue), quiescent (red) and immortalized (orange) fibroblasts treated with either 0.1% DMSO (circles) or 10 μM MG132 (squares) for 8 hours. Ovals denote

clustering of DMSO or MG132 conditions. B) MDS analysis of the proteostasis network's (chaperone, proteasome and lysosome genes) transcriptional response to proteasome inhibition in proliferating (purple), senescent (blue), quiescent (red) and immortalized (orange) fibroblasts. Ovals denote clustering of aggresome forming or lacking cell-states. C) Heat maps depicting differential expression of chaperone, proteasome or autophagy genes in response to MG132 in proliferating, senescent, quiescent or immortalized fibroblasts. D) Average log2(fold change) values for all chaperone, proteasome or autophagy genes as proliferating (purple), senescent (blue), quiescent (red) and immortalized (orange) fibroblasts respond to MG132 treatment. E) Transcript per million counts of representative genes implicated in aggresome formation in proliferating (purple), senescent (blue), quiescent (red) and immortalized (orange) fibroblasts treated with DMSO (circles) or MG132 (squares). F-G) GO and KEGG analysis of the signaling pathways significantly differentially regulated in response to MG132 in proliferating, senescent, quiescent, and immortalized cells. The dotted line in each panel separates cell-states that either do or do not form the aggresome.

autophagy genes (Fig. 5.6C-D). We observed stronger upregulation of chaperone and proteasome genes in response to proteasome inhibition, though autophagy also became upregulated in all four cell-states (Fig 3D). Surprisingly, no one feature clearly correlated with aggresome presence, further suggesting that the differences driving aggresome formation in each cell-state are lesser than the differences driving each cell-state's identity.

To gain insight into why some fibroblast cell-states form the aggresome and some do not, we reasoned that one explanation could be reduced expression of genes essential for aggresome formation. Therefore, we examined the expression of known genes essential for aggresome formation or genes known to function at the aggresome (Fig. 5.6E). However, we observed robust expression of all known aggresome-related genes we examined in all cell-states. While it is likely that there are additional factors essential for aggresome formation that have yet to be revealed, this finding suggests that aggresome presence or absence across cell-states is not due to the lack of components to form the aggresome, but rather a decision each cell makes in their response to proteasome inhibition.

Therefore, we next hypothesized that cells which form or do not form the aggresome differ in how they use their systems to respond to proteasome inhibition. To identify which features and signaling pathways would be associated with the presence or absence of the aggresome, we performed Gene Ontology (GO) and Kyoto Encyclopedia of Genes and Genomes (KEGG) analyses on each fibroblast cell-state's transcriptional response to proteasome inhibition individually, and probed for signaling pathways unique to aggresome-forming or aggresome-lacking cells (Fig. 5.6F-G). We observed

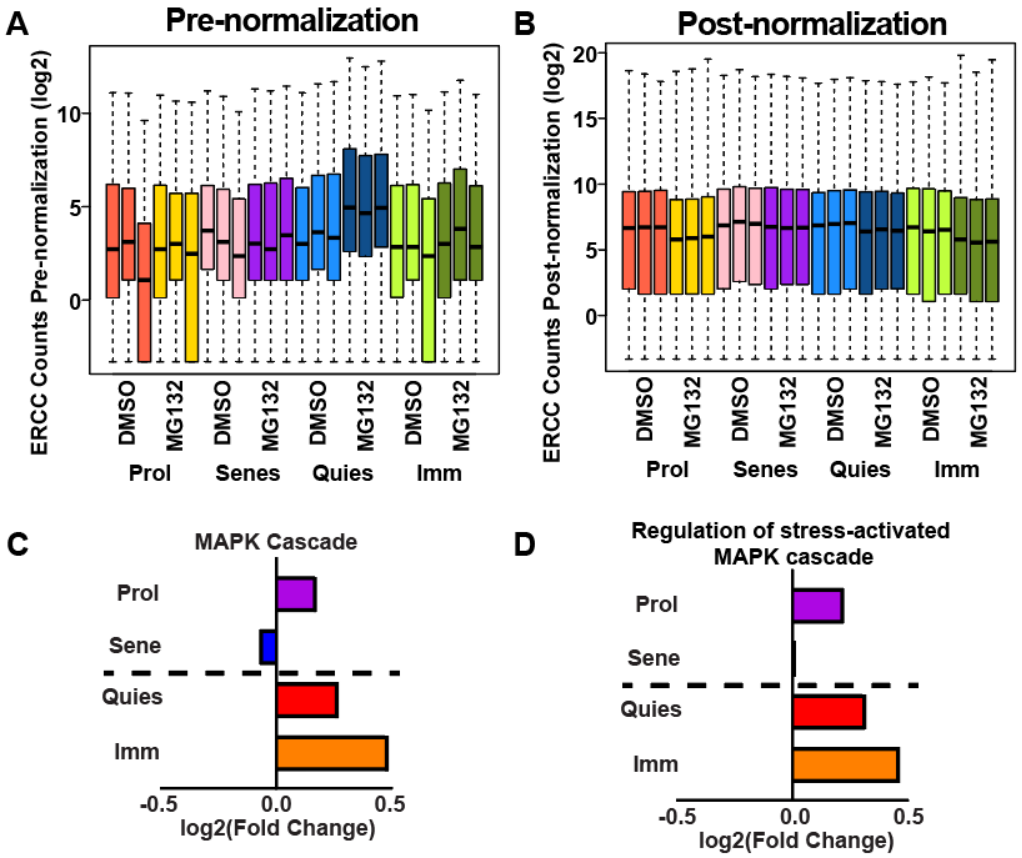

Figure 5.7 – A-B) ERCC spike-in counts relative to other transcripts in proliferating, senescent, quiescent and immortalized fibroblasts treated with DMSO or MG132 pre-ERCC normalization (A) or post-ERCC normalization (B). C-D) Average log2(fold change) values for all MAPK Cascade or Regulation of stress-activated MAPK Cascade genes as proliferating (purple), senescent (blue), quiescent (red) and immortalized (orange) fibroblasts respond to MG132 treatment.

that the aggresome-forming quiescent and immortalized fibroblasts significantly differentially regulated the stress-activated node of MAPK signaling, whereas the aggresome-lacking proliferating and senescent fibroblasts did not (Fig 3F). Supporting these analyses, we calculated the average log fold change of genes in the MAPK pathway generally, and more specifically in the stress-activated MAPK gene node, and found that in both cases, aggresome forming fibroblasts exhibited the strongest induction of MAPK/stress-activated MAPK signaling (Fig. 5.7C-D). This observation also confirms recent studies that revealed an essential role for p38 MAPK (stress-induced MAPKs) in aggresome formation in a human embryonic kidney cell line (HEK293), AD293 (Zhang, Gao et al. 2018, Qin, Jiang et al. 2019). Specifically, Zhang and colleagues found that p38δ MAPK (MAPK13) played a role in aggresome formation in a human embryonic kidney cell line (HEK293), AD293 cells, through phosphorylating p62 (SQSTM1) at threonine 269 and serine 272 (T269/S272) (Fig. 5.8A). Therefore, we hypothesized that this mechanism would work similarly to drive aggresome formation in quiescent and immortalized primary adult mouse dermal fibroblasts.

p38δ MAPK is not associated with aggresome formation in fibroblasts

To test the hypothesis that stress-activated p38 MAPK activation underlies aggresome formation in specific cell-states of our mouse dermal fibroblasts, we first examined p62 T269/S272 phosphorylation in response to proteasome inhibition in proliferating, senescent, quiescent and immortalized fibroblasts, as well as in HEK293 cells (Fig. 5.8C). Interestingly, while we were able to detect p62 T269/S272 phosphorylation in HEK293 cells in the MG132 treated condition, we were unable to

observe substantial p62 T269/S272 in any fibroblast cell-state. This finding suggests that p62 T269/S272 phosphorylation may not be involved in aggresome formation in fibroblasts and that fibroblasts form the aggresome in response to MG132 through mechanisms distinct from that of HEK293 cells.

MAP3K7 promotes aggresome formation in fibroblasts

While p38δ MAPK and P-p62 at T269/S272 did not appear to play a role in aggresome formation in fibroblasts as seen in HEK293 cells, another stress-activated MAPK, MAP3K7 (also called TAK1), has been reported to phosphorylate p62 at a different serine residue (S349 in human; S351 in mouse) (Fig. 5.8B) (Hashimoto, Simmons et al. 2016, Kehl, Soos et al. 2019). As p62 is essential for aggresome formation (Matsumoto, Inobe et al. 2018, Zhang, Gao et al. 2018), we next hypothesized that MAP3K7 could play a role in aggresome formation in quiescent and immortalized primary mouse dermal fibroblasts. To test this hypothesis, we performed immunoblots to measure p62 S351 phosphorylation. Fitting with our hypothesis, we observed p62 S351 phosphorylation in fibroblasts treated with MG132 (Fig. 5.8C). Additionally, immunostaining for p62 S351 phosphorylation revealed that p62 S351 phosphorylation was localized to the aggresome in both quiescent and immortalized fibroblasts, further supporting the notion that this phosphorylation could be involved in aggresome formation. To determine whether MAP3K7 was responsible for p62 S351 phosphorylation in response to proteasome inhibition in fibroblasts, we challenged quiescent fibroblasts with MG132 and either Takinib, a MAP3K7 inhibitor which blocks ATP hydrolysis by MAP3K7,

blocking its kinase activity, or DMSO. Expectedly, we observed that the addition of Takinib to cells

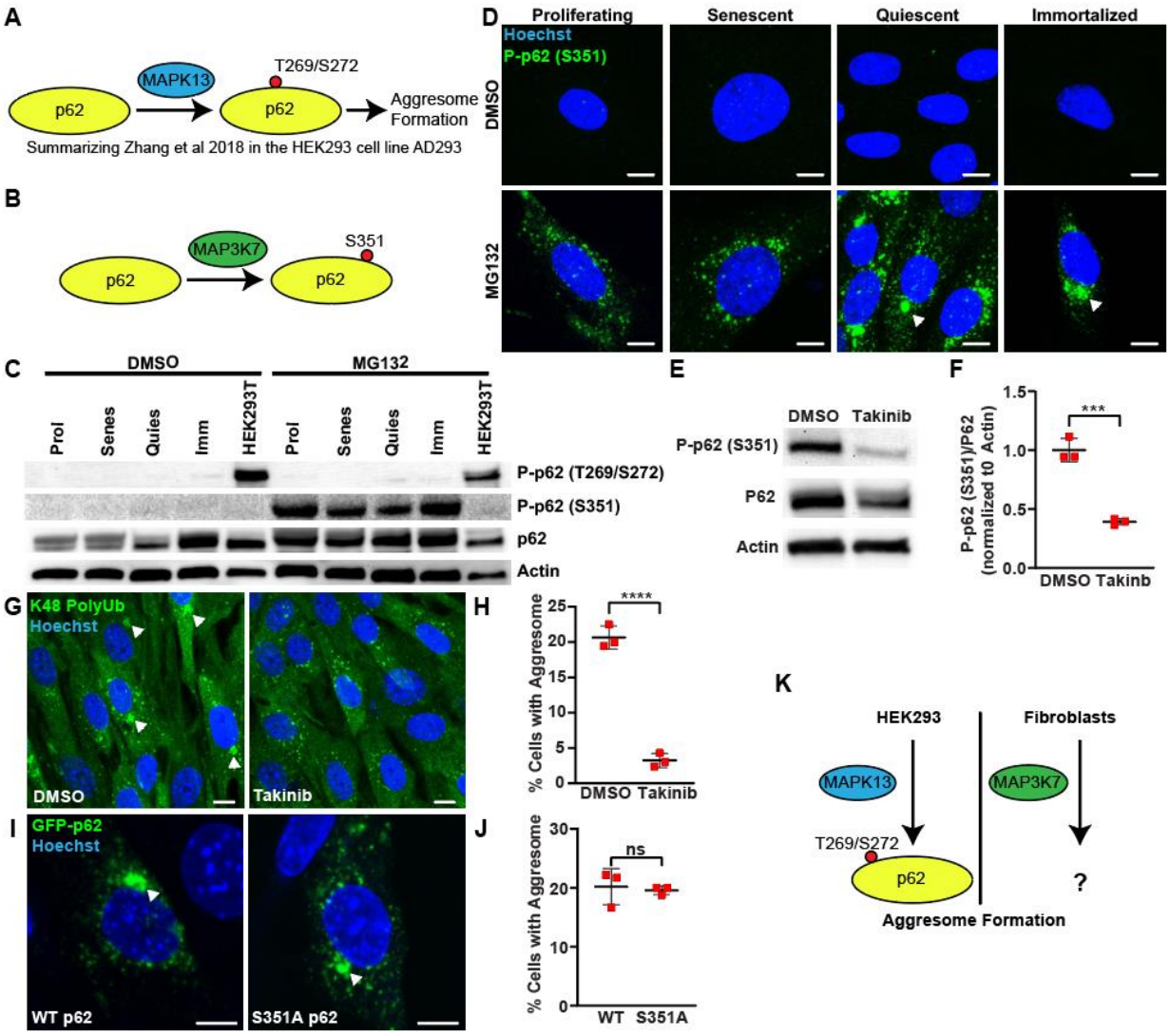

Figure 5.8 – MAP3K7 inhibition suppresses aggresome formation in quiescent fibroblasts. A) Schematic summarizing how p38δ MAPK (MAPK13) phosphorylates p62 at T269/S272 to promote aggresome formation in HEK293 cells (Zhang, Gao et al. 2018). B) Schematic illustrating how MAP3K7 can phosphorylate p62 at S351. C) Proliferating, senescent, quiescent, and immortalized fibroblasts and HEK293T cells were treated with 0.1% DMSO or 10 μM MG132 for 8 hours and then total protein was analyzed by western

blot for actin, p62, P-p62 S351 and P-p62 T269/S272. D) Proliferating, senescent, quiescent, and immortalized fibroblasts were treated with 0.1% DMSO or 10 μM MG132 for 8 hours and then immunostained for P-p62 S351 (green) and stained for nuclei (Hoechst; blue). Arrows denote P-p62 S351 localized to the aggresome. E-F) Quiescent fibroblasts were treated with either 0.1% DMSO or 62 μM Takinib for 24 hours preceding 10 μM MG132 for 8 hours and then total protein was analyzed by western blot for actin, p62 and P-p62 S351 (N=3; Student's t-test; mean ± SD). G-H) Quiescent fibroblasts were treated with either 0.1% DMSO or 62 μM Takinib for 24 hours preceding 10 μM MG132 for 8 hours and then fixed and immunostained for K48 PolyUb (green) and stained for nuclei (Hoechst; blue). White arrows denote aggresomes (N=3; Student's t-test; mean ± SD). I-J) Quiescent fibroblasts were transduced with with either WT or S351A GFP-p62, treated with 10 μM MG132 for 8 hours and then fixed and immunostained for GFP (green). Nuclei were stained with Hoechst (blue) (N=3; Student's t-test; mean ± SD). K) Model of cell-type specific MAPK-related mechanisms for promoting aggresome formation. Scale bars, 10 μm. ***p<0.001, ****p<0.0001.

treated with MG132 was associated with a significant reduction in p62 S351 phosphorylation (Fig. 5.8E-F). Finally, we asked whether MAP3K7 p62 S351 phosphorylation would be functionally important for a quiescent fibroblast's ability to form the aggresome. To this end, we applied MG132 and either Takinib or DMSO to quiescent fibroblasts and quantified the percentage of cells forming the aggresome. We found that addition of Takinib culminated in a significant reduction in the percentage of cells forming a K48 polyUb-rich aggresome, suggesting the MAP3K7 plays a role in promoting aggresome formation in quiescent fibroblasts.

We next asked whether Takinib would similarly block aggresome formation in immortalized fibroblasts, which also exhibited p62 S351 phosphorylation in response to proteasome inhibition. Surprisingly, we found that immortalized fibroblasts treated with MG132 and Takinib trended towards less aggresome formation, but did not display significantly reduced aggresome formation (Fig. 5.9A-B). To determine if Takinib similarly inhibited p62 S351 phosphorylation in immortalized fibroblasts, we performed immunoblots and found that Takinib reduced p62 S351 phosphorylation only to 65% of control levels in immortalized fibroblasts as compared to 39% in quiescent fibroblasts (Fig. 5.9C-D). Several kinases have been reported to phosphorylate p62 S351, and thus it is possible that immortalized fibroblasts use different kinases to form the aggresome in response to proteasome inhibition (Sanchez-Martin and Komatsu 2018). It is also possible that MAP3K7 is critical for aggresome formation in immortalized fibroblasts, but in response to MAP3K7 inhibition by Takinib, immortalized fibroblasts are able to compensate to form the aggresome through other kinases, while quiescent fibroblasts are unable to do so. Regardless, when Takinib is able to suppress p62 S351

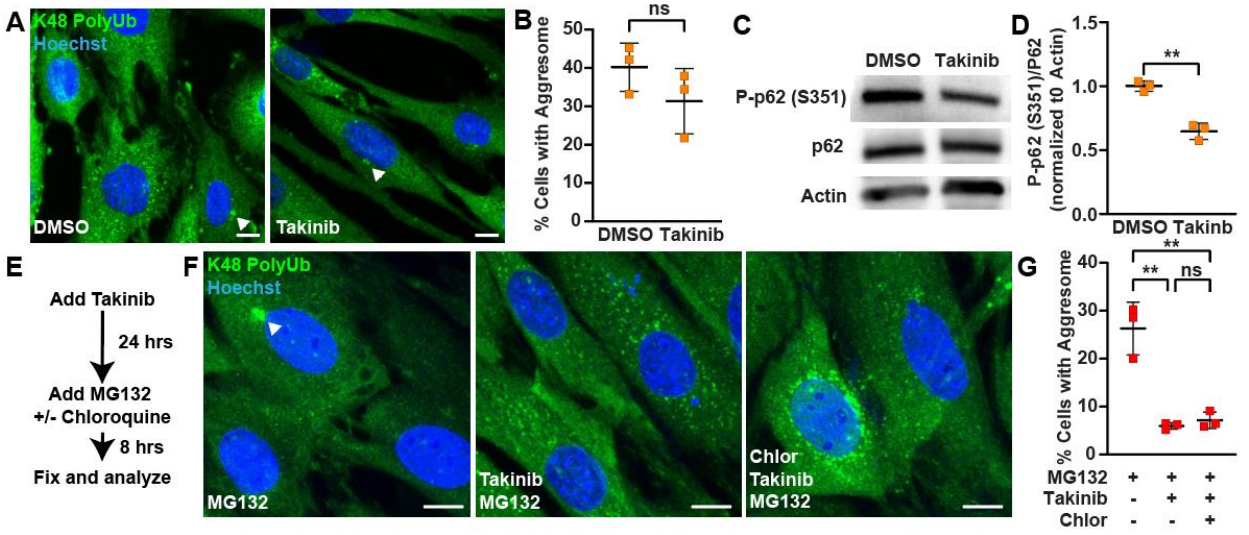

Figure 5.9 – A-B) Immortalized fibroblasts were treated with either 0.1% DMSO or 62 µM Takinib for 24 hours preceding 10 µM MG132 for 8 hours and then fixed and immunostained for K48 PolyUb (green) and stained for nuclei (Hoechst; blue). White arrows denote aggresomes (N=3; Student's t-test; mean ± SD). C-D) Immortalized fibroblasts were treated with either 0.1% DMSO or 62 µM Takinib for 24 hours preceding 10 µM MG132 for 8 hours and then total protein was analyzed by western blot for actin, p62 and P-p62 S351 (N=3; Student's t-test; mean ± SD). E-G) Quiescent fibroblasts were treated with either 0.1% DMSO or 62 µM Takinib for 24 hours preceding 10 µM MG132 with or without 1 µM Chloroquine for 8 hours and then fixed and immunostained for K48 PolyUb (green) and stained for nuclei (Hoechst; blue). White arrows denote aggresomes (N=3; Two-way ANOVA with post-hoc Tukey's test; mean ± SD). Scale bars, 10 µm. **p<0.01.

phosphorylation (in quiescent fibroblasts) more potently, aggresome formation is reduced, whereas when Takinib is unable to suppress p62 S351 phosphorylation (in immortalized fibroblasts), aggresome formation is unaltered. Thus, our data in quiescent and immortalized fibroblasts treated with Takinib collectively support the notion that higher levels of MAP3K7 activity drive aggresome formation.

We next asked whether MAP3K7 drives aggresome formation through its kinase activity on p62 at S351. To address this question, we obtained a vector for transiently expressing WT GFP-p62 and generated a S351 phospho-dead mutant GFP-p62 by replacing S351 with an alanine (S351A). We transduced fibroblasts with these constructs, induced quiescence and then challenged the cells with MG132 to induce aggresome formation. We observed that both WT and S351A p62 was able to localize to the aggresome in quiescent fibroblasts (Fig. 5.8I-J). This result suggests that S351 is not required for aggresome formation and that MAP3K7 is driving aggresome formation through other targets. The identity of these targets at this point remains unclear.

To confirm that our reduction in aggresome formation with Takinib in quiescent fibroblasts was not due to an upregulation of autophagy, we simultaneously challenged fibroblasts with MG132 to induce aggresome formation, Takinib to stop aggresome formation, and chloroquine to inhibit autophagy. While we observed aggresome formation in our MG132 only condition, and a reduction in aggresomes in MG132 and Takinib treatment, fibroblasts treated with the combination of MG132, Takinib, and chloroquine did not display an increase in the percentage of cells forming aggresomes, suggesting that Takinib does not reduce aggresome formation through increasing autophagy (Fig.

5.8E-F). Therefore, Takinib blocks aggresome formation by blocking a signaling pathway associated with aggresome formation.

Thus, here we report a novel kinase, MAP3K7, critical for aggresome formation in fibroblasts. As primary adult mouse fibroblasts form the aggresome through mechanisms at least in part distinct from what was previously reported in HEK293 cells, our data support a model that cells harbor multiple distinct mechanisms for forming the aggresome (Fig. 5.8K).

Here we demonstrate that primary adult mouse dermal fibroblasts use the aggresome in the quiescent and immortalized cell-state, but not in the proliferating and senescent cell-state. We find that aggresome formation is not simply a reflection of a cell's preference for protein degradation by autophagy, but rather, that each fibroblast cell-state employs a unique proteostasis network to maintain proteostasis. Transcriptomic analysis of the fibroblast response to proteasome inhibition revealed features associated with cells that form or do not form aggresomes. Among these features, we found stronger activation of stress-activated MAPK signaling is associated with aggresome formation, supporting recent work showing stress-activated MAPK signaling drives aggresome formation in HEK293 cells (Zhang, Gao et al. 2018, Qin, Jiang et al. 2019). Interestingly, our data suggest that fibroblasts use distinct mechanisms to form the aggresome compared to HEK293 cells, using MAP3K7, compared to HEK293 cells which use p38δ MAPK to drive aggresome formation. Thus, our data support a critical role for stress-activated MAPK signaling in aggresome formation, but suggest that the mechanisms driving aggresome formation across cell types are not the same. Taken together, we demonstrate that

aggresome formation is not a universal component of the cell's response to disrupted proteostasis, a novel role for MAP3K7 in aggresome formation, and suggest that mechanisms for aggresome formation across cell types are at least partially distinct.

5.5 Discussion

Here we demonstrate that preference to degrade protein through the aggresome is cell-type and cell-state specific. However, it is unclear whether the absence of aggresome formation is a reflection of proliferating and senescent fibroblasts making a decision to not form the aggresome through suppression of a pathway compared to an inability to form the aggresome due to missing expression of unknown aggresome formation machineries. Regardless, if the aggresome is cytoprotective as evidence suggests (Tanaka, Kim et al. 2004), it is not clear why some cells would not evolve to use this mechanism for maintaining proteostasis, while other cells conserved this mechanism. One possibility could be that redundancy in the cell's proteostasis network allowed for cell types to evolve divergently in how they maintain proteostasis. It also could be that we still don't fully understand the function of the aggresome and that there may be more nuanced contexts which dictate when the aggresome would be the most useful for a cell's fitness.

These data also provide an important cautionary note regarding the use of immortalized cell lines to study biology that is reflective of cell behavior *in vivo*. The majority of aggresome literature to date has investigated the aggresome in immortalized cells *in vitro*. However, our data demonstrate that the *simple* act of immortalizing cells is sufficient to drive cells that would not otherwise do so, to use the aggresome. Additionally, cell immortalization drove widespread remodeling of the proteostasis network. While

initial studies of the aggresome in immortalized cell-lines *in vitro* have provided great utility towards an understanding of aggresome function and mechanisms of aggresome formation and should not be discounted, our data highlights the importance of translating immortalized cell line findings to primary cell lines *in vitro* and to cells in tissue *in vivo*.

Identification of MAP3K7 as a mediator of aggresome formation in fibroblasts is timely, as recent work has described a role for aggresome-like structures as a program implicated in the cell's inflammasome (Magupalli, Negro et al. 2020). When specific types of inflammasomes form, an HDAC6-dependent perinuclear puncta of proteins implicated in the cell's response to infection forms. MAP3K7 is also known as transforming growth factor β activated kinase 1 (TAK1), and thus, our data provides additional connections between aggresome formation and the cell's immune system. MAP3K7 also was recently found to interact with p62 to promote p62's signaling actions. Thus, MAP3K7 inhibition could prevent this interaction and free p62 to be more active in the aggresome pathway (Kehl, Soos et al. 2019). Identification of MAP3K7 as a mediator of aggresome formation also corroborates a recent concept that MAPK signaling plays a role in aggresome formation (Zhang, Gao et al. 2018, Qin, Jiang et al. 2019). In this previous report in a HEK293 cell line (AD293), p38δ MAPK was required for aggresome formation through phosphorylation of p62 at T269/S272. In contrast, we find no evidence in mouse fibroblasts that p38δ MAPK is required for aggresome formation, however, we do still find that a stress-activated MAPK is critical for aggresome formation through its action phosphorylating p62. Together, our reports suggest that cells have multiple distinct mechanisms for inducing aggresome formation which converge on p62. It is still unclear

how much overlap there is or isn't in these two systems and further how many other mechanisms there may be for cells to from the aggresome.

In summary, we identify primary adult mouse dermal fibroblast cell-states as a model to understand aggresome formation and function, and further use this system to reveal the aggresome as a non-universal, but tunable mechanism cells can activate through multiple strategies, specifically through stress-activated MAPK signaling, to maintain proteostasis.

5.6 Materials and Methods

Fibroblast Isolation, Cell-State Generation, and Culture

Following a previously established protocol, fibroblasts were taken from tail snips of male 4 week-old C57Bl6 mice (Khan and Gasser 2016). To isolate the fibroblasts for *in vitro* culturing, tail snips were incubated in 70% ethanol for 5 minutes at room temperature. Tail snips were then cut into smaller pieces with scissors and put into an enzyme solution (20 µM Protease (Sigma P8811), 35 µM Collagenase D (Sigma 11088866001), 1.5 mM Tris Buffer and 62.5 µM EDTA) to dissociate the tissue and release cells at 37°C for 90 minutes. Samples were then mashed for 2 minutes with a plunger from a syringe and then filtered through a 70 µm cell strainer. The sample was then washed by adding 10 mL of fibroblast culture media (FCM; RPMI with Glutamine (Invitrogen 11875-093), 10% FBS (Invitrogen 16000044), 55 µM β-Mercaptoethanol (Invitrogen 21985-023), 100 µM asparagine and 100 µg/ml Penicillin-Streptomycin (Invitrogen 15140122), 25 µg/mL Amphoterecin B (Sigma-Aldrich A9528)) and cells were pelleted at ~580 x g for 7 minutes. Cells were washed a second time with 10 mL of FCM

and spun down similarly. Cell pellets were then resuspended and plated into one well of a 6 well plate (Fisher Scientific 1483211). Cells were left to sit for 5 days at 37°C and 5% CO_2 after initial plating and were only fed once after three days by adding an additional volume of FCM. After 1-2 weeks fibroblasts expanded and were ready for experiments and were fed at least once every 3 days with FCM.

Confluent fibroblasts were washed once with PBS, trypsinized with 0.25% trypsin-EDTA (Gibco 25200072) for 3-4 minutes at 37°C and 5% CO_2, spun down at 400 x g for 4 minutes, and then resuspended and plated into FCM. To generate proliferating fibroblast cultures, fibroblasts were seeded at ~30% confluence and allowed to sit for 2-3 days prior to analysis and prior to reaching greater than 80% confluence. To generate senescent fibroblasts (β-galactosidase+), fibroblasts were plated at 10% confluence and then passaged sequentially at 10% confluence until the cultures no longer expanded. After cultures stopped expanding, all cultures were left for at least 7 days to develop a mature senescence phenotype, with regular media changes at least every 3 days. To generate quiescent fibroblasts (EdU-), fibroblasts were seeded at 70-80% confluence. After reaching 100% confluence, cultures were left for at least 3 additional days to develop a mature quiescent phenotype, and during this time still fed at least once every 3 days. To immortalize fibroblasts (SV40t+), low passage proliferating fibroblasts (P0-2) were seeded at 50% confluence and then transduced with retroviral particles harboring SV40t (as described in the “HEK Culture” and “Viral Particle Production” section). After transduction, fibroblasts were seeded at 5% confluence and then immortalized cells brought the dish to confluency. After 2 passages, the cultures were pure for immortalized cells as detected by Sv40t immunostaining.

HEK293T Culture and Viral Particle Production

HEK293T cells (gift from Dr. Subhojit Roy) were cultured in HEK293T media (DMEM, high glucose, pyruvate, no glutamine (Thermo 10313021) supplemented with 10% FBS (Invitrogen 16000044) and Penicillin-Streptomycin (Invitrogen 15140122) at 37°C and 5% CO_2. When 100% confluent, cells were trypsinized with TrypLE Express Enzyme (Invitrogen 12604013) for 3 minutes at room temperature and spun down at 120 x g for 4 minutes prior to being resuspended in HEK293T media and replated. To generate viral particles, HEK293T cells were transfected using lipofectamine (Invitrogen 11668019) with CMV-GP (Gift from Dr. Fred Gage), pCMV-VSV-G (Gift from Dr. Fred Gage) and a transfer plasmid (SV40T; gift from Dr. Peter Lewis). 48 hours after transfection, viral particles were collected in the supernatant, sterile filtered to remove HEK293T debris, and applied directly to fibroblasts.

Microscopy

All images were taken with either a Nikon C2 confocal microscope or a Zeiss widefield epifluorescent microscope. Typically in figures 1-4, images represent max intensity projections of z-stacks taken to capture the entire cell with 1 μm step sizes. For live-cell experiments, cells were kept in a stage-top incubator to maintain humidity, 37°C, and 5% CO_2. Images were analyzed using Fiji.

Immunostaining

To immunostain fibroblasts to detect vimentin (1:1,000; Sigma-Aldrich AB5733), K48 Polyubiquitin (1:500; Millipore Sigma 05-1307), Lamin B1 (1:500; Abcam ab16048), SV40T (1:500; Abcam ab234426) and P-p62 S351 (1:500; Abcam ab211324), fibroblasts were fixed in 4% paraformaldehyde (PFA) for 15 minutes at room temperature. Samples were then permeabilized with 0.25% triton for 15 minutes at room temperature and blocked with 20% donkey serum (Millipore Sigma S30-100ML) in an antibody buffer (150mM sodium chloride, 50mM tris base, 1% bovine serum albumin (Sigma-Aldrich A2153-50G), 100mM L-lysine, 0.04% sodium azide, pH 7.4). Primary antibodies were diluted as listed above in antibody buffer and then applied to samples overnight at 4°C. The following day, samples were washed 3 times with PBS for 10 minutes at room temperature and then stained with secondary antibodies (1:500) for 1.5 hours at room temperature. Following secondary staining, samples were washed 3 times with PBS for 10 minutes. In the second to last wash, samples were treated with Hoechst to label nuclei (1:10,000; Thermo Fisher Scientific 62249).

To immunostain fibroblasts with γ-tubulin (1:250; Sigma-Aldrich T5326) and K48 Polyubiquitin (1:500; Millipore Sigma 05-1307), cells were stained for K48 Polyubiquitin as described above. Following staining for K48 Polyubiquitin, cells were further stained to detect γ-tubulin by performing the following protocol. Cells were permeabilized with ice-cold methanol (pre-chilled for 1 hour at -80°C) for 10 minutes at -20°C. Samples were then blocked and stained with primary and secondary antibodies as described above.

Western Blotting

Western blots probing for p62 (1:1,000; Sigma-Aldrich P0067), P-p62 T269/S272 (1:1,000; PhosphoSolutions p196-269), P-p62 S351 (1:1,000; Abcam ab211324), actin (1:1,000; Bio Rad VMA00048), HSP90β (1:1,000; GeneTex GTX101448) and puromycin (1:1,000; Millipore Sigma MABE343) were performed using the following protocol. To extract soluble proteins, cell pellets were resuspended in a soluble lysis buffer (10 mM Tris/HCl, 150 mM NaCL, 0.5 mM EDTA, 0.5% NP40, with protease inhibitor added) and placed on ice for 30 minutes. To extract total protein fractions, cell pellets were resuspended in total lysis buffer (10 mM Tris/HCl, 1% Triton, 150 mM NaCl, 10% Glycerol, 4% SDS, with DNAse and protease inhibitor added) and lysed for 30 minutes. Following lysis, samples were sonicated with a probe sonicator 15 times for 1 second on low power, and then clarified by centrifugation at 15,000 x g for 10 minutes. Samples were then quantified using the DC assay (Bio-Rad 5000112) and then ~5 µg of protein per sample was run through an SDS-PAGE gel. SDS-PAGE gels were transferred onto a membrane at 100V for 1.5 hours at 4°C. Membranes were then blocked in TBS-T with 5% milk for 30 minutes at room temperature. Primary antibodies were diluted in 5% milk and incubated on membranes overnight diluted as indicated above at 4°C on a tube roller. Primary antibody was washed off 3 times with TBS-T for 5 minutes/wash at room temperature on a tube roller. Secondary antibodies were applied to membranes in 5% milk in TBS-T for 1.5 hours at room temperature and then washed off 3 times with TBS-T for 5 minutes/wash on a tube roller. Following washing off secondary, protein expression was detected using a UVP Imaging system after treated blots with an ECL reaction. To quantify protein expression, blots were analyzed in ImageJ. In brief, ROIs were drawn around each band and measured, background signal was subtracted, and all

proteins were normalized to housekeeping genes, or as otherwise noted in the figure legends. All experiments were repeated at least 3 times to ensure reproducibility.

EdU Pulse

Fibroblasts were pulsed for 1 hour with 10 μm EdU (Invitrogen C10337) at 37°C to label cells in S-phase and then fixed with 4% PFA for 15 minutes at room temperature. Cells were then treated per the manufacturer's recommendations to visualize EdU through click-chemistry (Invitrogen C10337). Cells were stained with Hoechst to label nuclei (1:10,000; Thermo Fisher Scientific 62249). Samples were then analyzed for the percentage of cells that were EdU+.

Aggresome Assays

To detect aggresomes in various conditions, cells were treated as described in each legend respectively. Equal volume DMSO was applied to cells as a vehicle control for compounds dissolved in DMSO. Cells were immunostained as described in the "Immunostaining" section of the methods and analyzed for the percentage of cells with an aggresome as determined by an observer blind to experimental conditions but trained to identify aggresomes. An aggresome was defined as a perinuclear enrichment of K48 PolyUb localizing to the nuclear bay. All aggresome quantification experiments were repeated at least 3 times.

B-Galactosidase Assays

Proliferating and Senescent mouse fibroblasts were washed twice with 1X PBS and fixed and stained for B-Gal activity using the Senescence B-Galactosidase Staining Kit per the manufacturer's instructions (Cell Signaling Technology 9860S). The following day cells were washed twice with 1X PBS and stained with Hoechst (Thermo Fisher Scientific 62249). After staining, cells were imaged using a white light microscope and the percentage of B-Gal+ cells was determined by taking the number of B-Gal+ cells over the number of Hoechst+ cells in each image. This experiment was repeated 3 times.

Proteasome Activity Assays

Protein was extracted from fibroblasts with conditions optimized to preserve proteasome activity by resuspending pellets in 50mM Tris-HCl, pH 7.5, 250mM sucrose, 5mM MgCl2, 0.5mM EDTA and 1mM dithiothreitol. Samples were then lysed by passing samples through a 27-gauge needle ten times. Samples were clarified through centrifugation for 10 minutes at 4°C at 15,000 x g. Protein concentration was quantified using the DC protein assay (Bio-Rad 5000112). To perform the assay 10-30 µg of protein were loaded for each sample (equal weight of total protein was loaded across samples in each experiment) into a reaction buffer comprised of: 2 mM adenosine triphosphate (Fisher ICN15026605), 0.37 mM proteasome substrate (trypsin - Boc-Leu-Arg-Arg-AMC) and then diluted to 100 µl in resuspension buffer. Samples were measured every 5 minutes over the course of 1 hour in a plate reader at 37°C by exciting at 380 nm and collecting at 460 nm. Three wells were averaged for each sample and the experiment was repeated 3 times on three separate days.

Lysotracker Assays

Live fibroblasts were treated with Lysotracker (1:1,000; Thermo Fisher Scientific L7528) and Hoechst (1:10,000; Thermo Fisher Scientific 62249) for 30 minutes at 37°C and 5% CO_2 to label lysosomes and nuclei respectively. Following dye labeling, cells were washed 3 times with media and immediately imaged. To analyze the data, z stacks were acquired, and raw integrated intensity normalized to area was calculated for each cell using ImageJ. 1 µM chloroquine was used as a positive control to validate Lysotracker. Each experiment was repeated at least 3 times.

Protein Synthesis Assays

Fibroblasts were pulsed with 10 µg/mL puromycin (Invitrogen A11138-03) for 10 minutes at 37°C and 5% CO_2 to label nascent proteins. As a control, samples were treated with the protein synthesis inhibitor 10 µM cycloheximide (Millipore Sigma C4859-1ML) for 10 minutes prior to puromycin treatment and during puromycin treatment. After treatment, protein was extracted and analyzed by western blot as described in the “Western Blot” section of the methods. This experiment was repeated 3 times.

RNA extraction, library preparation and sequencing

Fibroblast cell-states were generated as described in “Fibroblast Isolation, Cell-State Generation and Culture” and then treated with either a vehicle control dose of 0.1% DMSO or 10 µM MG132 for 8 hours to induce aggresome formation. After 8 hours, cells were trypsinized and counted and then pellets of equal cell number were created. Prior to RNA extraction, ERCC Spike-In Mix RNA was added to resuspended pellets at a ratio

of 0.5 uL (of 1:100 diluted from ERCC stock received from the manufacturer) to 100,000 cells to provide the capacity to normalize mRNA to cell number and probe for changes in global transcription across cell-states and treatments. Total RNA was extracted using a RNeasy Mini Kit (Qiagen 74104) according to the manufacturer's instructions. Extracted RNA was submitted to LC Sciences for poly(A) RNA sequencing.

Poly(A) RNA sequencing libraries were generated using Illumina's TruSeq-stranded-mRNA protocol. Poly(A) mRNAs were isolated using oligo-(dT) magnetic beads, fragmented using divalent cation buffer at elevated temperature and then used to construct DNA libraries for sequencing. Samples were quality controlled using an Agilent Technologies 2100 Bioanalyzer High Sensitivity DNA Chip and then sequenced as paired-end 140 base pair reads on an Illumina NovaSeq 6000 sequencing system.

RNA-seq data processing

Sequencing data was trimmed using Cutadapt (Martin 2011). Reference mouse transcripts were obtained from the Ensembl 99 build (GRCm38p6), and combined with the ERCC92 sequences, to create a common mapping reference index using kallisto 0.43.0 (Bray, Pimentel et al. 2016). Trimmed reads were mapped to the combined reference with default parameters.

Parsed pseudocount values were extracted for each sample, and data was imported into R 3.6.3 for processing. We leveraged the R package 'RUVseq' 1.20.0 (Risso, Ngai et al. 2014) to normalize counts as a function of the ERCC92 spike in count values using the RUVg function. RUV-normalized counts were then used as input to R

package DESeq2 version 1.30.1 to perform differential expression analysis for each fibroblast cell-state's response to proteasome inhibition. MDS analyses were performed using cmdsale() in R. Heat maps were created using pheatmap() in R scaling by row. KEGG analyses was performed using gseKEGG() in R with a p value cutoff of 0.05. GO analyses were performed using gseGO() in R with a p value cutoff of 0.05. Average fold change plots were generated by taking the average differential expression output from DESeq2 for each gene in each pathway respectively. Gene lists for each node of genes came from the Gene Ontology Browser (http://www.informatics.jax.org/vocab/gene_ontology). Transcript per million counts (TPM) were calculated by taking the raw gene counts normalized to ERCC spike-in and dividing by gene length in kilobases to get reads per kilobase (RPK) (https://www.rna-seqblog.com/rpkm-fpkm-and-tpm-clearly-explained/). Then RPK was divided by an RPK scaling factor equal to the sum of all RPK values in each sample divided by 1 million.

Molecular Cloning

To generate a GFP-p62 S351 phospho-dead mutation, WT GFP-p62 was obtained from Addgene (Addgene 38277) (Itakura and Mizushima 2011). Primers were designed to change the coding sequence of S351 from TCT (serine) to GCA (alanine) using the Q5 site-directed mutagenesis kit from NEB (NEB E0552S).

S351 Mutant Aggresome Experiments

To perform the mutant p62 aggresome experiment, proliferating fibroblasts were plated at 50% confluence and then transduced with retroviral particles harboring WT or

S351A GFP-p62 (generated as described in the “HEK293T Culture and Viral Particle Production” section of this protocol). Proliferating fibroblasts were then cultured for 7 days prior to induction of quiescence. After induction of quiescence, fibroblasts were challenged with MG132 as indicated in the legend and then fixed for immunostaining and analysis. This experiment was repeated three times. As transduction efficiency was poor (less than 1%), the quantitation represents analysis of all cells present in each well in each condition respectively.

Statistics

All experiments, unless otherwise noted, were repeated at least three times on three separate days with at least three technical replicates, as applicable. Typically data in the figures displays average values for technical replicates from one experiment that is representative of all experiments performed with error bars representing standard deviation. Significance tests were performed using GraphPad Prism using tests as indicated in each figure legend.

Chapter 6: Conclusion

6.1 Brief Summary and Discussion of Implications

In this dissertation, I discussed experiments we performed aimed at increasing our understanding of how NSCs exit quiescence as they begin to create new neurons in adult organisms. Studying NSC quiescence is particularly important in understanding adult neurogenesis as it has become increasingly recognized as the rate-limiting step in adult neurogenesis. In Chapter 2, I provided an introduction to NSC quiescence and adult neurogenesis, discussing the widespread remodeling of a NSC's biology that occurs during NSC quiescence exit and the numerous identified strategies for manipulating NSC quiescence *in vitro* and *in vivo*. I also highlighted shortcomings and existing open questions posed by the field. In Chapter 3, I described our efforts to answer some of these open questions and bridge technical gaps by creating a new tool to study NSC quiescence through imaging NSC autofluorescence. More specifically, we found that NSC autofluorescence could be used to classify NSC activation state and study NSC quiescence *in vitro* and *in situ*. In Chapter 4, I described data outlining a role for the protein turnover program called the aggresome in mediating NSC quiescence exit. Further, I described a role for the intermediate filament vimentin in maintaining cellular proteostasis, which we hypothesize is through localizing proteasomes to the aggresome for efficient protein degradation. Lastly, in Chapter 5, I discussed a study of the aggresome in primary mouse dermal fibroblasts. We found that the aggresome is not a universal feature of any cell's response to impaired proteostasis, but rather that cells can use the aggresome cell-state specifically. We also created a resource for better understanding aggresome function and formation by performing RNA sequencing on the fibroblast response to proteasome inhibition and used this resource to identify a novel regulator of aggresome

formation, MAP3K7. Together, these data broadly provide novel insight into the molecular events mediating NSC quiescence exit. More specifically, these data provide mechanistic insight into the events which must occur for efficient NSC quiescence exit, and highlight a role for proteostasis in this process. Further, these data provide a newly developed tool which will help bridge technical gaps in studying NSC quiescence.

These data have many strengths and weaknesses and pose numerous interesting follow up studies. More specific future directions are outlined in each chapter in each discussion section respectively. Although the focus of this dissertation is narrowly placed on NSC quiescence, it is our hope that these data can contribute to translational work which can ultimately impact public health. Brain aging is implicated in a number of diseases and pathologies, such as Alzheimer's Disease and many other types of neurodegeneration. Many of these diseases and pathologies remain without effective therapies. Although NSCs are present and producing newborn neurons throughout life, their ability to do so during healthy aging or in pathology or disease is heavily limited. Identifying strategies to increase the activity of the endogenous stem cell pool in the brain during aging could be a desirable approach to increase brain rejuvenation and promote healthy brain aging. Thus, while our work is focused on NSC quiescence, our work has broader ties towards tackling brain aging at large, and all diseases and pathologies which fall under this umbrella.

To this end, in these experiments we have identified novel processes which regulate the activity of NSCs, all of which could prove effective targets to modulate adult neurogenesis during aging. For example, identifying ways to increase the efficiency of protein turnover at the aggresome or modulate vimentin expression could provide

strategies to increase adult neurogenesis. Further, beyond specifically identifying targets or processes to modulate NSC quiescence and adult neurogenesis, our work provides basic scientific advances which will contribute to a broader understanding of NSC quiescence and shape the field and brain development and regeneration more generally. Altogether, there are many far-reaching implications for these data.

References

1. Abramov, A. Y., M. Gegg, A. Grunewald, N. W. Wood, C. Klein and A. H. Schapira (2011). "Bioenergetic consequences of PINK1 mutations in Parkinson disease." PLoS One **6**(10): e25622.
2. Adam, C., A. Fekete, G. Bogel, Z. Nemeth, N. Tokesi, J. Ovadi, K. Liliom, S. Pesti, M. Geiszt and L. Buday (2015). "Accumulation of the PX domain mutant Frank-ter Haar syndrome protein Tks4 in aggresomes." Cell Commun Signal **13**: 33.
3. Adolf, A., G. Leondaritis, A. Rohrbeck, B. J. Eickholt, I. Just, G. Ahnert-Hilger and M. Holtje (2016). "The intermediate filament protein vimentin is essential for axonotrophic effects of Clostridium botulinum C3 exoenzyme." J Neurochem **139**(2): 234-244.
4. Alvarez-Buylla, A., M. Theelen and F. Nottebohm (1988). "Birth of projection neurons in the higher vocal center of the canary forebrain before, during, and after song learning." Proc Natl Acad Sci U S A **85**(22): 8722-8726.
5. Andy Liaw, M. W. (2002). "Classification and Regression by randomForest." R News **2**(3): 18-22.
6. Antfolk, D., M. Sjoqvist, F. Cheng, K. Isoniemi, C. L. Duran, A. Rivero-Muller, C. Antila, R. Niemi, S. Landor, C. V. C. Bouten, K. J. Bayless, J. E. Eriksson and C. M. Sahlgren (2017). "Selective regulation of Notch ligands during angiogenesis is mediated by vimentin." Proc Natl Acad Sci U S A **114**(23): E4574-E4581.

7. Audesse, A. J., S. Dhakal, L. A. Hassell, Z. Gardell, Y. Nemtsova and A. E. Webb (2019). "FOXO3 directly regulates an autophagy network to functionally regulate proteostasis in adult neural stem cells." PLoS Genet **15**(4): e1008097.
8. Banerjee, I., Y. Miyake, S. P. Nobs, C. Schneider, P. Horvath, M. Kopf, P. Matthias, A. Helenius and Y. Yamauchi (2014). "Influenza A virus uses the aggresome processing machinery for host cell entry." Science **346**(6208): 473-477.
9. Bannikova, S., D. B. Zorov, R. L. Shoeman, G. V. Tolstonog and P. Traub (2005). "Stability and association with the cytomatrix of mitochondrial DNA in spontaneously immortalized mouse embryo fibroblasts containing or lacking the intermediate filament protein vimentin." DNA Cell Biol **24**(11): 710-735.
10. Bardag-Gorce, F., N. E. Riley, L. Nan, R. O. Montgomery, J. Li, B. A. French, Y. H. Lue and S. W. French (2004). "The proteasome inhibitor, PS-341, causes cytokeratin aggresome formation." Exp Mol Pathol **76**(1): 9-16.
11. Bargagna-Mohan, P., A. Hamza, Y. E. Kim, Y. Khuan Abby Ho, N. Mor-Vaknin, N. Wendschlag, J. Liu, R. M. Evans, D. M. Markovitz, C. G. Zhan, K. B. Kim and R. Mohan (2007). "The tumor inhibitor and antiangiogenic agent withaferin A targets the intermediate filament protein vimentin." Chem Biol **14**(6): 623-634.
12. Barral, J. M., S. A. Broadley, G. Schaffar and F. U. Hartl (2004). "Roles of molecular chaperones in protein misfolding diseases." Semin Cell Dev Biol **15**(1): 17-29.
13. Bartolome, F. and A. Y. Abramov (2015). "Measurement of mitochondrial NADH and FAD autofluorescence in live cells." Methods Mol Biol **1264**: 263-270.

14. Baruch, K., A. Deczkowska, E. David, J. M. Castellano, O. Miller, A. Kertser, T. Berkutzki, Z. Barnett-Itzhaki, D. Bezalel, T. Wyss-Coray, I. Amit and M. Schwartz (2014). "Aging. Aging-induced type I interferon response at the choroid plexus negatively affects brain function." Science **346**(6205): 89-93.
15. Baser, A., M. Skabkin and A. Martin-Villalba (2017). "Neural Stem Cell Activation and the Role of Protein Synthesis." Brain Plast **3**(1): 27-41.
16. Bauer, P. O., R. Hudec, A. Goswami, M. Kurosawa, G. Matsumoto, K. Mikoshiba and N. Nukina (2012). "ROCK-phosphorylated vimentin modifies mutant huntingtin aggregation via sequestration of IRBIT." Mol Neurodegener **7**: 43.
17. Bauer, P. O., R. Hudec, S. Ozaki, M. Okuno, E. Ebisui, K. Mikoshiba and N. Nukina (2011). "Genetic ablation and chemical inhibition of IP3R1 reduce mutant huntingtin aggregation." Biochem Biophys Res Commun **416**(1-2): 13-17.
18. Beaudoin, S., K. Goggin, C. Bissonnette, C. Grenier and X. Roucou (2008). "Aggresomes do not represent a general cellular response to protein misfolding in mammalian cells." BMC Cell Biol **9**: 59.
19. Beckervordersandforth, R. (2017). "Mitochondrial Metabolism-Mediated Regulation of Adult Neurogenesis." Brain Plast **3**(1): 73-87.
20. Ben Abdallah, N. M. B., L. Slomianka, A. L. Vyssotski and H. P. Lipp (2010). "Early age-related changes in adult hippocampal neurogenesis in C57 mice." Neurobiology of Aging **31**(1): 151-161.
21. Benayoun, B. A., E. A. Pollina, P. P. Singh, S. Mahmoudi, I. Harel, K. M. Casey, B. W. Dulken, A. Kundaje and A. Brunet (2019). "Remodeling of epigenome and

transcriptome landscapes with aging in mice reveals widespread induction of inflammatory responses." Genome Res **29**(4): 697-709.

22. Berg, D. A., L. Belnoue, H. Song and A. Simon (2013). "Neurotransmitter-mediated control of neurogenesis in the adult vertebrate brain." Development **140**(12): 2548-2561.
23. Biskou, O., V. Casanova, K. M. Hooper, S. Kemp, G. P. Wright, J. Satsangi, P. G. Barlow and C. Stevens (2019). "The type III intermediate filament vimentin regulates organelle distribution and modulates autophagy." PLoS One **14**(1): e0209665.
24. Bjorkoy, G., T. Lamark, A. Brech, H. Outzen, M. Perander, A. Overvatn, H. Stenmark and T. Johansen (2005). "p62/SQSTM1 forms protein aggregates degraded by autophagy and has a protective effect on huntingtin-induced cell death." J Cell Biol **171**(4): 603-614.
25. Bjorkoy, G., T. Lamark and T. Johansen (2006). "p62/SQSTM1: a missing link between protein aggregates and the autophagy machinery." Autophagy **2**(2): 138-139.
26. Blacker, T. S. and M. R. Duchen (2016). "Investigating mitochondrial redox state using NADH and NADPH autofluorescence." Free Radic Biol Med **100**: 53-65.
27. Blanchette, P., P. Wimmer, F. Dallaire, C. Y. Cheng and P. E. Branton (2013). "Aggresome formation by the adenoviral protein E1B55K is not conserved among adenovirus species and is not required for efficient degradation of nuclear substrates." J Virol **87**(9): 4872-4881.

28. Boareto, M., D. Iber and V. Taylor (2017). "Differential interactions between Notch and ID factors control neurogenesis by modulating Hes factor autoregulation." Development **144**(19): 3465-3474.
29. Bodas, M. and N. Vij (2019). "Adapting Proteostasis and Autophagy for Controlling the Pathogenesis of Cystic Fibrosis Lung Disease." Front Pharmacol **10**: 20.
30. Bohnekamp, J., D. E. Cryderman, D. A. Thiemann, T. M. Magin and L. L. Wallrath (2016). "Using Drosophila for Studies of Intermediate Filaments." Methods Enzymol **568**: 707-726.
31. Bonaguidi, M. A., M. A. Wheeler, J. S. Shapiro, R. P. Stadel, G. J. Sun, G. L. Ming and H. Song (2011). "In vivo clonal analysis reveals self-renewing and multipotent adult neural stem cell characteristics." Cell **145**(7): 1142-1155.
32. Boraas, L. C. and T. Ahsan (2016). "Lack of vimentin impairs endothelial differentiation of embryonic stem cells." Sci Rep **6**: 30814.
33. Bottes, S., B. N. Jaeger, G. A. Pilz, D. J. Jorg, J. D. Cole, M. Kruse, L. Harris, V. I. Korobeynyk, I. Mallona, F. Helmchen, F. Guillemot, B. D. Simons and S. Jessberger (2021). "Long-term self-renewing stem cells in the adult mouse hippocampus identified by intravital imaging." Nat Neurosci **24**(2): 225-233.
34. Bowman, A. N., R. van Amerongen, T. D. Palmer and R. Nusse (2013). "Lineage tracing with Axin2 reveals distinct developmental and adult populations of Wnt/beta-catenin-responsive neural stem cells." Proc Natl Acad Sci U S A **110**(18): 7324-7329.

35. Boyette, L. B. and R. S. Tuan (2014). "Adult Stem Cells and Diseases of Aging." J Clin Med **3**(1): 88-134.

36. Bray, N. L., H. Pimentel, P. Melsted and L. Pachter (2016). "Near-optimal probabilistic RNA-seq quantification." Nat Biotechnol **34**(5): 525-527.

37. Brown, M. J., J. A. Hallam, E. Colucci-Guyon and S. Shaw (2001). "Rigidity of circulating lymphocytes is primarily conferred by vimentin intermediate filaments." J Immunol **166**(11): 6640-6646.

38. Bufalino, M. R., B. DeVeale and D. van der Kooy (2013). "The asymmetric segregation of damaged proteins is stem cell-type dependent." J Cell Biol **201**(4): 523-530.

39. Catley, L., E. Weisberg, T. Kiziltepe, Y. T. Tai, T. Hideshima, P. Neri, P. Tassone, P. Atadja, D. Chauhan, N. C. Munshi and K. C. Anderson (2006). "Aggresome induction by proteasome inhibitor bortezomib and alpha-tubulin hyperacetylation by tubulin deacetylase (TDAC) inhibitor LBH589 are synergistic in myeloma cells." Blood **108**(10): 3441-3449.

40. Challa, A. A. and B. Stefanovic (2011). "A novel role of vimentin filaments: binding and stabilization of collagen mRNAs." Mol Cell Biol **31**(18): 3773-3789.

41. Chance, B., B. Schoener, R. Oshino, F. Itshak and Y. Nakase (1979). "Oxidation-reduction ratio studies of mitochondria in freeze-trapped samples. NADH and flavoprotein fluorescence signals." J Biol Chem **254**(11): 4764-4771.

42. Chen, K., Z. Hu, Z. Xia, D. Zhao, W. Li and J. K. Tyler (2015). "The Overlooked Fact: Fundamental Need for Spike-In Control for Virtually All Genome-Wide Analyses." Mol Cell Biol **36**(5): 662-667.

43. Chen, M., T. B. Puschmann, P. Marasek, M. Inagaki, M. Pekna, U. Wilhelmsson and M. Pekny (2018). "Increased Neuronal Differentiation of Neural Progenitor Cells Derived from Phosphovimentin-Deficient Mice." Mol Neurobiol **55**(7): 5478-5489.

44. Cheng, F., Y. Shen, P. Mohanasundaram, M. Lindstrom, J. Ivaska, T. Ny and J. E. Eriksson (2016). "Vimentin coordinates fibroblast proliferation and keratinocyte differentiation in wound healing via TGF-beta-Slug signaling." Proc Natl Acad Sci U S A **113**(30): E4320-4327.

45. Cheung, T. H. and T. A. Rando (2013). "Molecular regulation of stem cell quiescence." Nat Rev Mol Cell Biol **14**(6): 329-340.

46. Choi, S. H., E. Bylykbashi, Z. K. Chatila, S. W. Lee, B. Pulli, G. D. Clemenson, E. Kim, A. Rompala, M. K. Oram, C. Asselin, J. Aronson, C. Zhang, S. J. Miller, A. Lesinski, J. W. Chen, D. Y. Kim, H. van Praag, B. M. Spiegelman, F. H. Gage and R. E. Tanzi (2018). "Combined adult neurogenesis and BDNF mimic exercise effects on cognition in an Alzheimer's mouse model." Science **361**(6406).

47. Chovatiya, R. and R. Medzhitov (2014). "Stress, inflammation, and defense of homeostasis." Mol Cell **54**(2): 281-288.

48. Codega, P., V. Silva-Vargas, A. Paul, A. R. Maldonado-Soto, A. M. Deleo, E. Pastrana and F. Doetsch (2014). "Prospective identification and purification of quiescent adult neural stem cells from their in vivo niche." Neuron **82**(3): 545-559.

49. Collins, G. A. and A. L. Goldberg (2017). "The Logic of the 26S Proteasome." Cell **169**(5): 792-806.

50. Colucci-Guyon, E., Y. R. M. Gimenez, T. Maurice, C. Babinet and A. Privat (1999). "Cerebellar defect and impaired motor coordination in mice lacking vimentin." Glia **25**(1): 33-43.

51. Colucci-Guyon, E., M. M. Portier, I. Dunia, D. Paulin, S. Pournin and C. Babinet (1994). "Mice lacking vimentin develop and reproduce without an obvious phenotype." Cell **79**(4): 679-694.

52. Corcoran, L. J., T. J. Mitchison and Q. Liu (2004). "A novel action of histone deacetylase inhibitors in a protein aggresome disease model." Curr Biol **14**(6): 488-492.

53. Cristofani, R., V. Crippa, P. Rusmini, M. E. Cicardi, M. Meroni, N. V. Licata, G. Sala, E. Giorgetti, C. Grunseich, M. Galbiati, M. Piccolella, E. Messi, C. Ferrarese, S. Carra and A. Poletti (2017). "Inhibition of retrograde transport modulates misfolded protein accumulation and clearance in motoneuron diseases." Autophagy **13**(8): 1280-1303.

54. Crowther, A. J., S. A. Lim, B. Asrican, B. H. Albright, J. Wooten, C. Y. Yeh, H. Bao, D. H. Cerri, J. Hu, Y. Y. Ian Shih, A. Asokan and J. Song (2018). "An Adeno-Associated Virus-Based Toolkit for Preferential Targeting and Manipulating Quiescent Neural Stem Cells in the Adult Hippocampus." Stem Cell Reports **10**(3): 1146-1159.

55. Cummings, C. J., M. A. Mancini, B. Antalffy, D. B. DeFranco, H. T. Orr and H. Y. Zoghbi (1998). "Chaperone suppression of aggregation and altered subcellular

proteasome localization imply protein misfolding in SCA1." Nat Genet **19**(2): 148-154.

56. Cummings, J. L., T. Morstorf and K. Zhong (2014). "Alzheimer's disease drug-development pipeline: few candidates, frequent failures." Alzheimers Res Ther **6**(4): 37.
57. Da, Q., M. Behymer, J. I. Correa, K. V. Vijayan and M. A. Cruz (2014). "Platelet adhesion involves a novel interaction between vimentin and von Willebrand factor under high shear stress." Blood **123**(17): 2715-2721.
58. Danielsson, F., M. K. Peterson, H. Caldeira Araujo, F. Lautenschlager and A. K. B. Gad (2018). "Vimentin Diversity in Health and Disease." Cells **7**(10).
59. Dantuma, N. P., T. A. Groothuis, F. A. Salomons and J. Neefjes (2006). "A dynamic ubiquitin equilibrium couples proteasomal activity to chromatin remodeling." J Cell Biol **173**(1): 19-26.
60. Datta, R., T. M. Heaster, J. T. Sharick, A. A. Gillette and M. C. Skala (2020). "Fluorescence lifetime imaging microscopy: fundamentals and advances in instrumentation, analysis, and applications." J Biomed Opt **25**(7): 1-43.
61. Dehvari, N., T. Mahmud, J. Persson, T. Bengtsson, C. Graff, B. Winblad, A. Ronnback and H. Behbahani (2012). "Amyloid precursor protein accumulates in aggresomes in response to proteasome inhibitor." Neurochem Int **60**(5): 533-542.
62. Dikic, I. (2017). "Proteasomal and Autophagic Degradation Systems." Annu Rev Biochem **86**: 193-224.
63. dos Santos, G., M. R. Rogel, M. A. Baker, J. R. Troken, D. Urich, L. Morales-Nebreda, J. A. Sennello, M. A. Kutuzov, A. Sitikov, J. M. Davis, A. P. Lam, P.

Cheresh, D. Kamp, D. K. Shumaker, G. R. Budinger and K. M. Ridge (2015). "Vimentin regulates activation of the NLRP3 inflammasome." Nat Commun **6**: 6574.

64. Douglas, P. M. and A. Dillin (2010). "Protein homeostasis and aging in neurodegeneration." J Cell Biol **190**(5): 719-729.
65. Dulken, B. W., M. T. Buckley, P. Navarro Negredo, N. Saligrama, R. Cayrol, D. S. Leeman, B. M. George, S. C. Boutet, K. Hebestreit, J. V. Pluvinage, T. Wyss-Coray, I. L. Weissman, H. Vogel, M. M. Davis and A. Brunet (2019). "Single-cell analysis reveals T cell infiltration in old neurogenic niches." Nature **571**(7764): 205-210.
66. Dulken, B. W., D. S. Leeman, S. C. Boutet, K. Hebestreit and A. Brunet (2017). "Single-Cell Transcriptomic Analysis Defines Heterogeneity and Transcriptional Dynamics in the Adult Neural Stem Cell Lineage." Cell Rep **18**(3): 777-790.
67. Engler, A., R. Zhang and V. Taylor (2018). "Notch and Neurogenesis." Adv Exp Med Biol **1066**: 223-234.
68. Fabunmi, R. P., W. C. Wigley, P. J. Thomas and G. N. DeMartino (2000). "Activity and regulation of the centrosome-associated proteasome." J Biol Chem **275**(1): 409-413.
69. Frazee, A. C., G. Pertea, A. E. Jaffe, B. Langmead, S. L. Salzberg and J. T. Leek (2015). "Ballgown bridges the gap between transcriptome assembly and expression analysis." Nat Biotechnol **33**(3): 243-246.
70. French, B. A., F. van Leeuwen, N. E. Riley, Q. X. Yuan, F. Bardag-Gorce, K. Gaal, Y. H. Lue, N. Marceau and S. W. French (2001). "Aggresome formation in

liver cells in response to different toxic mechanisms: role of the ubiquitin-proteasome pathway and the frameshift mutant of ubiquitin." Exp Mol Pathol **71**(3): 241-246.

71. French, S. W., M. Masouminia, S. Samadzadeh, B. C. Tillman, A. Mendoza and B. A. French (2017). "Role of Protein Quality Control Failure in Alcoholic Hepatitis Pathogenesis." Biomolecules **7**(1).
72. French, S. W., A. S. Mendoza and Y. Peng (2016). "The mechanisms of Mallory-Denk body formation are similar to the formation of aggresomes in Alzheimer's disease and other neurodegenerative disorders." Exp Mol Pathol **100**(3): 426-433.
73. Galou, M., E. Colucci-Guyon, D. Ensergueix, J. L. Ridet, M. Gimenez y Ribotta, A. Privat, C. Babinet and P. Dupouey (1996). "Disrupted glial fibrillary acidic protein network in astrocytes from vimentin knockout mice." J Cell Biol **133**(4): 853-863.
74. Galou, M., J. Gao, J. Humbert, M. Mericskay, Z. Li, D. Paulin and P. Vicart (1997). "The importance of intermediate filaments in the adaptation of tissues to mechanical stress: evidence from gene knockout studies." Biol Cell **89**(2): 85-97.
75. Garthe, A., J. Behr and G. Kempermann (2009). "Adult-generated hippocampal neurons allow the flexible use of spatially precise learning strategies." PLoS One **4**(5): e5464.
76. Geerts, A., C. Eliasson, T. Niki, A. Wielant, F. Vaeyens and M. Pekny (2001). "Formation of normal desmin intermediate filaments in mouse hepatic stellate cells requires vimentin." Hepatology **33**(1): 177-188.

77. Gerhardt, M. J., J. A. Marsh, M. Morrison, A. Kazlauskas, A. Khadka, S. Rosenkranz, M. M. DeAngelis, M. Saint-Geniez and S. M. P. Jacobo (2017). "ER stress-induced aggresome trafficking of HtrA1 protects against proteotoxicity." J Mol Cell Biol **9**(6): 533.

78. Goncalves, J. T., S. T. Schafer and F. H. Gage (2016). "Adult Neurogenesis in the Hippocampus: From Stem Cells to Behavior." Cell **167**(4): 897-914.

79. Gouras, G. K., T. T. Olsson and O. Hansson (2015). "beta-Amyloid peptides and amyloid plaques in Alzheimer's disease." Neurotherapeutics **12**(1): 3-11.

80. Grin, B., S. Mahammad, T. Wedig, M. M. Cleland, L. Tsai, H. Herrmann and R. D. Goldman (2012). "Withaferin a alters intermediate filament organization, cell shape and behavior." PLoS One **7**(6): e39065.

81. Guignot, J. and A. L. Servin (2008). "Maintenance of the Salmonella-containing vacuole in the juxtanuclear area: a role for intermediate filaments." Microb Pathog **45**(5-6): 415-422.

82. Guo, M., A. J. Ehrlicher, S. Mahammad, H. Fabich, M. H. Jensen, J. R. Moore, J. J. Fredberg, R. D. Goldman and D. A. Weitz (2013). "The role of vimentin intermediate filaments in cortical and cytoplasmic mechanics." Biophys J **105**(7): 1562-1568.

83. Hao, R., P. Nanduri, Y. Rao, R. S. Panichelli, A. Ito, M. Yoshida and T. P. Yao (2013). "Proteasomes activate aggresome disassembly and clearance by producing unanchored ubiquitin chains." Mol Cell **51**(6): 819-828.

84. Harris, L., P. Rigo, T. Stiehl, Z. B. Gaber, S. H. L. Austin, M. D. M. Masdeu, A. Edwards, N. Urban, A. Marciniak-Czochra and F. Guillemot (2021). "Coordinated

changes in cellular behavior ensure the lifelong maintenance of the hippocampal stem cell population." Cell Stem Cell **28**(5): 863-876 e866.

85. Hashimoto, K., A. N. Simmons, R. Kajino-Sakamoto, Y. Tsuji and J. Ninomiya-Tsuji (2016). "TAK1 Regulates the Nrf2 Antioxidant System Through Modulating p62/SQSTM1." Antioxid Redox Signal **25**(17): 953-964.
86. Heaster, T. M., M. Humayun, J. Yu, D. J. Beebe and M. C. Skala (2020). "Autofluorescence Imaging of 3D Tumor-Macrophage Microscale Cultures Resolves Spatial and Temporal Dynamics of Macrophage Metabolism." Cancer Res **80**(23): 5408-5423.
87. Henrion, D., F. Terzi, K. Matrougui, M. Duriez, C. M. Boulanger, E. Colucci-Guyon, C. Babinet, P. Briand, G. Friedlander, P. Poitevin and B. I. Levy (1997). "Impaired flow-induced dilation in mesenteric resistance arteries from mice lacking vimentin." J Clin Invest **100**(11): 2909-2914.
88. Herrmann, H. and U. Aebi (2004). "Intermediate filaments: molecular structure, assembly mechanism, and integration into functionally distinct intracellular Scaffolds." Annu Rev Biochem **73**: 749-789.
89. Herrmann, H., M. Haner, M. Brettel, S. A. Muller, K. N. Goldie, B. Fedtke, A. Lustig, W. W. Franke and U. Aebi (1996). "Structure and assembly properties of the intermediate filament protein vimentin: the role of its head, rod and tail domains." J Mol Biol **264**(5): 933-953.
90. Hipp, M. S., P. Kasturi and F. U. Hartl (2019). "The proteostasis network and its decline in ageing." Nat Rev Mol Cell Biol **20**(7): 421-435.

91. Holmstrom, K. M., L. Baird, Y. Zhang, I. Hargreaves, A. Chalasani, J. M. Land, L. Stanyer, M. Yamamoto, A. T. Dinkova-Kostova and A. Y. Abramov (2013). "Nrf2 impacts cellular bioenergetics by controlling substrate availability for mitochondrial respiration." Biol Open **2**(8): 761-770.

92. Horowitz, A. M., X. Fan, G. Bieri, L. K. Smith, C. I. Sanchez-Diaz, A. B. Schroer, G. Gontier, K. B. Casaletto, J. H. Kramer, K. E. Williams and S. A. Villeda (2020). "Blood factors transfer beneficial effects of exercise on neurogenesis and cognition to the aged brain." Science **369**(6500): 167-173.

93. Hutter, E., H. Unterluggauer, F. Uberall, H. Schramek and P. Jansen-Durr (2002). "Replicative senescence of human fibroblasts: the role of Ras-dependent signaling and oxidative stress." Exp Gerontol **37**(10-11): 1165-1174.

94. Ibrayeva, A., M. Bay, E. Pu, D. J. Jorg, L. Peng, H. Jun, N. Zhang, D. Aaron, C. Lin, G. Resler, A. Hidalgo, M. H. Jang, B. D. Simons and M. A. Bonaguidi (2021). "Early stem cell aging in the mature brain." Cell Stem Cell.

95. Islam, M. S., M. Honma, T. Nakabayashi, M. Kinjo and N. Ohta (2013). "pH dependence of the fluorescence lifetime of FAD in solution and in cells." Int J Mol Sci **14**(1): 1952-1963.

96. Itakura, E. and N. Mizushima (2011). "p62 Targeting to the autophagosome formation site requires self-oligomerization but not LC3 binding." J Cell Biol **192**(1): 17-27.

97. Iwata, A., B. E. Riley, J. A. Johnston and R. R. Kopito (2005). "HDAC6 and microtubules are required for autophagic degradation of aggregated huntingtin." J Biol Chem **280**(48): 40282-40292.

98. Jacobs, B. L. (2002). "Adult brain neurogenesis and depression." Brain Behav Immun **16**(5): 602-609.

99. Jacobs, B. L., H. van Praag and F. H. Gage (2000). "Adult brain neurogenesis and psychiatry: a novel theory of depression." Mol Psychiatry **5**(3): 262-269.

100. Jacquier, A., C. Delorme, E. Belotti, R. Juntas-Morales, G. Sole, O. Dubourg, M. Giroux, C. A. Maurage, V. Castellani, A. Rebelo, A. Abrams, S. Zuchner, T. Stojkovic, L. Schaeffer and P. Latour (2017). "Cryptic amyloidogenic elements in mutant NEFH causing Charcot-Marie-Tooth 2 trigger aggresome formation and neuronal death." Acta Neuropathol Commun **5**(1): 55.

101. Jana, N. R., E. A. Zemskov, G. Wang and N. Nukina (2001). "Altered proteasomal function due to the expression of polyglutamine-expanded truncated N-terminal huntingtin induces apoptosis by caspase activation through mitochondrial cytochrome c release." Hum Mol Genet **10**(10): 1049-1059.

102. Jia, B., Y. Wu and Y. Zhou (2014). "14-3-3 and aggresome formation: implications in neurodegenerative diseases." Prion **8**(2).

103. Jia, B., Y. Xue, X. Yan, J. Li, Y. Wu, R. Guo, J. Zhang, L. Zhang, Y. Li, Y. Liu and L. Sun (2018). "Autophagy inhibitor chloroquine induces apoptosis of cholangiocarcinoma cells via endoplasmic reticulum stress." Oncol Lett **16**(3): 3509-3516.

104. Jiang, S. X., J. Slinn, A. Aylsworth and S. T. Hou (2012). "Vimentin participates in microglia activation and neurotoxicity in cerebral ischemia." J Neurochem **122**(4): 764-774.

105. Jiu, Y., J. Peranen, N. Schaible, F. Cheng, J. E. Eriksson, R. Krishnan and P. Lappalainen (2017). "Vimentin intermediate filaments control actin stress fiber assembly through GEF-H1 and RhoA." J Cell Sci **130**(5): 892-902.

106. Johnston, J. A., M. E. Illing and R. R. Kopito (2002). "Cytoplasmic dynein/dynactin mediates the assembly of aggresomes." Cell Motil Cytoskeleton **53**(1): 26-38.

107. Johnston, J. A., C. L. Ward and R. R. Kopito (1998). "Aggresomes: a cellular response to misfolded proteins." J Cell Biol **143**(7): 1883-1898.

108. Jones, R. J., D. Jourd'heuil, J. C. Salerno, S. M. Smith and H. A. Singer (2007). "iNOS regulation by calcium/calmodulin-dependent protein kinase II in vascular smooth muscle." Am J Physiol Heart Circ Physiol **292**(6): H2634-2642.

109. Joung, J., S. Konermann, J. S. Gootenberg, O. O. Abudayyeh, R. J. Platt, M. D. Brigham, N. E. Sanjana and F. Zhang (2017). "Genome-scale CRISPR-Cas9 knockout and transcriptional activation screening." Nat Protoc **12**(4): 828-863.

110. Jucker, M. and L. C. Walker (2013). "Self-propagation of pathogenic protein aggregates in neurodegenerative diseases." Nature **501**(7465): 45-51.

111. Kaganovich, D., R. Kopito and J. Frydman (2008). "Misfolded proteins partition between two distinct quality control compartments." Nature **454**(7208): 1088-1095.

112. Kajitani, N., A. Satsuka, S. Yoshida and H. Sakai (2013). "HPV18 E1^E4 is assembled into aggresome-like compartment and involved in sequestration of viral oncoproteins." Front Microbiol **4**: 251.

113. Kalamakis, G., D. Brune, S. Ravichandran, J. Bolz, W. Fan, F. Ziebell, T. Stiehl, F. Catala-Martinez, J. Kupke, S. Zhao, E. Llorens-Bobadilla, K. Bauer, S. Limpert, B. Berger, U. Christen, P. Schmezer, J. P. Mallm, B. Berninger, S. Anders, A. Del Sol, A. Marciniak-Czochra and A. Martin-Villalba (2019). "Quiescence Modulates Stem Cell Maintenance and Regenerative Capacity in the Aging Brain." Cell **176**(6): 1407-1419 e1414.

114. Kawaguchi, Y., J. J. Kovacs, A. McLaurin, J. M. Vance, A. Ito and T. P. Yao (2003). "The deacetylase HDAC6 regulates aggresome formation and cell viability in response to misfolded protein stress." Cell **115**(6): 727-738.

115. Kehl, S. R., B. A. Soos, B. Saha, S. W. Choi, A. W. Herren, T. Johansen and M. A. Mandell (2019). "TAK1 converts Sequestosome 1/p62 from an autophagy receptor to a signaling platform." EMBO Rep **20**(9): e46238.

116. Khan, M. and S. Gasser (2016). "Generating Primary Fibroblast Cultures from Mouse Ear and Tail Tissues." J Vis Exp(107).

117. Khan, S., I. Khamis and J. J. Heikkila (2015). "The small heat shock protein, HSP30, is associated with aggresome-like inclusion bodies in proteasomal inhibitor-, arsenite-, and cadmium-treated Xenopus kidney cells." Comp Biochem Physiol A Mol Integr Physiol **189**: 130-140.

118. Kim, D., G. Pertea, C. Trapnell, H. Pimentel, R. Kelley and S. L. Salzberg (2013). "TopHat2: accurate alignment of transcriptomes in the presence of insertions, deletions and gene fusions." Genome Biol **14**(4): R36.

119. Knobloch, M., S. M. Braun, L. Zurkirchen, C. von Schoultz, N. Zamboni, M. J. Arauzo-Bravo, W. J. Kovacs, O. Karalay, U. Suter, R. A. Machado, M.

Roccio, M. P. Lutolf, C. F. Semenkovich and S. Jessberger (2013). "Metabolic control of adult neural stem cell activity by Fasn-dependent lipogenesis." Nature **493**(7431): 226-230.

120. Knobloch, M., G. A. Pilz, B. Ghesquiere, W. J. Kovacs, T. Wegleiter, D. L. Moore, M. Hruzova, N. Zamboni, P. Carmeliet and S. Jessberger (2017). "A Fatty Acid Oxidation-Dependent Metabolic Shift Regulates Adult Neural Stem Cell Activity." Cell Rep **20**(9): 2144-2155.

121. Knobloch, M., C. von Schoultz, L. Zurkirchen, S. M. Braun, M. Vidmar and S. Jessberger (2014). "SPOT14-positive neural stem/progenitor cells in the hippocampus respond dynamically to neurogenic regulators." Stem Cell Reports **3**(5): 735-742.

122. Kolenc, O. I. and K. P. Quinn (2019). "Evaluating Cell Metabolism Through Autofluorescence Imaging of NAD(P)H and FAD." Antioxid Redox Signal **30**(6): 875-889.

123. Kolodziejska, K. E., A. R. Burns, R. H. Moore, D. L. Stenoien and N. T. Eissa (2005). "Regulation of inducible nitric oxide synthase by aggresome formation." Proc Natl Acad Sci U S A **102**(13): 4854-4859.

124. Komatsu, S., S. Moriya, X. F. Che, T. Yokoyama, N. Kohno and K. Miyazawa (2013). "Combined treatment with SAHA, bortezomib, and clarithromycin for concomitant targeting of aggresome formation and intracellular proteolytic pathways enhances ER stress-mediated cell death in breast cancer cells." Biochem Biophys Res Commun **437**(1): 41-47.

125. Kopito, R. R. (2000). "Aggresomes, inclusion bodies and protein aggregation." Trends Cell Biol **10**(12): 524-530.

126. Kovacs, I., K. M. Lentini, L. M. Ingano and D. M. Kovacs (2006). "Presenilin 1 forms aggresomal deposits in response to heat shock." J Mol Neurosci **29**(1): 9-19.

127. Kueper, T., T. Grune, S. Prahl, H. Lenz, V. Welge, T. Biernoth, Y. Vogt, G. M. Muhr, A. Gaemlich, T. Jung, G. Boemke, H. P. Elsasser, K. P. Wittern, H. Wenck, F. Stab and T. Blatt (2007). "Vimentin is the specific target in skin glycation. Structural prerequisites, functional consequences, and role in skin aging." J Biol Chem **282**(32): 23427-23436.

128. Kuhn, H. G., H. Dickinson-Anson and F. H. Gage (1996). "Neurogenesis in the dentate gyrus of the adult rat: age-related decrease of neuronal progenitor proliferation." J Neurosci **16**(6): 2027-2033.

129. Labbadia, J. and R. I. Morimoto (2015). "The biology of proteostasis in aging and disease." Annu Rev Biochem **84**: 435-464.

130. Lakowicz, J. R., H. Szmacinski, K. Nowaczyk and M. L. Johnson (1992). "Fluorescence lifetime imaging of free and protein-bound NADH." Proc Natl Acad Sci U S A **89**(4): 1271-1275.

131. Langlois, B., E. Belozertseva, A. Parlakian, M. Bourhim, J. Gao-Li, J. Blanc, L. Tian, D. Coletti, C. Labat, Z. Ramdame-Cherif, P. Challande, V. Regnault, P. Lacolley and Z. Li (2017). "Vimentin knockout results in increased expression of sub-endothelial basement membrane components and carotid stiffness in mice." Sci Rep **7**(1): 11628.

132. Langmead, B. and S. L. Salzberg (2012). "Fast gapped-read alignment with Bowtie 2." Nat Methods **9**(4): 357-359.

133. Leeman, D. S., K. Hebestreit, T. Ruetz, A. E. Webb, A. McKay, E. A. Pollina, B. W. Dulken, X. Zhao, R. W. Yeo, T. T. Ho, S. Mahmoudi, K. Devarajan, E. Passegue, T. A. Rando, J. Frydman and A. Brunet (2018). "Lysosome activation clears aggregates and enhances quiescent neural stem cell activation during aging." Science **359**(6381): 1277-1283.

134. Legesse-Miller, A., I. Raitman, E. M. Haley, A. Liao, L. L. Sun, D. J. Wang, N. Krishnan, J. M. Lemons, E. J. Suh, E. L. Johnson, B. A. Lund and H. A. Coller (2012). "Quiescent fibroblasts are protected from proteasome inhibition-mediated toxicity." Mol Biol Cell **23**(18): 3566-3581.

135. Levin, E. C., N. K. Acharya, J. C. Sedeyn, V. Venkataraman, M. R. D'Andrea, H. Y. Wang and R. G. Nagele (2009). "Neuronal expression of vimentin in the Alzheimer's disease brain may be part of a generalized dendritic damage-response mechanism." Brain Res **1298**: 194-207.

136. Lewis, C. A., S. J. Parker, B. P. Fiske, D. McCloskey, D. Y. Gui, C. R. Green, N. I. Vokes, A. M. Feist, M. G. Vander Heiden and C. M. Metallo (2014). "Tracing compartmentalized NADPH metabolism in the cytosol and mitochondria of mammalian cells." Mol Cell **55**(2): 253-263.

137. Liao, L., D. Cheng, J. Wang, D. M. Duong, T. G. Losik, M. Gearing, H. D. Rees, J. J. Lah, A. I. Levey and J. Peng (2004). "Proteomic characterization of postmortem amyloid plaques isolated by laser capture microdissection." J Biol Chem **279**(35): 37061-37068.

138. Lie, D. C., S. A. Colamarino, H. J. Song, L. Desire, H. Mira, A. Consiglio, E. S. Lein, S. Jessberger, H. Lansford, A. R. Dearie and F. H. Gage (2005). "Wnt signalling regulates adult hippocampal neurogenesis." Nature **437**(7063): 1370-1375.

139. Liu, C. Y., H. H. Lin, M. J. Tang and Y. K. Wang (2015). "Vimentin contributes to epithelial-mesenchymal transition cancer cell mechanics by mediating cytoskeletal organization and focal adhesion maturation." Oncotarget **6**(18): 15966-15983.

140. Liu, Y., A. Shevchenko, A. Shevchenko and A. J. Berk (2005). "Adenovirus exploits the cellular aggresome response to accelerate inactivation of the MRN complex." J Virol **79**(22): 14004-14016.

141. Livak, K. J. and T. D. Schmittgen (2001). "Analysis of relative gene expression data using real-time quantitative PCR and the 2(-Delta Delta C(T)) Method." Methods **25**(4): 402-408.

142. Llorens-Bobadilla, E., S. Zhao, A. Baser, G. Saiz-Castro, K. Zwadlo and A. Martin-Villalba (2015). "Single-Cell Transcriptomics Reveals a Population of Dormant Neural Stem Cells that Become Activated upon Brain Injury." Cell Stem Cell **17**(3): 329-340.

143. Lopez-Otin, C., M. A. Blasco, L. Partridge, M. Serrano and G. Kroemer (2013). "The hallmarks of aging." Cell **153**(6): 1194-1217.

144. Lu, M., C. Boschetti and A. Tunnacliffe (2015). "Long Term Aggresome Accumulation Leads to DNA Damage, p53-dependent Cell Cycle Arrest, and Steric Interference in Mitosis." J Biol Chem **290**(46): 27986-28000.

145. Luciani, A., V. R. Villella, S. Esposito, N. Brunetti-Pierri, D. Medina, C. Settembre, M. Gavina, L. Pulze, I. Giardino, M. Pettoello-Mantovani, M. D'Apolito, S. Guido, E. Masliah, B. Spencer, S. Quaratino, V. Raia, A. Ballabio and L. Maiuri (2010). "Defective CFTR induces aggresome formation and lung inflammation in cystic fibrosis through ROS-mediated autophagy inhibition." Nat Cell Biol **12**(9): 863-875.

146. Luciani, A., V. R. Villella, S. Esposito, N. Brunetti-Pierri, D. L. Medina, C. Settembre, M. Gavina, V. Raia, A. Ballabio and L. Maiuri (2011). "Cystic fibrosis: a disorder with defective autophagy." Autophagy **7**(1): 104-106.

147. Lugert, S., O. Basak, P. Knuckles, U. Haussler, K. Fabel, M. Gotz, C. A. Haas, G. Kempermann, V. Taylor and C. Giachino (2010). "Quiescent and active hippocampal neural stem cells with distinct morphologies respond selectively to physiological and pathological stimuli and aging." Cell Stem Cell **6**(5): 445-456.

148. Lundkvist, A., A. Reichenbach, C. Betsholtz, P. Carmeliet, H. Wolburg and M. Pekny (2004). "Under stress, the absence of intermediate filaments from Muller cells in the retina has structural and functional consequences." J Cell Sci **117**(Pt 16): 3481-3488.

149. Magupalli, V. G., R. Negro, Y. Tian, A. V. Hauenstein, G. Di Caprio, W. Skillern, Q. Deng, P. Orning, H. B. Alam, Z. Maliga, H. Sharif, J. J. Hu, C. L. Evavold, J. C. Kagan, F. I. Schmidt, K. A. Fitzgerald, T. Kirchhausen, Y. Li and H. Wu (2020). "HDAC6 mediates an aggresome-like mechanism for NLRP3 and pyrin inflammasome activation." Science **369**(6510).

150. Martin, M. (2011). "Cutadapt Removes Adapter Sequences From High-Throughput Sequencing Reads." EMB - Bioinformatics in action **17**(1).

151. Martynoga, B., J. L. Mateo, B. Zhou, J. Andersen, A. Achimastou, N. Urban, D. van den Berg, D. Georgopoulou, S. Hadjur, J. Wittbrodt, L. Ettwiller, M. Piper, R. M. Gronostajski and F. Guillemot (2013). "Epigenomic enhancer annotation reveals a key role for NFIX in neural stem cell quiescence." Genes Dev **27**(16): 1769-1786.

152. Matsumoto, G., T. Inobe, T. Amano, K. Murai, N. Nukina and N. Mori (2018). "N-Acyldopamine induces aggresome formation without proteasome inhibition and enhances protein aggregation via p62/SQSTM1 expression." Sci Rep **8**(1): 9585.

153. McNaught, K. S., P. Shashidharan, D. P. Perl, P. Jenner and C. W. Olanow (2002). "Aggresome-related biogenesis of Lewy bodies." Eur J Neurosci **16**(11): 2136-2148.

154. Mercier, F. and V. Douet (2014). "Bone morphogenetic protein-4 inhibits adult neurogenesis and is regulated by fractone-associated heparan sulfates in the subventricular zone." J Chem Neuroanat **57-58**: 54-61.

155. Millward, M., T. Price, A. Townsend, C. Sweeney, A. Spencer, S. Sukumaran, A. Longenecker, L. Lee, A. Lay, G. Sharma, R. M. Gemmill, H. A. Drabkin, G. K. Lloyd, S. T. Neuteboom, D. J. McConkey, M. A. Palladino and M. A. Spear (2012). "Phase 1 clinical trial of the novel proteasome inhibitor marizomib with the histone deacetylase inhibitor vorinostat in patients with

melanoma, pancreatic and lung cancer based on in vitro assessments of the combination." Invest New Drugs **30**(6): 2303-2317.

156. Min, T., M. Bodas, S. Mazur and N. Vij (2011). "Critical role of proteostasis-imbalance in pathogenesis of COPD and severe emphysema." J Mol Med (Berl) **89**(6): 577-593.

157. Mira, H., Z. Andreu, H. Suh, D. C. Lie, S. Jessberger, A. Consiglio, J. San Emeterio, R. Hortiguela, M. A. Marques-Torrejon, K. Nakashima, D. Colak, M. Gotz, I. Farinas and F. H. Gage (2010). "Signaling through BMPR-IA regulates quiescence and long-term activity of neural stem cells in the adult hippocampus." Cell Stem Cell **7**(1): 78-89.

158. Mishima, Y., L. Santo, H. Eda, D. Cirstea, N. Nemani, A. J. Yee, E. O'Donnell, M. K. Selig, S. N. Quayle, S. Arastu-Kapur, C. Kirk, L. H. Boise, S. S. Jones and N. Raje (2015). "Ricolinostat (ACY-1215) induced inhibition of aggresome formation accelerates carfilzomib-induced multiple myeloma cell death." Br J Haematol **169**(3): 423-434.

159. Miyahara, K., H. Kazama, H. Kokuba, S. Komatsu, A. Hirota, J. Takemura, K. Hirasawa, S. Moriya, A. Abe, M. Hiramoto, T. Ishikawa and K. Miyazawa (2016). "Targeting bortezomib-induced aggresome formation using vinorelbine enhances the cytotoxic effect along with ER stress loading in breast cancer cell lines." Int J Oncol **49**(5): 1848-1858.

160. Moore, D. L., M. G. Blackmore, Y. Hu, K. H. Kaestner, J. L. Bixby, V. P. Lemmon and J. L. Goldberg (2009). "KLF family members regulate intrinsic axon regeneration ability." Science **326**(5950): 298-301.

161. Moore, D. L. and S. Jessberger (2017). "Creating Age Asymmetry: Consequences of Inheriting Damaged Goods in Mammalian Cells." Trends Cell Biol **27**(1): 82-92.

162. Moore, D. L., G. A. Pilz, M. J. Arauzo-Bravo, Y. Barral and S. Jessberger (2015). "A mechanism for the segregation of age in mammalian neural stem cells." Science **349**(6254): 1334-1338.

163. Mor-Vaknin, N., M. Legendre, Y. Yu, C. H. Serezani, S. K. Garg, A. Jatzek, M. D. Swanson, M. J. Gonzalez-Hernandez, S. Teitz-Tennenbaum, A. Punturieri, N. C. Engleberg, R. Banerjee, M. Peters-Golden, J. Y. Kao and D. M. Markovitz (2013). "Murine colitis is mediated by vimentin." Sci Rep **3**: 1045.

164. Moran Luengo, T., M. P. Mayer and S. G. D. Rudiger (2019). "The Hsp70-Hsp90 Chaperone Cascade in Protein Folding." Trends Cell Biol **29**(2): 164-177.

165. Moreno-Jimenez, E. P., M. Flor-Garcia, J. Terreros-Roncal, A. Rabano, F. Cafini, N. Pallas-Bazarra, J. Avila and M. Llorens-Martin (2019). "Adult hippocampal neurogenesis is abundant in neurologically healthy subjects and drops sharply in patients with Alzheimer's disease." Nat Med **25**(4): 554-560.

166. Moriya, S., S. Komatsu, K. Yamasaki, Y. Kawai, H. Kokuba, A. Hirota, X. F. Che, M. Inazu, A. Gotoh, M. Hiramoto and K. Miyazawa (2015). "Targeting the integrated networks of aggresome formation, proteasome, and autophagy potentiates ER stressmediated cell death in multiple myeloma cells." Int J Oncol **46**(2): 474-486.

167. Morrow, C. S., T. J. Porter, N. Xu, Z. P. Arndt, K. Ako-Asare, H. J. Heo, E. A. N. Thompson and D. L. Moore (2020). "Vimentin Coordinates Protein

Turnover at the Aggresome during Neural Stem Cell Quiescence Exit." Cell Stem Cell.

168. Munoz-Moreno, R., L. Barrado-Gil, I. Galindo and C. Alonso (2015). "Analysis of HDAC6 and BAG3-aggresome pathways in African swine fever viral factory formation." Viruses **7**(4): 1823-1831.

169. Nassar, M., H. Samaha, M. Ghabriel, M. Yehia, H. Taha, S. Salem, K. Shaaban, M. Omar, N. Ahmed and S. El-Naggar (2017). "LC3A Silencing Hinders Aggresome Vimentin Cage Clearance in Primary Choroid Plexus Carcinoma." Sci Rep **7**(1): 8022.

170. Nawrocki, S. T., J. S. Carew, M. S. Pino, R. A. Highshaw, R. H. Andtbacka, K. Dunner, Jr., A. Pal, W. G. Bornmann, P. J. Chiao, P. Huang, H. Xiong, J. L. Abbruzzese and D. J. McConkey (2006). "Aggresome disruption: a novel strategy to enhance bortezomib-induced apoptosis in pancreatic cancer cells." Cancer Res **66**(7): 3773-3781.

171. Neufeld, D. S., S. Ripley, A. Henderson and H. L. Ozer (1987). "Immortalization of human fibroblasts transformed by origin-defective simian virus 40." Mol Cell Biol **7**(8): 2794-2802.

172. Nieminen, M., T. Henttinen, M. Merinen, F. Marttila-Ichihara, J. E. Eriksson and S. Jalkanen (2006). "Vimentin function in lymphocyte adhesion and transcellular migration." Nat Cell Biol **8**(2): 156-162.

173. Nozawa, N., Y. Yamauchi, K. Ohtsuka, Y. Kawaguchi and Y. Nishiyama (2004). "Formation of aggresome-like structures in herpes simplex virus type 2-

infected cells and a potential role in virus assembly." Exp Cell Res **299**(2): 486-497.

174. Ogrodnik, M., H. Salmonowicz, R. Brown, J. Turkowska, W. Sredniawa, S. Pattabiraman, T. Amen, A. C. Abraham, N. Eichler, R. Lyakhovetsky and D. Kaganovich (2014). "Dynamic JUNQ inclusion bodies are asymmetrically inherited in mammalian cell lines through the asymmetric partitioning of vimentin." Proc Natl Acad Sci U S A **111**(22): 8049-8054.

175. Olanow, C. W., D. P. Perl, G. N. DeMartino and K. S. McNaught (2004). "Lewy-body formation is an aggresome-related process: a hypothesis." Lancet Neurol **3**(8): 496-503.

176. Olzmann, J. A., L. Li and L. S. Chin (2008). "Aggresome formation and neurodegenerative diseases: therapeutic implications." Curr Med Chem **15**(1): 47-60.

177. Ouyang, H., Y. O. Ali, M. Ravichandran, A. Dong, W. Qiu, F. MacKenzie, S. Dhe-Paganon, C. H. Arrowsmith and R. G. Zhai (2012). "Protein aggregates are recruited to aggresome by histone deacetylase 6 via unanchored ubiquitin C termini." J Biol Chem **287**(4): 2317-2327.

178. Pandit, L., K. E. Kolodziejska, S. Zeng and N. T. Eissa (2009). "The physiologic aggresome mediates cellular inactivation of iNOS." Proc Natl Acad Sci U S A **106**(4): 1211-1215.

179. Park, D., A. P. Xiang, F. F. Mao, L. Zhang, C. G. Di, X. M. Liu, Y. A. Shao, B. F. Ma, J. H. Lee, K. S. Ha, N. Walton and B. T. Lahn (2010). "Nestin Is

Required for the Proper Self-Renewal of Neural Stem Cells." Stem Cells **28**(12): 2162-2171.

180. Park, S. H., S. J. Yoon, S. Choi, J. S. Kim, M. S. Lee, S. J. Lee, S. H. Lee, J. K. Min, M. Y. Son, C. M. Ryu, J. Yoo and Y. J. Park (2020). "Bacterial type III effector protein HopQ inhibits melanoma motility through autophagic degradation of vimentin." Cell Death Dis **11**(4): 231.

181. Paul, A., Z. Chaker and F. Doetsch (2017). "Hypothalamic regulation of regionally distinct adult neural stem cells and neurogenesis." Science **356**(6345): 1383-1386.

182. Pekny, M., C. B. Johansson, C. Eliasson, J. Stakeberg, A. Wallen, T. Perlmann, U. Lendahl, C. Betsholtz, C. H. Berthold and J. Frisen (1999). "Abnormal reaction to central nervous system injury in mice lacking glial fibrillary acidic protein and vimentin." J Cell Biol **145**(3): 503-514.

183. Perez-Sala, D., C. L. Oeste, A. E. Martinez, M. J. Carrasco, B. Garzon and F. J. Canada (2015). "Vimentin filament organization and stress sensing depend on its single cysteine residue and zinc binding." Nat Commun **6**: 7287.

184. Perreau, J., A. Lilienbaum, M. Vasseur and D. Paulin (1988). "Nucleotide sequence of the human vimentin gene and regulation of its transcription in tissues and cultured cells." Gene **62**(1): 7-16.

185. Pertea, M., G. M. Pertea, C. M. Antonescu, T. C. Chang, J. T. Mendell and S. L. Salzberg (2015). "StringTie enables improved reconstruction of a transcriptome from RNA-seq reads." Nat Biotechnol **33**(3): 290-295.

186. Peuhu, E., R. Virtakoivu, A. Mai, A. Warri and J. Ivaska (2017). "Epithelial vimentin plays a functional role in mammary gland development." Development **144**(22): 4103-4113.

187. Pilecka, I., L. Sadowski, Y. Kalaidzidis and M. Miaczynska (2011). "Recruitment of APPL1 to ubiquitin-rich aggresomes in response to proteasomal impairment." Exp Cell Res **317**(8): 1093-1107.

188. Pilz, G. A., S. Bottes, M. Betizeau, D. J. Jorg, S. Carta, B. D. Simons, F. Helmchen and S. Jessberger (2018). "Live imaging of neurogenesis in the adult mouse hippocampus." Science **359**(6376): 658-662.

189. Qin, S., C. Jiang and J. Gao (2019). "Transcriptional factor Nrf2 is essential for aggresome formation during proteasome inhibition." Biomed Rep **11**(6): 241-252.

190. Rajendran, P., A. M. Alzahrani, H. N. Hanieh, S. A. Kumar, R. Ben Ammar, T. Rengarajan and M. A. Alhoot (2019). "Autophagy and senescence: A new insight in selected human diseases." J Cell Physiol **234**(12): 21485-21492.

191. Ran, F. A., P. D. Hsu, J. Wright, V. Agarwala, D. A. Scott and F. Zhang (2013). "Genome engineering using the CRISPR-Cas9 system." Nat Protoc **8**(11): 2281-2308.

192. Riley, N. E., F. Bardag-Gorce, R. O. Montgomery, J. Li, W. Lungo, Y. H. Lue and S. W. French (2003). "Microtubules are required for cytokeratin aggresome (Mallory body) formation in hepatocytes: an in vitro study." Exp Mol Pathol **74**(2): 173-179.

193. Riley, N. E., J. Li, L. W. McPhaul, F. Bardag-Gorce, Y. H. Lue and S. W. French (2003). "Heat shock proteins are present in mallory bodies (cytokeratin aggresomes) in human liver biopsy specimens." Exp Mol Pathol **74**(2): 168-172.

194. Risso, D., J. Ngai, T. P. Speed and S. Dudoit (2014). "Normalization of RNA-seq data using factor analysis of control genes or samples." Nat Biotechnol **32**(9): 896-902.

195. Rodriguez-Fernandez, I. A., Y. Qi and H. Jasper (2019). "Loss of a proteostatic checkpoint in intestinal stem cells contributes to age-related epithelial dysfunction." Nat Commun **10**(1): 1050.

196. Rogel, M. R., P. N. Soni, J. R. Troken, A. Sitikov, H. E. Trejo and K. M. Ridge (2011). "Vimentin is sufficient and required for wound repair and remodeling in alveolar epithelial cells." FASEB J **25**(11): 3873-3883.

197. Rohwedder, A., Q. Zhang, S. A. Rudge and M. J. Wakelam (2014). "Lipid droplet formation in response to oleic acid in Huh-7 cells is mediated by the fatty acid receptor FFAR4." J Cell Sci **127**(Pt 14): 3104-3115.

198. Ross, C. A. and M. A. Poirier (2004). "Protein aggregation and neurodegenerative disease." Nat Med **10 Suppl**: S10-17.

199. Ross, C. A. and M. A. Poirier (2005). "Opinion: What is the role of protein aggregation in neurodegeneration?" Nat Rev Mol Cell Biol **6**(11): 891-898.

200. Roy, S., A. Kapoor, F. Zhu, R. Mukhopadhyay, A. K. Ghosh, H. Lee, J. Mazzone, G. H. Posner and R. Arav-Boger (2020). "Artemisinins target the intermediate filament protein vimentin for human cytomegalovirus inhibition." J Biol Chem **295**(44): 15013-15028.

201. Rudrabhatla, P., H. Jaffe and H. C. Pant (2011). "Direct evidence of phosphorylated neuronal intermediate filament proteins in neurofibrillary tangles (NFTs): phosphoproteomics of Alzheimer's NFTs." FASEB J **25**(11): 3896-3905.

202. Rujano, M. A., F. Bosveld, F. A. Salomons, F. Dijk, M. A. van Waarde, J. J. van der Want, R. A. de Vos, E. R. Brunt, O. C. Sibon and H. H. Kampinga (2006). "Polarised asymmetric inheritance of accumulated protein damage in higher eukaryotes." PLoS Biol **4**(12): e417.

203. Runembert, I., S. Couette, P. Federici, E. Colucci-Guyon, C. Babinet, P. Briand, G. Friedlander and F. Terzi (2004). "Recovery of Na-glucose cotransport activity after renal ischemia is impaired in mice lacking vimentin." Am J Physiol Renal Physiol **287**(5): F960-968.

204. Sabath, N., F. Levy-Adam, A. Younis, K. Rozales, A. Meller, S. Hadar, S. Soueid-Baumgarten and R. Shalgi (2020). "Cellular proteostasis decline in human senescence." Proc Natl Acad Sci U S A **117**(50): 31902-31913.

205. Sagar, M. A. K., J. N. Ouellette, K. P. Cheng, J. C. Williams, J. J. Watters and K. W. Eliceiri (2020). "Microglia activation visualization via fluorescence lifetime imaging microscopy of intrinsically fluorescent metabolic cofactors." Neurophotonics **7**(3): 035003.

206. Sahay, A. and R. Hen (2007). "Adult hippocampal neurogenesis in depression." Nat Neurosci **10**(9): 1110-1115.

207. Sahay, A., K. N. Scobie, A. S. Hill, C. M. O'Carroll, M. A. Kheirbek, N. S. Burghardt, A. A. Fenton, A. Dranovsky and R. Hen (2011). "Increasing adult

hippocampal neurogenesis is sufficient to improve pattern separation." Nature **472**(7344): 466-470.

208. Sala, A. J., L. C. Bott and R. I. Morimoto (2017). "Shaping proteostasis at the cellular, tissue, and organismal level." J Cell Biol **216**(5): 1231-1241.

209. Salemi, L. M., A. W. Almawi, K. J. Lefebvre and C. Schild-Poulter (2014). "Aggresome formation is regulated by RanBPM through an interaction with HDAC6." Biol Open **3**(6): 418-430.

210. Sanchez-Martin, P. and M. Komatsu (2018). "p62/SQSTM1 - steering the cell through health and disease." J Cell Sci **131**(21).

211. Schaffeld, M., H. Herrmann, J. Schultess and J. Markl (2001). "Vimentin and desmin of a cartilaginous fish, the shark Scyliorhinus stellaris: sequence, expression patterns and in vitro assembly." Eur J Cell Biol **80**(11): 692-702.

212. Schiffers, P. M., D. Henrion, C. M. Boulanger, E. Colucci-Guyon, F. Langa-Vuves, H. van Essen, G. E. Fazzi, B. I. Levy and J. G. De Mey (2000). "Altered flow-induced arterial remodeling in vimentin-deficient mice." Arterioscler Thromb Vasc Biol **20**(3): 611-616.

213. Schipper-Krom, S., K. Juenemann, A. H. Jansen, A. Wiemhoefer, R. van den Nieuwendijk, D. L. Smith, M. A. Hink, G. P. Bates, H. Overkleeft, H. Ovaa and E. Reits (2014). "Dynamic recruitment of active proteasomes into polyglutamine initiated inclusion bodies." FEBS Lett **588**(1): 151-159.

214. Schulze, R. J., E. W. Krueger, S. G. Weller, K. M. Johnson, C. A. Casey, M. B. Schott and M. A. McNiven (2020). "Direct lysosome-based autophagy of lipid droplets in hepatocytes." Proc Natl Acad Sci U S A **117**(51): 32443-32452.

215. Shi, X., C. Fan and Y. Jiu (2020). "Unidirectional Regulation of Vimentin Intermediate Filaments to Caveolin-1." Int J Mol Sci **21**(20).

216. Shin, J., D. A. Berg, Y. Zhu, J. Y. Shin, J. Song, M. A. Bonaguidi, G. Enikolopov, D. W. Nauen, K. M. Christian, G. L. Ming and H. Song (2015). "Single-Cell RNA-Seq with Waterfall Reveals Molecular Cascades underlying Adult Neurogenesis." Cell Stem Cell **17**(3): 360-372.

217. Shivalingappa, P. C., R. Hole, C. V. Westphal and N. Vij (2016). "Airway Exposure to E-Cigarette Vapors Impairs Autophagy and Induces Aggresome Formation." Antioxid Redox Signal **24**(4): 186-204.

218. Silva-Vargas, V., A. R. Maldonado-Soto, D. Mizrak, P. Codega and F. Doetsch (2016). "Age-Dependent Niche Signals from the Choroid Plexus Regulate Adult Neural Stem Cells." Cell Stem Cell **19**(5): 643-652.

219. Smith, L. K., Y. He, J. S. Park, G. Bieri, C. E. Snethlage, K. Lin, G. Gontier, R. Wabl, K. E. Plambeck, J. Udeochu, E. G. Wheatley, J. Bouchard, A. Eggel, R. Narasimha, J. L. Grant, J. Luo, T. Wyss-Coray and S. A. Villeda (2015). "beta2-microglobulin is a systemic pro-aging factor that impairs cognitive function and neurogenesis." Nat Med **21**(8): 932-937.

220. Sontag, E. M., R. S. Samant and J. Frydman (2017). "Mechanisms and Functions of Spatial Protein Quality Control." Annu Rev Biochem **86**: 97-122.

221. Spalding, K. L., R. D. Bhardwaj, B. A. Buchholz, H. Druid and J. Frisen (2005). "Retrospective birth dating of cells in humans." Cell **122**(1): 133-143.

222. Spector, M. (2018). "Biomedical materials to meet the challenges of the aging epidemic." Biomed Mater **13**(3): 030201.

223. Steven, A. C., J. F. Hainfeld, B. L. Trus, J. S. Wall and P. M. Steinert (1983). "The distribution of mass in heteropolymer intermediate filaments assembled in vitro. Stem analysis of vimentin/desmin and bovine epidermal keratin." J Biol Chem **258**(13): 8323-8329.

224. Stoll, E. A., R. Makin, I. R. Sweet, A. J. Trevelyan, S. Miwa, P. J. Horner and D. M. Turnbull (2015). "Neural Stem Cells in the Adult Subventricular Zone Oxidize Fatty Acids to Produce Energy and Support Neurogenic Activity." Stem Cells **33**(7): 2306-2319.

225. Strouhalova, K., M. Prechova, A. Gandalovicova, J. Brabek, M. Gregor and D. Rosel (2020). "Vimentin Intermediate Filaments as Potential Target for Cancer Treatment." Cancers (Basel) **12**(1).

226. Sun, Y., Y. Zheng, C. Wang and Y. Liu (2018). "Glutathione depletion induces ferroptosis, autophagy, and premature cell senescence in retinal pigment epithelial cells." Cell Death Dis **9**(7): 753.

227. Sun Y. Maybury-Lewis, A. K. B., Mitchell Yeary, Anna Sloutskin, Shleshma Dhakal, Brendan McCarthy-Sinclair, Tamar Juven-Gershon, Ashley E. Webb (2020). "Changing and stable chromatin accessibility supports transcriptional overhaul during neural stem cell activation." Bioarxiv.

228. Sunchu, B., R. T. Riordan, Z. Yu, I. Almog, J. Dimas-Munoz, A. C. Drake and V. I. Perez (2020). "Aggresome-Like Formation Promotes Resistance to Proteotoxicity in Cells from Long-Lived Species." J Gerontol A Biol Sci Med Sci **75**(8): 1439-1447.

229. Szklarczyk, D., A. Franceschini, S. Wyder, K. Forslund, D. Heller, J. Huerta-Cepas, M. Simonovic, A. Roth, A. Santos, K. P. Tsafou, M. Kuhn, P. Bork, L. J. Jensen and C. von Mering (2015). "STRING v10: protein-protein interaction networks, integrated over the tree of life." Nucleic Acids Res **43**(Database issue): D447-452.

230. Takahashi, M., H. Kitaura, A. Kakita, T. Kakihana, Y. Katsuragi, M. Nameta, L. Zhang, Y. Iwakura, H. Nawa, M. Higuchi, M. Komatsu and M. Fujii (2018). "USP10 Is a Driver of Ubiquitinated Protein Aggregation and Aggresome Formation to Inhibit Apoptosis." iScience **9**: 433-450.

231. Tanaka, M., Y. M. Kim, G. Lee, E. Junn, T. Iwatsubo and M. M. Mouradian (2004). "Aggresomes formed by alpha-synuclein and synphilin-1 are cytoprotective." J Biol Chem **279**(6): 4625-4631.

232. Taylor, J. P., F. Tanaka, J. Robitschek, C. M. Sandoval, A. Taye, S. Markovic-Plese and K. H. Fischbeck (2003). "Aggresomes protect cells by enhancing the degradation of toxic polyglutamine-containing protein." Hum Mol Genet **12**(7): 749-757.

233. Taylor, R. C. and A. Dillin (2013). "XBP-1 is a cell-nonautonomous regulator of stress resistance and longevity." Cell **153**(7): 1435-1447.

234. Terzi, F., D. Henrion, E. Colucci-Guyon, P. Federici, C. Babinet, B. I. Levy, P. Briand and G. Friedlander (1997). "Reduction of renal mass is lethal in mice lacking vimentin. Role of endothelin-nitric oxide imbalance." J Clin Invest **100**(6): 1520-1528.

235. Thibaudeau, T. A., R. T. Anderson and D. M. Smith (2018). "A common mechanism of proteasome impairment by neurodegenerative disease-associated oligomers." Nat Commun **9**(1): 1097.

236. Tolstonog, G. V., R. L. Shoeman, U. Traub and P. Traub (2001). "Role of the intermediate filament protein vimentin in delaying senescence and in the spontaneous immortalization of mouse embryo fibroblasts." DNA Cell Biol **20**(9): 509-529.

237. Tran, I., C. Ji, I. Ni, T. Min, D. Tang and N. Vij (2015). "Role of Cigarette Smoke-Induced Aggresome Formation in Chronic Obstructive Pulmonary Disease-Emphysema Pathogenesis." Am J Respir Cell Mol Biol **53**(2): 159-173.

238. Urban, N., I. M. Blomfield and F. Guillemot (2019). "Quiescence of Adult Mammalian Neural Stem Cells: A Highly Regulated Rest." Neuron **104**(5): 834-848.

239. Urban, N., D. L. van den Berg, A. Forget, J. Andersen, J. A. Demmers, C. Hunt, O. Ayrault and F. Guillemot (2016). "Return to quiescence of mouse neural stem cells by degradation of a proactivation protein." Science **353**(6296): 292-295.

240. Vakhrusheva, A., S. Endzhievskaya, V. Zhuikov, T. Nekrasova, E. Parshina, N. Ovsiannikova, V. Popov, D. Bagrov, C. Minin Acapital A and O. S. Sokolova (2019). "The role of vimentin in directional migration of rat fibroblasts." Cytoskeleton (Hoboken) **76**(9-10): 467-476.

241. van Engeland, N. C. A., F. Suarez Rodriguez, A. Rivero-Muller, T. Ristori, C. L. Duran, O. Stassen, D. Antfolk, R. C. H. Driessen, S. Ruohonen, S. T.

Ruohonen, S. Nuutinen, E. Savontaus, S. Loerakker, K. J. Bayless, M. Sjoqvist, C. V. C. Bouten, J. E. Eriksson and C. M. Sahlgren (2019). "Vimentin regulates Notch signaling strength and arterial remodeling in response to hemodynamic stress." Sci Rep **9**(1): 12415.

242. van Loosdregt, I., G. Weissenberger, M. van Maris, C. W. J. Oomens, S. Loerakker, O. Stassen and C. V. C. Bouten (2018). "The Mechanical Contribution of Vimentin to Cellular Stress Generation." J Biomech Eng **140**(6).

243. Verdoes, M., B. I. Florea, V. Menendez-Benito, C. J. Maynard, M. D. Witte, W. A. van der Linden, A. M. van den Nieuwendijk, T. Hofmann, C. R. Berkers, F. W. van Leeuwen, T. A. Groothuis, M. A. Leeuwenburgh, H. Ovaa, J. J. Neefjes, D. V. Filippov, G. A. van der Marel, N. P. Dantuma and H. S. Overkleeft (2006). "A fluorescent broad-spectrum proteasome inhibitor for labeling proteasomes in vitro and in vivo." Chem Biol **13**(11): 1217-1226.

244. Vilaboa, N. E., L. Garcia-Bermejo, C. Perez, E. de Blas, C. Calle and P. Aller (1997). "Heat-shock and cadmium chloride increase the vimentin mRNA and protein levels in U-937 human promonocytic cells." J Cell Sci **110 (Pt 2)**: 201-207.

245. Vilchez, D., L. Boyer, I. Morantte, M. Lutz, C. Merkwirth, D. Joyce, B. Spencer, L. Page, E. Masliah, W. T. Berggren, F. H. Gage and A. Dillin (2012). "Increased proteasome activity in human embryonic stem cells is regulated by PSMD11." Nature **489**(7415): 304-308.

246. Vilchez, D., I. Saez and A. Dillin (2014). "The role of protein clearance mechanisms in organismal ageing and age-related diseases." Nat Commun **5**: 5659.

247. Vilchez, D., M. S. Simic and A. Dillin (2014). "Proteostasis and aging of stem cells." Trends Cell Biol **24**(3): 161-170.

248. Villeda, S. A. and T. Wyss-Coray (2013). "The circulatory systemic environment as a modulator of neurogenesis and brain aging." Autoimmun Rev **12**(6): 674-677.

249. Villella, V. R., S. Esposito, E. M. Bruscia, M. Vicinanza, S. Cenci, S. Guido, M. Pettoello-Mantovani, R. Carnuccio, M. A. De Matteis, A. Luini, M. C. Maiuri, V. Raia, G. Kroemer and L. Maiuri (2013). "Disease-relevant proteostasis regulation of cystic fibrosis transmembrane conductance regulator." Cell Death Differ **20**(8): 1101-1115.

250. Vora, S. M. and B. T. Phillips (2016). "The benefits of local depletion: The centrosome as a scaffold for ubiquitin-proteasome-mediated degradation." Cell Cycle **15**(16): 2124-2134.

251. Walsh, A. J., K. P. Mueller, K. Tweed, I. Jones, C. M. Walsh, N. J. Piscopo, N. M. Niemi, D. J. Pagliarini, K. Saha and M. C. Skala (2021). "Classification of T-cell activation via autofluorescence lifetime imaging." Nat Biomed Eng **5**(1): 77-88.

252. Walther, D. M., P. Kasturi, M. Zheng, S. Pinkert, G. Vecchi, P. Ciryam, R. I. Morimoto, C. M. Dobson, M. Vendruscolo, M. Mann and F. U. Hartl (2015).

"Widespread Proteome Remodeling and Aggregation in Aging C. elegans." Cell **161**(4): 919-932.

253. Wang, A. S., P. F. Ong, A. Chojnowski, C. Clavel and O. Dreesen (2017). "Loss of lamin B1 is a biomarker to quantify cellular senescence in photoaged skin." Sci Rep **7**(1): 15678.

254. Wang, K., L. K. Bekar, K. Furber and W. Walz (2004). "Vimentin-expressing proximal reactive astrocytes correlate with migration rather than proliferation following focal brain injury." Brain Research **1024**(1-2): 193-202.

255. Wang, Q. and K. Andreasson (2010). "The organotypic hippocampal slice culture model for examining neuronal injury." J Vis Exp(44).

256. Wigley, W. C., R. P. Fabunmi, M. G. Lee, C. R. Marino, S. Muallem, G. N. DeMartino and P. J. Thomas (1999). "Dynamic association of proteasomal machinery with the centrosome." J Cell Biol **145**(3): 481-490.

257. Wilhelmsson, U., M. Faiz, Y. de Pablo, M. Sjoqvist, D. Andersson, A. Widestrand, M. Potokar, M. Stenovec, P. L. Smith, N. Shinjyo, T. Pekny, R. Zorec, A. Stahlberg, M. Pekna, C. Sahlgren and M. Pekny (2012). "Astrocytes negatively regulate neurogenesis through the Jagged1-mediated Notch pathway." Stem Cells **30**(10): 2320-2329.

258. Wilhelmsson, U., A. Pozo-Rodrigalvarez, M. Kalm, Y. de Pablo, A. Widestrand, M. Pekna and M. Pekny (2019). "The role of GFAP and vimentin in learning and memory." Biol Chem.

259. Wong, E. and A. M. Cuervo (2010). "Autophagy gone awry in neurodegenerative diseases." Nat Neurosci **13**(7): 805-811.

260. Wong, E. S., J. M. Tan, W. E. Soong, K. Hussein, N. Nukina, V. L. Dawson, T. M. Dawson, A. M. Cuervo and K. L. Lim (2008). "Autophagy-mediated clearance of aggresomes is not a universal phenomenon." Hum Mol Genet **17**(16): 2570-2582.

261. Xiao, H. S., Q. Xie, J. Y. Zhong, B. Gerald Rukundo, X. L. He, Y. L. Qu and H. Cao (2018). "[Effect of vimentin on activation of NLRP3 inflammasome in the brain of mice with EV71 infection]." Nan Fang Yi Ke Da Xue Xue Bao **38**(6): 704-710.

262. Xu, B., Y. Gao, S. Zhan, F. Xiong, W. Qiu, X. Qian, T. Wang, N. Wang, D. Zhang, Q. Yang, R. Wang, X. Bao, W. Dou, R. Tian, S. Meng, W. P. Gai, Y. Huang, X. X. Yan, W. Ge and C. Ma (2016). "Quantitative protein profiling of hippocampus during human aging." Neurobiol Aging **39**: 46-56.

263. Xu, Y. F., T. F. Gendron, Y. J. Zhang, W. L. Lin, S. D'Alton, H. Sheng, M. C. Casey, J. Tong, J. Knight, X. Yu, R. Rademakers, K. Boylan, M. Hutton, E. McGowan, D. W. Dickson, J. Lewis and L. Petrucelli (2010). "Wild-type human TDP-43 expression causes TDP-43 phosphorylation, mitochondrial aggregation, motor deficits, and early mortality in transgenic mice." J Neurosci **30**(32): 10851-10859.

264. Xu, Z., K. Graham, M. Foote, F. Liang, R. Rizkallah, M. Hurt, Y. Wang, Y. Wu and Y. Zhou (2013). "14-3-3 protein targets misfolded chaperone-associated proteins to aggresomes." J Cell Sci **126**(Pt 18): 4173-4186.

265. Yamaguchi, M., H. Saito, M. Suzuki and K. Mori (2000). "Visualization of neurogenesis in the central nervous system using nestin promoter-GFP transgenic mice." Neuroreport **11**(9): 1991-1996.

266. Yamashita, T., M. Akamatsu and S. Kwak (2017). "Altered Intracellular Milieu of ADAR2-Deficient Motor Neurons in Amyotrophic Lateral Sclerosis." Genes (Basel) **8**(2).

267. Yan, J. (2014). "Interplay between HDAC6 and its interacting partners: essential roles in the aggresome-autophagy pathway and neurodegenerative diseases." DNA Cell Biol **33**(9): 567-580.

268. Yang, C., W. Tan, C. Whittle, L. Qiu, L. Cao, S. Akbarian and Z. Xu (2010). "The C-terminal TDP-43 fragments have a high aggregation propensity and harm neurons by a dominant-negative mechanism." PLoS One **5**(12): e15878.

269. Yeh, C. Y., B. Asrican, J. Moss, L. J. Quintanilla, T. He, X. Mao, F. Casse, E. Gebara, H. Bao, W. Lu, N. Toni and J. Song (2018). "Mossy Cells Control Adult Neural Stem Cell Quiescence and Maintenance through a Dynamic Balance between Direct and Indirect Pathways." Neuron **99**(3): 493-510 e494.

270. Yehia, M., H. Taha, A. Salama, N. Amer, A. Mosaab, O. Hassanain, A. Refaat, D. Yassin, A. El-Hemaly, S. Ahmed, M. El-Beltagy, O. Shaalan and S. El-Naggar (2019). "Association of Aggresomes with Survival Outcomes in Pediatric Medulloblastoma." Sci Rep **9**(1): 12605.

271. Yu, L., Y. Chen and S. A. Tooze (2018). "Autophagy pathway: Cellular and molecular mechanisms." Autophagy **14**(2): 207-215.

272. Yung, C., D. Sha, L. Li and L. S. Chin (2016). "Parkin Protects Against Misfolded SOD1 Toxicity by Promoting Its Aggresome Formation and Autophagic Clearance." Mol Neurobiol **53**(9): 6270-6287.

273. Zhang, C., J. Gao, M. Li, Y. Deng and C. Jiang (2018). "p38delta MAPK regulates aggresome biogenesis by phosphorylating SQSTM1 in response to proteasomal stress." J Cell Sci **131**(14).

274. Zhang, R., M. Boareto, A. Engler, A. Louvi, C. Giachino, D. Iber and V. Taylor (2019). "Id4 Downstream of Notch2 Maintains Neural Stem Cell Quiescence in the Adult Hippocampus." Cell Rep **28**(6): 1485-1498 e1486.

275. Zhang, R., A. Engler and V. Taylor (2018). "Notch: an interactive player in neurogenesis and disease." Cell Tissue Res **371**(1): 73-89.

276. Zhou, L., H. Wang, D. Chen, F. Gao, Z. Ying and G. Wang (2014). "p62/sequestosome 1 regulates aggresome formation of pathogenic ataxin-3 with expanded polyglutamine." Int J Mol Sci **15**(9): 14997-15010.

277. Zhou, Y., A. M. Bond, J. E. Shade, Y. Zhu, C. O. Davis, X. Wang, Y. Su, K. J. Yoon, A. T. Phan, W. J. Chen, J. H. Oh, N. Marsh-Armstrong, K. Atabai, G. L. Ming and H. Song (2018). "Autocrine Mfge8 Signaling Prevents Developmental Exhaustion of the Adult Neural Stem Cell Pool." Cell Stem Cell **23**(3): 444-452 e444.